~~The Physical Characterisation and Crystallisation of Lactose in Pharmaceutical Systems.~~

THE STUDY OF THE CHARACTERISATION AND CRYSTALLISATION OF LACTOSE SPRAY DRIED AND PHYSICAL MIXED PRODUCTS'

Magda Daifi

Submitted for the Degree of Doctor of Philosophy in the Faculty of Medicine, University of London.

Department of Pharmaceutics

The School of Pharmacy

January, 2004

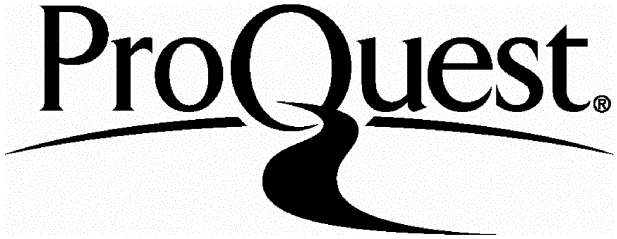

Abstract

The general aim of this thesis was to study binary spray dried composite particles of lactose with either polyvinylpyrrolidone (PVP K-25) or sodium dodecyl sulphate (SDS). The research was based on the characterisation and crystallisation of these products, with special interest directed to the stability of amorphous lactose. Lactose, PVP and SDS are used widely in pharmaceutics but have not been studied thoroughly in combination as binary systems.

The spray dried (SD) and physical mixed (PM) products of lactose and PVP (K-25) or SDS were produced at varying concentrations of the latter two excipients with amorphous lactose. The effects of PVP were further studied in combination with partially amorphous lactose.

Initially lactose and PVP (K-25) were studied as single components to investigate their physical properties. The effects of feed concentrate with reference to spray drying for lactose was investigated. The production of amorphous content was quantified and found to decrease with increase lactose concentration. Crystallisation kinetics using Avrami equation was determined by dynamic vapour sorption and near infrared spectroscopy (DVS-NIRS). The results showed that amorphous lactose alone and in the presence of seed crystals crystallised in a similar rate and manner. Amorphous lactose with a high quantity of crystalline material crystallised in a rapid and cooperative manner.

The addition of polymer was found to increase the induction time of crystallisation of amorphous lactose and also crystal growth at concentrations higher than 10% of PVP. This delay in nucleation and inhibition of crystallisation is due to hydrogen bonding and an increase in viscosity (depicted by a raised glass transition). The PM products were relatively unaffected up until 40% polymer concentration. Partially amorphous lactose also showed a delay in the onset of crystallisation; however crystal growth was not hindered due to seeding which was found using NIRS.

SDS produced the opposite effect in relation to PVP, where the increase wetting of amorphous lactose in the SD composite particle decreased both the induction and propagation time.

The study of the stability of amorphous and partially amorphous lactose under the influence of PVP and SDS has been successfully investigated with the employment of a variety of analytical tools in parallel combination. However the use of the novel technique DVS-NIRS proved vital to the work accomplished.

Acknowledgments

I would like to thank GOD.

The work presented in this thesis has formed a major part of my life at the most interesting time of my life, but it would not have been possible without the following people. I would like to thank Prof. Graham Buckton for his unwavering support, guidance and encouragement in believing that I have the ability to complete this PhD.

A great big thank you to Dr Fariba Koosha (Glaxo-SmithKline), for all her support, kindness and understanding throughout the course of this work. The financial support of GlaxoSmithKline is gratefully appreciated.

I would like to thank the staff in the pharmaceutics department; Mac, Keith, Lionel and the gang for providing me with the technical support I needed. I would also like to mention my old colleagues; Shazia Ali, Juliette Guaquiere, Leticia Bariocanal, Ajay Shah and Ann Vibookiat who have made these past few years enjoyable and memorable. A special mention and thank you to Roy Lane and Dr Simon Gaisford for all the long chats about the TAM, DSC, etc and providing me with the scientific insight to accomplish my studies.

Finally I would like to thank my loving family for their patience, support, time and effort in helping me achieve my goal especially my mother, my father, my husband and my beautiful daughters. Thank you!

This thesis is dedicated in loving remembrance to my mother- in-law.

abs.	Absorbance
amo.	Amorphous
der.	Derivative
DSC	Differential Scanning Calorimetry
DVS	Dynamic Vapour Sorption
endo.	endothermic
exo.	exothermic
FTIR	Fourier Transform Infrared Spectroscopy
FWHM	Full Width Half Maximum
GC	Gas Chromotography
H-bond	Hydrogen bond
MLR	Multiple Linear Regression
MTDSC	Modulated Temperature Differential Scanning Calorimetry
NIRS	Near Infrared Spectroscopy
Pa. amo.	Partially amorphous
PEG	Polyethylene Glycol
PM	Physical Mix
PVP	Polyvinylpyrrolidone
PXRD	Powder X-ray Diffraction
RH	Relative Humidity
SD	Spray Dried
SDS	Sodium Dodecyl Sulphate
SEM	Scanning Electron Microscopy
SEMS	Scanning Electron Micrographs
SMS	Surface Measurement Systems
SNV	Standard Normal Variate
TAM	Thermal Activity Monitor
TGA	ThermoGravimetric Analysis

Prologue

Multi-component systems have been investigated in pharmaceutical science over the past two decades (Sekikawa et al., 1978; Corrigan et al., 1984; Shamblin et al., 1996; Chidavaenzi et al., 1998; Van der Mooter et al., 2001). The research has equipped scientists with better knowledge and understanding of how components may influence each other under pharmaceutical processes and dosage form design. However with evolving analytical equipment and the unpredictability of some systems under different experimental conditions, there has been increased interest into the research of multi-component systems (Chidavaenzi, 1999; Nair et al., 2001; Van den Mooter et al., 2001).

The significance of studying such systems provides important information on pharmaceutical subjects. The nature of a formulation seldom consists of one component hence the study of interactions between components from film coating to the effects of crystallisation and amorphous composition have been investigated (Sekizaki et al., 1995; Shamblin et al., 1998; Chidavaenzi et al., 2001; Nair et al., 2001). New formulation designs using more than two components are always at the forefront of pharmaceutical research (Tantishaiyakul et al., 1999; Imamura et al., 2001). Scientific concepts are tested using multi-component systems, for example exploring the factors which affect the amorphous to crystalline phase transition of a compound (Van Scoik and Cartensen, 1990). The factors which influence the crystallisation process are essential to the stability of the final product. Many formulations are required to remain in the most bioavailable state, which is usually in the amorphous form. So the prevention of crystallisation is essential to maintain the stability and the bioavailability of a product. These are a few of the many reasons why multi-component systems are studied.

The general objective of this thesis has been to investigate the effects of the polymer polyvinylpyrrolidone (PVP, K-25) and the surfactant sodium dodecyl sulphate (SDS) on lactose. This was proposed following a previous study of spray dried (SD) lactose and the polymer PEG 4000 (Chidavaenzi, 1999). The results documented from this report were unpredictable in terms of the effects PEG 4000 had on lactose in the final binary SD product. From this study it was found that there was very few literature reports based on the effects that excipients have on amorphous and partially amorphous lactose systems. This is significant as lactose is a widely used exicpient in the pharmaceutical and food industry as well as research where it is used as a model material.

The binary systems were investigated as spray dried (SD) and physical mix (PM) products at varying concentrations of lactose and PVP or SDS. The following points have been the focus of this study to achieve the main objective;

- To study the amorphous to crystalline phase transition of amorphous and partially amorphous lactose as a single component.
- To investigate the co-spray drying of lactose with PVP in solution and suspension.
- To study the stability of amorphous and partially amorphous lactose under the influence of PVP when co-spray dried and as a PM.
- To investigate the co-spray drying of lactose with SDS in solution.
- To study the amorphous to crystalline phase transition of the binary products of amorphous lactose and SDS.

A general introduction into the pharmaceutical concepts related to the work conducted are described in chapter one. This is fundamental to the understanding of the work presented in this thesis. The different physical states in which a material can exist are defined. All the aims and objectives were achieved by using a combination of calorimetric and non-calorimetric techniques described in chapter two. In particular the novel hyphenation of dynamic vapour sorption (DVS) and near infrared spectroscopy (NIRS). Chapter three details the preliminary studies conducted on lactose, PVP and SDS as single components. Chapter four focuses on the study of amorphous and partially amorphous lactose and PVP (K-25) and finally chapter five describes the work conducted on amorphous lactose and SDS. To complete the work a general conclusion along with ideas of future work is presented.

Chapter One
Introduction

1.1 Introduction

Most materials around us exist in one form or another, in pharmaceutics the state of a material can be broadly classified into two forms crystalline or amorphous which can be further subdivided. An introduction into these states is described in this chapter. Further topics are also discussed which include the production, physical properties, the advantages and disadvantages and how they are exploited accordingly with regards to the amorphous and crystalline form.

The amorphous to crystalline phase transition is also an area which is tackled, describing the nucleation and crystal growth phase and how it is observed experimentally. The phase transition is an important step in defining factors which can stabilise the amorphous material which is usually the desired form. All of these areas are important in pharmaceutical science and provide the basis for the work conducted in this thesis.

1.2 The Crystalline State

A crystalline solid is a material where the molecules organise themselves into a regular pattern of long-range order leading to periodicity and symmetry (Byrn, 1982; Flink, 1983). This phenomenon is responsible for many of the unique physicochemical properties of crystals, which range from crystal habits to polymorphism. The importance of the crystalline state and the degree of crystallinity are by no means understated in pharmaceutics. This is with respect to drug and excipient formulation, stability and bioavailability. Most pharmaceutical materials encountered are crystalline or possess a high degree of crystallinity with a small amount of amorphous material depending on manufacturing processes.

The state of a compound is also important to its physical properties for example a very well defined melting point indicates a crystalline lattice, where the breakdown of the crystals occurs at a fixed energy level (Flink, 1983). Pharmaceutical properties such as chemical stability, water uptake and loss, solubility, dissolution rate, mixing, flow and compaction can be influenced by the degree of crystallinity, which can be explained by two concepts illustrated in Fig 1.1 (York, 1983; Suryanarayanan and Mitchell, 1985).

Fig 1.1. A schematic representation of the two models of crystallinity (adapted from Suryanarayanan and Mitchell, 1985).

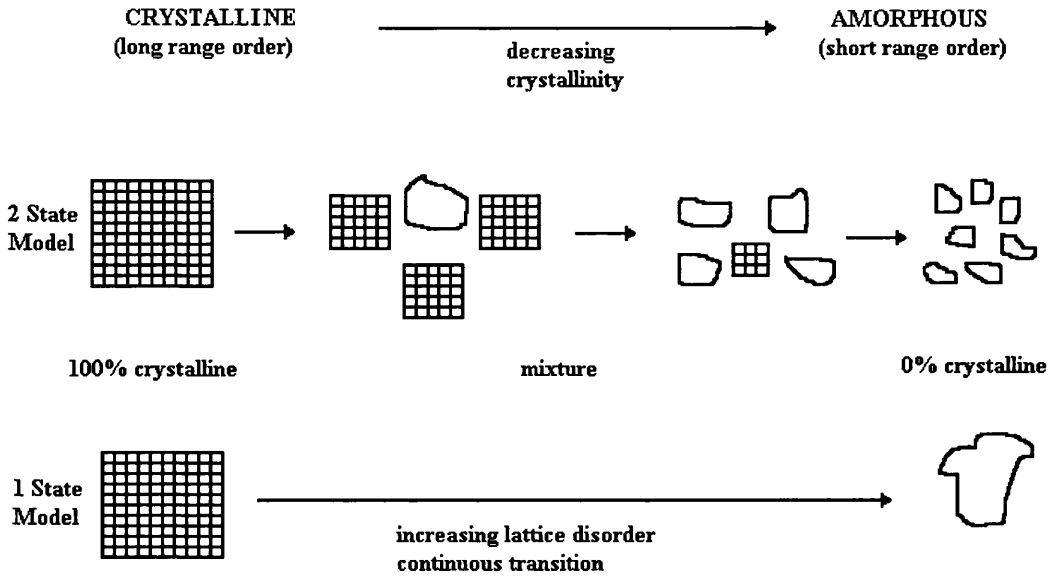

A two state model represents a mixture of two states: crystalline and amorphous material, the degree of crystallisation depending on the fraction of crystalline material in the mixture. An alternative concept is that the degree of crystallinity has a value located on a continuous scale, which varies between 100% (perfect crystal) and 0% (amorphous) depending on the state of order/disorder in the lattice (Huttenrauch, 1978 via Suryanarayanan and Mitchell, 1985). Since there is no sharp distinction between the crystalline and amorphous state this is referred to as the one state model. It is accepted that these concepts are over simplified and that more complex transitions occur and that other models can exist but nevertheless these models are accepted and adopted (Suryanarayanan and Mitchell, 1985).

Understanding the mechanisms of crystallisation is essential in material science as it is a means of providing control of the final product for the operator. Crystals are produced by inducing a change from the liquid to a solid state where nucleation and growth are involved. There are two options by which this can be achieved: cooling a molten sample through its melting point or crystallising via a supersaturated solution. The latter process can be achieved through a number of routes: cooling crystallisation, which entails cooling the solution until the solute solidifies. Evaporation crystallisation is another route where the solvent is evaporated leaving a crystal solid of what was once the solute. Drowning-out or salting out is another method by which crystallisation can take place. This

particular route is achieved by adding another component, either a solvent or solute that is inert (David and Giron, 1998; Buckton, 2002). During these processes in order for crystallisation to occur nucleation and growth need to be achieved.

1.2.1 Nucleation

Nucleation is the process by which crystallisation takes place, it may occur spontaneously or may be induced artificially by agitation, mechanical shock, friction and extreme pressures within solutions and melts. Once nucleation and subsequent crystallisation occurs the origins by which it has taken place are not always possible to identify. The actual concept can be divided into two headings: primary and secondary.

Primary nucleation can be further divided into homogenous, which occurs spontaneously, or heterogeneous where nucleation is induced by foreign particles. In a homogenous sample the formation of a crystal nucleus is still not understood because the process is complex. The molecules need to have the correct orientation to adhere to the growing nucleus and also resist re-dissolving to form a critical size. A critical size in order for nucleation to proceed represents the minimum size of a stable nucleus. Particles smaller than the arbitiuary size will dissolve or evaporate in order to achieve a reduction in the free energy. Particles larger than this will continue to grow because by stabilising and settling down there is also a decrease in free energy (Mullins, 1993). Turnball and Fisher, (1949) summarise the rate of homgenous nucleation in an equation which is dependent on two parameters; Gibbs free energy change for the formation of a nucleus of a critical size and the free energy associated with the transport of molecules across the nucleus/amorphous matrix interface. Many of the potential nucleus-forming sites may never become active nucleus sites as they become consumed by the growth of other nuclei. Alternatively the growing nuclei will eventually impinge on one another (Jacobs, 1997).

The process of true homogenous nucleation rarely takes place. It would be very difficult to achieve a sample that is completely contaminant free of foreign bodies in every day practice. Therefore heterogeneous nucleation is a more likely event where the heteronucleus is a foreign body that could be added intentionally or occur accidentally. The size of the foreign body is important and there is evidence to suggest that the most active heteronuclei in liquid solutions lie in the range of 0.1-1μm (Mullins, 1993).

When crystals of the solute are already present or deliberately added (seeding) nucleation takes place more readily and at faster rate, this is termed secondary nucleation. The occurrence of secondary nuclei may also arise from the production of breakage fragments due to collisions from existing crystals. Secondary nucleation differs from primary heterogenous nucleation, as the nuclei are small pieces of the solute that have been displaced from existing crystals. An example of secondary nucleation is a supersaturated solution, which has been agitated leading to fragmented crystals, which become secondary nuclei sites. A summary of these concepts is shown in figure 1.2. Once crystallisation has been established crystal growth takes place.

Fig 1.2. A schematic summary of nucleation.

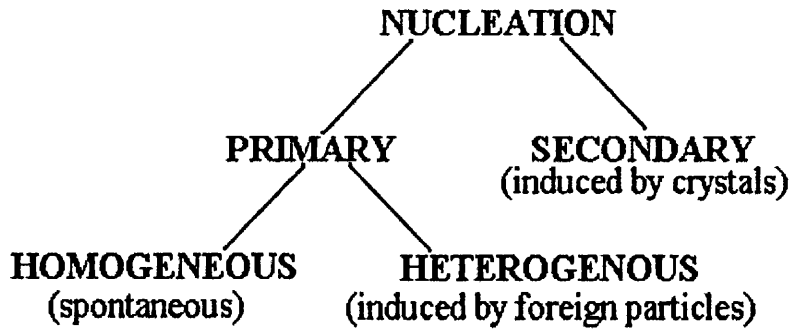

1.2.2 Crystal Growth And Defects

Crystal growth is essentially the increase in size of the nuclei. There are two steps involved: diffusion of the solute molecule through the solvent and integration of the solute molecule into the nuclei, which can be termed interfacial incorporation. The latter step is influenced by a number of factors, such as the nature of the solvent and surface roughness. In order to be in favour of crystallisation and crystal growth the interaction between solute molecules needs to be greater than that between the solute and solvent molecule. There also needs to be dislocations where molecules can lodge and grow.

There are many growth models that have been proposed for crystalline growth, a few will be mentioned here but for a more comprehensive review Mullins, (1993) can be referred to. Continuous growth is a model which is diffusion rate-limited, the molecules bond and attach to the rough surface of the emerging crystalline structure, so this growth is highly unlikely to be seen on smooth crystal surfaces and is directly proportional to the supersaturation of the liquid. Spiral growth is similar to the above but the nuclei attach to

imperfections or dislocations during crystallisation. As a result they spiral out of the dislocation hence the name. Surface nucleation is a model that occurs on smooth surfaces. The nuclei form on the plain surface but a few molecules need to converge together and deposit on the surface at the same time and place to create a rough surface for crystal growth. This leads to two types of morphological states: layered crystal or spherulites. This type of growth is also integration rate limited as it depends on the molecules of the supersaturated solution forming nuclei of critical size and the need for the supersaturated solution to return to equilibrium. Fig 1.3 illustrates the three different growth models.

Fig 1.3. A schematic representation of crystal growth for (a) continuous (b) spiral and (c) surface nucleation models.

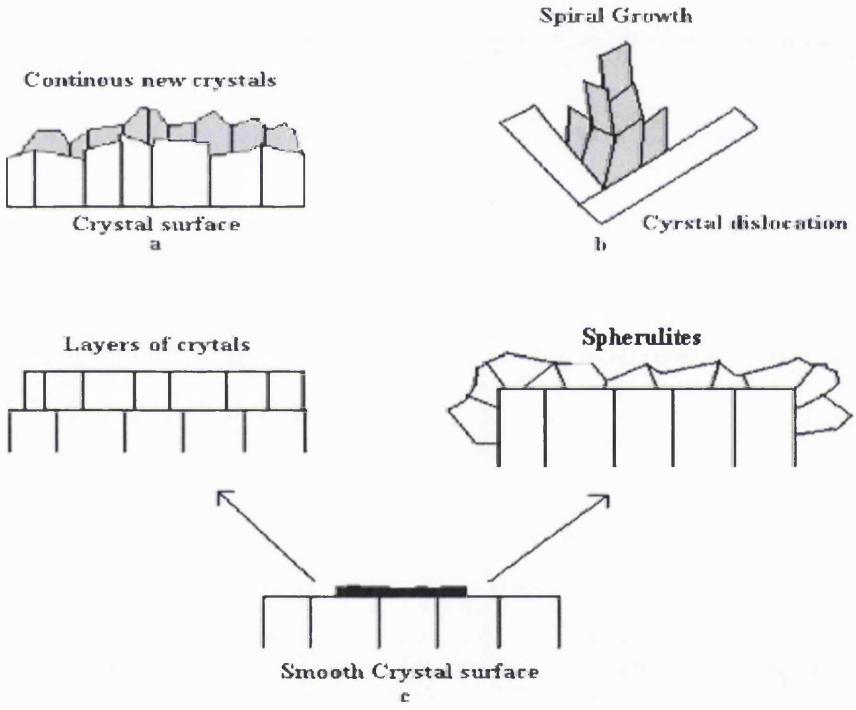

It follows from the above explanation that crystalline solids contain within their lattice, defects which can influence their physical and mechanical properties and their processing. These defects and dislocations occur during growth of the crystalline structure. They can be broadly classified into two categories: point and lattice. Point defects are localised imperfections, and are generally thermodynamically stable. They occur due to vacancies of molecules or extra molecules, which can be foreign or of the same specie, occupying substitutional positions in the crystal lattice. Lattice defects encompass line defects or dislocations that are thermodynamically unstable (Read, 1953). These defects have been shown to influence chemical reactivity, enhance the dissolution rate and as a consequence increase the bioavailability (Burt and Mitchell, 1981; Byrn,

1982). The concentration and density of lattice defects can also be altered as a result of stress induced during processing and therefore the pharmaceutical properties of the material need to be maintained throughout the process, causing minimum disruption to the surface of the sample.

Once nucleation and crystal growth is established the type of bonding that occurs between molecules during the crystallisation process is responsible for holding the crystals together which is quantified by molecular binding energies. Non-covalent interactions, which can be either hydrogen-bonded, or a form of non-covalent attractive forces holds the crystal lattice together. The symmetry of the lattice structure is also of importance thermodynamically. Molecules with symmetries that allow them to fit together in a close-packed arrangement form better crystals and crystallise more easily than less symmetrical systems (Byrn, 1982).

1.2.3 Crystal Habit

Once crystal growth is complete, the external shape of a crystal that has formed is called its habit. The shape can be of various morphology depending on the rate at which different faces grow and the internal packing of molecules. The crystal habit can therefore provide us with information on the molecular organisation of a material. In terms of characterisation a material would have an identical internal structure but several different crystal habits. This would provide us with identical powder X-ray diffraction pattern as well as physicochemical properties such as melting point and enthalpy of fusion etc. In terms of pharmaceutical properties a difference in crystal habit can have a profound effect on the properties of a product. Dissolution rate, powder flow characteristics and suspension syringeability are properties that need to be reviewed with a change in crystal habit. It is possible to produce the desired external shape in a number of ways: controlling the crystallisation conditions and manipulating the rate of growth of the different faces of the crystal. The latter is done by intentionally adding a small amount of impurity to the solution crystallising, which would preferentially favour one face of the growing crystal. This will stop the growth on that face and allow the remaining faces to grow (Byrn, 1982; Buckton, 2002).

1.2.4 Polymorphism

A material undergoing crystallisation may have the ability to crystallise as more than one form through different internal packing arrangements of atoms or molecules. This is defined as polymorphism and it has been suggested that every organic medicinal compound can exist in different polymorphic forms, a comprehensive list of drugs exhibiting polymorphism can be found in the published review by Giron, (1995). The difference in crystal structure naturally leads to different physical and chemical properties. This occurs because of a difference in energy contents due to the change in molecular binding energies. For a given set of physical conditions the polymorph with the lowest free energy is the most stable, whilst the others are termed metastable, trying to convert to the most stable form. The physicochemical properties which are affected by the type of polymorphic form are: crystal shape, density, melting point, solubility, hardness, dissolution rate, and various flow properties (York, 1983). However, for pharmaceutical agents the non-equivalence of crystal structure requires that non-equivalent X-ray powder diffractograms be observed for polymorphic materials (Brittain, 1997).

Since medicinal compounds exhibit polymorphism, it is absolutely essential in pharmaceutics to choose the form that provides the required bioavailability and therapeutic levels and maintain this throughout formulation and shelf life. For example polymorphism has been shown to occur during spray drying of various materials including lactose (Fell and Newton, 1970), hydroflumethiazide and phenobarbitione (Corrigan, 1982) and many more (York, 1983). It has also been observed that transitions can also occur during milling and grinding (Ibrahim et al., 1977).

1.2.5 Solvates

The formation of a solvate occurs when crystallisation takes place in a solvent system and a solvent molecule is incorporated within the structure. Hence crystals that contain solvents of crystallisation are termed solvates and can be in stoichiometric or non-stoichiometric amounts. A solvent can play a differential role in holding the crystal lattice together depending on whether the solvent molecule is incorporated or not by the host molecules. An interaction between solvent and host molecule in the form of hydrogen bonding leads to incorporation. The removal of the solvent (termed desolvation) in this case would prompt recrystallisation and the formation of a new crystal form. However if

the solvent molecule is excluded and only occupies voids in the crystal, if desolvation was to occur the crystal form would remain intact and unaltered. These events and hence definitions can be termed crystal pseudopolymorphism. Solvates that transform to another crystalline form upon desolvation are called polymorphic solvates. Solvates that remain in the same crystal form are termed pseudopolymorphic solvates. Both forms have stable and unstable members (Byrn, 1982).

1.3 The Amorphous State

An important aspect of a material in the pharmaceutical industry is whether the sample is amorphous or crystalline in nature. An amorphous material may be defined as a system where there is no three-dimensional long-range order but are structurally more similar to liquids where the arrangement of the molecules is random. They also have physical properties different from those of their corresponding crystalline states (Angell, 1995; Hancock and Zografi, 1997). This state may be produced intentionally or unintentionally depending on the requirements of the operator. Four common ways of producing an amorphous material have been identified which are shown in figure 1.4.

Fig 1.4. A schematic diagram of the common ways of producing an amorphous sample (adapted from Hancock and Zografi, 1997).

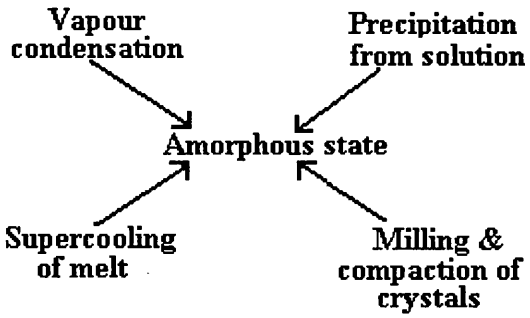

Precipitation from solution to produce an amorphous material usually entails freeze or spray drying the material in question. In the case of spray drying, the material is dissolved in the appropriate solvent and passed through the spray dryer into a high temperature environment under a short space of time causing rapid precipitation and the production of an amorphous material. In this case the molecules have little time to align in the correct way and interact to form a crystal. The milling and compaction of crystals is routinely

used in pharmaceutics to produce an amorphous material. Authors have used this method of production for subsequent studies of quantification of low amorphous content (Otsuka and Kaneniwa, 1990; Mackin et al., 2002). Vapour condensation entails the rapid cooling of vapour onto a substrate producing an amorphous film. A variety of techniques are used to vaporise the material including thermal evaporation, which is achieved by vaporising the chosen material in vacuum. Sputtering is also another technique by which the material can be vaporised (Elliott, 1994).

The amorphous state also exists within large molecular structures because of size. For example natural and synthetic polymers tend to always be partially amorphous and may completely lack crystallinity, as it is not possible for them to align perfectly to form crystals. For synthetic polymers the degree of crystallinity may also vary depending on the processing parameters (White and Cakebread, 1966; Ediger et al., 1996; Buckton, 2002). Low levels of disorder can also be attained by the presence of small amounts of impurities and additives, which are incorporated during crystallisation to cause impurity defects within the crystal lattice. This gives rise to a disordered state within an ordered environment (Pikal and Grant, 1987). The final way of producing an amorphous material is by supercooling a melt, this is described in the following section.

1.3.1 The Supercooling of a Melt

The supercooling of a melt or melt quenching can be described by Fig 1.5. Many crystalline solids when heated above their melting point (T_m) and are rapidly cooled through this parameter do not immediately crystallise but form a supercooled liquid, which is a liquid at a temperature below its melting point (Ediger et al., 1996). The crystalline solid is heated to form a liquid, which is followed by an increase in the specific volume and enthalpy. Upon rapid ($>10^5 K\ s^{-1}$) cooling we enter into the supercooled liquid state, which is an equilibrium line that may be stable for a very long time. However on further cooling the viscosity of the liquid increases and the molecules which comprise it move more and more slowly. At some temperature molecular mobility will be so slow that rearrangement to achieve the equilibrium state before further cooling is not attained. At this point the specific volume of the system deviates from the equilibrium value and the molecular mobility is described as "frozen". This change in slope is seen at the characteristic temperature known as the glass transition temperature (T_g). This leads to a glassy material, which is in a non-equilibrium state that possess an elevated amount of enthalpy, entropy and a high specific volume than a supercooled

liquid or crystalline material (Ediger et al., 1996; Hancock and Zografi, 1997; Walstra, 2003).

The Kauzmann temperature (denoted T_k, Kauzmann, 1948) that is illustrated in Fig 1.5 represents the temperature at which the entropy of the disordered supercooled liquid state is equal to that of the ordered crystalline state. This is a highly improbable event and in reality the entropy crises is avoided by the intervention of the T_g (Kauzmann, 1948; Shamblin et al., 1999; Zhou et al., 2002).

Fig 1.5. The formation of an amorphous material from a supercooled liquid (adapted from Hancock and Zografi, 1997; Zhou et al., 2002).

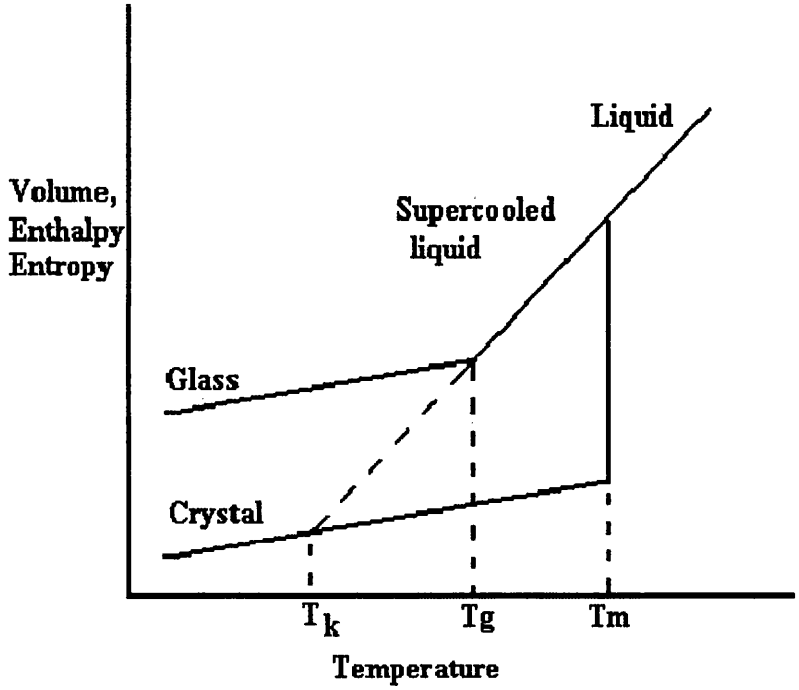

1.3.2 Pharmaceutical Properties of An Amorphous Material

The difference in physical properties of an amorphous material to its crystalline counterpart is due to the high-energy state described as unstable because of the disordered nature. Thermodynamically the stable crystalline form is favoured and an amorphous region will always try to revert to this state (Schmitt et al., 1999). Many of the advantages and disadvantages of this system are based on this concept. Improving dissolution and bioavailability of poorly soluble drugs can often be achieved by using amorphous preparations as a lower energetic barrier needs to be overcome in order to enter solution

than a regular structured crystalline solid. However, the disadvantages are the increased chemical and physical instabilities due to an increase in moisture uptake (Simonelli et al., 1976; Byrn et al., 1995; Hancock et al., 1995).

Amorphous material that has been induced by pharmaceutical processes usually resides on the surface of a crystalline solid and therefore a small amount of disorder (by weight of the sample) can be a very substantial amount on the powder surface, which can be represented by the one state model (Suryanarayanan and Mitchell, 1985; Buckton and Darcy, 1999). This leads to various pharmaceutical problems such as a change in the final physicochemical properties of the product, which are not known or have not been considered. This systematically leads to change in the product performance. Therefore whether the amorphous state occupies the bulk of a material or resides on the surface and occupies a small percentage, it still possess the ability to be detrimental to the stability of the final product. However, this can be overcome at times by the addition of stabilising agents if the amorphous state is favourable. Rapid drying or cooling can also be conducted to retard molecular mobility of the amorphous material over a meaningful pharmaceutical time scale (Hancock et al., 1995).

1.3.3 Definition of Glass Transition Temperature (T_g)

The glass transition temperature (T_g) is a characteristic temperature of any amorphous material; it is usually defined by the molecular mobility. Below this temperature, the molecules are held in a "kinetically frozen" metastable glassy state, there is very little molecular motion and the material is classed as amorphous. Above the T_g the molecules gain energy, leading to an increase in molecular motion, and the material is described as been in a "rubbery state." The T_g is an experimental parameter that is material specific and has been shown to vary with experimental heating and cooling rates, sample molecular mass, sample history, sample geometry and purity (Ahlneck and Zografi, 1990; Hancock and Zografi, 1997). The T_g is a second order transition where a change in kinetics is observed (Walstra, 2003).

Most amorphous materials have a glass transition temperature above room temperature, for example dry lactose has a T_g of 115°C and therefore is held in the amorphous state at ambient temperatures. The employment of certain conditions can lower the T_g of a system to produce the crystalline state. The additions of certain materials that are termed plasticizers lower the T_g, as described in Fig 1.6 with water vapour. Anitplasticizers or stabilising agents can often be added to an amorphous material to prevent the material

from crystallising by raising the T_g (Hancock and Zografi, 1994). Heating the material to the glass transition temperature also leads to the stable crystalline form.

Fig 1.6. A solute-water state diagram that shows the effects of water plasticization and its effects on T_g. Tm denotes temperature of melt of amorphous solid (adapted from Ahlneck and Zografi, 1990).

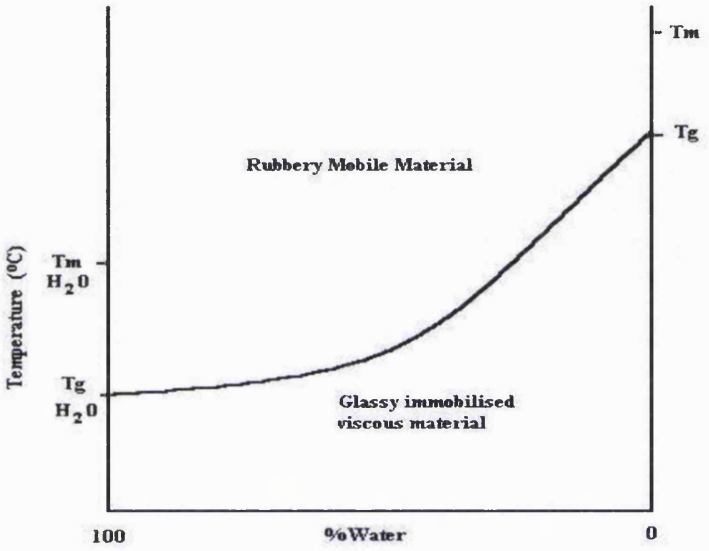

1.3.4 The Physical Parameters of the Amorphous state at the glass transition temperature (T_g)

The T_g of an amorphous solid is a kinetic parameter, which determines its chemical and physical stability as well as its viscoelastic properties. It is therefore of importance where relevant that the T_g of a material can be measured. It has been shown that many physical properties change when the T_g of a material is crossed from the supercooled liquid to the amorphous state. There is increased molecular motion when a material goes from glass (amorphous) to a rubbery liquid state. This molecular motion has been quantified as an average range $10\text{-}10^4$ seconds for many materials at the T_g. Below the T_g, in the amorphous state the material is kinetically "frozen" and molecular motions will occur over a period in excess of 100 seconds. The material is referred to as "frozen" as the molecular rearrangements become long compared to the time scale of the experimental observations but in actual fact it has been found that for molecular motions to become

insignificant it is necessary to cool the product to 50K below the Tg (Hancock et al., 1995; Ediger et al., 1996; Hancock and Zografi, 1997).

With a change in molecular motion there is also a change in the free volume of the system, this is defined by Flink (1983) as the volume unoccupied by the "solid matter" of the molecules and hence represents the volume available for free movement. The free volume originates from the molecule's translational, rotational, and vibrational movements. As long as this parameter extends throughout the system, the molecules are able to change structure and undergo crystallisation. However, when molecular motion slows down significantly, free volume no longer extends through out the system, the structure that exists at that moment is said to be "frozen" and hence a glassy state is established. At this stage, if we consider Fig 1.5 non-equilibrium conditions exist, as there is space in the system that would not exist under an equilibrium environment. This fractional free volume that occurs at T_g and remains below this temperature has been measured for polymers at 0.025. In general an increase in free volume leads to a decrease in T_g, as the molecules will be provided with space to complete a phase transition from amorphous to a crystalline state. It therefore follows that with a decrease in free volume there is an increase in T_g. Factors which affect free volume are listed as molecular weight, steric hindrance, and diluents (Flink, 1983; Shalaev and Franks, 1995).

The change in molecular motion and free volume also brings a change in viscosity, which has also been quantified. At T_g the viscosity for many amorphous materials would be in the range of 10^{12}-10^{14} Pa S, which in reality is too viscous to allow crystallisation. However above this parameter, viscosity has been noted to drop to approximately 10^8 Pa S where collapse of the material is observed (Levine and Slade, 1987). With a decrease in viscosity there is an increase in free volume, and hence an increase in the molecular motion leading to the event of crystallisation. The opposite effect is seen when the viscosity is increased and the free volume is reduced as a consequence.

Other major physical properties that change at the T_g as a consequence of molecular mobility, free volume and viscosity are; heat capacity, heat content and thermal expansion coefficient. The heat capacity (C_p) is an important parameter for the characterisation of the amorphous state and generally there is an increase in the heat capacity of a material when it is heated through the glass transition into the supercooled liquid state. The measured C_p has also been reported to depend on thermal history of the material in a similar manner to that of the T_g (Shamblin et al., 1999). A difference between the thermal expansion coefficient below and above the T_g can be measured and

arises due to a change in the free volume between the amorphous and supercooled liquid state (Flink, 1983). The change in the physical properties at T_g can be summarised in Fig 1.7 as well as Fig 1.5. The measurement of T_g and the definition of the amorphous state are based on these properties (White and Cakebread, 1966).

Fig 1.7. Physical characteristics of the transition from the glassy to the liquid state (adapted from White and Cakebread, 1966).

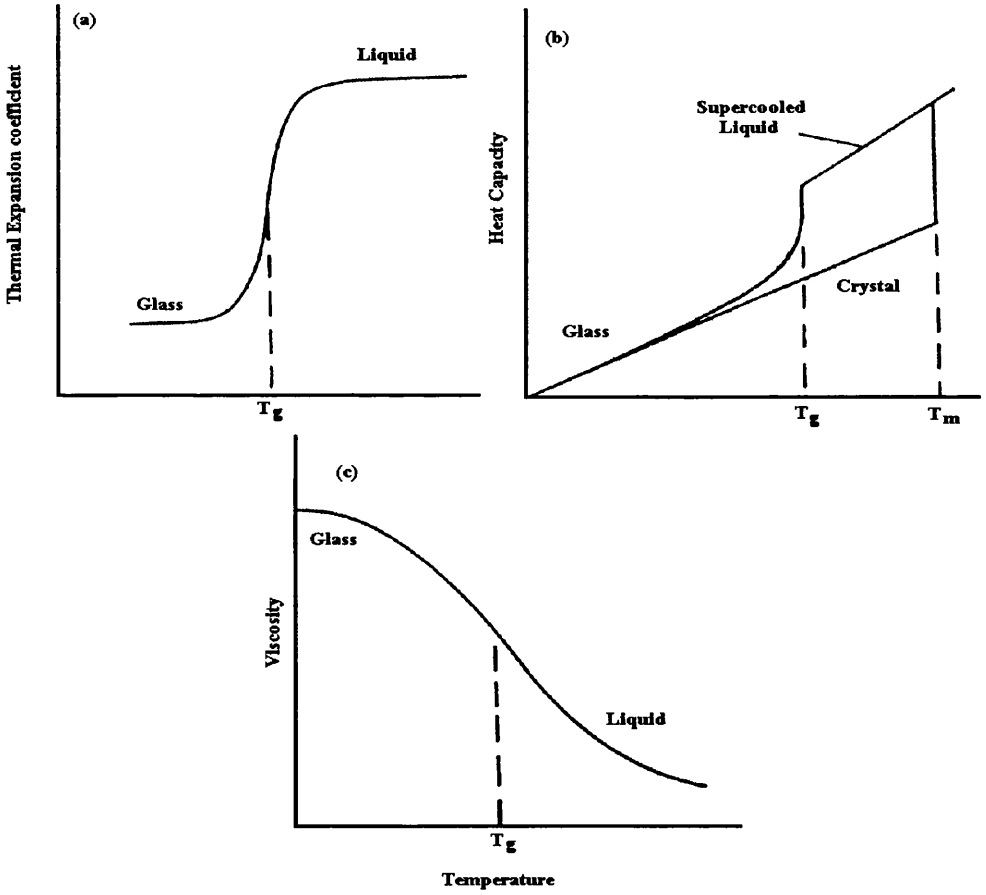

1.3.5 Structural Relaxation

From the above discussion the amorphous phase has been described as a non-equilibrium metastable state which if given the appropriate conditions revert to the stable (equilibrium) crystalline state. However even if crystallisation does not occur on an experimental time scale, amorphous solids will "relax" towards the equilibrium supercooled liquid state (the process is also referred to as aging) (Liu et al., 2002). As

structural relaxation is occurring and moving in the direction of the equilibrium state, energy along with free volume will gradually decrease (Fig 1.5). Structural order will increase due to relaxation and hence the configurational entropy will decrease. The energy dissipated from this process can be measured and is termed the enthalpy relaxation and the experiments carried out to measure this are referred to as aging experiments. The study of structural relaxation is becoming increasingly important simply because it is shown to occur due to molecular mobility which leads to degradation of the system. Hancock et al., (1995) were able to determine that molecular mobility can exist at 50K below the T_g by measuring the enthalpy relaxation.

Structural relaxation can be modelled to a multi-exponential decay from the amorphous state where the molecular configurations are frozen during the processing, towards the equilibrium state. Often the Kohlrausch-Williams-Watts (KWW) equation is used to represent the decay (equation 1.1). The two important factors in equation 1.1 are the constants τ which represents the mean molecular relaxation time and β which is defined as the stretch power, reflecting the distribution of independently relaxing states (Hancock and Zografi, 1997; Liu et al., 2002). There are variable factors that reflect the mean relaxation time, such as thermal history, moisture content, temperature effects and also the nature of the material (Liu et al., 2002).

$$\Phi(t) = \exp[-(t/\tau)^{\beta}] \qquad \text{.....equation 1.1}$$

1.3.6 Measuring the T_g

The T_g for single and binary components can be determined by a variety of methods, which expose the change in the physical properties when a material undergoes the glass transition event: calorimetric, thermomechanical, volumetric, and spectroscopic. Differential Scanning Calorimetry (DSC) has widely been reported to accurately determine the T_g (Hancock and Zografi, 1994; Kerc and Srcic, 1995). More recently the addition of modulated temperature differential scanning calorimetry (MTDSC), which is a highly sensitive version of the DSC has superseeded the use of DSC in this area of science (Haines, 2002). The T_g is recorded by a change in heat capacity, where four characteristic temperatures may be defined in the measurement, Fig 1.8 illustrates this.

Fig 1.8. The transitions of glass-forming material, which shows the onset temperature (T_f), midpoint temperature (T_{mid}), maximum anomalous endothermic peak temperature (T_m), and extrapolated end temperature (T_e) (adapted from Kerc, and Srcic, 1995).

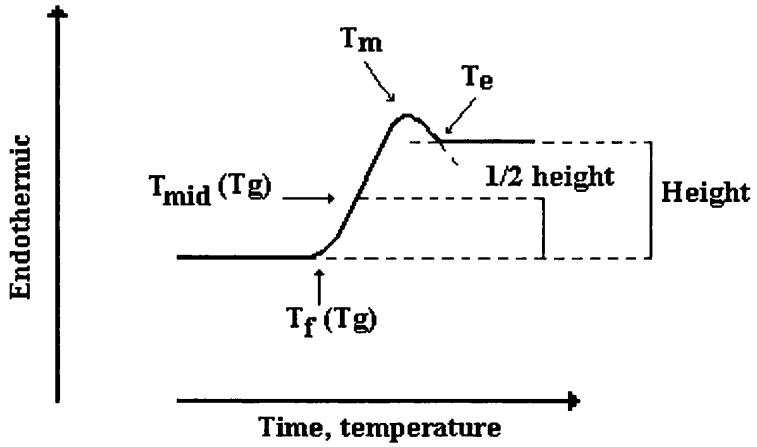

It is clear from Fig 1.8 that two T_g values can be reported in literature: the onset and midpoint. Usually one of these values is chosen by the author to be reported, but when a comparison is drawn it is important to note that the T_g is not a sharply defined point but can span over a 20°C region and so differences in observed values will arise.

The T_g of a binary blend can also be predicted theoretically using the Gordon-Taylor equation (Gordon and Taylor, 1952) as well as using analytical tools. The Gordon-Taylor equation was originally derived for polymers but can be applied to any pharmaceutical system. The equation assumes perfect volume additivity with no specific interaction between the components, the T_g can be calculated as:

$$T_{gmix} = \emptyset_1 T_{g1} + \emptyset_2 T_{g2} \qquad \text{.....equation 1.2}$$

where Ø represents the volume fraction and the subscripts represents the two components. This can then be rearranged for weight fractions (Hancock and Zografi, 1994) giving:

$$T_{gmix} = (w_1 T_{g1}) + (K w_2 T_{g2}) / (w_1 + (K w_2)) \qquad \text{.....equation 1.3}$$

where w_1 and w_2 represents the weight fractions of the components and K is a constant which can be calculated from the density (ρ) and Tg of each individual component.

$$K = (\rho_1 T_{g1}) / (\rho_2 T_{g2}) \qquad \text{.....equation 1.4}$$

The equation can be expanded to accommodate a system that have more than two components and has been used to predict the strength of intermolecular bonding that can occur in multi-component systems. The use of the Gordon-Taylor equation also facilitates the calculation of the quantity of water required to lower the T_g to room temperature and in doing so provides an indication of the stability of the system under various storage conditions. Generally a sharp glass transition event will be seen if the multi-component system is totally miscible, otherwise individual T_gs are seen (Hancock and Zografi, 1997; Nair et al., 2001).

1.4 Water-Solid Interactions of Amorphous and Crystalline States

Most pharmaceutical solids will contain residual water that arises from prolonged exposure to an atmosphere containing water vapour, or as a result of processing, such as spray drying, lyophilisation, or wet granulation (Ahlneck and Zografi, 1990). So the interaction of water with a pharmaceutical material is an important feature and depends on whether the material is either an amorphous or crystalline material.

A crystalline solid can interact with water in three different ways: adsorption of water vapour onto the solid-air interface, crystal hydrate formation and deliquescence. Water molecules can adsorb to the surface of a crystalline solid by hydrogen bonding and form a monolayer; subsequent layers (at most 2-3) may also form at higher relative humidities, which can all be reversed by a small increase in temperature or a decrease in the relative humidity (Thiel and Madey, 1987). Therefore the adsorption and desorption of water on a crystalline surface is a reversible process. The quantity of water, which may also be adsorbed, also depends on the available surface area and also the nature of surface of the solid. Water at room temperature shows little tendency to adsorb to non-polar surfaces relative to polar surfaces (Zografi, 1988). Generally adsorbed water does not threaten the stability of a crystalline solid, as the molecules do not have the form of bulk water. This however changes if condensation was to occur which would lead to instability (Buckton, 2000).

Amorphous regions have been described in literature as "active sites" within the material as they tend to be sensitive to moisture and hence lead to absorption of water vapour (Sebhatu et al., 1994). The amount of water absorbed is dependent on the total mass of amorphous material available. The effects of water on the amorphous solid have been discussed briefly where the term "plasticiser" has been used. Water is of a small molecular size and as a consequence can penetrate into an amorphous solid and increase

its free volume by reducing the hydrogen bonding between adjacent molecules (Levine and Slade, 1987; Zografi, 1988). As a result the T_g of the system is lowered (Fig 1.6) by an increase in the molecular mobility and the glass to liquid state is facilitated hence disrupting the stability of the system, this event is termed plasticisation. Other than lowering the T_g of a material, the absorbed water also promotes chemical degradation due to the increase in the molecular mobility and can also act as a chemical reactant where hydrolysis and oxidation occur (Ahlneck and Zografi, 1990).

1.5 The Collapsed State

The collapsed state is a phenomenon that occurs when an amorphous particulate system is on the path of crystallisation. An amorphous material will absorb water as a consequence the rubbery amorphous system is unable to support its weight under gravity with the excess water and so collapses resulting in flow of the glassy matrix. The causes of collapse have been listed as high residual water content, plasticisation and high storage temperature. All these factors are able to decrease the viscosity of the amorphous solid (White and Cakebread, 1966; To and Flink, 1978).

The collapsed phenomena can be observed by DSC and also visually. Once the T_g is surpassed and the viscosity of the system has dropped to the order of 10^6-10^7 Pa S, a temperature referred to as a softening or the sticky point (T_s) is observed. The material is then referred to in the collapsed state (Shalaev and Franks, 1995); visually the powder becomes sticky and agglomerates. To and Flink, (1978) provide a good interpretation of collapse as a visual result of the amorphous solid undergoing viscous flow when it takes on a liquid like property. Levine and Slade (1987) have also described that structural relaxation occurs within the rate defined by the Williams Landel-Ferry equation (1955) during the process of collapse.

Collapsed systems have different properties from pre-collapsed and crystalline states and varying degrees of structural collapse can be exhibited. Diffusion of the plasticising material, which in most cases is water, is very slow in comparison to a non-collapsed state. It is worth noting that the water content in a collapsed system is not freely available to the powder mass but localised to the collapsed region due to slow diffusion. Also the crystallisation of a collapsed material will occur at a lower temperature when induced by heat relative to an amorphous material. Crystallisation can also be promoted by reducing the relative humidity allowing more water to diffuse out of the structure and the solute molecules to come together to crystallise. A collapsed state upon crystallisation may also

vary the polymorphic ratio of the final product (Buckton and Darcy, 1996; Darcy and Buckton, 1997).

Therefore pre-collapsed and collapsed structures behave differently and will do so in pharmaceutical products. One problem that can be identified is the different drying rates, which an amorphous material will possess with a small region of a collapsed state. There are also varying degrees of structural collapse, which are more likely to posses varying drying rates. The vast amount of water, which is stored in the collapsed state although not freely available is also not bound, may have a detrimental effect on the final product that possesses such a state.

1.6 The Amorphous to Crystalline Phase Transition

A discussion of the crystalline and amorphous states in detail would not be complete if we did not explain about the amorphous to crystalline phase transition. Two major steps of this process have been described in detail in section 1.2.1 and 1.2.2 as nucleation and crystal growth. In this field early researchers Makower and Dye (1956) investigated the crystallisation of spray dried sucrose and glucose at different relative humidities. When inducing crystallisation the authors observed a lag or induction period followed by expulsion of water. The induction time was attributed to the formation of stable nuclei in order for propagation to follow. Microscopic studies looking at the expulsion of water described the progressive growth of crystals with respect to first order kinetics.

Other studies have followed (Jolley, 1970; Levine and Slade, 1987; Saleki-Gerhardt and Zografi, 1994) where the process of nucleation and propagation have been described under temperature induced conditions. Fig 1.9 summarises the temperature dependence of both nucleation and crystal growth and the overall effect of temperature on the rate of crystallisation and hence the crystallisation temperature (T_c), which occurs intermediate to T_g and T_m (the melting temperature).

Fig 1.9. A schematic representation of the crystallisation kinetics from the amorphous state above T_g and below T_m (adapted from Jolley, 1970).

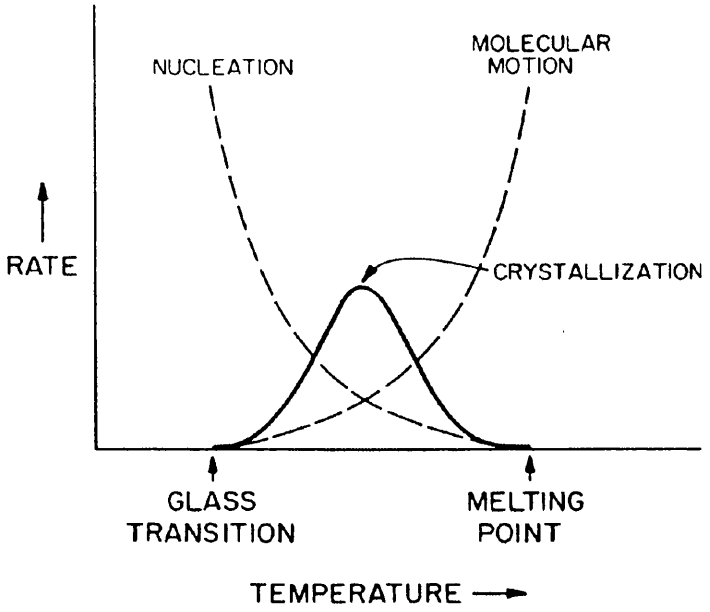

In fig 1.9 both nucleation and propagation rates are shown to have an exponential dependence on temperature. The rate of nucleation increases exponentially with a decrease in temperature to $T = T_g$ while the rate of propagation increases exponentially with an increase in temperature up to $T = T_m$. The rate of propagation is seen to increase with temperature as this step requires motion and hence a higher energy state which the elevating temperature provides. The nucleation rate is seen to increase with a decrease in temperature below T_m as supercooling increases, as there is a higher probability of finding the molecules in their lower energy states to form stable nuclei. However with such a decrease in temperature there is also an increase in viscosity that will affect molecular mobility and diffusion across the amorphous matrix. Therefore there is a balance in the loss of molecular motion and the increase in nucleation rate that leads to a maximum crystallisation rate at T_c that is intermediate of T_g and T_m for the above reasons (Jolley, 1970; Levine and Slade, 1987; Saleki-Gerhardt and Zografi, 1994).

1.6.1 Crystallisation Kinetics

The amorphous to crystalline phase transition can also be described using crystallisation kinetics where the process can be quantified and compared for different materials. Recently several scientists (Roos and Karel, 1992; Arvanitoyannis and Blanshard, 1994; Mazzobre et al., 2001) have used more than one model to quantify the phase transition

with the aim of understanding the crystallisation process under different experimental conditions and additives. A few models will be mentioned here starting with the Williams-Landel-Ferry equation (Williams et al., 1955). This was initially developed to look at the kinetics of molecular relaxation processes that will occur on a practical time frame between the T_g and T_m. The equation has been used to describe the temperature dependence of viscosity for amorphous materials through the relationship between relaxation time processes and free volume. The justification for the use of this equation to describe the crystallisation kinetics is based on the reasoning that crystallisation depends on the viscosity of the sample (Roos and Karel, 1992).

Another model that is used to describe crystallisation kinetics is the Vogel-Tammann-Fulcher model (VTF). This is similar to WLF equation, where the temperature dependence of the molecular motions in terms of relaxation times is represented exponentially (Hancock et al., 1997; Mazzobre et al., 2001). The equation has also been shown to describe the ranking of amorphous material in terms of strength and fragility (Angell, 1995). The Avrami equation (Avrami, 1940), which will be described in a subsequent chapter, is another model where the nucleation rate alongside the crystallisation half time is determined for a crystallising material.

1.7 Characterisation, Detection and Quantification of Amorphous and Crystalline Content

The importance of an amorphous material and the degree of crystallinity has been explained and therefore the detection, along with identification and in some cases quantification is of great importance. Characterising the state of a material uses a number of techniques that have long been established. In a review by Brittain et al., (1991) analytical techniques are grouped under the headings of particulate, molecular and bulk level. Powder X-ray diffraction (PXRD) is a favoured technique in identifying whether a material is either crystalline or amorphous. An amorphous and crystalline material can be detected directly and indirectly by two ways: The degree of order and the degree of disorder, both are generally interrelated. However it has been reported in literature that different techniques are more sensitive to different characteristics of the solid (Saleki-Gerhardt et al., 1994; Sebhatu et al., 1994). The degree of crystallinity relates to the degree of order and techniques often used to measure this reflect the direct average measurement throughout the bulk of the solid. PXRD (Black and Lovering, 1977), density (Duncan-Hewitt and Grant, 1986), infrared (IR) (Black and Lovering, 1977) and

solid state NMR spectroscopy (Hancock and Zografi, 1997) all assess the material by looking at the average degree of order directly detected by the measurement. Therefore they can indirectly assess the material for amorphous content although they present a limited capability when measuring small amounts of disorder. The limit of detection can vary with each technique; PXRD has been quoted to have a detection limit of 10% w/w amorphous content along with density measurements (Saleki-Gerhardt et al., 1994).

Techniques that are sensitive in measuring the degree of disorder and hence the higher state of energy are usually employed to detect low levels of amorphous content. The thermal techniques: Isothermal microcalorimetry and solution calorimetry are well established for this purpose. The heat evolved from crystallisation of an amorphous material is used to quantify and assess the degree of disorder in an amorphous system. The techniques also have a detection limit, differential scanning calorimetry (DSC) like PXRD has been quoted to have a detectation limit of 10% w/w (Saleki-Gerhardt et al., 1994) but isothermal microcalorimetry is far superior and can detect an amorphous content as low as 0.5% w/w (Buckton et al., 1995; Mackin et al., 2002). Water vapour sorption studies also have the ability to quantify the amorphous content of a sample with a detection limit of approximately 0.5-1% w/w (Saleki-Gerhardt et al., 1994; Hogan and Buckton, 2001; Mackin et al., 2002) using very sensitive balances. Recently near infrared spectroscopy has been added to the list for the detection of low amorphous content (approx. 1%, Hogan and Buckton, 2001). The use of solution calorimetry in the quantification of low levels of amorphous content ranging from 0-10% w/w have also been reported (Hogan and Buckton, 2000).

1.8 Summary

From this chapter we can see that there are many areas which are associated with the amorphous and crystalline state. Theses areas have been and continue to be researched as they are fundamental in understanding and predicting the behaviour of the material. An amorphous sample is usually the preferred form with advantages for pharmaceutical bioavailability. However the problem of maintaining the amorphous form will always be at the forefront of pharmaceutics. New research into molecular movement and relaxation will help explain and improve our understanding as well as the phase transition between the amorphous and crystalline state. The study of multi-component systems also helps to define factors which effect the amorphous and crystalline phase. Much information has been documented as has been demonstrated in this chapter, but as a result there are always new questions and hypothesis which necessitate further research.

Chapter Two

Experimental Techniques And Method

2.1 Introduction

A number of techniques have been established in the characterisation of materials over the years that provide accurate results on the state of a sample and quantification of its experimental parameters. Classic techniques such as differential scanning calorimetry (DSC), thermogravimetric analysis (TGA) and Fourier transform infrared spectroscopy (FTIR) have been tried, tested and have also formed the basis for new techniques. With the increased use of sophisticated computer software there is an increase in the speed of data generation and analysis. However most systems do remain operator dependent and there are wide variations in the way the software is used to understand and analyse the data. There is also a need to standardise data analysis so that comparisons can be drawn for identical instruments. In the course of this thesis, the method of analysis adopted has been consistent. Non-thermal, thermal and gravimetric studies have been employed throughout. The use of an innovative hyphenated technique has also been highlighted along with more established and readily available analytical tools. All have been used in conjunction to characterise the spray dried (SD) and physical mix (PM) products on a molecular and particulate level.

2.2 Spray drying

2.2.1 Introduction

Rapid precipitation from solution or suspension via spray drying has been described in section 1.3 (chapter one) as one of the paths leading to the production of amorphous material and has been the chosen technique for this project. Spray drying is a member of the suspended particle processing systems (SPP), were particles are dried whilst suspended in air. The mechanism of spray drying is to convert a solution, suspension, emulsion or paste into a dry particulate system in a one step process. This system is widely used in the chemical, ceramic, food and pharmaceutical industry. In the latter two industries it has been used to convert crystalline material to an amorphous state. It is also used for micro encapsulation, where a liquid/solid product is embedded in a mixture of solids.

The spray drying process is essentially composed of four stages: atomisation of feed which occurs in the atomiser, spray-air contact which takes place in or outside the atomiser depending on the type used, drying of spray which occurs in the drying

chamber, separation of dry product from air which happens in the cyclone. A schematic diagram shown in Fig 2.1 summarises the four basic stages of spray drying. Each process is subject to many variable factors that need to be controlled or optimised so that the desired or ideal product is produced (Masters, 1990).

Fig. 2.1. A schematic diagram of the four basic stages of spray drying.

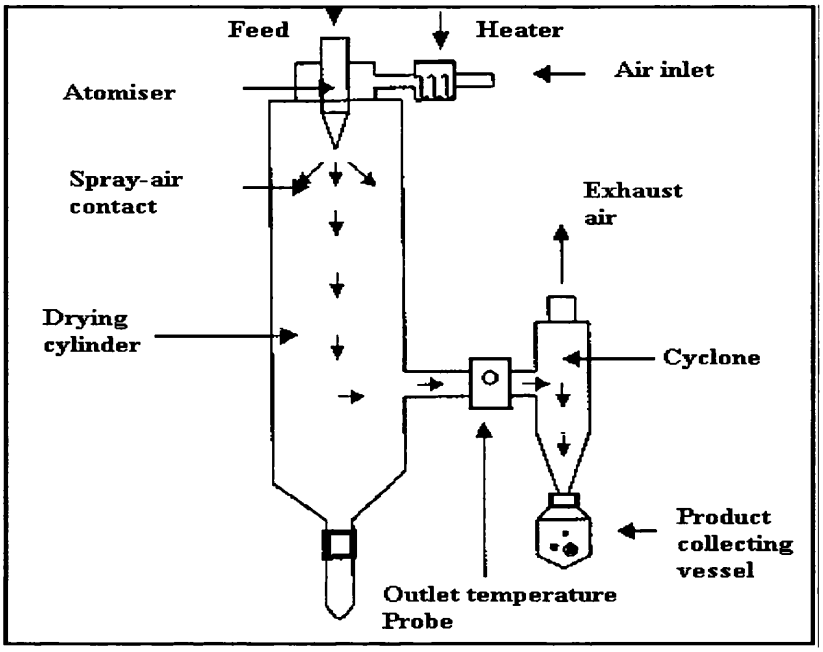

Atomisation of feed; Atomisation is the initial critical stage where the aim is to convert a fluid feed material into a spray that will eventually pass into the drying chamber. Hence the definition of atomisation is the liquid break up into the individual droplets forming a spray. The fluid feed can be a solution, suspension or paste, which once subjected to the spray drying process will lead to powder, granules, or agglomerates respectively (Masters, 1990; Coulson and Richardson, 1991).

Spray - air contact; The second stage of spray drying is defined as spray-air contact, this describes the number of ways by which the air can be drawn from the atmosphere and heated to dry the atomised droplets. The importance of spray-air contact will influence droplet behaviour during the third stage of drying (Masters, 1990: Broadhead et al, 1992).

Drying; Drying is the third stage of the process and essentially is the removal of solvents from the spray. It consists of simultaneous heat and mass transfer between atomised droplets and drying air. The drying of the product along with other factors will finally

dictate the powder properties of a material such as particle size distribution, moisture content, density, and particle strength.

Separation of powder and air (Product recovery); The final stage of the spray drying operation is the separation of the powder from the drying air. The product may be separated from the air either by cyclonic airflow, which takes place in the cyclone after leaving the drying chamber, or by the ability of the particles to fall out of the airflow to a flat chamber base (Masters, 1990).

2.2.2 Spray drying Experimental Parameters and Powder Properties.

The experimental conditions of the spray drying process are important in determining the powder properties. These experimental parameters are the inlet and outlet temperature, the aspirator setting, the spray flow rate and the feed rate. The aspirator setting and the spray flow rate govern the two types of airflow within the spray dryer. The spray flow rate is provided by the compressed air, which is attached to the spray dryer to break up the liquid jet into fine droplets (atomisation). The aspirator governs the airflow rate, which sucks in air from the atmosphere; this is then heated by resistance and enters the drying chamber. This drives the particles into the cyclone separates and enters out into the open air if the spray dryer is an open cycle system. Closed cycle systems operate when organic solvents are used, the air is replaced by inert gas usually nitrogen and is continuously recirculated (Masters, 1990).

All the experimental parameters are interdependent; therefore an operator cannot alter one experimental parameter without altering the other if the same physical properties of the powder are to be maintained. This proves to be advantageous to the operator as the final powder characteristics are controllable. The powder properties affected by experimental design provided that each experimental parameter is altered alternatively are described in this section.

Particle size: The spray flow rate can alter the particle size; by increasing this parameter we produce a small particle size or a mean particle size that is small. The spray flow rate has been described above as the air that breaks up the liquid jet so therefore we would expect a change in particle size to be seen. The feed rate will also have an effect on particle size, if this parameter is increased alone, the high velocity air which is controlled by the spray flow rate is not enough to penetrate the liquid jet and a large mean particle size is obtained (Masters, 1990).

Residual Moisture Content of product: This is affected by the aspirator setting which if increased will increase the airflow rate within the open cycle system. As a result this decreases the residence time in the drying chamber of particles which leads to an increase in residual moisture content of the material. An increase in the feed rate also increases the residual moisture content, as the particles produced will be relatively large and concentrated in solvent to undergo sufficient drying. Maintaining the outlet temperature within a narrow range will produce a product of constant moisture content (Masters, 1990).

Surface morphology: Drying the material has an effect on the particle size and structure of the particles. The inlet temperature of the spray dryer controls drying, therefore by increasing the inlet temperature you increase the evaporation rates at the surface of the material you are spray drying. High initial drying rates will lead to larger particles with thin shells and low density. Low initial drying rates will lead to smaller particles with thick shells and high density. The types of particles produced on spray drying are shown in a schematic diagram in Fig 2.2 (Masters, 1990; Oakley, 1997).

Fig 2.2. A schematic diagram of the types of particles produced during spray drying (adapted from Oakley, 1997).

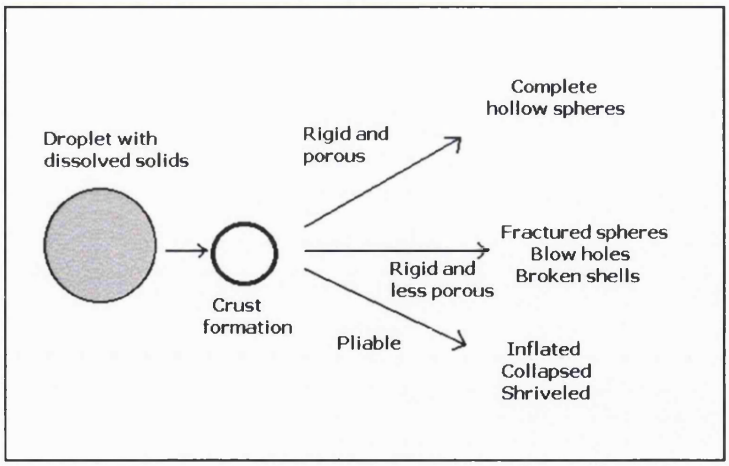

Bulk density: An increase in inlet temperature has been shown to produce a powder that is porous and fragmented; this then leads to a material that possess a low bulk density. An increase in the feed rate may increase the bulk density of a material as the particles produced may be large dense particles or coarse depending on the nature of the material (Masters, 1990).

The degree of disorder: This has been shown to alter the percentage of amorphous material. Kawashima et al., (1983) prepared a pyrabarbital complex, which showed a greater degree of amorphous content when the fluid feed material was dried at a temperature of 145 °C as opposed to 85 °C. This was attributed to the rapid evaporation rates that occur at higher temperatures. It has also been cited that the type of atomiser may also affect the amorphous content.

2.2.2 Instrumentation

Spray drying on a laboratory scale is employed using a variety of instruments in this case the Buchi-190 mini spray dryer was used. The instrument consists of a pneumatic atomiser and uses co-current air to dry the material, which is suitable for heat sensitive material. The SD product is recovered by cyclonic separation into a collecting vessel.

2.2.3 Experimental Method

The spray drying parameters were established from a previous study (Chidavaenzi, 1999) and they have been maintained through out the course of this thesis. The pump rate and heating dial are varied accordingly to maintain the outlet and inlet readings at the desired temperatures respectively. At the end of the procedure the material is immediately collected, weighed and stored at 0 % RH (P_2O_5) in a desiccator.

Table 2.1. Operating parameters for the preparation of spray products using a Buchi-190 mini spray dryer.

Operating parameters	Conditions.
Inlet temperature (°C)	185 -190 °C
Outlet temperature (°C)	85-90 °C
Atomiser airflow rate (normliter/hr).	400
Aspirator (dial setting)	12
Heating (dial setting)	10-12
Pump (ml/min)	varied

2.3 Isothermal Microcalorimetry

2.3.1 Introduction

Microcalorimetry may be used to study and quantify small degrees of heat change for any physical or chemical process. The heat evolved or absorbed during a reaction is recorded as a function of time; the results are then presented as power (dq /dt or W) versus time (t in s). In this study microcalorimetry was employed to characterise and quantify the amorphous content of the samples. The onsets of crystallisation as well as the crystallisation kinetics were also determined using this technique.

The advantages of the system are simple in that it is non-invasive and non-destructive and does not rely on sample form, therefore the material may be solid, liquid, or gas (Buckton and Beezer, 1991). The sensitivity of the equipment is also well documented, and as the name suggests detects enthalpy changes as small as 10^{-6}°C. Applications of the technique are numerous from biological studies to drug targeting and have been reviewed by Buckton and Beezer (1991); Buckton (1995); and Phipps and Mackin (2000).

2.3.2 Instrumentation

In isothermal microcalorimetry, the heat flow or the heat leakage principle is used. Any heat produced or absorbed by a sample is ideally, completely exchanged with a surrounding heat sink. A Thermal Activity Monitor (TAM, Thermometric 2277 AB, Sweden) was utilised where the heat sink is a 25 litre water thermostat and is maintained at a constant temperature. This provides a sensitive environment where the water thermostat is maintained at $\pm$ 2 $\times$ 10^{-4} °C within a temperature range of 5–80°C (TAM manual). When a thermal energy change occurs in the sample, a temperature difference is created relative to the heat sink, in order to maintain isothermal conditions heat is forced to flow, either to or from the heat sink. The magnitude of the heat flow is directly proportional to the temperature difference created as a consequence of the thermal event. Very sensitive thermopiles are placed around the sample and are used to measure and quantify the heat flow. The potential generated by the thermopiles is then amplified and recorded as heat flow (power) as a function of time. Fig 2.3 illustrates this principle (TAM manual).

Fig 2.3. The Operating principles of the TAM (Thermometric 2277).

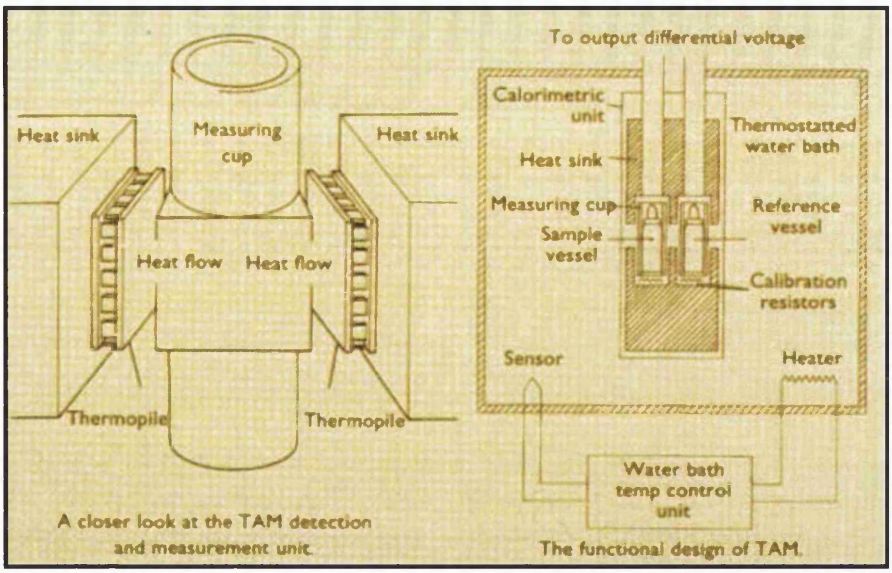

The TAM consists of four channels, which allow four different experiments to run concurrently. Each channel consists of a sample and reference side, accepting steel ampoules (5ml capacity) and glass ampoules (3ml capacity). Different ampoules are used with regards to the experimental set up employed. Fig 2.4 represents a diagram of a TAM.

Fig 2.4. A diagram of a TAM (Thermometric 2277).

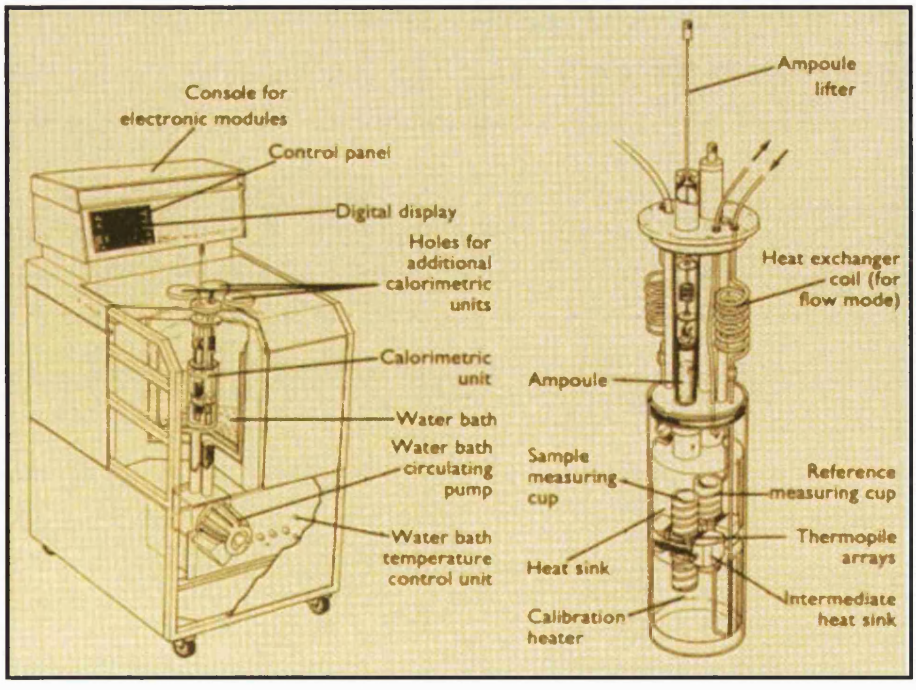

2.3.3 Calibration

An electrical calibration is required if experimental conditions are changed, a power-off condition has occurred, or once every fortnight as standard practice. The exact experimental conditions are applied and an accurate known power level is supplied to the channel via an electrical resistor that is located in the measuring cup. Ampoules (3 ml capacity) were used in all of the experiments. Mini hydrostats containing the salt solution sodium chloride, which generated a relative humidity (RH) of 75%, were sealed within the ampoule by crimping a rubber and aluminium seal. The ampoules were placed at equilibration position and monitored for a baseline, once this was stable indicating that equilibration had been acheived the ampoules were lowered into the measuring cups. Once the system had stabilised again, the baseline was adjusted using the zeroing dial to 0.000 ± 0.1 μW. At this point the calibration is turned on via computer software and a specific amount of current is supplied to the calibration resistor. A known amount of thermal heat was dissipated and this was recorded as an exothermic peak by Digitiam 4.1 for Windows software. All the experimental calibrations were conducted at 3000μW unless otherwise stated in the subsequent chapters and sections.

2.3.4 Experimental Method

Ampoule experiments were employed to assess the amorphous content of a material at 75% RH. The experiment was carried out in an identical way to the calibration method except 30mg of powder was added to an ampoule and placed in the sample channel. Equilibration of the ampoules was usually achieved within 30 mins prior to lowering the ampoules into the measuring cups. All experiments were carried out at 25.0°C.

2.4. Differential Scanning Calorimetry (DSC)

2.4.1 Introduction

Differential Scanning Calorimetry (DSC) is currently the most widely used thermal analysis technique in pharmaceutics. The advantages and uses of the DSC are reasons why it is a favoured technique. Small sample size "as received" along with rapidity of which the experiment can be carried out aids the popularity of this technique. Applications of DSC include qualitative studies such as identification of unknown samples as well as polymorphic forms and the study of phase diagrams in

pharmaceuticals have proved valuable. Quantitative data can also be obtained with enthalpies of crystallisation, fusion, and heat capacities being recorded. Recently the determination of chemical kinetics has been added to the list of quantitative measurements, which has all been possible with new computerised software allowing data to become more manageable (Haines, 2002). In this study DSC has been employed to characterise the physical state of the SD and PM products and also to detect the different anomeric forms of lactose.

2.4.2 Instrumentation

The term differential relates to an important feature of the technique, two identical measuring sensors are used corresponding to sample and reference site. The difference between the responses of the two sensors provides the signal that represents the thermal change to be studied. Scanning relates to method of operation and calorimetry is defined as the measurement of heat. Power compensation DSC-7 (Perkin Elmer instruments, UK) was employed where the instrument's principle is similar to that of isothermal microcalormetry. The DSC-7 consists of sample and reference pans, which are placed in two identical micro furnaces, these are embedded in an aluminium block which represents a heat sink. Each micro furnace contains 2 identical platinum resistance elements, one provides the furnace with power (heat) and the other is a sensor, which detects the change in the temperature of the furnace. The platinum ring as shown in fig 2.5 is distributed over the full area of the furnace and so provides a full monitoring of temperature and heat at all points along the sample and reference pans.

Fig 2.5. The functional principle of power compensation DSC, (Perkin Elmer, DSC-7)

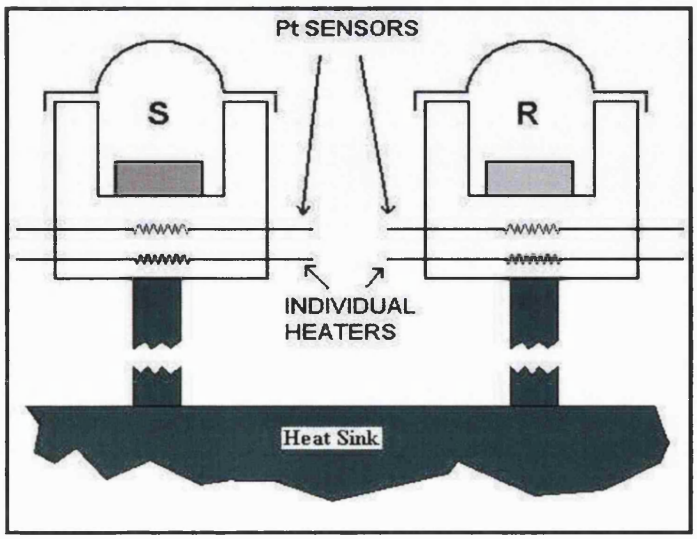

The heat sink is held isothermally below the temperature range of the experiment to ensure effective dissipation of heat from the micro furnace to the aluminium block. The design of two micro furnaces along with two separate heaters is based on the thermal null principle. When there is no physical and chemical change occurring in the sample, there is no temperature difference between the sample and the reference pan. However, when a phase transition takes place, heat is either taken in or dissipated. The sensors detect this and suppress the temperature rise or fall by providing the correct amount of heat to maintain a thermal null. This is directly proportional to energy change of the system and is read by computer software as a signal (Haines, 2002). In this case the instrument is operated by Pyris software for Windows, version 3.81 (provided by Perkin Elmer Instruments, UK).

2.4.3 Calibration

Calibration checks were conducted daily or if the experimental conditions were changed or after the instrument has been turned off. This was achieved by using high purity standard materials, indium and zinc. A sample pan holding either indium or zinc was placed in the sample holder alongside a reference pan that is empty. Aluminium pans and lids (Perkin Elmer) were crimped and non-hermatically sealed. The scanning rate used to calibrate the reference materials were identical to that of the experiment at 10°C/ min and all experiments were conducted under a nitrogen flow rate of 20-30 psi. The temperatures and enthalpy that the metals were calibrated against are shown in table 2.2.

Table 2.2. The onset temperatures and enthalpy of fusion for indium and zinc respectively.

Reference Material	Onset temp. (°C)	Enthalpy of fusion (J/g)
Indium	156.60	28.45
Zinc	419.47	---

2.4.4 Experimental Method

Sample masses of 3-5mg were loaded in aluminium pans and were non-hermatically sealed in an identical way to the calibrants. A temperature range of 40-270°C was set, with a ramp rate of 10°C/min. All other conditions were identical to that of the calibration.

2.5. Step Scan DSC

2.5.1 Introduction

Modulated Temperature Differential Scanning Calorimetry (MTDSC) has been represented as a revolution in thermal analysis in the same way as power compensation DSC was once described. MTDSC is an extension of the original DSC technique in which a regular modulation is superimposed onto the linear temperature change hence the name modulated temperature. In the original form of the technique introduced in 1993 the modulation was sinusoidal since then various manufacturers have developed different modulations in which the step scan method is one of them. The advantages of the system are an increased sensitivity and resolution as well as the ability to separate thermal events (Haines, 2002). One of the major uses of MTDSC is in the study of glass transition temperatures that are often masked by other thermal events using conventional DSC.

Step Scan DSC is very similar to MTDSC in that thermal events of a material can be separated and enhanced characterisation of physical properties of samples can be achieved. The method does not apply a sinusoidal modulation but rather a series of heat-hold steps, which produces results that are very similar to MTDSC. The method is straightforward, accurate and free of experimental problems such as gradients, sine wave distortions or phase lag. It is also able to provide a direct measurement of heat capacity and no Fourier transform or deconvolution is needed (Sichina, technical note). The employment of step scan DSC was to determine the T_g of the binary SD products that were investigated.

2.5.2 Instrumentation

Step Scan DSC requires a DSC instrument with a very high resolution and responsiveness and is only functional with the power compensated Pyris 1 DSC supplied by Perkin Elmer. The outline of the instrument is very similar to that of the DSC 7, which has been described in section 2.4.2.

2.5.3 Calibration

Calibration is conducted prior to the experimental run and if the following conditions were altered: a change in experimental conditions, nitrogen flow or if the instrument had

been switched off. The calibration is identical to that of DSC-7 using indium and zinc. A furnace calibration is also conducted which is carried out by the computer software (Pyris software for Windows, version 3.81). Once again the calibration was conducted at a scanning rate identical to the experimental run, which in this case is 2.5°C/min and under a nitrogen flow rate of 20-30psi.

2.5.4 Experimental Method

A number of cycles are required in order to establish the true Tg of a material. By exposing the sample to a heating cycle followed a cooling period, which was then followed by another heating method it is believed that the thermal history of the material is erased and that a true representation of Tg will emerge. This method also removes any absorbed moisture within the sample with the aid of non-hermatically sealed pans.

The experimental method was first established at a ramp rate of 2.5°C/min along with an isothermal hold time of 0.4 min (24 seconds). This particular section was repeated until the desired minimum or maximum temperature was reached. Once this cycle was complete the cooling cycle commenced at the same ramp rate and isothermal hold time to the minimum desired temperature that was usually the starting experimental temperature. This was then followed by the previous heating cycle. Unless otherwise stated the temperature range employed was 40-150°C. Samples of approximately 10-12 mg were placed in aluminium pans identical to those used for DSC and were non-hermatically sealed. The pan is flattened by a spatula to aid contact between the sample pan and furnace. A thermograph representing step scan data is shown in Fig 2.6.

Fig 2.6. Step scan DSC showing repetitive heat-hold segments.

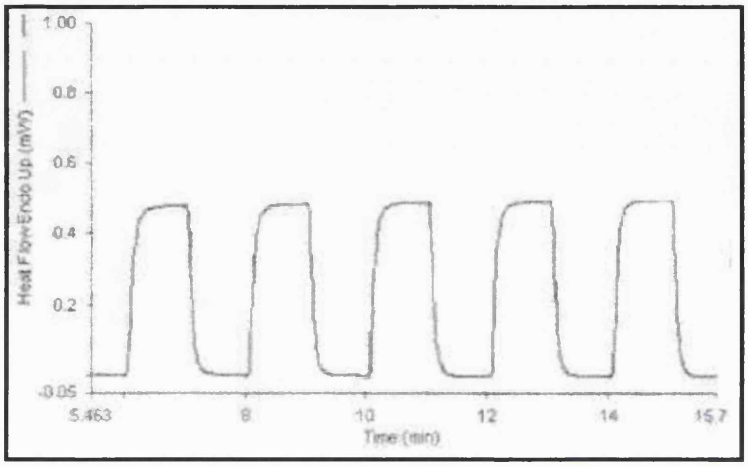

2.6 Thermogravimetric Analysis (TGA)

2.6.1 Introduction

Thermogravimetric analysis is a technique in which the mass change of a substance is measured as a function of temperature whilst the sample is subjected to a controlled temperature programme (Haines, 2002). Mass loss is only seen when a volatile component diffuses out of the system, this could be a solvent absorbed or bound to the chemical structure. The temperature at which the solvent is lost gives the operator an indication of type of solvent-sample bonding and percentage that is present. For example water removed from a sample below 100 °C is defined as absorbed or "free" water (Darcy and Buckton, 1997) and that which is removed above this temperature is more likely to be bound to the internal structure. Suffice to say that the major use of TGA is the quantitative determination of moisture content as has been in this study.

2.6.2 Instrumentation

The most important features of the instrument are the furnace and balance hence the name thermobalance. A 2950 Thermogravimetric analyser (TA instruments,) was employed which was based on the null deflection system. Any mass loss detected from the sample pan causes a movement of the balance beam from its null position, this is sensed and a restoring force is applied to return the beam to its null position. The TA instrument applies this principle via the use of two light emitting photodiodes.

The instrument comprises of a thermobalance, furnace and a computer using TGA software (TGA Autoanalysis, version 1.0). The microbalance consists of a small flag on top of the balance, which blocks light (emitted from an infrared LED) from reaching the photodiodes. If there is a weight change in the sample pan, which is connected to the microbalance via a kapton loop and hangdown wire, the position of the balance beam and flag are displaced from their original position. This causes an unequal amount of light to reach the two photodiodes that is detected as an unbalanced signal and is nulled by control circuitory. This causes movement to bring the balance arm to the null position. The consequent change in current is proportional to the mass change and is recorded by the TGA software as a weight change. A purge of nitrogen is needed through out the course of the experimental run. There are two flows rates, which were used at 60cc/min through the purge inlet and 40cc/min through the balance inlet. The purpose of this was to

eliminate any decomposition products or evolved gases out of the furnace using the large flow of gas and also the balance chamber using the small flow of gas. A thermocouple is also positioned ~ 2mm above the sample pan and is used to monitor the environmental temperature (TA instruments manual). A diagram of the TA instrument used is shown in Fig 2.7.

Fig 2.7. A diagram of the TA instrument used in this study.

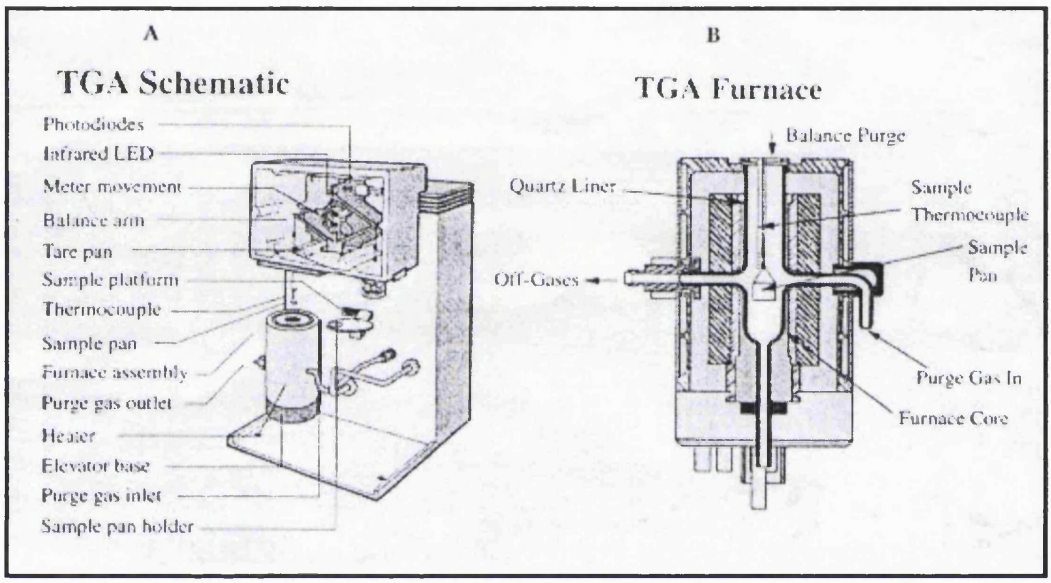

2.6.3 Calibration

Calibration is based on two important features of the instrument, the weight and the temperature. Weight calibration is preformed once a month using 100mg and 1g standards. Temperature calibration is undertaken if one of the following is changed: heating rate, purge gas and flow rate and/or if thermocouple is repositioned. An indium standard is used to calibrate the thermocouple at 156.6°C.

2.6.4 Experimental Method

The experiments were conducted under a nitrogen atmosphere, using aluminium pans (Perkin-Elmer) as crucibles. A sample weight of 5-10 mg was loaded for all experimental runs and a ramp rate of 10°C/min from 25-250°C was used to scan the samples.

2.7 Fourier Transform Infrared Spectroscopy (FTIR)

2.7.1 Introduction

Infrared spectroscopy is an established analytical tool in the study of molecular properties. The technique has been described as a powerful method for the study of pharmaceutical solids and provides high quality spectra, which is diagnostic for compounds (Brittain et al., 1991).

The infrared region lies between the visible and microwave region of the electromagnetic spectrum, absorbing radiation in the range of 5×10^6- 700 nm. The region can be divided into far, middle and near infrared depending on the transitions that arise when characteristic wavelengths are absorbed by the molecules (table 2.3). Samples subjected to infrared radiation absorb definite quanta of energy leading to molecular vibrations and rotational motions of the atoms within the molecules. This energy can be quantified by the following equation.

$$\Delta E = h\upsilon = E_1 - E_2 \qquad \text{equation 2.1}$$

Where h is Planck's constant and υ is the frequency of radiation. This transition undergone by the sample can be related to wavelength and hence spectral terms by the following relationship, where c is the speed of light.

$$\lambda = c / \upsilon \qquad \text{equation 2.2}$$

Table 2.3. The divisions of the infrared region along with their properties (adapted from Osborne et al., 1993).

Region	Characteristic transitions	Wavelength range (nm)	Wavenumber range (cm^{-1})
Near infrared (NIR)	Overtones combinations	700-2500	14 300 - 4000
Middle infrared (IR)	Fundamental vibrations	2500-5×10^4	4000-200
Far infrared	Rotations	5×10^4 - 10^6	200-10

2.7.2 Instrumentation

IR spectrometers consist of two basic components: an optical bench and a computer with the appropriate software. The optical bench measures the intensity of a specially encoded infrared beam after it has passed through a sample. The resulting signal (called an interferogram) contains information about all the frequencies present in the beam. The computer reads the interferogram and uses Fourier transform to decode the information and presents the spectra.

The IR source emits radiation at frequencies of interest, which is reflected via a mirror into an interferometer, here spectral encoding takes place. Once this is complete the encoded beam is deflected by a mirror and directed onto the sample. Here the encoded beam interacts with the sample where certain frequencies may be fully or partially absorbed. As a result a weak beam emerges which is deflected by a mirror into the detector. To increase the intensity of the beam a laser, which is inert and of single frequency follows an identical path to that of the beam to strengthen the interferogram. The detector feeds the result to the computer, which then decodes the interferogram using Fourier transform (Fig 2.8).

Fig 2.8. A schematic representation of FTIR.

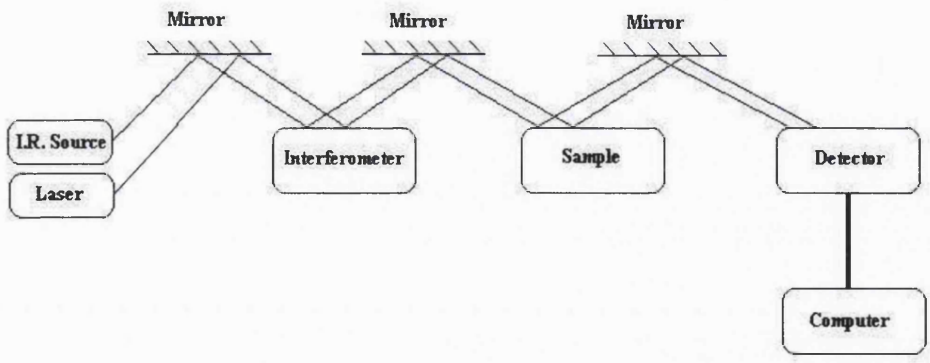

The optical bench was a Nicolet Avatar 360, which was connected to the computer using EZ OMNIC (version 5.0) software. An average of 32 scans were taken, where each scan took one second to be recorded. The result was then presented as wavenumber (cm^{-1}) versus absorption (Nicolet Avatar manual).

2.7.3 Experimental Method

Initially before the first experiment of the day and every 15 minutes thereafter, a background reading was taken. The instrument was operated in an identical manner on collecting a reference spectrum but with no sample with the aim of subtracting the spectrum from the sample spectra. The sample was then placed on a crystal plate in the path of the encoded beam and pressed down by the head of a metallic rod. The computer was directed to take an interferogram via the optical bench. The sample is then removed using a wooden rod and the mirror cleaned using acetone.

2.8 Dynamic Vapour Sorption – Near Infrared Spectroscopy (DVS-NIRS)

2.8.1 Introduction

Dynamic Vapour Sorption (DVS) as the name suggests is a gravmetric technique, which measures the sorption/desorption of a solvent to a powder. The change in weight when the solvent probes the powder or is removed is measured by a microbalance of which reference and sample pans are hung from either side. The instrument is enclosed in an incubator in which the relative humidity and temperature are controlled providing greater accuracy to the data collected. Water sorption has been used to study the amorphous form in single and binary systems (Buckton and Darcy, 1995a; Stubberud and Forbes, 1998) as well as in the use of quantifying amorphous content (Hogan and Buckton, 2001). Advantages of the system pertain to the accuracy of the sensitive microbalance and the accurately controlled incubator.

Until recently the employment of NIRS has predominately been in the analysis of food substances. This is surprising especially when you consider the advantages of NIRS as a non-invasive, rapid, simple analytical tool that requires no sample preparation. The technique provides us with a vast amount of physical and chemical information by recording absorption of overtones and combinations, which derive from fundamental molecular vibrations occurring from the mid-infrared region, hence the name near infrared. NIRS measures the overtones and combinations of the molecules vibrational modes principally those involving hydrogen. As a direct consequence NIRS is particularly useful for the study of hydrogen bonding and is therefore exploited in the study of the state of water in a system (Osborne et al., 1993).

The use of NIR in pharmaceutical sciences is in its infancy stage with researchers trying to overcome the disadvantages of the technique, which are mainly associated with transferability of data. Nevertheless the uses of NIR broadly include the study of polymorphic material (Aldridge et al., 1996), mutarotation of samples (Buckton et al., 1998), quantification of amorphous content (Hogan and Buckton, 2001). Other common applications include the identification of raw materials, and quality control (Yoon et al., 1998). The hyphenation of DVS and NIRS is a unique combination, which has been validated (Lane and Buckton, 2000) to show that adaptation of both techniques has not altered the performance of the instruments.

2.8.2 Instrumentation

A schematic representation of the DVS is shown in Fig 2.9. The instrument used is a DVS-1 apparatus provided by Surface Measurement Systems (SMS) which consists of a sensitive Cahn D-200 microbalance, which is capable of measuring changes in sample mass to 1 ± 10^{-4} mg. The sample and reference pans, which are glass quartz are located on opposite sides and are attached to the microbalance by hang down wires. When the pans are not in use by the operator they are completely sealed from the environment by two parts of glass tubing that are held together by a metal clip. Accessing the pans simply takes place by lowering the lower portion of tubing. The lower part of the glass tubing also has a secondary shoulder on either side which houses the temperature and humidity probe and in the case of the sample pan there is also an NIR probe attached directly under the pan.

A mixture of nitrogen and dry air is used to provide the desired relative humidity via two mass flow controllers and a solvent vapour controller, which essentially is a liquid reservoir of experimental choice. One mass controller solely provides 0% RH by delivering dry nitrogen only and the other controller provides the operator 100% RH by pumping nitrogen through a stainless steel tube into the reservoir containing the liquid probe in this case water. The two mass controllers are then used in combination to provide the desired RH. The incubator temperature can range from 0-80°C (SMS). The instrument was computer controlled (DVS-1 software, SMS) allowing for programming of experimental runs and the choice of sorption/desorption ramp or step cycles depending on the operator.

Fig 2.9. A schematic representation of the DVS-NIR instrument used.

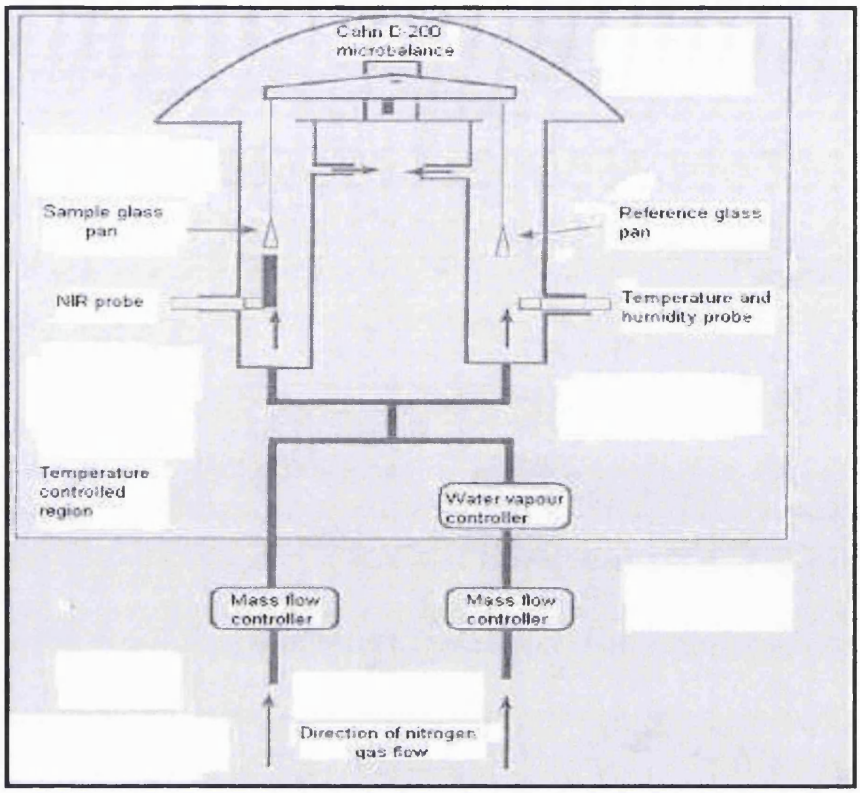

The specially adapted fibre optic reflectance NIR probe (FOSS NIRSystems) is attached approximately 4mm below the DVS sample pan. Diffuse reflectance is recorded and the reciprocal of this parameter is plotted to give absorbance. Vision software (version 2.2.1) is used to collect and analyse the data.

2.8.3 Calibration

A weight calibration was conducted for DVS, which was preformed on a monthly basis, if the operating temperature was changed or if the instrument was switched off. A 100mg standard is used once the sample pan has been tared. Any difference between the expected and the observed value is recorded and adjusted by the software.

The NIR calibration was conducted weekly, if the lamp has been switched off, or for the first initial experiment. A ceramic reference spectrum is taken which provides background spectra for experimental data. In addition a performance test and if necessary following that test, wavelength linearisation were carried out monthly to ensure optimum performance of the lamp.

2.8.4 Experimental Method

Prior to an experimental run, thorough cleaning of sample pan was required, soaking and rinsing the pan in distilled water followed by absolute alcohol was the method used. The pan was then returned to the balance to dry at 0% relative humidity (RH). In order to remove any static build up, pans were exposed to 90% RH for approximately 10 mins. The RH was then returned to 0% and the balance zeroed and observed for a steady baseline. Once this had been achieved the sample was loaded at a mass range of 30-40mg. The programme was then initiated which exposed the mass to 0% RH for 6 hours (drying period) followed by 75% RH for 12 hours (crystallisation period) and then returned to 0% RH for 6 hours unless otherwise stated. NIR spectra was recorded in conjunction with spectra taken every 10 mins, the mean of 32 scans over the wavelength range of 1100-2500 nm was recorded.

2.9 Powder X-ray diffraction (PXRD)

2.9.1 Introduction

Powder X-ray diffraction is an analytical tool greatly used in the investigation of the structure of solids. The technique provides information on the crystal lattice of a solid or the absence of this if dealing with an amorphous material. Hence drug polymorphism can be characterised. Experimentally it is a simple technique to use and the information it provides is routinely used in industry. Many drugs and excipients exhibit polymorphism and this alters the physical properties of these materials. Manufacturing and formulation processes can easily alter the crystal state of a material; therefore it is of importance to confirm the crystalline structure (Brittain et al., 1991).

2.9.2 Instrumentation

Information with regards to the crystal state is obtained by the scatter of x-rays on the solid, this scattered radiation is unique to each crystalline structure and is called the diffraction pattern. The incident ray, which is monochromatic, runs parallel rays through the powdered sample at an angle θ reflecting off planes of the crystalline structure at the same angle (Fig 2.10). These angels are correlated to the spacings between planes of molecules in the lattice using Braggs law (Brittain et al., 1991, Atkins, 1998).

$n\lambda = 2d \sin \theta$ .....equation 2.3

where n = order of the diffraction pattern

λ = wavelength of incident beam

d = distance between the planes of the crystals

θ = angle of beam of diffraction

Equation 2.3 is used to calculate the spacing between planes, which are exposed in one of two ways: the sample or detector are either rotated. The diffraction characteristics of a sample are recorded in a diffractogram as the intensity of the peaks versus the angle at which they occur (2θ).

Fig 2.10. An x-ray beam bombarding a crystal particle and the angle of deflection.

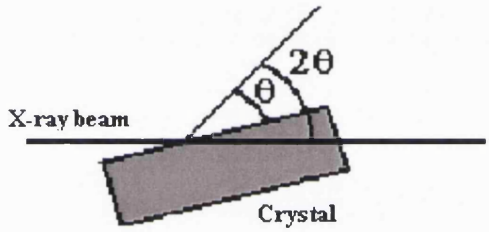

2.9.3 Calibration

A monthly calibration was preformed by conducting a full range linearity check over the range of 20 -100° 2θ. The deviations of the maxima peak from the theoretical values are listed. The values are then used to calculate the difference between the largest and smallest values, which should not exceed 0.075° 2θ.

2.9.4 Experimental Method

A Philips PW3710 X-ray powder diffractometer was employed for all the studies. The sample was compressed in a metal sample holder and approximately 100mg was mounted. All measurements were taken at 40kV and 30mA using a copper anode emitting X-ray photons.

2.10 Gas Chromatography (GC)

2.10.1 Introduction

Chromatography is an analytical method that is employed for the separation, detection and determination of chemical components in a chemical mixture. It is a well-established technique used routinely in most industrial and academic laboratories because of its capability of high resolution, selectivity and sensitivity. Martin and Synge first introduced the system in 1941, since then numerous techniques have evolved.

Chromatography consists of a mobile phase and a stationary phase, where the mobile phase is gas this is referred to as GC. The stationary phase can either be a solid or a liquid, Gas solid chromatography comprises all techniques with an active solid as a stationary phase and gas liquid chromatography involves a liquid stationary phase. The basic components of GC remain the same for both systems (Robards et al., 1994).

2.10.2 Instrumentation

In GC the sample is injected and vapourised onto the head of a chromatographic column. Elution is brought about by the flow of an inert gaseous mobile phase. In contrast to most other types of chromatography, the mobile phase does not interact with molecules of the analyte; its only function is to transport the analyte through the column. The analytes distribute or partition between the two phases depending on their relative affinities for the phases, as determined by molecular structure and intermolecular forces. Analytes, which have a high affinity for the stationary phase, will move through the system very slowly and vice versa for the mobile phase, which is also known as the carrier gas. This difference in migration rates results in separation of the components as they move through the column (Robards et al., 1994).

The instrument comprises a pressure or flow controller for the carrier gas, injection port, separation column (which is housed in an oven), a detector, and chart recorder. The sample is introduced into the chromatograph via the sample inlet into a continuous flow of carrier gas, which in this case is helium. The sample is vapourised in the inlet system by the high temperature and transported by the carrier gas to the thermostatted column, where separation occurs. The individual components give rise to an electrical signal in the

detector; in this case a flame ionisation detector was used. A schematic representation of GC is shown in Fig 2.11.

Fig 2.11. A schematic representation of GC.

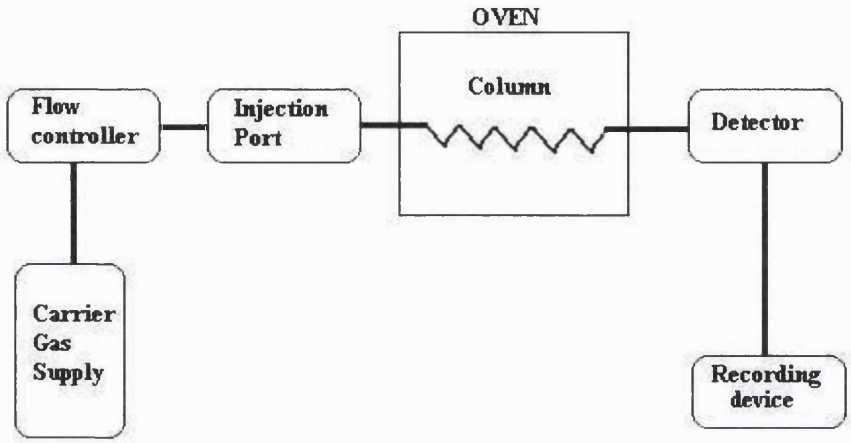

2.10.3 Experimental Method

Once the need for GC studies was established, the samples were chemically derivatised using a mixture of trimethysilymidazole (Lancaster) (22%), dimethyl sulphoxide (Sigma) (19.5 %) and pyridine (Aldrich) (58.5%). The method of sample preparation is based on Dwivedi and Mitchell, (1989) quoting the advantages as been quick and accurate compared to previous derivatistions. The samples were then sonicated for ~1 mins and were kept at room temperature for 20 minutes until derivatision was complete. The instrument used in this study was the Carlo, Erba, HRGC 5300, which is fitted with a flame ionisation detector. The conditions at which the experiments were run are summarised in table 2.4. The carrier gas used was helium.

Table 2.4. The experimental conditions used for GC.

Experimental Parameters	Temperature (°C)
Injection port	300
Column	230
Detector	280

2.10.4 Validation of Technique

The technique was validated using known ratios of α-lactose monohydrate and β-anhydrous. The anomeric forms of lactose used were not entirely pure but this is naturally difficult to obtain due to manufacturing processes (Olano et al., 1983; Wade and Wellar, 1994). An average of four results were taken and standard deviation calculated (table 2.5).

Table 2.5. Validation of the GC where the actual and observed results of α- and β-lactose composition are presented (n=4).

Theoretical		Actual composition		GC result	
α (%)	β (%)	α (%)	β (%)	α (%)	β (%)
100	0	94	6	94 ± 0.5	6 ± 0.8
0	100	26	74	24.2 ± 0.8	75.8 ± 0.9
25	75	43	57	45.4 ± 1.7	54.6 ± 2.6
50	50	60	40	65.5 ± 2.8	34.5 ± 2.8
75	25	77	23	79.0 ± 1.3	21 ± 1.3

2.11 Pycnometer

2.11.1 Introduction

The term pyconmeter is derived from the greek word pyknos, which has been identified with volume measurements. Hence the instrument is used to derive the true density of a material. One application of density measurement has been in the use of quantifying the amorphous content of a material. Saleki-Gerhardt et al., (1994) reported that a detection limit of 10% could be achieved using pyconmetry although large standard deviations associated with these measurements existed. Density measurements in this study have been used in collaboration with the Gordon-Taylor equation (Gordon and Taylor, 1952) to determine the glass transition temperature.

2.11.2 Instrumentation

The multipyconmeter is an instrument that is designed to measure the true volume of solid materials. This measurement is achieved based on Archimedes principle of fluid

replacement to determine the volume. Archimedes principle states that a body floating in a fluid displaces a weight of fluid equal to its own weight. In this case the displaced fluid is helium gas that can penetrate the finest pores to assure maximum accuracy due to its small atomic dimensions. The multipycnometer determines the true density of a solid or a powder sample by measuring the pressure difference when a known quantity of helium under pressure is allowed to flow from a precisely known reference volume into a sample cell containing the solid or powdered material. Through mathematical derivation the working equation used is shown below.

$$V_p = V_c - V_r [(P_1 / P_2) - 1] \quad \text{.....equation 2.3}$$

Where V_p = powder volume

V_c = sample cell volume

V_r = reference cell volume

P_1 = pressure reading after pressurising the reference volume

P_2 = pressure reading including V_c

The volume calculated is placed in the following equation with a known sample weight and the powder density calculated.

Powder density = Sample weight (g) / True powder volume (cm^3)

The instrument used was a Quantachrome multipycnometer (Model number MVP-1).

2.11.3 Calibration

A calibration of the instrument had to be conducted on a daily basis and involves the calculation of sample and reference cell volume. Both are calibrated using two micro spheres of combined known volume 2.1544 cm^3 and a micro sample cell is inserted in place of the small sample cell, the working equation used to calculate the volumes is shown below.

$$V_r = 2.1544 / [(P1/P2) -1] - [(P_1/P_2) -1] \quad \text{.....equation 2.4}$$

Where P1 = pressure in V_r with no calibration spheres in the cell

P2 = pressure in V_r and micro sample cell with no calibration spheres in the cell.

P_1 = pressure in V_r with the calibration spheres in the cell

P_2 = pressure in V_r and micro sample cell with the calibration spheres in the cell.

The value V_r is then used in the following equation to calculate V_c. These values are then placed in the working equation and subsequently used to calculate the powder density.

$$V_c = 2.1544 + V_r \ [(P_1/P_2) - 1] \qquad \text{.....equation 2.5}$$

2.12 Particle Sizing

2.12.1 Introduction

Particle size of powders is routinely measured in pharmaceutics. The bioavailability of pharmaceutical formulations for all systemic routes is dependent on particle size of a product. The mixing of materials and the avoidance of segregation is dominated by the particle size, where the particles of equivalent size are better at producing homogenously mixed powders relative to particles of a wide distribution. Flow characteristics of powders are also of importance and dependent on particle size as well as particle morphology during tablet and capsule formulation. Particle morphology is rarely spherical, in order to obtain measurements many particle sizing methods are based on the equivalent "parameter" theory. In the case of the Malvern this is based on the equivalent volume of a sphere.

2.12.2 Instrumentation.

Particle sizing has been conducted for this study using the Malvern mastersizer model MS7. The particle size is obtained by passing a laser light through the dispersed particles. In general large particles will scatter light at large angles and small particles will scatter light at small angles. These measurements are recorded and are related to a sphere of equivalent scattering intensity. The volume of sphere is then used to provide the particle size hence this is referred to as the equivalent sphere theory. In essence the software estimates a particle size distribution based on the scattering pattern. The Mie theory, which is a mathematical model, also uses the particle size distribution to calculate the scattering intensities. A comparison of the fitted and experimental patterns is then observed, which is termed the residual. A low residual (< 1%) indicates a difference between the fitted and the experimental patterns, therefore a good fit. A high residual (> 1

%) is related to a bad fit and consequently leads to an incorrect particle size distribution, this is often related to an incorrect refractive index. A refractive index for the material, medium and the absorption part of the refractive index (also known as the imaginary refractive index) needs to be known by the operator in order for the residual to be calculated and the Mie scattering theory to be used.

The Malvern has five distinctive parts; the transmitter module, which contains the laser light, the source was a low power helium-neon laser of a monochromatic wavelength of 0.63 μm. The advantage of this source is the stability of the laser which permits highly reproducible measurements. The intensity of the laser source allows sensitive measurements of all particle sizes and of relatively low concentrations. Lenses are needed to collimate the laser beam in order for scattering of particles to take place in the sample region and also to collect scattered light into the detector. Finally a computer is required with the appropriate software (in this case Malvern mastersizer, version 2.15) to transform the scattered light into particle size data.

2.12.3 Experimental Method

The solutions used to disperse the powders was cyclohexane (Aldrich). Initially great difficulty was found in dispersing the sample in the organic solvent so lecthin was employed as a dispersant at a concentration of 0.1% w/v and the samples were also sonicated for approximately 2 mins. Another experimental factor, which was taken into consideration, was the refractive index chosen for the mixtures of excipients. A specific calculated refractive index was chosen for each excipient and combination of spray dried material under the guidance of the Malvern reference manual.

Table 2.6. The excipients and dispersant used along with their refractive index.

Excipient	Refractive Index
Lactose	1.345
Polyvinylpyrrolidone (PVP)	1.580
Sodium dodecyl sulphate (SDS)	1.500
Dispersant	------
Cyclohexane	1.426

2.13 Scanning Electron Microscopy (SEM)

2.13.1 Introduction

Microscopy is one of the preferred methods for the study of pharmaceutical materials, giving an insight into the particle morphology and an estimation of particle size. Flow properties of materials as described previously are reliant on these properties. Amorphous and crystalline structures can also be identified amongst other properties from optical and scanning electron microscopy (Brittain et al., 1991). SEM is the technique used for the study of particle morphology in this thesis.

2.13.2 Instrumentation

The SEM provides a focused electron beam, which scans the sample in a series of parallel tracks. These electrons interact with the sample to produce various signals, including secondary electron emission, back scattered electrons and X-rays each of which can be detected. A secondary electron detector was employed attached to the SEM used, which monitored the intensity. An advantage of this technique is the great depth of focus producing images of an excellent quality. Coating the sample with a metal is standard procedure in order to prevent charge build up on the surface, which also increases secondary electron emission. The choice of metal is based on the magnification and in this case gold is used (Shaw, 1992).

2.13.3 Experimental Method

A Philips XL20 SEM was employed to produce electron micrographs for each sample. This was achieved by mounting each sample to adhesive carbon discs attached to SEM stubs. The samples were then transferred to an Emitech K550 sputter coater where they were coated with gold for 4 mins at 30mA prior to being photographed.

2.14 Summary

An introduction into the experimental techniques and methodology has been the aim of this chapter, with the belief that a background understanding will help the reader realise why the techniques were chosen. The characterisation and crystallisation of SD and PM products has been conducted using these analytical tools in the hope to investigate the

physical properties of the systems. Chapter three describes the excipients used as single components and investigates the physical properties that pertain to each material.

Chapter Three

The Excipients

3.1 Introduction

Characterising pharmaceutical drugs and excipients in industry is important in order to predict and understand how the chemical entity will behave both as a single and in a multi-component system. The preliminary study also identifies and provides details on the phyisco-chemical properties, which allows prediction of behaviour, stability and degradation once the material is in a multi-component system. Thus the aim of this study was to characterise the excipients; lactose, PVP and SDS and establish their physical properties using calorimetric and non-calorimetric techniques before introducing them to a binary system. Lactose was also studied as four feed concentrates (as solution and suspension) to investigate the effects the feed concentrate will have on the amorphous content. Another objective was to also follow the amorphous to crystalline phase transition using DVS-NIRS and to determine the crystallisation kinetics.

3.2 Lactose

3.2.1 Chemical and Physical Properties of Lactose

Lactose belongs to a group of sugars called the disaccharides and is composed of galactose and glucose. Lactose exists, in two optically isomeric forms, α- and β-lactose. These anomeric structures with, the incorporation of water where appropriate, produces the different forms of lactose, which are used in the pharmaceutical industry. A hydrate form of β-lactose does not exist because of its compact structure, which is not able to accommodate a water molecule. Evidence for this was obtained from density and thermal data acquired from differential scanning calorimetry (DSC) and sorption studies (Berlin et al., 1971). The β-anhydrous form is also relatively more soluble than α-lactose monohydrate (Olano et al, 1983).

Fig 3.1. The structure of α- and β-lactose and the difference in the anomeric forms.

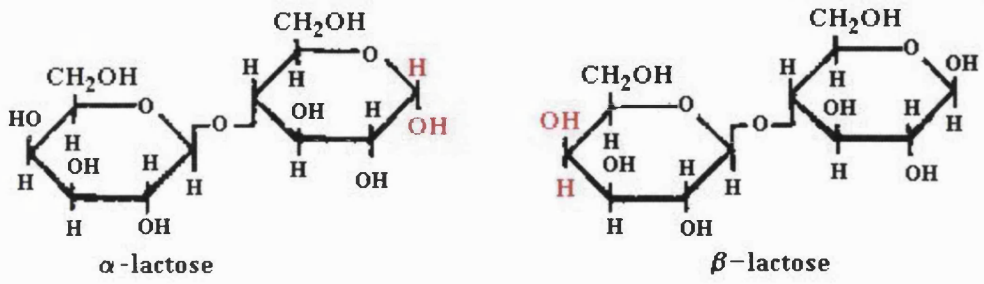

3.2.2 Pharmaceutical Applications of Lactose

Lactose is extensively used in the pharmaceutical industry as a diluent in capsule and tablet filling, where the primary aim is to increase the bulk of a solid dosage form when dealing with a potent drug. The reason for the diluent's popularity is due to its stability in the presence of many drug substances. Lactose can also be found in combination with sucrose (ratio 1:3) in the preparation of sugar coating solutions. The diluent is also used as a carrier in dry inhalation, where control over particle size and density is required to target the lung (Kibbe, 2000; Brittain et al., 1991b).

There are various grades of lactose, which dictate the nature of use of the excipient. For example direct compression grades of lactose are more fluid and more compressible than crystalline or powdered lactose. These grades are composed of spray-dried lactose, which is a combination of α-lactose monohydrate and amorphous lactose. Various lactose grades are commercially available which have different physical properties such as particle size and flow characteristics depending on their composition. This allows the most suitable material to be chosen for the appropriate application. For example fine grades of lactose are chosen in the preparation of tablets by the wet-granulation method. Direct compression grades as described above are chosen for tablet formulation where the composition of amorphous and crystalline lactose of lactose is approximately 15 and 85% respectively. At this level the amorphous content is enough to increase compactability and hardness profile. This is achieved by the amorphous content forming a binding layer over the α-monohydrate crystals which results in good binding characteristics (Kussendrager et al., 1981; Vormans et al., 1987; Kibbe, 2000). Lactose can also be spray dried as a solution to produce a sample that is a 100% amorphous with particles that are spherical in nature and seem to form aggregates (Fig 3.2). The particle size produced is of a narrow range. It is the spherical morphology that is responsible for the good flow characteristics.

Fig 3.2. SEM of a 100% amorphous lactose sample from this study.

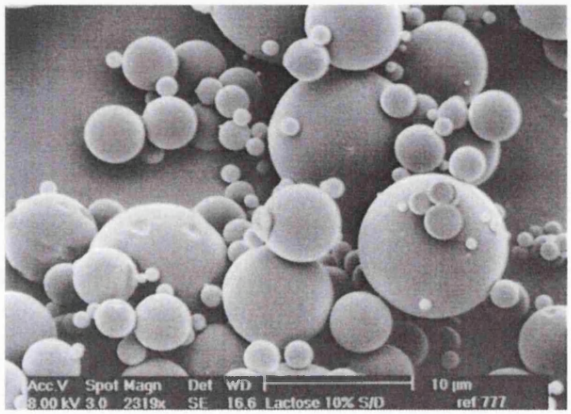

3.2.3 Characterisation and Analysis of Lactose

Many techniques have been used to study lactose; the excipient is described as a model material, which is a common and versatile pharmaceutical component in formulations. Lerk et al., (1984) studied various grades of lactose using DSC and identified dehydration, crystallisation and melting points. It has also been reported that amorphous lactose crystallises into several different forms: α-lactose monohydrate, anhydrous β-lactose, stable and unstable anhydrous α-lactose, and an anhydrous mixture of α/β-lactose in different molar ratios which have been established using PXRD and polarimtery (Olano et al., 1977; Lerk et al., 1984; Briggner et al., 1994; Jouppila et al., 1997; Schmitt et al., 1999).

Lactose crystallisation by the induction of water has been studied using the TAM, where the apparent enthalpy of crystallisation of amorphous lactose is well documented (Sebhatu et al., 1994; Briggner et al., 1994; Chidavaenzi et al., 1997). Other literature reports concerning lactose are centred on the detection limit and quantification of amorphous content for experimental techniques. This has been achieved for the TAM (Buckton et al., 1995), DVS-NIR (Hogan and Buckton, 2001) and solution calorimetry (Hogan and Buckton, 2000). Gravimetric studies of amorphous lactose (100%) and the sorption and desorption of water has been studied, with particular reference to the collapsed state of the material (Buckton and Darcy, 1996; Darcy and Buckton, 1997).

The crystallisation kinetics of lactose have also been investigated, with Roos and Karel (1992) modelling the rates of crystallisation at various experimental conditions. Schmitt et al., (1999) found that at 57.5% RH amorphous lactose crystallises to approximately 30% α-lactose monohydrate, 70% β anhydrous and a small amount of α-anhydrous. The growth mechanism of crystallisation of amorphous lactose seemed to be determined by surface incorporation rather than diffusion.

3.2.4 Mutarotation

Under different experimental conditions, the anomeric forms of lactose mutarotate to their respective counterparts. For example β-lactose mutarotates to α-lactose under the influence of *water vapour*. These findings were reported by Angberg et al., (1991) using the TAM where it was discovered that at a high relative humidity (94% RH) β-anhydrous mutarotates to α-anhydrous and incorporates water molecules to form the monohdyrate.

When lactose is exposed to *heat* the opposite process occurs, α-lactose mutarotates to the β-form. Also under the influence of *heat and water* all forms of β-lactose were seen to mutarotate to the α-form, this was achieved using closed DSC pans (Olano and Castro, 1983; Lerk et al., 1984 (a)).

The influence of pharmaceutical processes also induces mutarotation of lactose. Otsuka et al. (1991) showed that α-lactose can mutarotate to the β-form and vice versa depending on the starting material. For example the α-lactose content of ground monohydrate decreased with increasing grinding time. Roetman and Van Schaik (1975) presented information that mutarotation takes place in solution prior to drying during the spray/freeze drying process and in the final dried product during storage. It was also found that mutarotation occured when amorphous lactose underwent crystallisation (Roetman and Van Schaik (1975).

Thus in conclusion the different physical forms of lactose have lead to the availability of various commercial qualities. This reason coupled with the versatility and the inert nature of lactose makes the excipient an interesting material to research.

3.3 Materials

α-lactose monohydrate (Lactochem, supplied by GlaxoSmithKline) was used to prepare the SD products and also used as a reference material for DSC, PXRD, TGA, NIRS, TAM, and GC experiments. β-lactose anhydrous (Sigma-Aldrich) was used as a reference material for PXRD and GC experiments. For both starting materials the anomeric composition was determined using the experimental method listed in Chapter Two (section 2.10.3), where it was found that α-lactose monohydrate consists of 94% α- and 6% β-lactose. β-lactose was found to contain 75.8% β- and 24.2% α-lactose.

The starting material (as received) lactose monohydrate was checked for amorphous content to confirm whether the sample was indeed approximately 100% crystalline. This was accomplished using the TAM and exposing the material to 75% RH. The TAM as described in Chapter Two (section 2.3.1) is highly sensitive and can detect small amounts of amorphous content (0.5%, Buckton et al., 1995(b)). No crystallisation peak was seen; only a steady baseline was recorded as seen in Fig 3.3. Thus no detectable amorphous material exists and the starting material is ~ 100% crystalline.

Fig 3.3. A steady baseline for "as received" lactose monohydrate in the TAM at 75% RH.

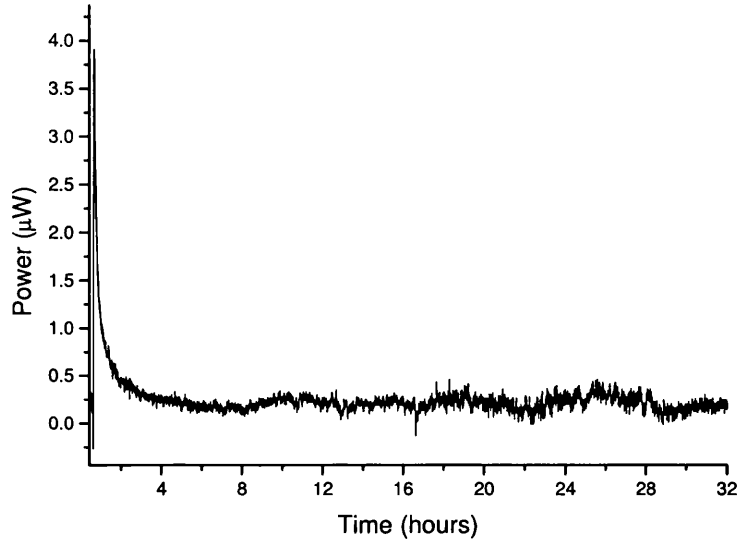

3.4 Sample Preparation

Feed samples of α-lactose monohydrate were prepared by weighing 10, 20, 30, and 40g of lactose in a 100ml conical flask and distilled water added. Lactose 10 and 20% w/v were solutions at room temperature in comparison to lactose 30 and 40%, which were suspensions under the same ambient conditions (293K ± 2K, 50% ± 5% RH) (Hogan and Buckton, 2001). The feed concentrates were spray dried, collected and then stored in a desiccator at 0% RH over P_2O_5.

3.5 Experimental Methodology

The Buchi-190 mini spray dryer was employed under the experimental conditions listed in Chapter Two, section 2.2.3. All the experimental parameters were kept essentially the same for the spray drying of each feed concentrate except for the pump rate. During the spray drying process the feed suspensions (Lactose 30 and 40% w/v) were maintained in a homogenised state using a magnetic stirrer.

DSC and PXRD were used to characterise the lactose SD products under the experimental conditions described in Chapter Two (section 2.4.4 and 2.9.4 respectively). TGA was used to determine the water content of the SD samples; the experimental method used is listed in Chapter Two (section 2.6.4.) Crystallisation of the SD materials was induced by water vapour at 75% RH and 25°C using the TAM (experimental method, chapter two,

section 2.3.4.) The TAM was calibrated at 3000μW for SD products containing lactose concentration 30 and 40% w/v. For lactose 10 and 20% w/v SD, the TAM was calibrated at 1000μW to determine a more accurate result for the apparent enthalpy of crystallisation for each SD product.

The hyphenated technique of DVS-NIRS was used to induce and follow crystallisation and allow comparison of data obtained from TAM. The DVS cycle along with the calibration was described in Chapter Two (section 2.8.4). NIR spectra were taken every ten minutes throughout the experimental run and analysed using Vision (2.21) software. Diffuse reflectance was recorded and the reciprocal (1/R) of this parameter was plotted to give absorbance. However the spectra are influenced by physical and chemical information and in order to minimise the effect of scatter caused by physical properties such as particle size and morphology, the spectra are treated mathematically. In this case the standard normal variate (SNV) was employed to diminish any influence, for example the offset in baseline, which is characteristic of NIR spectra. This is due to the effect of factors such as the particle size of the sample. Other mathematical treatments such as the second derivative of the spectra allow enhancement of the peak resolutions (Blanco et al., 1998; Buckton et al., 1998).

One experimental parameter that was investigated to identify whether it exerted any significant effect on NIR SNV-2nd derivative spectra was sample weight. Hogan and Buckton (2001) expressed a concern with quantification work whether the effect of sample size would affect the intensity of the NIR reflectance signal when coupled with DVS. To investigate this, NIR spectra of samples of increasing weight were taken manually at 25°C and 0% RH using dried amorphous lactose as the reference material. The NIR spectrum was not taken manually until the sample weight was stabilised to 0.001% weight change with time. The experiment was preformed in duplicate.

The result shown in Fig 3.4(a) represents spectra of different experimental weights recorded, which showed very small changes in the intensity with an increase in weight above 5mg using SNV 2nd derivative spectra. However the difference seen by peaks at 2064 and 2100nm may be due to incomplete covering of the quartz pan. If we consider mathematically untreated data (Fig 3.4 (b)), there was a visual difference between sample masses up to a certain weight, which is ~35 mg. The absorbance baseline shifts downwards with increasing weight. Above 35 mg the absorbance spectra was independent of the sample weight, with the generated spectrum being placed within the previous spectra (Fig 3.4 (c)).

Fig 3.4. The effects of sample weight on NIR spectra (log 1/R) represented by (a) SNV 2nd derivative and (b) untreated absorbance data up to 45 mg and (c) all the sample weight investigated.

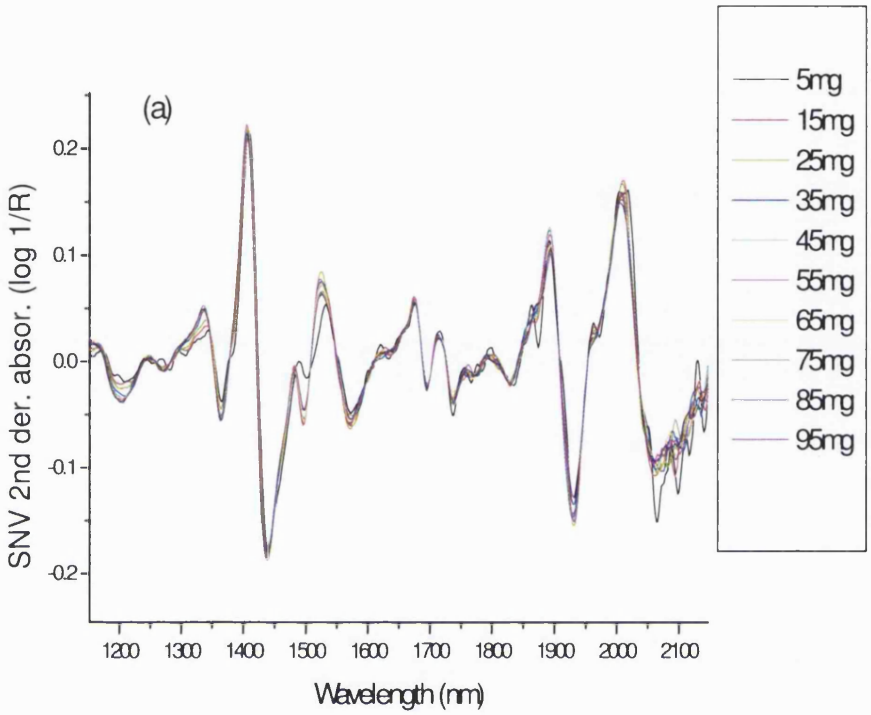

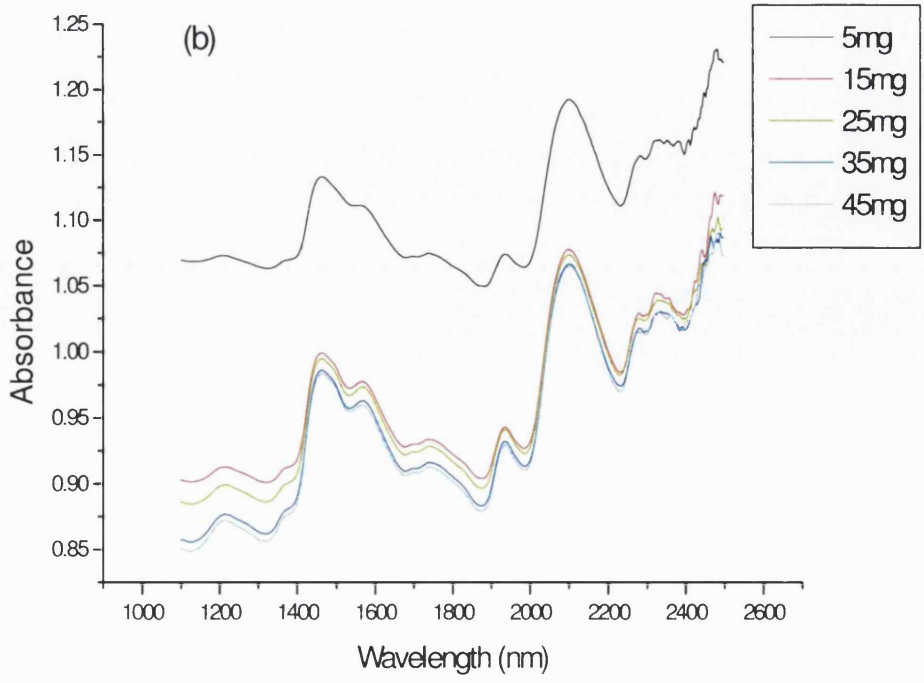

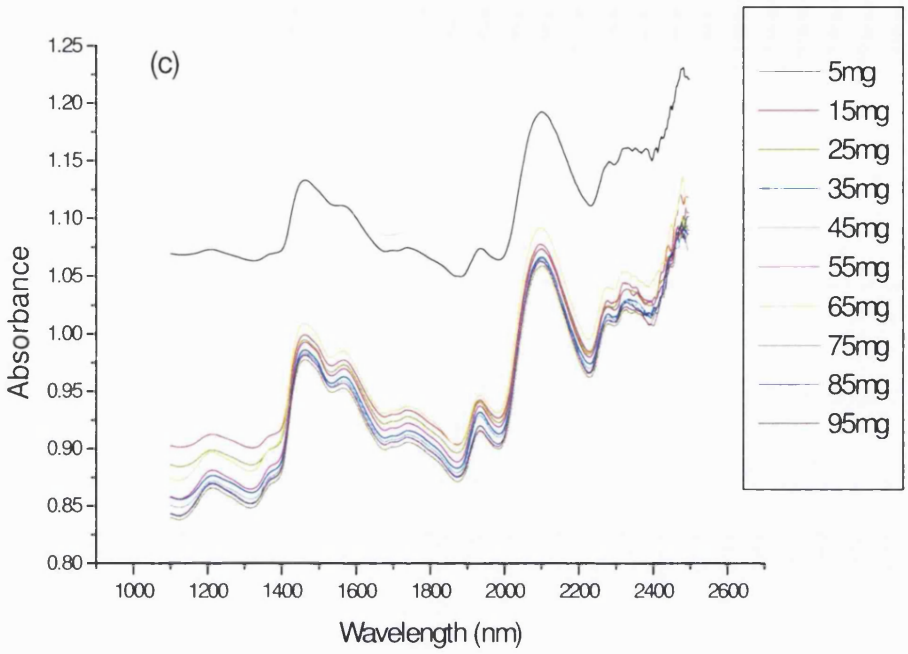

Yoon et al. (1998) also described these findings with a more thorough investigation on the sample thickness of a material amongst other parameters. The NIR reflectance values become independent of the sample thickness above a certain value, this is termed the "infinite thickness" which was also found to be dependent on the material. However the effects of sample thickness were less pronounced than other experimental parameters.

For quantitative work that is conducted in this study, the sample material needs to be above 30-35mg in order to eliminate the effects of sample weight however small. Although by mathematically treating the data we eliminate the effects of particle size and morphology and other physical factors in this case the effects of sample weight are also reduced relative to the SNV 2nd derivative absorbance spectra.

3.6 Results and Discussion

3.6.1 Characterisation of SD Lactose

3.6.1.1 DSC and PXRD

DSC and PXRD were used to identify whether the SD materials were amorphous or crystalline. DSC has the advantage that it is able to identify anomeric forms of a material but in the case of α-lactose mutarotation to the β-form can occur during heating

conditions. However, the data remain a good indication of the anomeric content (Lerk et al., 1984(a); Chidavaenzi et al., 1997; Schmitt et al., 1999) and have also proved to be useful in this study.

The characterisation of lactose SD products using DSC is shown in Fig 3.5. The thermograph for SD lactose from a 10% w/v feed (Figure 3.5 (a)) had an exothermic peak at ~180°C which represents amorphous material crystallising, this was followed by an α-anhydrous melt at ~210°C. A similar result was also seen for SD samples derived from 20% and 30% w/v feed concentrates. For the SD product from a high feed concentrate 40% w/v a dehydration of α-lactose monohydrate at ~143°C was observed, which was evidence that a quantity of crystalline material was present within the sample. Thus, not all the material spray dried had been able to convert to the amorphous state for the 40% w/v feed suspension. Following the dehydration process, crystallisation and an α-melt were seen to occur at ~165°C and 210°C respectively. To confirm these results PXRD was also employed.

Fig 3.5. DSC thermographs of lactose SD products from feed concentrates (a) 10% w/v and (b) 40% w/v. The DSC thermographs for SD products from 20 and 30% w/v were similar to that of 10% w/v.

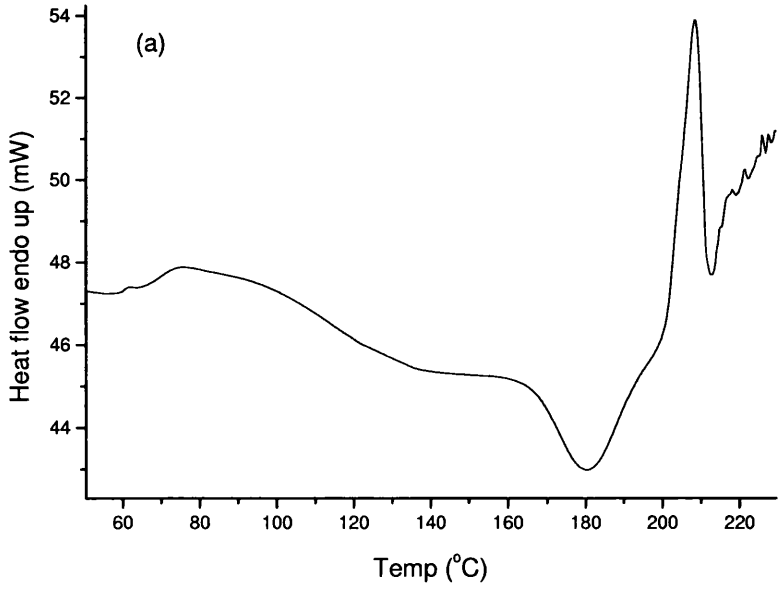

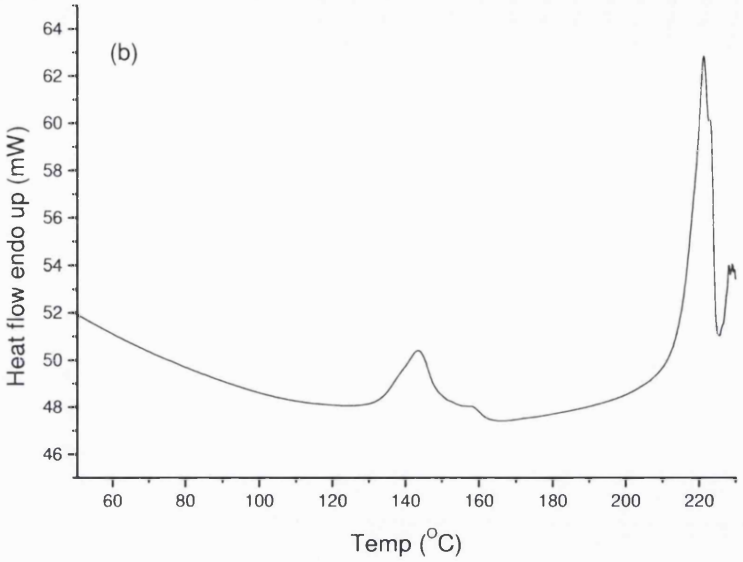

Fig 3.6. X-ray diffraction data of (a) β-lactose anhydrous (b) α- lactose mono (c) SD lactose 10% w/v (which is also representative of SD lactose from a 20% w/v solution), (d) SD lactose 30% w/v, (e) SD lactose 40% w/v.

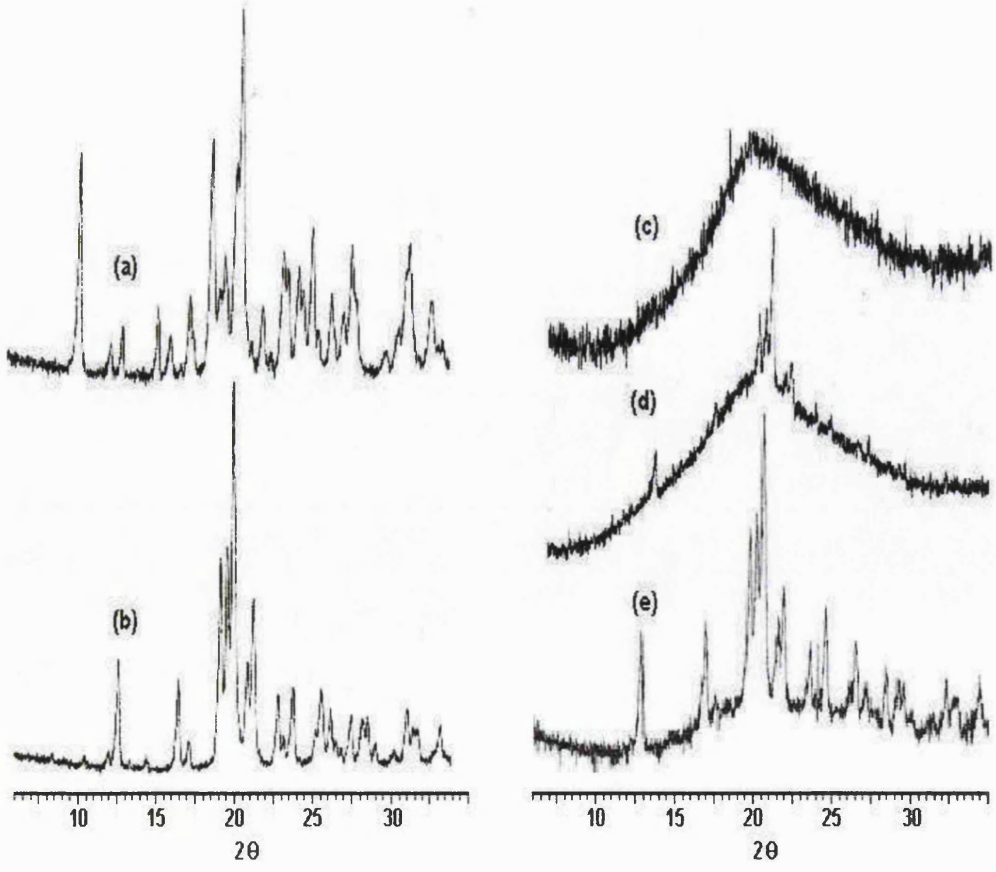

The X-ray diffraction results for the SD products of 10%, 20% and 40% w/v feed concentrates correlate with the DSC data. An X-ray diffractogram of the SD product 10% w/v showed an amorphous halo with no peaks in comparison to materials which were totally crystalline as shown in Fig 3.6 (a) and (b) representative of β-lactose anhydrous and α-lactose monohydrate respectively. The SD sample produced by the feed concentrate lactose 40% w/v showed a peak at 12.6° that corresponds to α-lactose monohydrate. This can be deduced from X-ray analysis of α-lactose monohydrate and β-lactose anhydrous where the most prominent and characteristic peaks that distinguish the two anomers are 12.6° and 10.5° respectively. The diffractogram pattern within the range 19-22° (2θ) for lactose 40% w/v was of similar shape to α-lactose monohydrate.

For SD lactose of feed concentrate 30% w/v we also observe a peak at 12.6°, a range of peaks at 19-20° (2θ) and also at 22.0°, this is similar to α-lactose monohydrate but is also identical to that of stable α-anhydrous lactose (Jouppila et al., 1997; Chidavaenzi et al., 2001). However with the result from DSC where no α-monohydrate peak was detected for SD lactose from a 30% w/v suspension, the residing crystalline material can be identified as stable α-anhydrous lactose. This would manifest itself in a DSC thermograph as an anhydrous α-melt at ~210°C which was observed.

From the above analysis it is clear that each SD lactose product from their respective feed concentrates consists of different compositions of amorphous and crystalline material. To complete the characterisation process quantification of the amorphous and crystalline material was conducted for each SD product by employing the TAM.

3.6.2 The study of crystallisation using Isothermal Microcalorimetry (TAM)

The TAM is a very sensitive instrument; however, this can lead to confusion in the comparison of data. Lactose is a material, which poses such a dilemma. Various literature results have quoted enthalpies of crystallisations depending on the method and also the software used for calculation. An example of a typical TAM profile for amorphous lactose exposed to elevated RH is seen in Fig 3.7.

Fig 3.7. A TAM profile of SD amorphous lactose generated by exposure to 75% RH at 25 ℃ from this study.

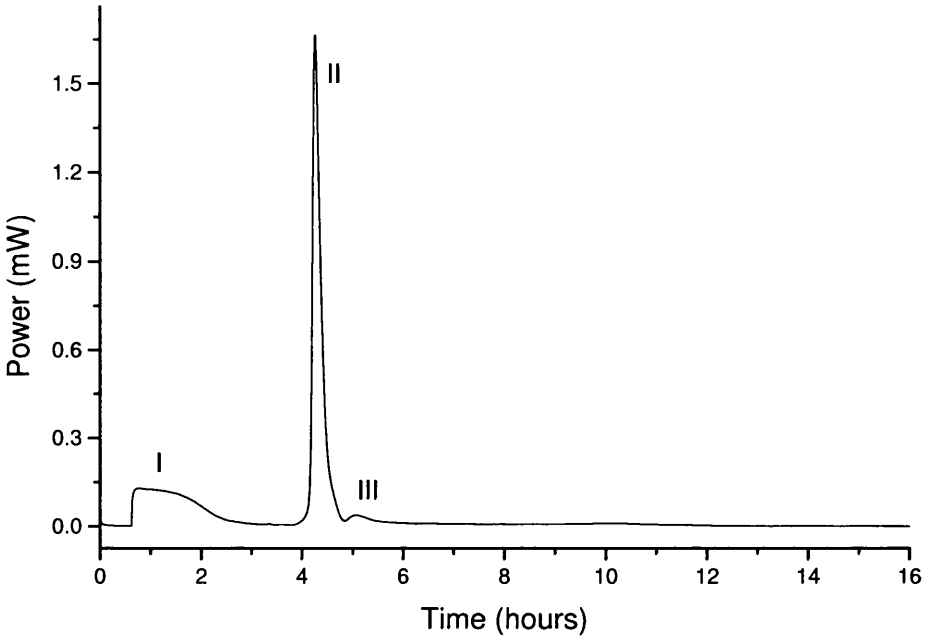

From the profile in Fig 3.7 it can be seen that several distinct phases exist within the trace, which can be identified, but nevertheless add to the confusion of analysis. Phase I is an exothermic peak, which arises from a number of events. The friction from lowering the ampoules into the measuring cups causes an exothermic response. This phase has also been attributed to evaporation of the salt solution in the hydrostat into the surrounding ampoule and wetting of the sample leading to an overall exothermic response (Sebhatu et al., 1994; Ahmed et al., 1996; Darcy and Buckton, 1998). Buckton and Darcy (1996) have also suggested that during this phase structural collapse of the material may also be taking place amongst other events.

Phase II represents the crystallisation response of the sample. This response is a net effect of the expulsion of the absorbed plasticising water (endothermic) and the crystallisation process itself (exothermic). However there will also be other contributing factors due to the lack of specificity of the TAM (Buckton and Darcy, 1999) and hence the area under the graph represents the apparent enthalpy of crystallisation. For amorphous lactose the material has been shown to be in a crystalline state at the end of this phase as described by Briggner et al. (1994). The response has also been described as a highly cooperative process by which the entire powder bed crystallises in a one step process having set up a concentration gradient of absorbed water through the powder mass (Briggner et al., 1994;

Buckton and Darcy, 1995(c)). However in other cases for example salbutamol sulphate, phase II is slightly more complex, where the sample does not readily desorb water form the crystalline mass but releases it over several days therefore significantly altering the apparent enthalpy of crystallisation (Columbano et al., 2002).

Phase III is a shoulder peak, which may or may not be observed, that has been attributed to a number of processes according to literature. Angberg et al., (1991) has shown that mutarotation of β to α-lactose occurs under the influence of water vapour, which occurs at the highest RH (94 %) but to a lesser extent at lower RH (75, 81, and 84%), where there is influence of hydration of the anhydrous α-lactose. Briggner et al. (1994) attributes this process to mutarotation and has suggested that an estimation of the anomeric forms is possible from the size and the shape of the subsequent transition peak. Sebhatu et al., (1994) has explained that this peak could be due to incorporation of water into the anhydrous α-lactose to form the monohydrate. However these are all conjectures and no conclusive evidence has been reported on the cause of phase III and whether it should be integrated as part of the crystallisation peak. It is for this reason that confusion arises on the calculation of the apparent enthalpy of crystallisation. Table 3.1 lists the various apparent enthalpies of crystallisations for 100% amorphous lactose samples as well as the experimental conditions.

Table 3.1. A literature comparison of the apparent enthalpy of crystallisation of 100% amorphous lactose and the experimental conditions which they were determined under.

Experimental conditions	Phase incorporation	(ΔH_c mJ/mg)	Reference
25°C, 57, 75, 84, 100% RH	Phase II only.	32 ± 4%.	Sebhatu et al., 1994.
25°C, 85% RH	Unspecified	44.9, 46.9 and 47.8	Briggner et al., 1994
25°C, 75% RH	Unspecified	50	Chidavaenzi et al., 1997
25°C, 75% RH	Phase II and III	48.9 (1.9)	Darcy and Buckton, 1998.

It is therefore difficult to assign a start and end point to the crystallisation process as many issues surround the event. However, with the help of an advanced software package (Origin 5.0) and consistency in the analysis of the results, the TAM can be used to quantify the amorphous content of amorphous and partially amorphous lactose SD products. In this case the samples were quantified for their amorphous content, by using a

method, which incorporated phase II only. This was chosen as phase III more often than not was not present especially for SD lactose from a 10% w/v feed concentrate. This sample is expected to be ~ 100% amorphous and will provide the standard value from which the amorphous content of partially amorphous samples will be determined. It also became apparent after many experimental runs for each SD lactose product and the information found in literature reports that the observation of phase III was very much dependent on the spray drying parameters of lactose (Angberg, 1995).

It is also important to mention that there are several parameters that affect the rate at which a sample crystallises. Firstly the quantity of amorphous material will influence the onset of crystallisation (time taken from the beginning of the experiment to phase II). An increase in amorphous content will also lead to a proportional increase in the onset time. This is because full saturation of the powder bed must first take place before instantaneous cooperative crystallisation occurs. This also explains why if we increase the weight of the sample we also increase the lag time. Secondly by altering the RH a change in the onset time will also be observed, powder bed saturation is achieved faster at a higher RH than a lower RH at constant experimental conditions. Other factors that have been investigated are surface area of the saturated salt solution and powder bed, if both are large the delay in the onset of crystallisation is short; if either is reduced the delay is increased (Briggner et al., 1994).

Factors that influence the enthalpy of crystallisation have also been investigated by Darcy and Buckton (1998). The study showed that altering both the temperature and RH can have a detrimental effect on the enthalpy of crystallisation for amorphous lactose. Increasing the temperature from 25 to 60°C was found to result in an increase in the enthalpy of crystallisation. Increasing the relative humidity was found to result in a lower value especially when the experiments were conducted at high temperatures.

3.6.2.1 The TAM response of SD lactose products

The SD lactose feed concentrates produced different TAM traces, as from the previous section on the characterisation it was apparent that each SD lactose sample had a different amorphous content. Fig 3.8 is a graphical representation of the SD lactose products from the four different feed concentrations under the influence of 75% RH. The shape of each SD sample illustrates the difference in crystallisation kinetics and the onset of crystallisation is an indication of the amount of amorphous content present.

Fig 3.8. A graphical representation of crystallised SD lactose from four feed concentrates (% w/v) (—) 10, (—) 20, (—) 30, (—) 40 at 75% RH and 25 ℃ in the TAM.

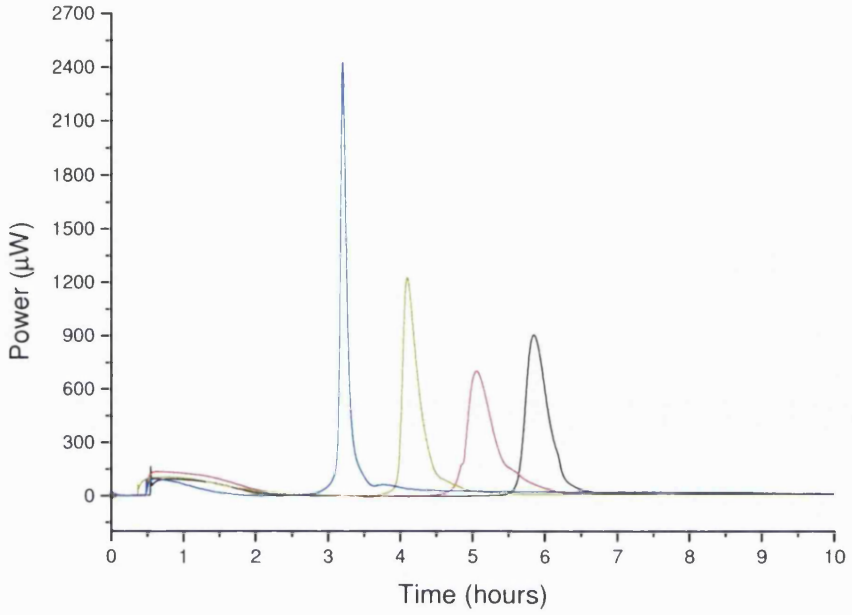

Table 3.2 summarises the onset of crystallisation for SD lactose samples. SD lactose 10% w/v takes the longest to crystallise at 5.3 hours, followed by SD samples from 20, 30 and finally 40% w/v feed concentrates. Therefore the amount of amorphous content in each SD product decreases in this order with SD lactose from a 10% feed containing approximately 100% amorphous material as all the lactose is in solution whereas the SD sample from 40% w/v suspension seems to contain approximately half the amorphous content.

Table 3.2. The onset of crystallisation with respect to the SD lactose product from different feed concentrations (n=5).

SD lactose product from feed concentrate (% w/v)	Onset of crystallisation (hours)
10	5.3 ± 0.4
20	4.7 ± 0.1
30	3.7 ± 0.6
40	2.6 ± 0.2

The actual percentage amorphous content for each lactose SD sample was calculated from the following equation (Briggner et al., 1994). Where Q represents the heat output of the test sample and Q_a is the heat output from a totally amorphous material. The blank

response represents the output obtained by loading the cell into the microcalorimeter. A blank response of zero was used in our calculation.

$$\% \text{ Amorphous} = 100 * (Q\text{-blank}) / (Q_a) \quad \text{.....equation 3.1}$$

Table 3.3. A summary of the % feed in solution, the apparent heat of crystallisation, and amorphous content for 30mg of each SD lactose product from the respective feed concentrates (n=5).

Feed concentrate g/100ml	(%) Dissolved	The apparent heat of crystallisation (mJ)	(%) Apparent amorphous content.
10	100	1369.5 ± 19.5	100
20	100	1312.0 ± 12.0	95.8
30	67	1227.1 ± 25.9	89.6
40	50	748.0 ± 43.7	54.7

The apparent amorphous content may be compared to table 3.2, where there was a good correlation with respect to the onset of crystallisation. The sample containing the greatest amount of amorphous content took the longest to crystallise and vice versa. The SD lactose sample from a 10% feed can be identified as ~100% amorphous as the starting material was all in solution as described earlier. The DSC along with PXRD also confirmed this, where no crystalline peak or diffraction pattern was seen for each technique respectively. The apparent enthalpy of crystallisation for this sample was 45.7mJ/mg (for a 30mg sample), which was in good agreement with literature (Briggner et al., 1994). SD lactose from a 20% feed concentrate contains a small percentage (4.2%) of crystalline material that was not detected by DSC or PXRD due to the sensitivity of the instruments. The amorphous content was still within the expected range, however the crystalline composition may have occurred due to the possibility that some nucleation sites may have remained as the solution is approximately at equilibrium solubility (Chidavenzi et al., 1997). SD lactose from a 30% w/v feed produced a greater amount of amorphous content than expected (89.6%) in comparison to the percentage in solution (67%). Any "excess amorphous material" was likely to be due to a combination of factors; the atomisation pressure during spray drying along with particle attrition may have induced a milling effect, which increased the amorphous content (Chidavaenzi et al., 1997). The SD sample from a 40% w/v feed also produced a slightly greater percentage of amorphous content (4.7%) in comparison to the percentage in solution, however the

majority remains in the crystalline state. The difference between the SD sample from a 30 and 40% w/v feed was more likely to be due to the increased pump rate during spray drying, which was increased significantly to maintain the outlet temperature. This reduced the residence time of the suspended feed concentrate in the atomiser with approximately half the material converted to the amorphous content.

Table 3.4. A comparison of the average increase in pump rate for the feed concentrates lactose 30 and 40% w/v when spray dried.

Lactose Feed concentrate (%)	Pump rate (%)
30	22-24
40	35-82

3.6.3 The Anomeric composition of SD lactose products

With the characterisation of the SD lactose samples before crystallisation and the TAM data, the anomeric forms were determined. From the X-ray diffractograms, DSC, and TAM, SD lactose from a feed of 10% w/v was found to be ~100% amorphous. SD lactose from a 20% w/v feed contained a small percentage (4.2%) of crystalline material that was not detected by DSC and PXRD. The nature of this material was more likely to be stable α-anhydrous as opposed to α-monohydrate because of the dehydration and drying that occurs during the spray drying process at a low pump rate setting. SD lactose product from a 30% w/v feed when crystallised in the TAM produced a sample that was ~89.6% amorphous. The remaining percentage is crystalline α-anhydrous, determined by PXRD and DSC, where no β-lactose was detected. TGA data for this sample (Fig 3.9) also showed no monohydrate peak for the SD sample.

SD lactose from a 40% w/v feed was found to be ~54.7% amorphous with the remaining percentage crystalline from TAM data. PXRD and DSC data showed that the SD product contained a substantial amount of monohydrate with no β-melt. The TGA data (Fig 3.10) for SD lactose sample from a 40% w/v feed can also be used to quantify the percentage monohydrate within the crystalline material (~50% monohydrate), which was similar to that of the TAM and therefore no α-anhydrous was produced within the detection limit of the TGA.

Fig 3.9. A TGA thermogram of lactose 30% (that is representative of lactose 10 and 20% w/v), which shows moisture removal below 100°C representing absorbed water only.

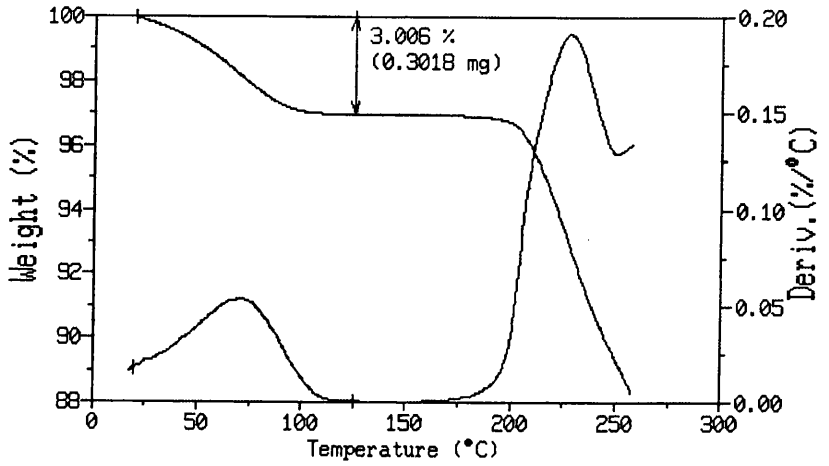

Fig 3.10 A TGA thermogram of lactose 40% showing that approximately 50% of moisture is absorbed and 50% is in the monohydrate region.

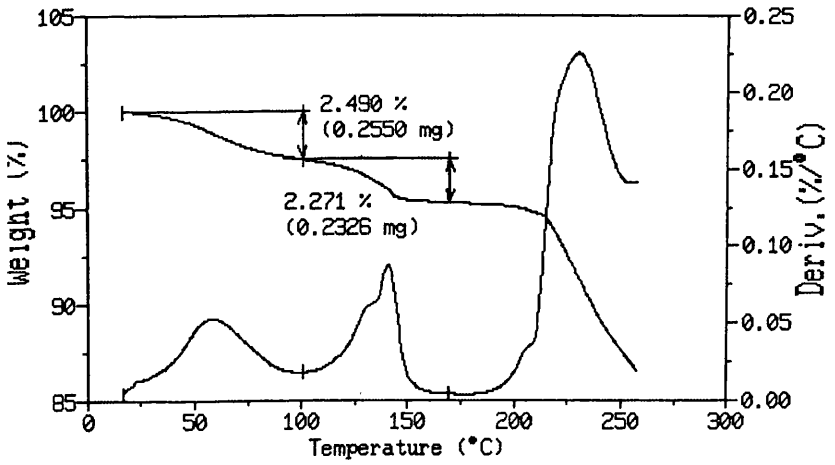

Therefore half of lactose 40% w/v SD was a monohydrate of lactose. This result supports the theory that the increase in load during spray drying and the increase in the pump rate provided the feed concentrate with a short residence time in the atomiser, unable to undergo dehydration and atomisation in order to convert to the amorphous state. Table 3.5 summarises the anomeric composition of each SD lactose product. The physical and anomeric composition of the products is important for the reason that the pharmaceutical properties are very much dependent on the state of the material.

Table 3.5. A summary of the amorphous and crystalline composition of the SD lactose products from different feed concentrates.

SD lactose feed concentrate (% w/v)	SD Product Composition (%)			
	Amorphous	α-monohydrate	α-anhydrous	β-anhydrous
10	100	0	0	0
20	95.8	0	4.2	0
30	89.6	0	10.4	0
40	54.7	45.3	0	0

3.6.4 The study of crystallisation using DVS

Isothermal microcalorimetry is better suited to quantify the amorphous content and assess the onset of crystallisation for each lactose SD product, however the crystallisation kinetics were not established. Understanding the crystallisation process (through kinetics) is of importance in defining the stability of the sample and adopting preventative measures to ensure that the material is maintained at the desired state. The DVS data (Fig 3.11) were studied in an attempt to understand the crystallisation kinetics of each SD lactose product. The samples were initially dried for 360 mins (6 hours) at 0% RH in the DVS system, and then crystallisation was induced by raising the RH to 75% for 720 mins (12 hours), followed by subsequent drying for 360 mins (6 hours). The absorption of water for each SD product was initially reported to provide us with information about the DVS profile and the amorphous content in comparison to the TAM.

Fig 3.11. DVS profiles of lactose SD products from feed concentrations of (% w/v): (—) 10, (—) 20, (—) 30, (—) 40.

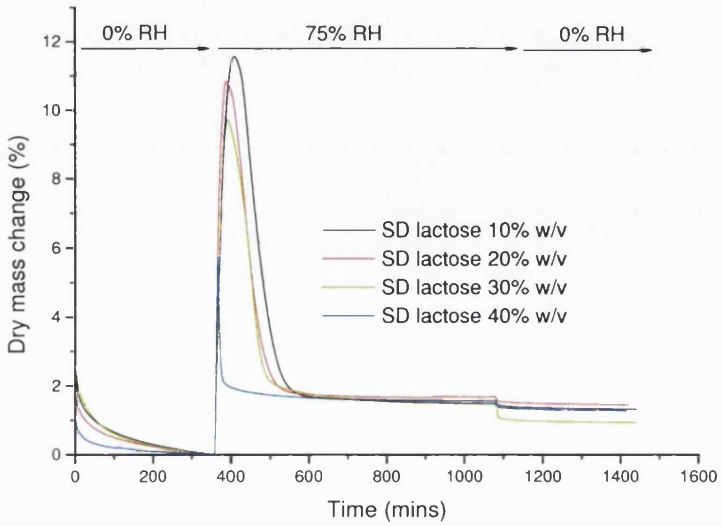

3.6.4.1 The Absorption of Water

The maximum amount of water absorbed by each SD lactose feed concentrate is an indication of the amount of amorphous material in the samples (Ahlneck and Zografi, 1990). From Fig 3.11 and table 3.6 the SD products produced from feed concentrates that were in solution (10 and 20% w/v) have absorbed the greatest amount of water reflecting the greater amorphous content. The SD sample produced from 40% w/v feed has taken up the least amount of water, which was approximately 50% the value of 10% w/v feed concentrate SD sample. The result supports the data provided by the TAM and TGA that half the sample is amorphous. The amount absorbed by a sample that is 100% amorphous lactose is in good agreement with literature under similar experimental conditions (Stubberud and Forbes, 1998; Lane and Buckton, 2000). In summary the experiment provides evidence that a simple preliminary study like the absorption of water by a material, in this case lactose is a good indicator of the amorphous content.

Table 3.6. The (%) water for SD lactose from different feed concentrations (n=4).

Feed concentrate (% w/v)	% Water Absorbed
10	11.75 ± 0.2
20	10.40 ± 0.5
30	9.45 ± 0.7
40	5.82 ± 0.5

3.6.4.2 Modelling DVS data using the Avrami equation

It has been the norm that crystallisation kinetics under isothermal conditions can be studied by techniques such as X-ray diffraction (Jouppila et al., 1997; Corrigan et al., 2002), and DSC (Kedward et al., 1998). Gravimetric studies have also been used by Andronis et al., (1997) and Schmitt et al., (1999). There are a number of parameters that can be reported to describe the Kinetics of crystallisation using the Avrami equation (Avrami, 1940) (equation 3.2). The equation describes the overall crystallisation process for a solid-state system under isothermal conditions and can be written in two ways.

$\theta = 1\text{-}\exp(-(kt)^n)$ or $\theta = 1\text{-}\exp(-K^*t^n)$ .....equation 3.2

Where θ is the fraction crystallised, t is time, k is the isothermal crystallisation rate constant at which the reaction proceeds, K* is the overall isothermal crystallisation rate

constant (both depend on the nucleation and growth rate constants), n is the Avrami exponent, which depends on the nucleation mechanism and the number of dimensions in which growth is occurring (Avrami, 1940; Andronis et al., 1997; Schmitt et al; 1999). A thorough description of the components in the equation and the way the raw data is transformed is discussed in the following sections prior to data presentation.

3.6.4.2.1 The Avrami exponent (n)

The Avrami exponent (n) can take several values and is a combination of the nucleation mechanism and the dimension of crystal growth. The nucleation mechanism can be of three types; continuous, where the formation and growth of nuclei continues to occur whilst crystals grow. Fixed number nucleation means that no more nuclei form during the growth of crystal, hence growth precedes from a fixed number of pre-existing nucleation sites. Site-saturated nucleation is the final nucleation mechanism that is a combination of the two previous cases. It follows that the dimensions of growth (growth mechanism (m)) from a fixed number of nuclei or from site saturation will equal the Avrami exponent (n = m). For growth from a constant rate of nucleation the Avrami exponent will equal the dimension of growth plus one (n = m + 1) (De Bruijn et al., 1981; Schmitt et al., 1999). A summary of these concepts is represented in table 3.7.

Table 3.7. A summary of possible values for n for different mechanisms (adapted from De Bruijn et al., 1981).

Dimension of growth (m)	Constant rate nucleation n = m + 1	Fixed number or site-saturated nucleation; n = m.
One-dimension (m=1)	2	1
Two-dimension (m=2)	3	2
Three-dimension (m=3)	4	3

3.6.4.2.2 The isothermal crystallisation rate constant (k/ K*)

As described in a previous section (section 3.6.4.2) two forms of the Avrami equation exist in the literature, and are related to each other by equation 3.3. k represents the isothermal crystallisation rate constant for one dimensional growth, whereas $K^{*(1/n)}$ is the bulk crystallisation rate constant which represents the overall value for all dimensions of growth. Both constants are related to each other through equation 3.3

$k = K^{*(1/n)}$ .....equation 3.3

In literature both versions can be found (Maffezzoli et al., 1995; Andronis et al., 1997; Schmitt et al., 1999; Kedward et al., 2000) and are manipulated accordingly, care must be taken when comparing data and the crystallisation rate constants.

3.6.4.2.3 The Corrected time

In order to determine the crystallisation kinetics using the Avrami model the time axis has to be reset and the induction time has to be established to determine the kinetic parameters. The induction time (t_i) may be defined "as the most probable time from the beginning of isothermal crystallisation to the point at which a stable crystal nucleus starts to grow" (Kedward et al., 2000).

In this case the induction time was taken from the onset exposure (time equals zero) of 75% RH to the maximum water uptake of the sample. Wetting and plasticization occurs on the uptake of water leading to an increase in molecular mobility of lactose. The loss of sorbed moisture signifies the phase transformation of amorphous lactose to the crystalline state. Therefore it would be appropriate to define the induction time in this way, as the likelihood that a stable nucleus has formed upon expulsion of water is highly probable.

3.6.4.2.4 The degree of Crystallinity (θ)

The DVS raw data initially needs to be converted to degree of crystallinity and hence the fraction crystallised as a function of time before any mathematical treatment can be conducted. The data were transformed using equation 3.4 (Schmitt et al., 1999) which produced the graph shown in Fig 3.12.

$\theta = (Wt_{max}-Wt_t / Wt_{max}-Wt_{final})$ .....equation 3.4

where Wt_{max} represents the maximum weight, Wt_t represents the weight at time (t) and Wt_{final} the final weight at the end of the crystallisation process. By using this approach we are calculating the fraction of amorphous material crystallised by subtraction and division to normalise the data.

Fig 3.12. A graphical representation of the fraction of amorphous material crystallised against corrected time for lactose SD products.

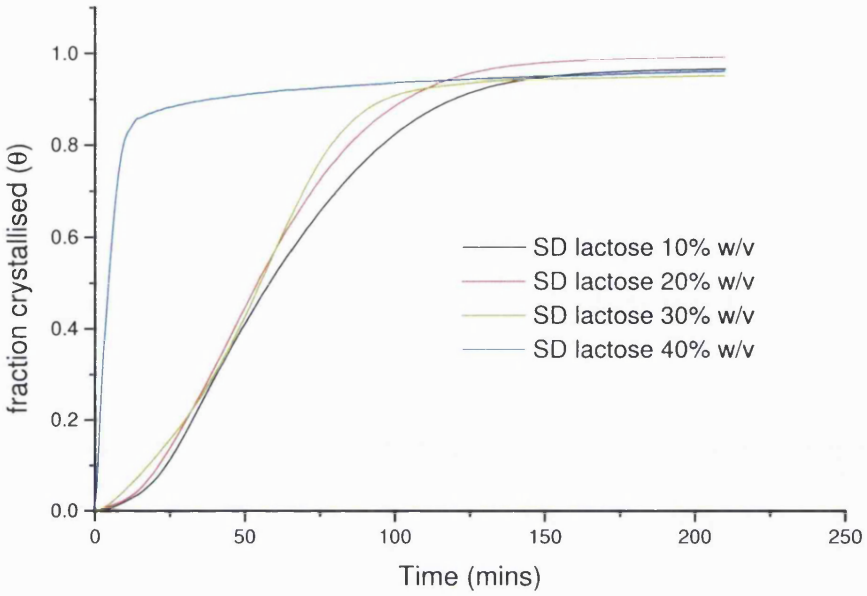

The difference in the shape of the graphs relates to the Avrami index, which describes the nucleation mechanism and number of directions in which growth is occurring (Kedward et al., 1998). In order to determine the index, the data generated can now be plotted using the linearised form of the Avrami equation (equation 3.5) between 30-70% degree of crystallinity, which is read from the above graph.

$$\log_{10}[-\ln(1-\theta)] = \log_{10}K^* + n\log_{10}t \qquad \text{.....equation 3.5}$$

The gradient of the linearised equation provides the value of (n), which can be used in the following rearrangement of the Avrami equation to provide a value of k, the actual isothermal crystallisation rate constant from the gradient of equation 3.6. Fig 3.13 shows an example of the graphs generated for SD lactose product from a 10% w/v feed concentrate.

$$[-\ln(1-\theta)]^{(1/n)} = kt \qquad \text{.....equation 3.6}$$

Fig 3.13. Transformation of DVS data within the region of 30-70% for SD lactose product from a 10% w/v feed concentrate. Graph (a) represents an example of data generated to determine the Avrami exponent (n) from the gradient. Graph (b) is derived from equation 3.6 where the gradient provides a value for k, the isothermal crystallisation rate constant.

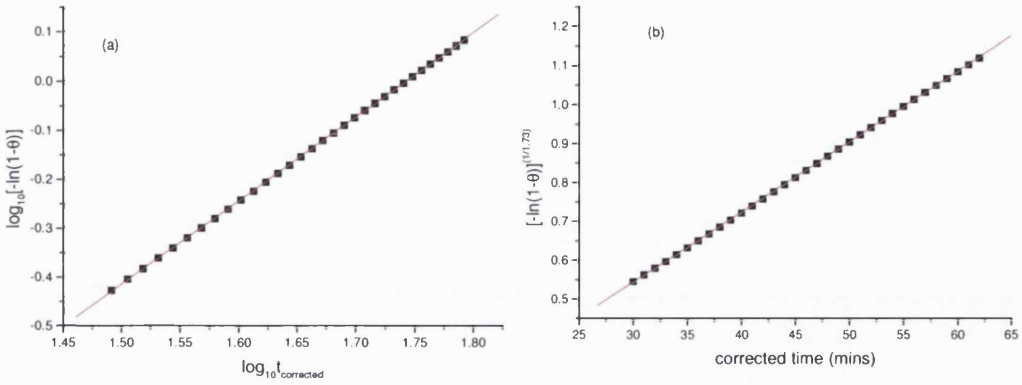

3.6.4.3 The Crystallisation kinetics for SD lactose from different feed concentrates

The overall crystallisation kinetics for SD lactose products from different feed concentrates are summarised in table 3.8. By exposing the samples to 75% RH using the DVS, the sample would be expected to crystallise rapidly. The addition of crystal material as is the case with an increase in the SD product feed concentrate, would be expected to influence the crystallisation process by increasing the rate of crystallisation and also affecting the nucleation mechanism. A change in the SD lactose from different feed concentrate leads to a decrease in (n). Schmitt et al., (1999) found at a low RH (57.5%) a 100% amorphous sample of lactose crystallised by site saturation and a sample which contained crystal seeds crystallised from a fixed number of pre-existing nuclei and that growth of crystals was limited by surface incorporation in both cases.

With SD lactose from 10% feed concentrate (which is 100% amorphous) n is equal to 1.73, which indicates growth from site saturation or from a fixed number of nuclei and in more than one dimension (see table 3.6, De Bruijn et al., 1981). This could be likely at a high RH, as the uptake of water is relatively fast causing supersaturation across the powder bed, an increase in mobility and formation of bridges to form nuclei before growth proceeds. The n values of SD lactose products from feed concentrates 20% and 30% w/v are similar to 10% w/v feed concentrate indicating growth from a fixed number

of nuclei in more than one dimension. SD lactose from feed concentrate 40% undergoes rapid crystallisation and this is reflected in the n value determined, where the approximation to 1 indicates growth from fixed pre-existing nuclei in one dimension.

Table 3.8. A summary of the crystallisation kinetics of SD lactose from respective feed concentrates, represented by the Avrami exponent (n), the isothermal crystallisation rate constant (k), and crystallisation half time ($t_{1/2}$) (n=3).

Lactose Feed concentrate	Avrami exp. (n)	linear fit (R^2)	Rate constant (k) (min^{-1})	linear fit (R^2)	Half–time ($t_{1/2}$) (min).
10%	1.73	1.0	0.0181	1.0	44.2
20%	1.68	1.0	0.0136	1.0	59.6
30%	1.61	0.99	0.0171	0.99	46.5
40%	1.08	0.99	0.1130	0.99	6.7

The isothermal crystallisation rate constant that describes the rate at which crystalline growth proceeds varies between SD lactose products from feed concentrates 10, 20 and 30% w/v. This may reflect the difference in crystallisation into different anomeric forms of lactose, which may affect the crystallisation kinetics and k value. Kedward et al., (2000) showed that a similar situation was arrived and explained that it could be due to different polymorphic forms, which develop during crystallisation. This may also explain why the $t_{1/2}$ calculated for the SD products are different. For SD lactose from a 40% w/v feed the k value is relatively high and this is shown in the $t_{1/2}$ calculated, where the assumption that the material is crystallising to the monohydrate with 50% of the material already a monohydrate and growth proceeding in one dimension. To further support the different rates of crystallisation NIRS taken during crystallisation may be investigated.

3.6.5 NIRS and the study of crystallisation

NIRS produces overtones and combinations, which arise when a sample is excited, most of the absorption bands arise from hydrogen vibrations as described in chapter two, section 2.8.1. It is for this reason NIRS is well suited in studying the interaction of water with compounds. The spectra shown here are SNV-2^{nd} derivative and hence have been mathematically treated as described in section 3.3.6. It should be noted that in the second derivative, only the negative peaks are of interest as they correspond directly with positively displaced peaks in the original spectrum. The aim of studying NIRS in

hyphenation is to follow the crystallisation process in conjunction with DVS and to see whether the NIR can distinguish between the different SD lactose products.

3.6.5.1 The Amorphous to crystalline phase transition.

Having established the crystallisation kinetics, the amorphous to crystalline phase transition of the four SD lactose products was followed using NIR as the DVS cycle proceeds. Lane and Buckton, (2000) have shown that it is possible to follow the crystallisation process of a sample that is 100% amorphous lactose using the hyphenated technique DVS-NIRS. Fig 3.14 (a) shows an example of a DVS profile for SD lactose sample from a 10% w/v feed concentrate, the diagram highlights the points along the profile at which spectra was chosen to be studied (Fig 3.14 (b)).

Fig 3.14(a). An example of a DVS cycle for SD lactose sample from 10% feed concentrate (100% amorphous lactose) and point's a-g which represent the spectra shown in Fig 3.14 (b). Both figures are also representative of SD lactose samples from 20 and 30% w/v feed concentrates.

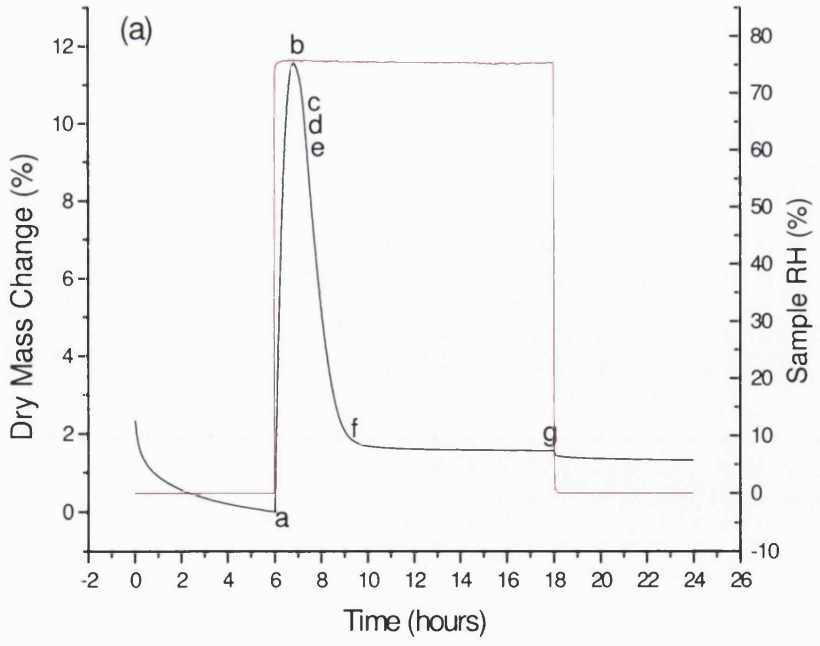

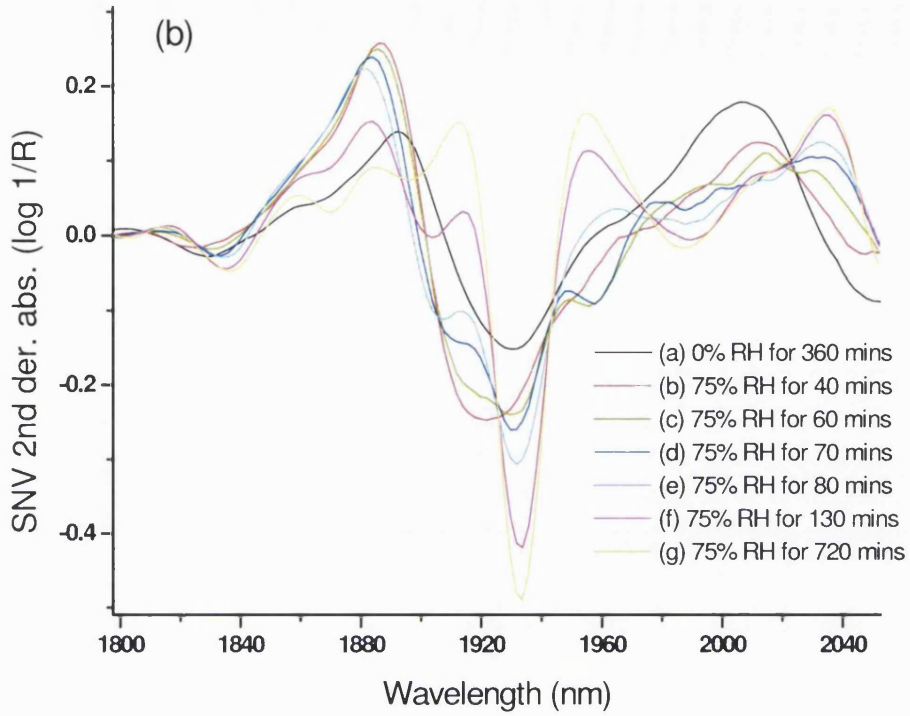

Spectrum (a) is for a dried SD lactose sample as it has been taken at the end of the drying stage, at 360 mins at 0% RH. Spectrum (b) is taken at the maximum point of water absorption, at 75% RH. Spectra (c), (d) and (e) represents spectra along the desorption phase of water at 75% RH which has been described as the region where crystallisation is occurring for amorphous lactose (Makower and Dye, 1956; Elamin et al., 1995; Stubberud and Forbes, 1998; Lane and Buckton, 2000). Spectra (f) at 75% RH represent the end of the desorption phase and finally spectra (g) at 75% RH for 720 mins represents the end of the cycle for 75% RH. The crystallisation of SD lactose sample from feed concentrate 10% w/v (amorphous lactose) is similar to the two feed concentrates 20 and 30% w/v with no visual difference in NIR second derivative spectra. The spectra shown in Fig 3.14(b) are representative of SD lactose from feed concentrates 10, 20 and 30% w/v.

The region of the spectra represented in Fig 3.14(b) is associated with O-H stretch and deformation in relation to water molecules and hence represents hydrate formation of lactose. Spectrum (a), which represents dry amorphous material lactose, is displaced at 1930 nm. The sample absorbs water and the spectra gradually shifts to lower wavelengths 1920 and 1926 nm for spectra (b) and (c) respectively. Multiple peaks form at 1908 and 1956 nm, indicating the onset of crystallisation which shift to higher energy states and

disappear once the crystallisation process is complete. Also during this stage the monohydrate peak becomes more sharply defined from 1926 to 1934 nm and increases in intensity (Buckton, et al., 1998; Lane and Buckton, 2000). The intensity and shape of the peak remains the same once crystallisation is complete by 180 mins with little change in spectra.

However for the SD lactose product from a 40% w/v feed concentrate (Fig 3.15), following the same spectral points along Fig 3.14(a) the monohydrate peak is seen initially and decreases in intensity at 20 and 30 mins with no change in the peak position. After which the peak at 1934 nm increase in intensity (to approximately 80%). The decrease and subsequent increase in intensity may be attributed to the rapid uptake of water preventing the spectral changes seen in Fig 3.14(b) from been observed. There was a slight deformation that occurred at spectrum (b) around 1902 and 1916 nm which disappeared at spectrum (c) to follow a smooth transition through the spectra until crystallisation is complete. By 40 mins the crystalline monohydrate has formed with very little change in the intensity seen after this point.

Fig 3.15. SNV 2nd der. NIR spectra for SD lactose from 40% feed concentrate during the crystallisation process.

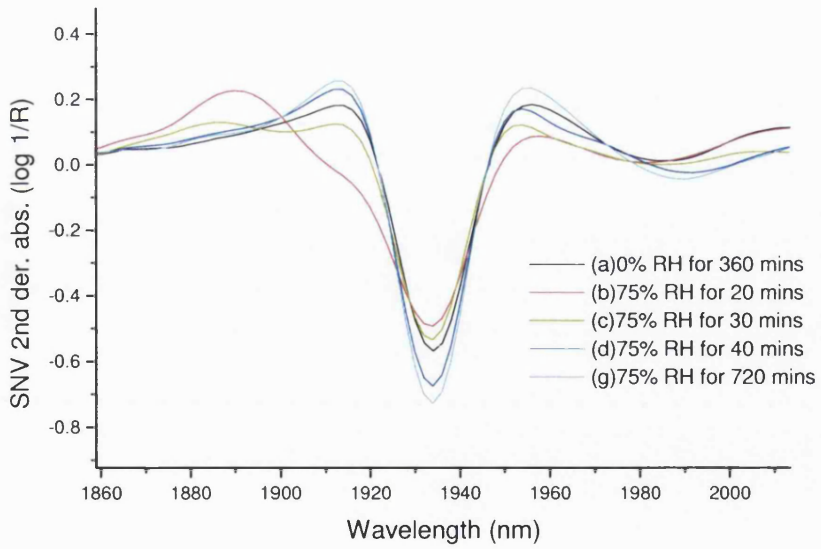

It seems that crystallisation was taking place rapidly with the SD lactose sample from 40% feed because only half the material is amorphous and spectra were taken every ten minutes, the collapse and displacement of wavelengths may have occurred quickly to be

recorded. These results support the data illustrated by the crystallisation kinetics for SD lactose from a 40% w/v feed using the Avrami equation. The isothermal crystallisation rate constant (k) was a relatively high value along with the $t_{1/2}$ which was 6.7mins indicating that crystallisation was occurring at a relatively high rate. The Avrami exponent (n) generated was ~1 which represents one-dimensional growth. The similarity in the crystallisation of SD lactose from a 10, 20 and 30% w/v feeds using NIRS correlates to the crystallisation kinetics generated by each SD product.

3.6.5.2 The Anomeric Region

A study of the spectra, in particular the anomeric region (2075-2160 nm), may provide us with an insight into the anomeric forms which occur during crystallisation for each SD lactose product. In Fig 3.16, an α-peak is seen at 2090 nm which relates to an O-H combination stretch and deformation. The peaks at 2104 and 2126 nm represent β-anhydrous formation that arises from O-H deformation and C-H stretching phenomena (Osborne et al., 1993; Lane and Buckton, 2000).

Fig 3.16. SNV 2nd der. NIR spectra of the anomeric region of SD lactose product from 10% w/v feed concentrate during crystallisation at 75% RH and 25 ℃. The figure is also representative of SD lactose from a 20 and 30% w/v feed concentrate.

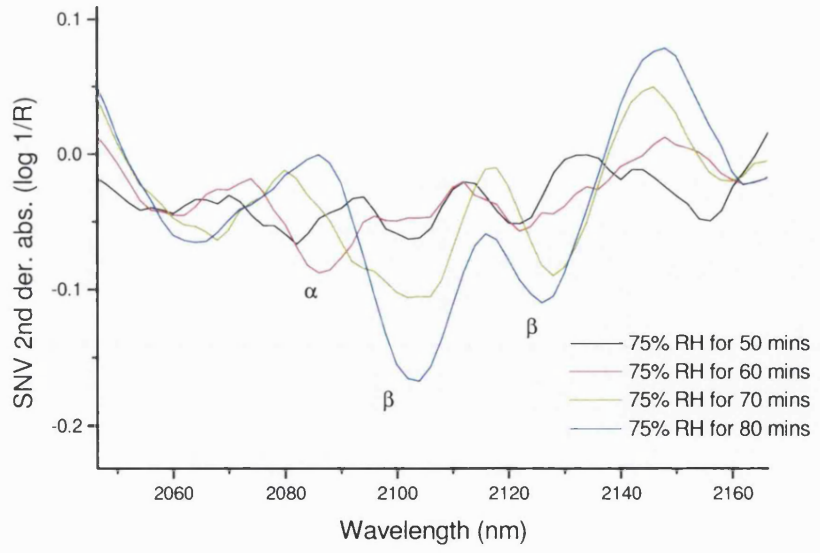

Fig 3.16 illustrates SD lactose sample from 10% w/v feed concentrate crystallising with time at 75% RH, this was similar for the SD lactose samples from feed concentrates 20 and 30% w/v. Following the exposure of 75% RH for 60 mins a peak formed at 2090 nm,

which corresponds to α-formation (Buckton et al., 1998; Lane and Buckton, 2000). At the same corresponding time if we consider the monohydrate region at 1925-1940 nm, the material is in the plasticized state (Fig 3.14(b)). After 70 mins at 75% RH characteristic peaks of NIR absorbance begin to emerge, there is an extra peak at 2126 nm with the peak at 2090 nm been permanently displaced at 2104 nm. These peaks represent β-anhydrous formation (Lane and Buckton, 2000). It is known that amorphous lactose crystallises to a combination of α- and β-forms (Briggner et al., 1994) and that the β-form mutarotates to the α-form under water vapour at high relative humdities (> 94% RH) (Angberg, 1995). It is therefore likely that amorphous lactose collapses to crystallise and form a mixture of α-monohydrate and β-anhydrous and highly unlikely that mutarotation takes place. The initial α-peak at 2090 nm could be due to the exaggerated response of the spectra during plasticization and collapse, which manifests itself as an α-peak. It could also be the emergence of β-lactose which is initially recorded at 2090 nm and progressively moves to its final position at 2104 nm.

For SD lactose from a 40% feed concentrate (Fig 3.17) the sample initially contained a large amount of α-lactose (~ 50%), which was easily detected in the anomeric region and increased in intensity as crystallisation proceeded. The final result indicates that there was no β-lactose in the sample but confirmation with other techniques should be applied as sensitivity of this region has not been reported.

Fig 3.17. SNV 2nd der. NIR spectra of the anomeric region for SD lactose from 40% w/v feed concentrate at 0 and 75% RH.

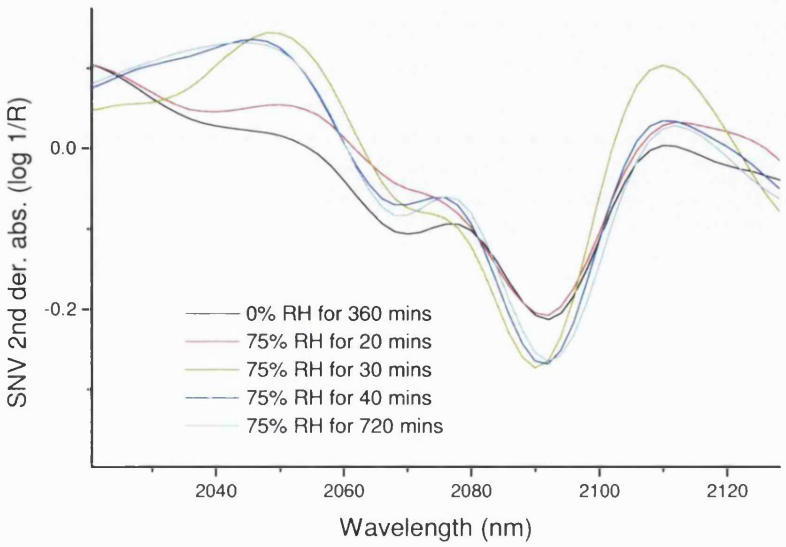

In conclusion, the study of NIR in conjunction with DVS has proved to be valuable in the study of the amorphous to crystalline phase transition. From the study it can be seen that the rapid uptake of water in samples containing a large amount of amorphous content (≥ 89.6%) caused wetting and plasticization to occur. The onset of crystallisation was not detected until desorption of water for ~ 30 mins had occurred (70 mins at 75% RH). This could be due to the sensitivity of the instrument or the actual time taken at which crystal growth and nucleation proceeded to an adequate level to be detected. NIRS also showed that despite the elevated RH for twelve hours, further crystallisation seized to occur after approximately 180 mins. This indicates that for a sample containing a large amount of amorphous material, the phase transition to a crystalline state is not an instantaneous but rather a gradual process. For a sample containing approximately 50% amorphous material, the maximum amount of water absorbed was achieved within 10 mins at 75% RH and crystallisation was complete approximately 40 mins at 75% RH. Any change in spectra after this point was minimal. It was difficult to assess whether crystallisation had began before desorption of water. The spectra collected for this sample was not sensitive enough to the changes occurring in the material due to the rapid crystallisation process and also because the starting material contained 45.3% crystalline material.

3.7. Polyvinylpyrrolidone (PVP)

3.7.1 Chemical and Physical properties of PVP

Polyvinylpyrrolidone (PVP) or Povidone is chemically known as poly(1-(2-oxo-1pyrrolidinyl)- ethylene) which consists of linear polymers of 1-vinylpyrrolidin-2-one. The soluble grades of PVP are obtained by free radical polymerisation of vinylpyrrolidone in water or 2-propanol. A simplified version of polymerisation of the monomer is shown in Fig 3.18, this may be visualised as coupling of the unsaturated alkene chain. The degree of polymerisation can be controlled, but polymers of various molecular weights are still produced and it is this physical property that allows us to characterise polymers. The polymer molecules are composed of between 12 and 1,350 monomer units (Robinson et al., 1990; Kreft, 1999).

Fig 3.18. The structural monomer N-vinyl-2-pyrrolidone which is polymerised to produce the PVP polymer (adapted from Kibbe, 2000).

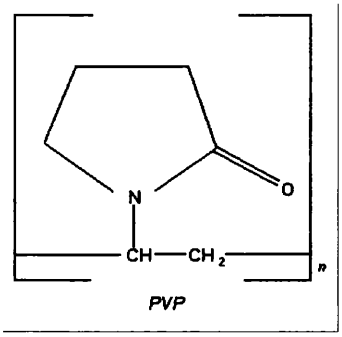

A parameter (K) is assigned to a polymer according to the viscosity of the material in aqueous solution, which is dependent on the molecular weight of the polymer, table 3.9 illustrates this. The K value is calculated using Fikentscher's equation (equation 3.7), where (z) is the relative viscosity of a solution of concentration (c) and (k) is the K-value multiplied 10^{-3} (Robinson et al., 1990; Kibbe, 2000).

$$\log z = c\left(\frac{75k^2}{1+1.5kc}\right)+k \qquad \text{.....equation 3.7}$$

Table 3.9. An example of the K values assigned with respect to the molecular weight of the polymer (adapted from Kibbe, 2000).

K value	Approx weight
12	2500
25	30 000
60	400 000
90	1 000 000
120	3 000 000

PVP is soluble in a variety of organic solvents and also in water, where the viscosity of the resulting solution determines its limit of water absorption. Under ambient conditions the polymer is stable as a solid and in solution, it is relatively inert to chemical modification (Robinson et al., 1990).

3.7.2 Pharmaceutical Applications of PVP

Polymers in general have a wide range of uses in the pharmaceutical industry and PVP is no exception. Its first medical use was in World War II where its was widely employed as a blood plasma substitute and extender. It possessed the advantages of being non-antigenic and required no cross matching. Now the polymer is used in a variety of industries and pharmaceutically it is used in a number of formulations including solid dosage forms, where it functions as a binding agent in tablet formulations and also as a coating agent in the end production. In topical and oral suspensions it is added because of its suspending, stabilising and viscosity properties. The quantity of PVP in a formulation will depend on its function; this is illustrated by table 3.10.

Table 3.10. A summary of the pharmaceutical uses of PVP and the different concentrations.

Pharmaceutical use	Concentration (%)
Carrier for drugs	10-25
Dispersing agent	Up to 5
Eye-drops	2-10
Suspending agent	Up to 5
Tablet binder, tablet diluent, or coating agent	0.5-5

PVP is marketed for its various uses at different average weights ranging from 2,500-1,200,000. K-12, K-15, K-17, K-30 are used for injectable human and veterinary preparations; K-25 and K-30 are used for oral pharmaceutical and food use and topical pharmaceutical and cosmetic use; K-90 is also used for topical and pharmaceutical use. The properties of the polymer also vary according to the average molecular weight (Robinson et al., 1990; Kibbe, 2000).

3.7.3 The Manufacture and Structure of PVP

PVP provides the pharmaceutical industry with a variety of uses and has also been widely studied, however being a polymer it does not present the physico-chemical properties that lactose seems to provide. PVP is a synthetic polymer and exists as an amorphous material that can be manufactured by two ways depending on the molecular weight of the polymer. Values of K lower than 90 are produced by spray drying and exist as spheres, higher K values are produced by drum drying and exist as plates (Kibbe, 2000). The

pharmaceutical grades of PVP are marketed under the trade names Kollidon (produced by BASF, Germany) and Plasdone (produced by GAF, USA). Non-pharmaceutical grades also exist under a variety of names (Robinson et al., 1990).

3.7.4 Characterisation of Polymers

Generally the physical state of a polymer can be amorphous as mentioned above for PVP, or partially amorphous and crystalline. The characterisation of polymers can be conducted in a variety of ways; calorimetric techniques such as DSC, MTDSC and DTA provide information on melting, crystallisation where appropriate and also glass transitions. Mechanical methods such as thermomechancial analysis (TMA) and torsional braid analysis (TBA) provide information on the liquid-liquid transition temperatures. Rheological studies are used to determine the molecular weight of a polymer (Ford and Timmins, 1989). More recently the use of NIR to qualitatively determine PVP has been undertaken by Kreft et al. (1999).

The basic characteristic property reported for polymers is the T_g, this is found in all amorphous polymers and in amorphous regions of partially crystalline polymers. The value of T_g is unaffected by the degree of crystallinity but the magnitude of the transition decreases with an increase in crystallinity. The result is that Tg becomes difficult to detect in highly crystalline polymers (Ford and Timmins, 1989).

A polymer above its T_g is flexible and rubbery, but below this parameter polymers exist as a glass, which can be, described as stiff, hard, brittle and may be of high optical clarity and transparency. The glass transition defines the change in state as explained in previous chapters and is a second order transition as it reflects secondary thermodynamics such as heat capacity and expansion coefficients. For polymers the T_g is governed by three molecular factors. Polymers with a stiff backbone and rigidly held bulky side groups have a high T_g for example polystyrene. The bulky side groups generally restrict polymer movement, whereas polymers that do not contain this entity have a low T_g for example polyethylene. The extent of attractive forces that the polymer chains show is the second factor, which affects the T_g. The higher the attractive forces between polymer chains the higher the T_g. Finally the T_g of homologous polymers of different molecular weights will increase with an increase in the molecular weight. For PVP this can be seen in Fig 3.19, which represents the glass transition as a function of molecular weight (Fox and Flory, 1950; Ford and Timmins, 1989; Robinson et al., 1990).

Fig 3.19. The relationship between the glass transition of PVP and molecular weight of the polymer (adapted from Robinson et al., 1990).

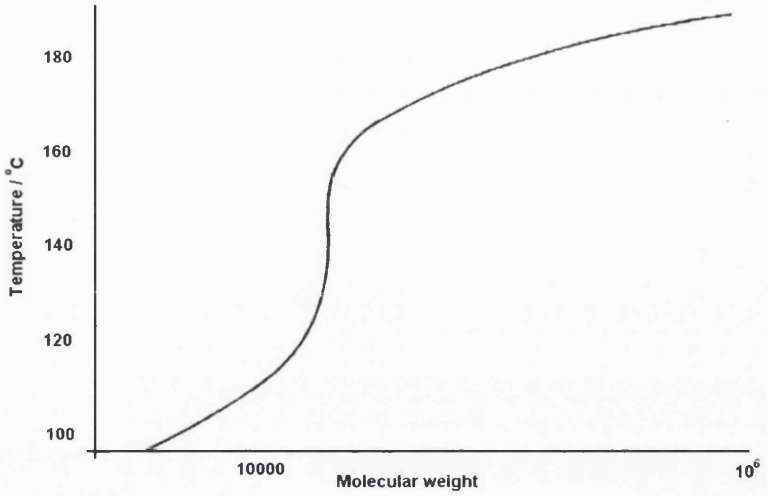

3.8 Material

PVP (K-25) was supplied by GlaxoSmithKline as Kollidon K-25. The material was spray dried at this molecular weight, which is confirmed by SEM (Fig 3.20), where the morphology of the sample is spherical with some fragmentation.

Fig 3.20. SEM of the excipient used as received in this study; PVP K-25.

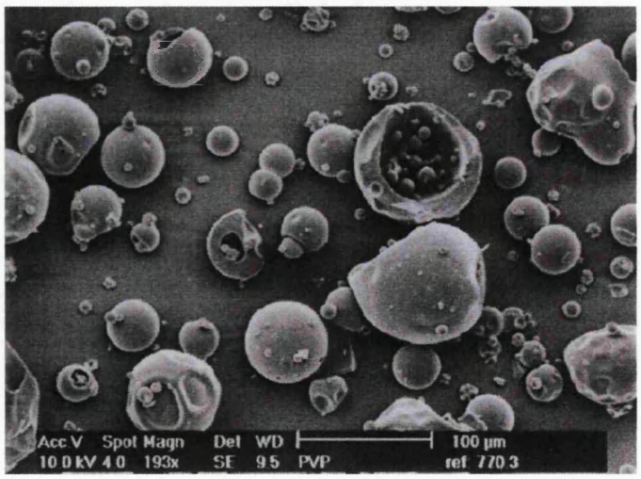

3.9 Experimental Methodology

A step scan DSC was employed to characterise the polymer by determination of the true T_g of PVP (K-25). This was achieved by drying a sample of PVP (100mg weight) at 80°C in a vacuum oven for 5 days. TGA and step scan runs of the sample were conducted throughout this time to determine that the sample was indeed dry, only when the results were repeatable was the material considered dry.

The samples were all heated and cooled approximately 30°C above and 100°C below the T_g in order to erase the thermal history. A third scan was then conducted and the T_g determined. The experimental method used a ramp rate of 2.5°C/min along with an isothermal hold time of 0.4 min (24 seconds). This particular section was repeated until the desired minimum or maximum temperature was reached. The temperature range employed was 50-200°C. The remaining experimental details are listed in chapter two section 2.5.3.

TGA samples of PVP (K-25) were taken to determine the amount of water present before and during storage in the vacuum oven. A sample weight of approximately 10mg was loaded onto a Perkin-Elmer aluminium pan and the experiment run under the conditions described in chapter two section 2.6.4.

TAM and DVS-NIRS were employed to assess the water absorption of PVP (K-25). The experimental conditions applied are listed in chapter two section 2.3.4 and 2.8.4 respectively. The TAM was calibrated at 100 μW.

Light microscopy was employed to assess the morphological change of PVP under the influence of water vapour at 75% RH. The samples were removed from the TAM at the required times and photomicrographs were taken under ambient conditions.

3.10 Results and Discussion

3.10.1 Determination of T_g

Table 3.11. The practical T_g value of PVP K-25 recorded in this study (red) in comparison to reported T_g values in literature (black).

PVP Sample	T_g reported value (°C)	Reference
K-25	Midpoint 172.3 ± 1.5 (n=6)	----
K-15	Midpoint 128	Turner and Schwartz, 1985
K-30	Midpoint 162	Turner and Schwartz, 1985
K-90	Midpoint 180	Turner and Schwartz, 1985
K-90	Onset 178	Shamblin et al, 1998
K-90	177	Okansen and Zografi, 1990
K-90	177	Hancock and Zografi, 1994
K-90	Onset 176	Taylor and Zografi, 1998
K-90	Onset 175	Tan and Challa, 1976
K-90	167.5	Feldstein, 2001

The T_g values of PVP reported in the literature are shown in table 3.11. The majority of results reported correspond to a larger molecular weight polymer, where there is a general increase in the T_g with an increase in the molecular weight (Fox and Flory, 1950; Turner and Schwartz, (1985); Ford and Timmins, 1989; Robinson et al., 1990). The literature results are in good agreement but discrepancies do arise when drying conditions and experimental designs vary. Turner and Schwartz (1985) replicated work by Tan and Challa, (1976) under "careful drying at the highest temperature possible, preferably under a nitrogen blanket. In order to obtain correct T_g values" and reported that "this advice was followed in the present work, but nevertheless, a wide range of T_g values were still obtained" (Turner and Schwatrz, 1985). The experimental T_g result achieved here at 172.3 ± 1.5 (n=6) is within the literature value and was taken after a consistent result was achieved after drying as described in section 3.7.1. Although careful drying was achieved residual water still existed in the polymer at a level of 2.01% ± 0.2 (n=4). Franks (1981) reported this with PVP and referred to the water as "bound" however the residual water would be removed during the step scan run and hence would not affect the T_g value of the polymer.

3.10.2 The study of drying and wetting of PVP using DVS-NIRS

PVP (K-25) is known to spontaneously absorb significant amounts of water from the environment even at low relative humidities. This property of PVP was studied using the

hyphenated technique DVS-NIRS in an attempt to follow the wetting, plasticization and drying of PVP (K-25) spectroscopically.

Fig 3.21. The DVS profile of PVP K-25 at a cycle of 0% RH for 360 mins (6 hours), 75% RH for 720 mins (12 hours) and finally 0% RH for 360 mins.

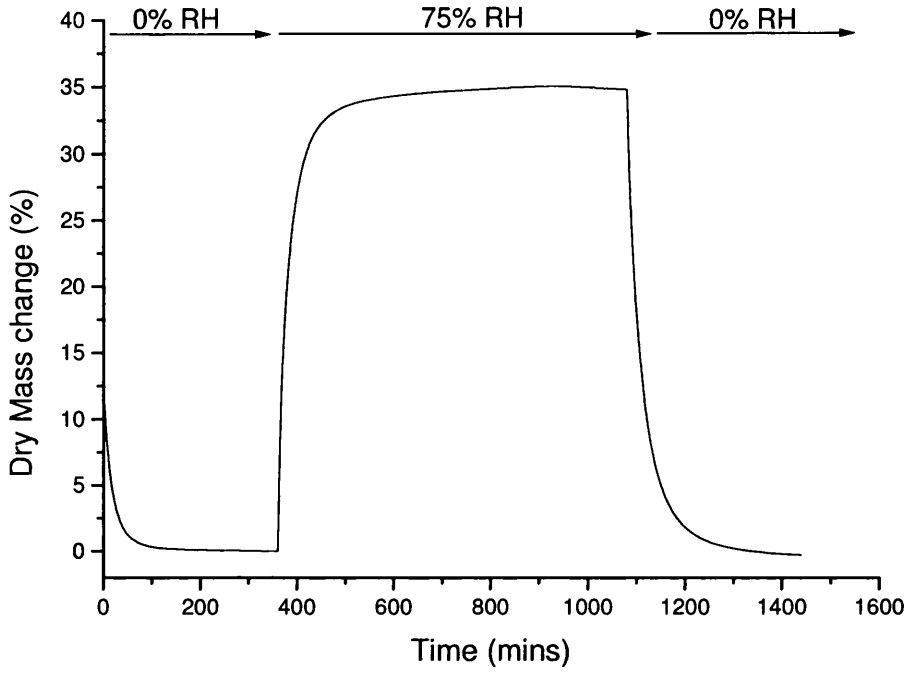

The DVS profile (Fig 3.21) shows that reversible water sorption and desorption does occur with PVP (K-25) and that the maximum water absorbed is 34.4% ± 0.1% (n=3) at 75% RH. This is in good agreement with Stubberud et al. (1996). Removal of water in the initial stage is successful with a plateau reached within 30 mins. Once the RH is increased to 75% RH a rapid uptake of water is achieved during the first 100 mins, after which there is a gradual increase in water uptake to the maximum value. This is similar to first order kinetics where the data can be modelled to exponential growth. At the end of this stage the sample is exposed to 0% RH where the previous rapid uptake of water is mirrored by the rapid removal of water. The DVS profile was further investigated by NIRS at the initial drying stage and during the elevated RH.

3.10.2.1 Drying of PVP (K-25)

The NIR spectra corresponding to the drying of the polymer is illustrated in Fig 3.22 where the most prominent wavelengths are represented. At 1932 nm, this peak relates to first overtone O-H stretch and deformation corresponding to water, the intensity of the

peak decreases with increase in drying with no change in the peak position. This indicates that previously absorbed water by the amorphous structure of the polymer is progressively been removed. At 2006 nm, which relates to C-H combination stretch and deformation, the peak increases in intensity with an increase in drying time and shifts to a lower wavelength 2004 nm. This depicts a change in the median interaction energy and a probable change in the state of water. The readily absorbed water from pharmaceutical processing and storage is removed and it is likely that bound water remains within the system.

Fig 3.22. SNV 2nd derivative NIR spectra during the drying of PVP (K-25) at 0% RH for 360 mins.

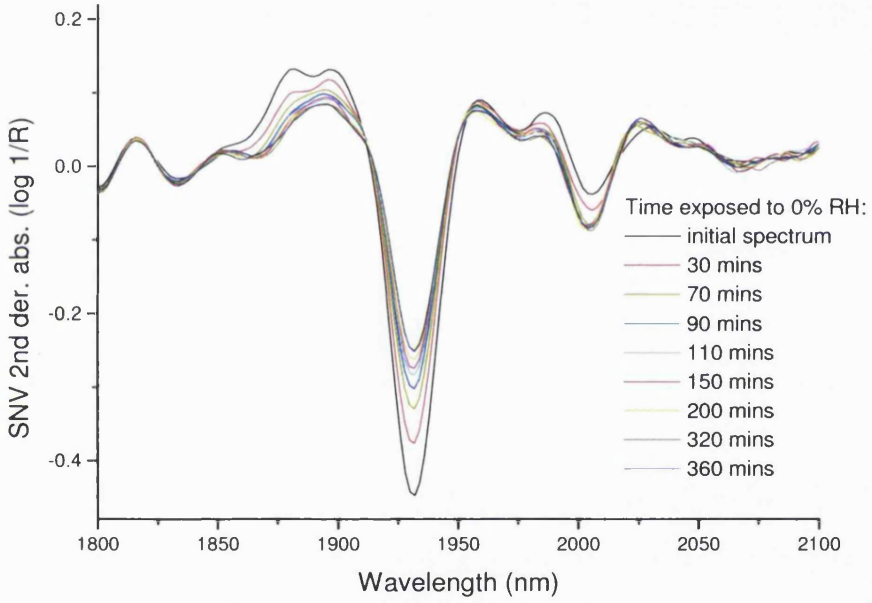

3.10.2.2 Wetting and Plasticization

After the drying stage PVP (K-25) was exposed to 75% RH where the process of wetting and plasticization was monitored. By considering mathematically untreated NIRS (Fig 3.23) there was an upward baseline shift with an increase time exposure to the elevated RH between 10 and 90 mins. After this time there were relatively small differences in the upward displacement of spectra. The change in baseline represents a change in particle size and morphology due to swelling as water is absorbed into the material. If we consider the DVS data alongside this information it is useful to note that the change in particle size and morphology occurs during the rapid uptake of moisture. After this stage

any change in the upward displacement of baseline corresponds to the small increments in moisture uptake (i.e. the change in % dry mass change).

Fig 3.23. Untreated absorbance spectra of PVP (K-25) at 75% RH.

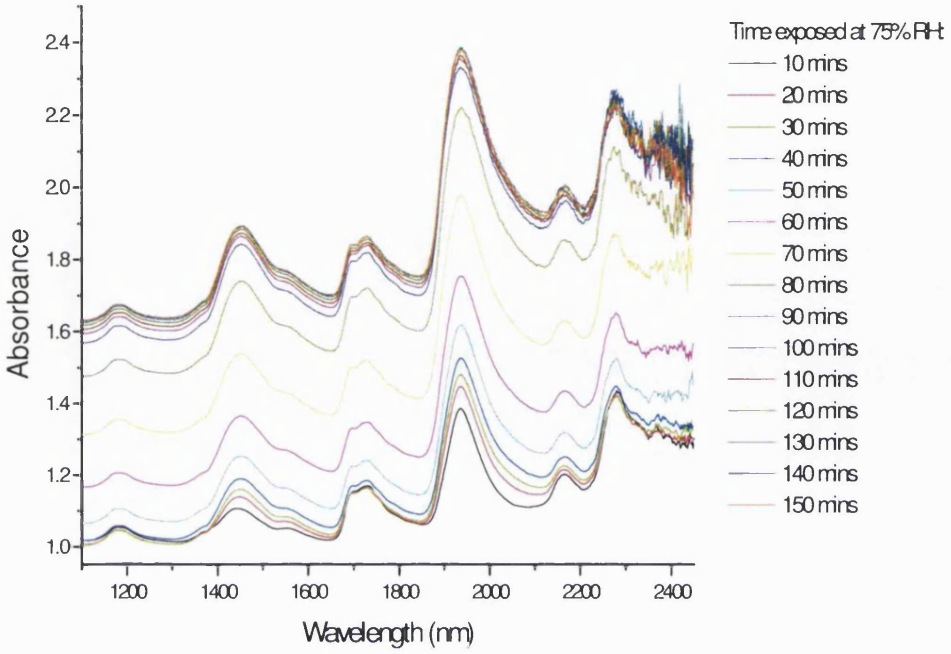

NIR spectra that has mathematically been treated is shown in Fig 3.24 between region 1600 to 1700 nm. The peak occurring at 1692 nm represents a first overtone C-H stretch, where with the increase in water uptake the intensity of the peak decreases but remains in the same position. The uptake of water would be expected to increase the intensity of the peak as seen during drying of PVP (K-25) where peak intensity decreased with removal of water. However at 75% RH PVP (K-25) is involved in a rapid uptake of water in a short space of time that may have prevented the predicted spectral changes from occurring. A study conducted by Lane and Buckton (2000) using the hyphenated technique of DVS-NIRS have also reported a decrease in peak intensity with an increase in water uptake for amorphous lactose at an elevated RH.

Fig 3.24. SNV 2nd der. NIR spectra during wetting and plasticization of PVP (K-25).

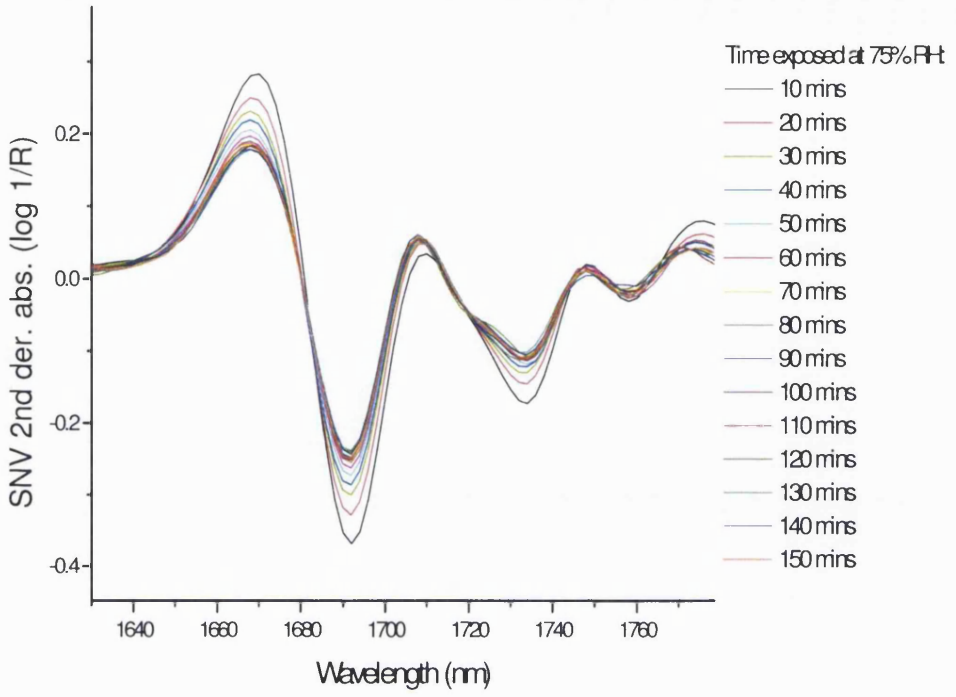

Further along the NIR spectra within the region 1850 and 2000 nm (fig 3.25), a peak seen at 1932 nm represents an O-H stretch and deformation in correspondence to water molecules. This peak decreases in intensity whilst a broad shoulder peak at 1904-1908 nm forms and increases in intensity with time. The formation of the latter peak represents a first overtone O-H stretch and the broad shape indicates that there is a spread of interaction energies and also a change in the energy state of water. From this analysis we can infer that with the increase in water uptake PVP (K-25) is interacting with water molecules, forming hydrogen bonds. This interaction is manifested as a broad shoulder peak at a higher energy state.

Fig 3.25. SNV 2nd der. NIR absorbance spectra of PVP (K-25) at 75% RH, where wetting and plasticization has occurred.

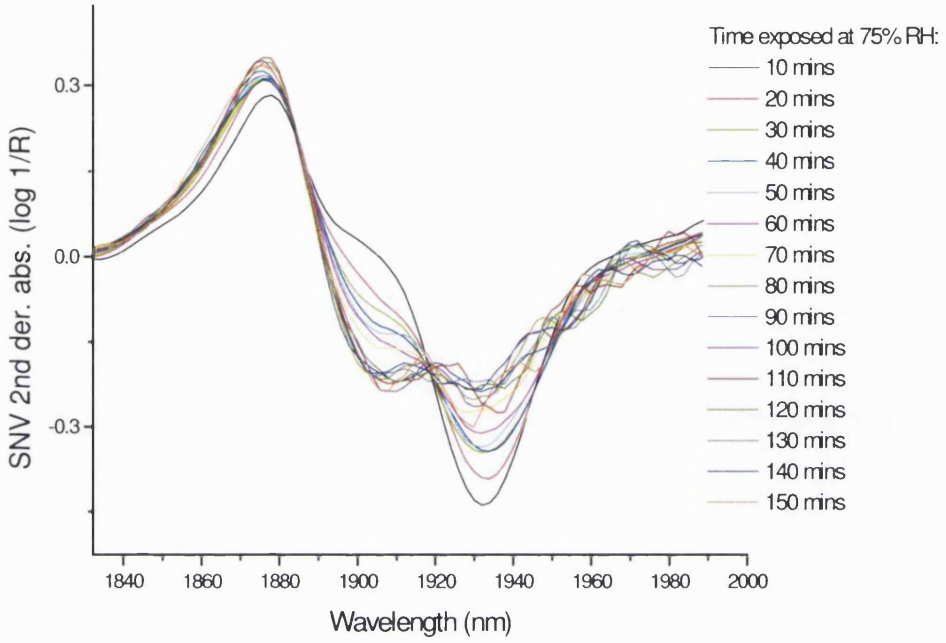

During the process of studying wetting and plasticization of PVP (K-25) using NIRS at some point the T_g of the polymer is suppressed to experimental conditions. This can be calculated and the spectra at which it occurs can be identified. The aim of this process was to see if any changes occurring at T_g can be identified by NIR. Rearranging the Gordon-Taylor equation (equation 3.8) we are able to calculate the % water uptake at which the T_g = experimental T.

$$w_1/w_2 = K\,(T_{g2}-T_{gmix}) / (T_{gmix}- T_{g1}) \qquad \text{.....equation 3.8}$$

Where w_1 and w_2 are equal to the weight fraction of PVP and water respectively; Tg_1 represents PVP (K-25) at 172.3°C (445.3K); Tg_2 represents water at –138 °C (135 K) (Sugisaki et al., 1968); the experimental temperature, which is 25°C (298K) is denoted by T_{gmix}. K is a constant as shown in equation 1.3 (chapter one, section 1.3.6). In this case the density of dry PVP was measured using the pycnometer at 1.23 g/cm^3 this is in good agreement with literature (Hancock and Zografi, 1994) and the density of water is taken as 1.0 g/cm^3. So therefore the calculated K value for PVP (K-25) and water is 4.06.

From this calculation it was found that approximately 22.3% water uptake (18.2% w/w, 30mg sample) was required to lower the T_g of PVP to the experimental temperature. So

therefore the polymer carries on absorbing water regardless of whether the Tg has been depressed to experimental conditions. This illustrates the high affinity that PVP (K-25) has for water. The maximum water uptake of PVP (K-25) was found to be 34.4% as previously mentioned, this suppresses the T_g to -8.53 °C. The increase in water uptake has been reported by Okansen and Zografi (1990) and has been attributed to a change in morphology, where a greater amount of water continues to be absorbed. At this stage the polymer exists with water as a rubbery polymer state. Untreated spectra shown in Fig 3.23 also shows that there is a change in particle size and hence morphology between the rapid and maximum uptake of water.

With the calculated water uptake at 22.3% it was found that T_g was suppressed to experimental temperature at ~25 mins at 75% RH. It follows that those spectra taken at 20 and 30 mins at the elevated RH should be just before and just after T_g = T respectively. Fig 3.26 shows greater differences between spectra taken at 10 and 20 mins that corresponds to the initial uptake of water. Within the region of 1400 nm, the peak occurring at 1434 nm at 10 mins was broadened and displaced to 1440 nm by 40 mins. This represents a combination of C-H stretches and deformation of the polymer structure. The shoulder peak (which has already been mentioned in Fig 3.25) between 20 and 40 mins at ~1908 nm begins to form. Various other changes along the NIR spectra are occurring but none coincide with the T_g of the polymer equating to the experimental temperature. Thus NIRS is unable to identify whether the T_g of the polymer has been surpassed.

Fig 3.26. SNV 2nd der. NIR spectra taken just before and just after the Tg of the polymer are equal to the experimental temperature (T_g = T).

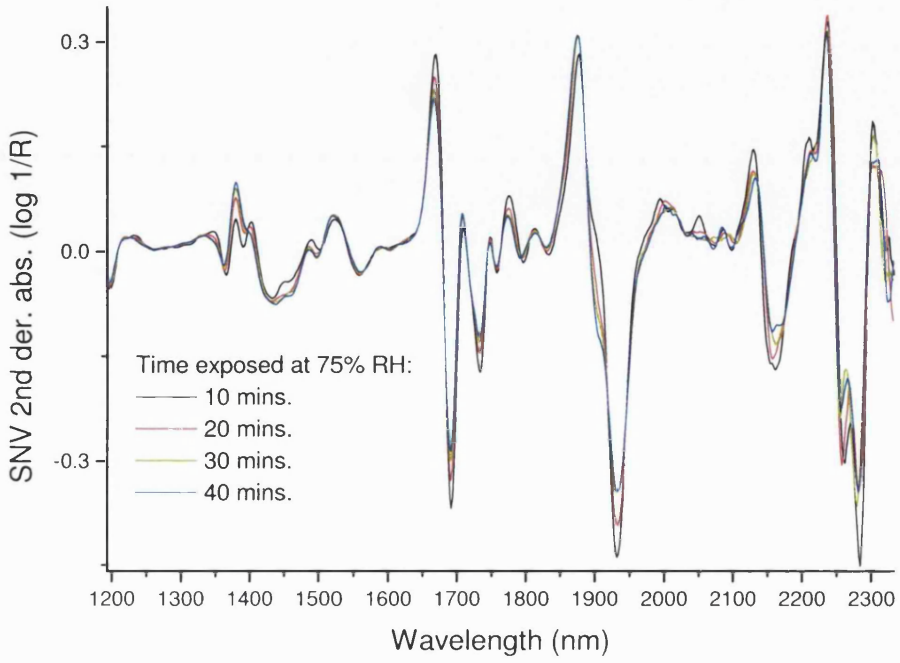

3.10.2.3 Drying PVP (K-25) from Wetting

After assessing the NIR spectra through the glass to rubber transition, PVP was dried for 6 hours, at this stage the last spectrum taken at the end of the 1st drying cycle and the 2nd drying cycle were compared. A comparison would confirm that no physical transition has taken place. Fig 3.27 shows untreated NIR spectra where a baseline shift is the difference between spectra. This could be attributed to insufficient drying of the polymer or the particle size and morphology. A comparison with the initial spectrum of the experiment where the sample has a greater amount of residual water would indicate that the difference in baseline can be attributed to irreversible change in the particle size and may also be due to a change in the physical particle morphology.

Fig 3.27. Untreated NIR spectra for PVP (K-25); the initial spectrum of the experiment; the final spectra from the first and second drying cycle.

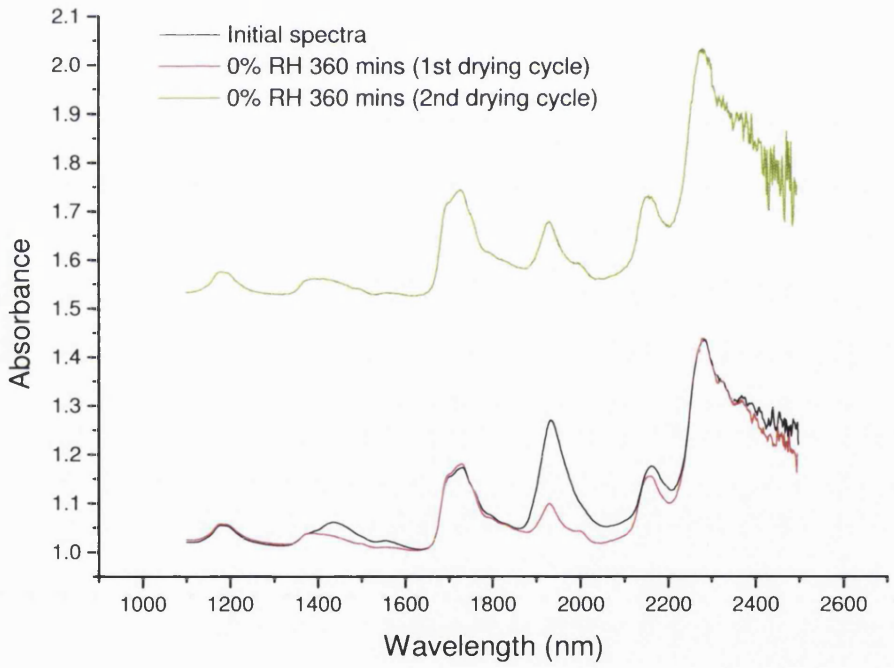

3.10.3 Isothermal Microcalorimetry: The Wetting Response

The wetting of PVP was studied using isothermal micorcalorimetry, it was observed from previous experiments that PVP produced a large wetting response relative to lactose, this can be seen in Fig 3.28 which shows phase I of the TAM graphs of PVP samples with different mass. The exothermic response increased with an increase in weight.

Fig 3.28. The TAM wetting response of PVP as a function of sample mass.

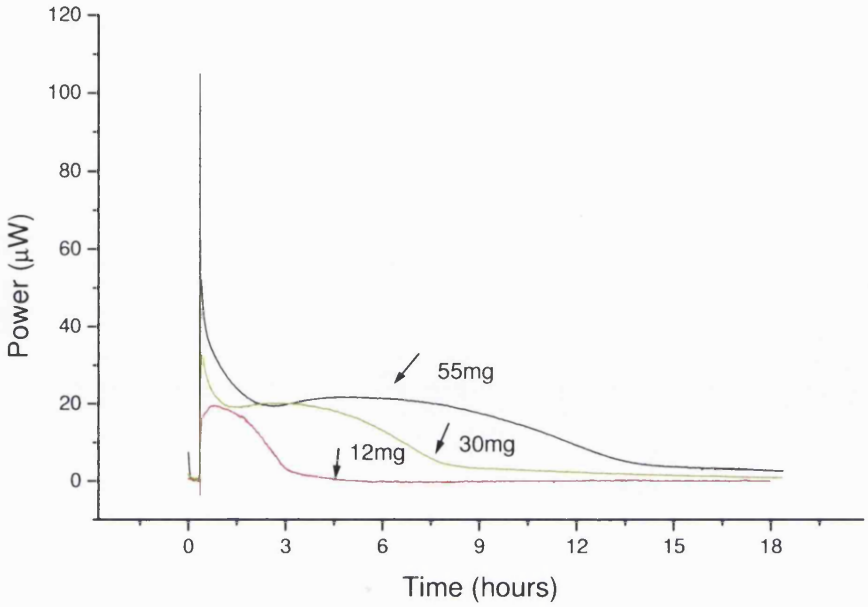

One material that has responded in the TAM this way is raffinose (Hogan and Buckton, 2001), where it was determined that this could not solely be due to a wetting response but to increased mobility of molecules. From Fig 3.28 it seems that some changes are taking place at approximately 2 and 7 hours of a 30 mg sample. To investigate this light microscopy was employed to study any morpohological change that may be occurring. The sample was removed from the TAM at set times along the thermograph: 0, 2, 3, 5, 7, 9, 24 hours for a 30mg sample.

The micrographs (Fig 3.29) over the period of time investigated show a subtle change in the morphology, there seems to be a slow transition from a "near" perfect sphere to a fragmented shape at the end of 9 hours, which is when the thermograph returns to an elevated pseudo-baseline (protratcted baseline). During the course of this time up to 18 hours the material has converted to a viscous material and hence the gel like appearance shown in Fig 3.29 (e).

Fig 3.29. Light microscopy of PVP K-25 (a) before experimental run and removed from the TAM at 75% RH (b) 3 (c) 5 (d) 9 (e) and 18 hours for 30mg samples.

(a)

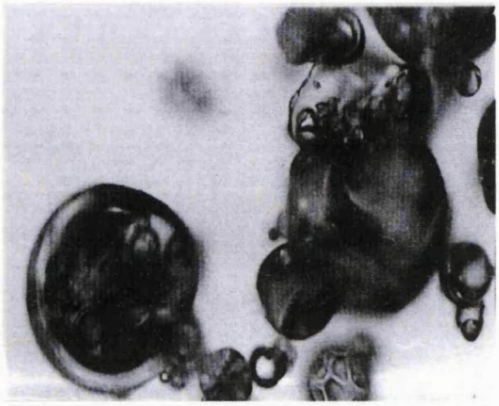

(b)

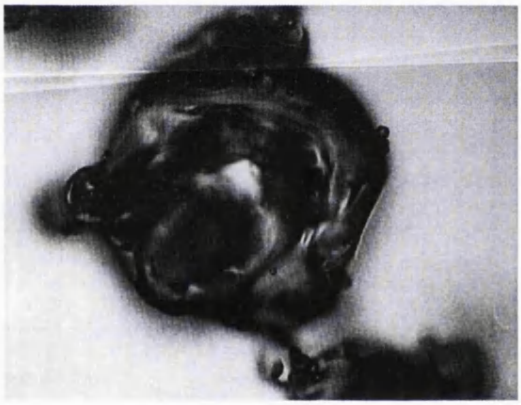

(c)

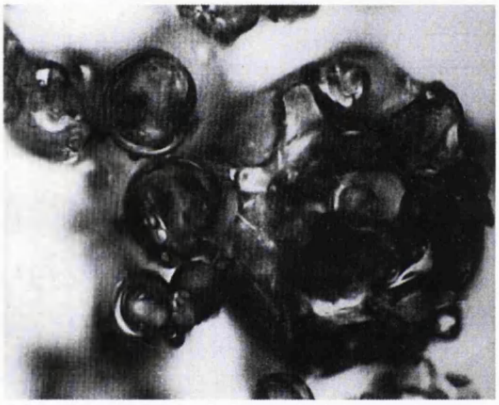

(d)

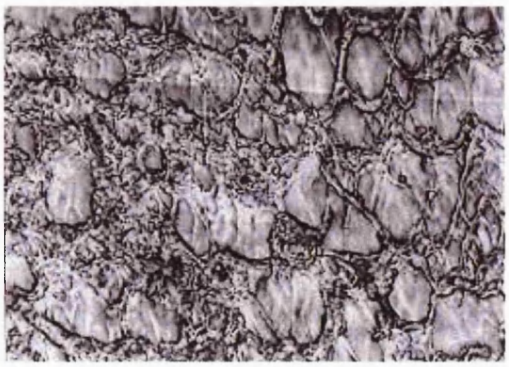

(e)

The micrographs seem to confer that the polymer is absorbing water during this phase and that distortion of the PVP structure is a result of this, although it is a slow and gradual process, which is partly due to the mini hydrostat providing a slow uptake of water. In terms of visual appearance there is no change in the creamy-white fine powder until it converts to the rubbery gel material.

The water uptake during the chosen experimental times was also investigated, to confirm that the polymer was indeed taking up water. The sample was removed at appropriate times and analysed using the TGA under the conditions outlined in section 3.6.4. These values were then used to determine at what point along the trace is the T_g depressed to the experimental value. Table 3.12 represents the sample type and (%) water absorbed and the calculated T_g values using the Gordorn-Taylor equation (equation 1.3, chapter one, section 1.3.6).

Table 3.12. The (%) moisture uptake of water during various points along the TAM graph of PVP (K-25) at 75% RH and the calculated Gordon-Taylor equation (equation 1.3, pg 17) values (n=3) for 30mg samples.

Sample	% TGA absorbed water con.	T_g (°C)
PVP @ RT (stored)	12.5% ± 0.29	67.5
PVP at 75% RH @ 2hrs	16.3 ± 0.28	48.2
PVP @ 75% RH @ 9hrs	18.6 ±0.44	38.1
PVP @ 75% RH @ 18 hrs	24.7 ± 0.40	16.2

The T_g of PVP (K-25) is suppressed to the experimental temperature between 9 and 18 hours, once the graph has returned to "baseline". In this case it is likely that the graph generated by PVP relates to the wetting, morphological change and increased mobility of the polymer, which are enthalpy changes that are detected by the TAM.

3.11 Sodium Dodecyl Sulphate (SDS)

3.11.1 Physical and Chemical Properties of SDS

Sodium dodecyl sulphate (SDS) is classified as a surface-active agent or a surfactant. This group of excipients have unique properties that are characterised by their chemical structure and their tendency to accumulate at the boundary between two phases. The chemical structure exists of two basic regions; one hydrophobic segment which usually consists of a saturated and unsaturated hydrocarbon chain. The hydrophilic portion is the second portion which can be termed anionic (- charge) cationic (+ charge) or nonionic (polar). Once this information is known surfactants are sub grouped according to the hydrophilic nature of their structure. SDS is an anionic surfactant and its basic structure is represented below.

Fig 3.30. The structure of SDS.

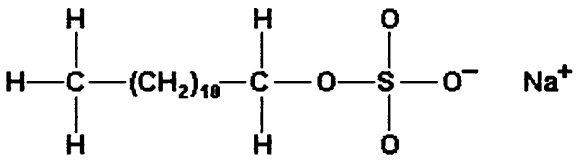

SDS is a material that is not hygroscopic but is freely soluble in water. The anionic surfactant is produced by sulphation of the lauryl alcohol, which is then followed by neutralisation with sodium carbonate. Hence under degradation conditions SDS hydrolyses to the lauryl alcohol and the sodium bisulphite (Kibbe, 2000).

3.11.2 Micelle Formation

When a surfactant molecule dissolves in a liquid medium because of its dual nature, one part of the molecule will be freely soluble in the medium whilst the other part is relatively insoluble. In order for the system to stabilize the insoluble moiety migrates to the interface leaving the soluble segment within the medium. Hence the molecule is said to adsorb onto the interface. This leads to a reduction in the surface tension of the liquid, which facilitates the miscibility of the two opposing phases for example, oil and water.

Another property of surfactants is the ability to form micelles. The reduction of surface tension has been established and can be reduced as the concentration of the surfactant increases as more surfactant molecules enter the surface or interfacial layer. Once the surface and layer is saturated another mechanism by which shielding of the insoluble segment occurs is by formation of spherical aggregates called micelles (Aulton, 2002).

3.11.3 Pharmaceutical Applications of SDS

The pharmaceutical applications of surfactants are based on the hydrophilic and hydrophobic segments. The lowering of interfacial tension is desired for emulsion formation. The wetting of an insoluble compound can be achieved by adsorption onto solid surfaces. Solubilisation occurs whereby a water-insoluble substance is brought into the aqueous medium by incorporation into micelles. The main uses of SDS are shown in the table below at various concentration levels. Other industries for example domestics and cosmetics also extensively use surfactants on a daily basis (Aulton, 2002).

Table 3.13. A summary of the pharmaceutical applications of SDS (adapted from Kibbe, (2000)).

Pharmaceutical Use	Concentration (%)
Anionic emlusifier	0.5-2.5
Detergent in medicated shampoos	~ 10
Solubiliser in concentrations > cmc	>0.0025
Tablet lubricant	1-2
Wetting agent	1-2

3.11.4 Characterisation of Surfactants

The characterisation of surfactants is normally conducted based on their physico-chemical characteristics. In the case of SDS many literature reports are based on the ability of the surfactant to lower the surface tension of materials and the formation of micelles, where the determination of the enthalpy of formation of micelles is the aim (Mysels, 1986; Volpe and Filho, 1995).

3.12 Experimental Methodology

3.12.1 Automated Wilhelmy Plate Method.

The purity of SDS (Sigma, > 99% pure) was determined using the automated wilhelmy plate method. Concentrations of SDS (mM) were chosen and the surface tension determined and compared to literature. The experiments were conducted at 24°C (room temperature) and calibrated with water and chloroform (table 3.14).

Table 3.14. The surface tension measurements for water and chloroform achieved for the calibration of the automated Wilhelmy plate in comparison to literature values.

Component	Surface tension Values (mNm^{-3})	
	Practical	Literature
Water	72.7	72.8
Chloroform	25.4	25.4

3.13 Results and Discussion

3.13.1 Determination of SDS Purity

Measuring the surface tension of a material is an indication of how pure the sample is. If there are any contaminants present they will weaken the bonds between the homogenous molecules in the bulk and also at the surface, which will manifest itself as a lowering of the surface tension of the material.

Table 3.15. A summary of the surface tension values of SDS at various concentrations and the comparison to literature.

SDS conc. (mM)	Surface tension (mNm^{-3})	Literature
0.12	68.2	71.0 Patel, (1999)
2.12	54.8	---
4.0	45.8	48.4-52.5 Mysels, (1986)
8.56	37.5 (0.2)	38.9(0.3) Patel, (1999)

The results are compared to literature, which deviate slightly, the main reason for this is that many of the authors purify SDS before commencing any study by means of foaming (Mysels, 1986; Patel, 1999). However in this study the use of SDS is limited to its exerting effects in a binary system, as long as the substance is not completely impure, the material can be used.

3.14 Conclusions

Lactose was investigated using four different feed concentrates in order to determine the amorphous content and the crystallisation process using the techniques provided prior to the addition of a second excipient. SD lactose from 10, 20, 30, and 40% w/v feed concentrates were found to yield different amounts of crystalline and amorphous material based on the amount of material in solution. The amorphous content decreased with decreasing lactose concentration in solution (% w/v). From the SD samples, it was found that SD lactose from a 30% w/v feed produced a product which contained a greater amount of amorphous lactose than was predicted from the percentage in solution. This

was due to a combination of factors including the atomising pressure during spray drying, the milling effect between particles and the low feed pump rate.

The amorphous to crystalline phase transition was followed successfully using DVS-NIRS, where the crystallisation kinetics determined using DVS and spectroscopic differences between the SD products showed a correlation. It was found that SD lactose from feed concentrates 10, 20, and 30% w/v crystallised in a similar time and manner from the isothermal crystallisation constant, Avrami index and NIRS. The absorption and plasticization, followed by collapse and crystallisation was observed by spectroscopy. SD lactose from a 40% feed concentrate contained a substantial amount of crystalline material (~46.4%) and hence crystallised rapidly with little change in the spectra occurring.

The wetting and plasticization of PVP (K-25) was followed using the DVS-NIRS and the TAM, where it was found that neither technique could detect the glass transition. However NIRS was successfully able to follow the change in particle size, the wetting and plasticization of PVP (K-25) where both the untreated and mathematically treated spectra were used in conjunction. The TAM data along with light microscopy and TGA data showed that the exothermic response observed was due to wetting and change in molecular mobility and particle morphology.

Chapter Four

Lactose and PVP K-25

4.1 Introduction

To date the combination of lactose and PVP has not been studied in detail. Both are abundant and commonly used materials which have been studied as single and in the case of PVP in binary components with other compounds. There are many pharmaceutical formulations where the addition of a sugar and polymer play a significant role. For example the interest in the formulation of peptides and proteins requires both a sugar and polymer to stabilise the system. It is believed that the glassy state of these excipients protects the conformational change of the proteins and inhibits the unfolding and aggregation of the macromolecules (Carpenter and Chang, 1996). The maintenance of the amorphous (glassy state) as described above is important in many pharmaceutical and non-pharmaceutical formulations. It is the aim of this chapter to study the stability of amorphous lactose under the influence of ascending PVP concentration. Both SD and PM products of the polymer and disaccharide have been investigated to help understand the behaviour of these binary systems.

4.1.1 Lactose

One of the few studies which have been conducted and which prompted this work is by Chidavaenzi et al., (2001). Spray granulates of lactose and polyethylene glycol (PEG 4000) at various concentrations of diluent and polymer were investigated. The authors reported that the polymer caused lactose to crystallise during the spray drying operation and so crystalline composites of lactose were produced, regardless of the concentration of PEG 4000. Corrigan et al., (2002) extended the work and found that some amorphous material was produced when lactose and PEG 4000 are spray dried simultaneously but explained this as a result of the difference in the spray drying parameters. Finally the combination of lactose and PVP (K-25) has been studied as a physical mix using DVS to assess the water absorption of the mixture by Stubberud and Forbes, (1998). This short study showed that lactose delayed the onset of crystallisation by acting as an internal desiccant.

4.1.2 PVP

PVP is a model polymer that has been used for the stabilisation of amorphous materials as described in section 4.1 and where appropriate in the enhancement of solubility of poorly soluble drugs. It has been reported that over 60 drugs have been dispersed in the polymer (Simonelli et al., 1969; Corrigan et al., 1985; Ford, 1986). The combination of PVP along with other disaccharides such as sucrose and trehalose has been researched (Shamblin et al., 1996; Zheng et al., 2001; Zhang and Zografi, 2001). The use of PVP as a model for protein in formulations has also been studied; this is based on its structural features as well as its behaviour. The polymer shows similarities to proteins via interactions with small molecules and its solubility in water (Molyneux, 1985).

A property of PVP, which has been widely documented in literature, is its effects on crystallisation of a compound when added as an excipient. Depending on the compound PVP has been shown to inhibit, retard or have no effect on the crystallisation of materials, for example Sekikawa et al., (1978) showed that PVP inhibits or retards crystallisation of sulfisoxazole, sulfmethizole, and sulfamerazine but has no effect on the crystallisation of nalidixic acid and caffeine. Other literature reports have shown that PVP inhibits the crystallisation of indomethacin and sucrose either spray dried or as a co-precipatate formulated by lyophilization (Corrigan et al., 1985; Yoshioka et al., 1995; Shamblin et al., 1996). The effects of PVP on the crystallisation of compounds are summarised in table 4.1 it should be noted that this is by no means a comprehensive list.

From the results (table 4.1) shown PVP can influence materials in a variety of ways. It has also been deduced that the mechanism by which PVP exerts its effects on certain materials is by hydrogen bonding which forms between the binary systems. The antiplasticizing property of PVP also plays a role by absorbing water and hence acting as an internal desiccant (Yoshioka et al., 1995; Shamblin et al., 1996; Taylor and Zografi, 1997; Taylor and Zografi et al., 1998; Shamblin et al., 1998). It is for these reasons that PVP is also known as a stabilising agent, based on its ability to hold a material in its amorphous state for a period of time and hence raise the Tg of a material.

Table 4.1. The effects of PVP on the crystallisation of materials.

Material	the effects of PVP on crystallisation			Reference
	inhibits	retards	no effect	
Sucrose	✓ >1%	x	x	Shamblin et al., (1996)
Indomethacin	✓ >5%	x	x	Imaizumi et al., (1983), Corrigan et al., (1985) Yoshioka et al., (1995)
Caffeine	x	x	✓	Sekikawa et al., (1978)
Nalidixic acid	x	x	✓	Sekikawa et al., (1978)
Sulfamethizole	✓ 0.01%	✓ <0.01%	x	Sekikawa et al., (1978)
Sulfamerazine	x	✓ <3%	x	Sekikawa et al., (1978)
Piroxicam	x	✓	x	Tantishaiyakul et al., (1999)
Ibuprofen	x	✓ > 50%	✓ < 50%	Corrigan et al., (1985) Broadhead et al., (1992)
Ketoprofen	x	✓ > 50%	✓ < 50%	Corrigan et al., (1985) Broadhead et al., (1992)
Ketoconazole	✓ 10%	x	x	Van den Mooter et al., (2001)
Hydroflumethiazde	x	✓ > 1%	x	Corrigan and Holohan, (1984)

SECTION A: Amorphous lactose And PVP K-25

4.2 Experimental Methodology

4.2.1 Sample preparation of lactose and PVP SD and PM products

The starting materials α-lactose monohydrate and PVP (K-25) were used to produce the SD products of varying concentrations. α-lactose monohydrate was weighed at 10g and added to a 100ml conical flask. PVP (K-25) was then added at a concentration of 5, 10, 25 and 40% w/w (by weight of lactose). The materials were made up to 100ml using distilled water. A Buchi 190 mini spray dryer was used to spray dry the solutions. The experimental spray drying parameters used have been discussed and listed in detail in chapter two (section 2.2.1). All of the powder recovered from the process was weighed,

with the percentage yield shown in table 4.2. The results show that there is a general increase in the amount of SD product with an increase in PVP content. The samples were stored over P_2O_5 at 0% RH.

Table 4.2. The (%) yield for each SD product under identical spray drying conditions (average of 6 results).

Sample (w/w)	(%) yield
Amorphous lactose	10.0
+ 5% PVP (K-25)	14.9
+ 10% PVP (K-25)	17.9
+ 25% PVP (K-25)	21.4
+ 40 PVP (K-25)	25.2

The PM products were produced by weighing ~ 1.5 grams of SD amorphous lactose, PVP (K-25) was then added at 5, 10, 25 and 40% w/w (by weight of lactose). Both samples were passed through a 425 μm sieve prior to mixing. The samples were placed in a glass vial (3g capacity). A turbula mixer was then used to mix the binary blend at 480 rpm for approximately 20 mins. The samples were then stored in a desiccator at 0% RH.

4.2.2 Experimental Techniques

For the characterisation of the SD and PM products of lactose and PVP (K-25), DSC, PXRD, and SEMS were employed. The experimental methodologies for these latter techniques are listed in chapter two under the relevant subheadings of each analytical tool. The Tg of the SD products was determined using step scan DSC, for which the experimental methodology is listed in section 2.5.3. A sample of the SD product (70 mg weight) was stored at 80°C in a vacuum-oven (~ 40 m Torr) for approximately five days. TGA and step scan runs of the sample were conducted throughout this time to determine that the sample was indeed dry. Density measurements of amorphous lactose and PVP (K-25) were obtained using pyconometry and used in the calculation of Tg. To complete the characterisation process FTIR was employed to assess hydrogen bonding between the dissacharide and the polymer for both the SD and PM products.

Crystallisation of SD and PM systems was induced using the TAM and DVS, which was achieved by using water vapour at 75% RH. The quantification of amorphous content and the onset of crystallisation were determined using the TAM. The crystallisation kinetics

to investigate the nucleation and propagation phases was established using the DVS data and the Avrami equation. NIRS in combination with DVS was employed to follow the amorphous to crystalline phase transition of the SD and PM products. NIRS was also employed to quantify the amount of polymer within the SD and PM systems at various physical states. The experimental methodology for these techniques can be found under section 2.3.4 and 2.8.3 for both the TAM and DVS-NIRS respectively.

After crystallisation characterisation of the SD and PM products was determined using DSC, TGA, and GC. The aim of this exercise was to establish the nature of the crystalline state of lactose and whether PVP had influenced the final crystalline composition. This part of the study was also carried out to lend support to other findings observed during the crystallisation of the SD and PM products using the TAM and DVS-NIR. The experimental methodology was described in chapter two, section 2.4.4, 2.6.4 and 2.10.3 for DSC, TGA and GC respectively.

4.3 Results and Discussion

4.3.1 Characterisation of SD products prior to crystallisation

In chapter three the characterisation of the excipients and how they behave under experimental conditions was investigated. It is hoped that this work will help provide an understanding and explanation of how lactose and PVP behave when combined as a binary system. Initially the characterisation of the SD and PM products prior to crystallisation was conducted using PXRD and DSC.

4.3.1.1 PXRD and DSC

Once the binary systems had been spray dried, they were checked for their amorphous content using PXRD. It was found that all four spray dried products were amorphous in nature with no crystalline content within the detection limit of the instrument. This was confirmed with an amorphous halo as shown in Fig 4.1 for amorphous lactose and the addition of 40% PVP (K-25), SD products containing 5, 10, and 25% w/w PVP (K-25) also showed identical diffractograms.

Fig 4.1. PXRD for (a) amorphous lactose and (b) + 40% w/w PVP (K-25).

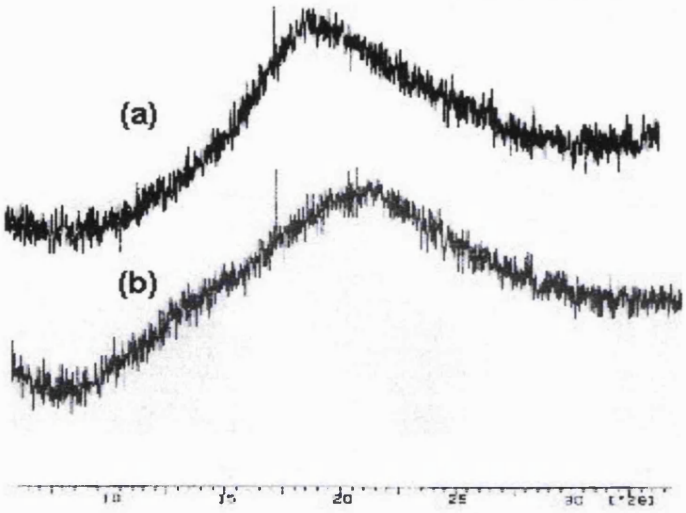

In chapter three, section 3.6.1 amorphous (amo.) lactose was investigated using the DSC, where the material was confirmed amorphous by an exothermic peak at ~180°C which represents crystallisation of the amorphous material, followed by melting of the alpha form ~ 210°C which corresponds to literature (Lerk et al., 1984). The addition of PVP at ascending concentration affected the crystallisation of lactose as can be seen in fig 4.2

Fig 4.2. The DSC thermographs of (—) amo. lactose alone (this thermograph is also representing SD products containing amo. lactose and PVP (K-25) 5 and 10% w/w), (—) + 25 % and (—) + 40% PVP (K-25) SD.

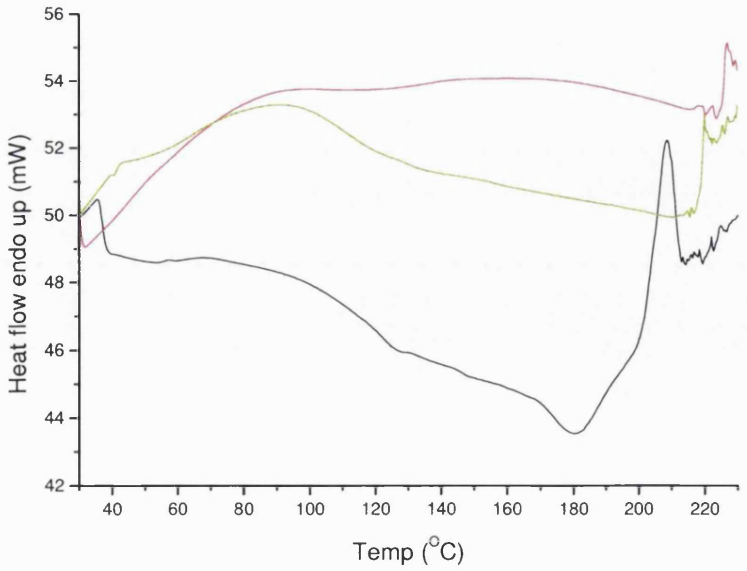

The addition of 5 and 10% PVP (not shown) produced an identical DSC trace to amorphous lactose alone. At higher concentrations of PVP (K-25) (25 and 40%) DSC thermographs showed no crystallisation peak at ~180°C. The results were compared to PM of amorphous lactose and PVP (K-25), which showed that crystallisation of amorphous lactose, was occurring regardless of the concentration of the polymer in the binary blend.

Fig 4.3. A DSC trace of amorphous lactose and PM of PVP (K-25) at 10 and 40% w/w. 5 and 25% w/w of PVP (K-25) are similar to the thermographs below.

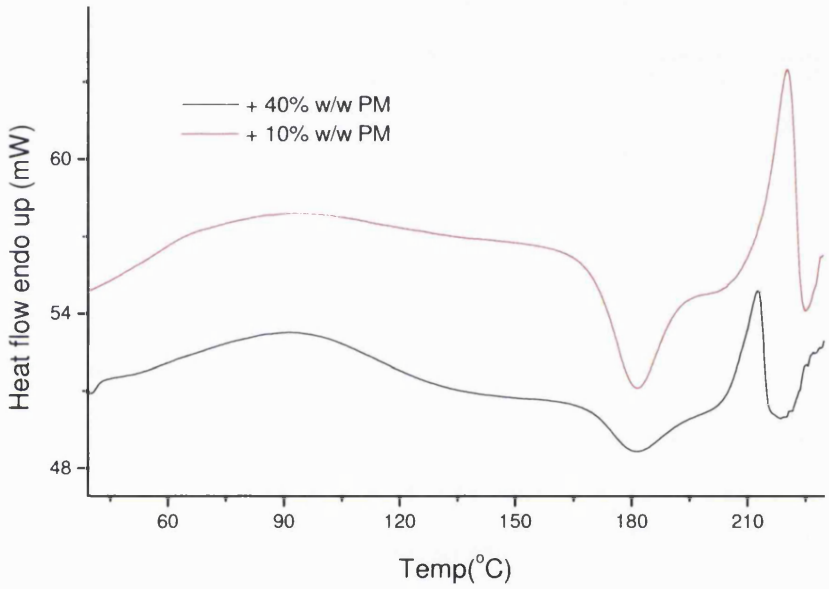

To further investigate the absence of crystallisation for co-spray dried lactose and PVP at higher concentrations, TGA and PXRD were employed. The experimental techniques were used as it was very difficult to retrieve the crimped sample after an experimental DSC run. A sample was placed in open aluminum pans in the TGA under the same operating conditions as the DSC. After the TGA run the sample was placed in the PXRD to check the physical state and whether crystallisation had occurred.

The diffractogram for the SD products investigated showed an amorphous halo (Fig 4.4) hence the material had not undergone crystallisation and still remained in the amorphous state. From the result it seemed that the SD products of amorphous lactose and PVP (K-25) at higher concentrations (25 and 40% w/w) were relatively stable to heat. However isothermal conditions were applied using DSC to see if amorphous lactose would crystallise.

Fig 4.4. The X-ray diffractogram for amorphous lactose and 40% PVP (K-25) SD at the end of a TGA run replicating DSC experimental conditions.

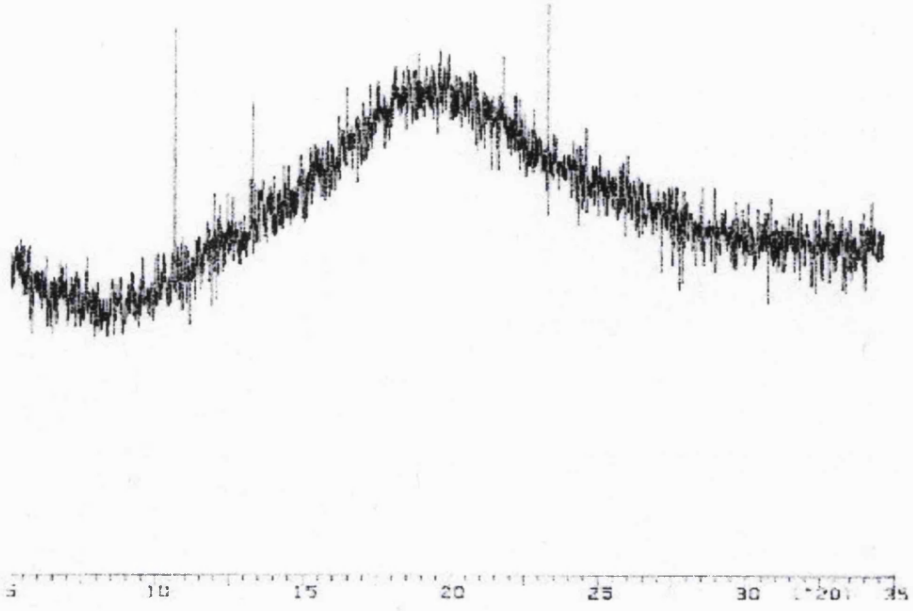

Isothermal crystallisation was achieved by heating the samples with an initial ramping rate of 200°C/min. to 160°C. The samples were then held isothermally until crystallisation occurred. For both concentrations of polymer (25 and 40%) the SD samples were seen to crystallise within ~ 5 mins (Fig 4.5).

Fig 4.5. A DSC thermograph of amorphous lactose and PVP 40% SD. The sample was held isothermally at 160 °C.

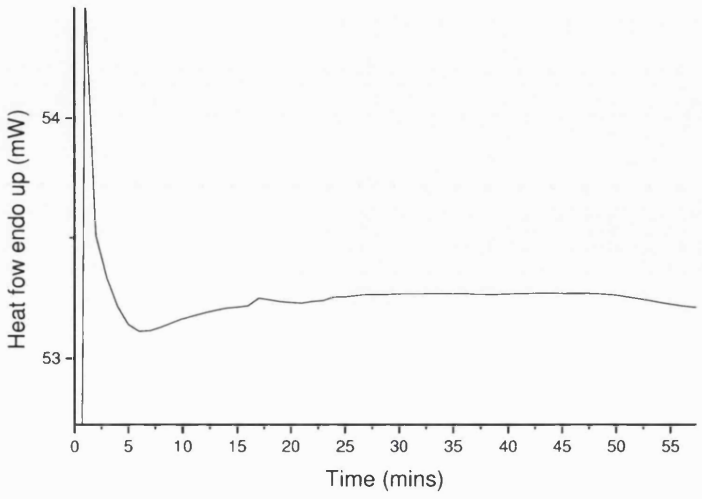

From this investigation crystallisation of amorphous lactose does take place at higher concentration of PVP (K-25) but was delayed. A better insight into the effects of PVP on amorphous lactose and crystallisation is the employment of isothermal microcalorimetry, where the delay and even the inhibition of crystallisation can be determined.

4.3.1.2 SEMS

SEMS of amorphous lactose and SD binary products were taken to determine any morphological changes. There also seemed to be a correlation between the DSC results and the micrographs as seen in Fig 4.6.

Amorphous lactose produced perfectly formed discrete spheres as did the products where 5 and 10% PVP (K-25) were added, which are not shown. The addition of 25 and 40% PVP (K-25) lead to products where the PVP and lactose molecules have agglomerated to form "pitted" and shriveled particles. The agglomeration of particles has also been reported between PVP and indomethacin at higher concentrations, and it was also found that there was a delay in the crystallisation of the drug with an increase in PVP content (Corrigan et al., 1985).

Fig 4.6. A comparison of SEMS for (a) amo. lactose and (b) 25% PVP (K-25) (c) 40% PVP (K-25).

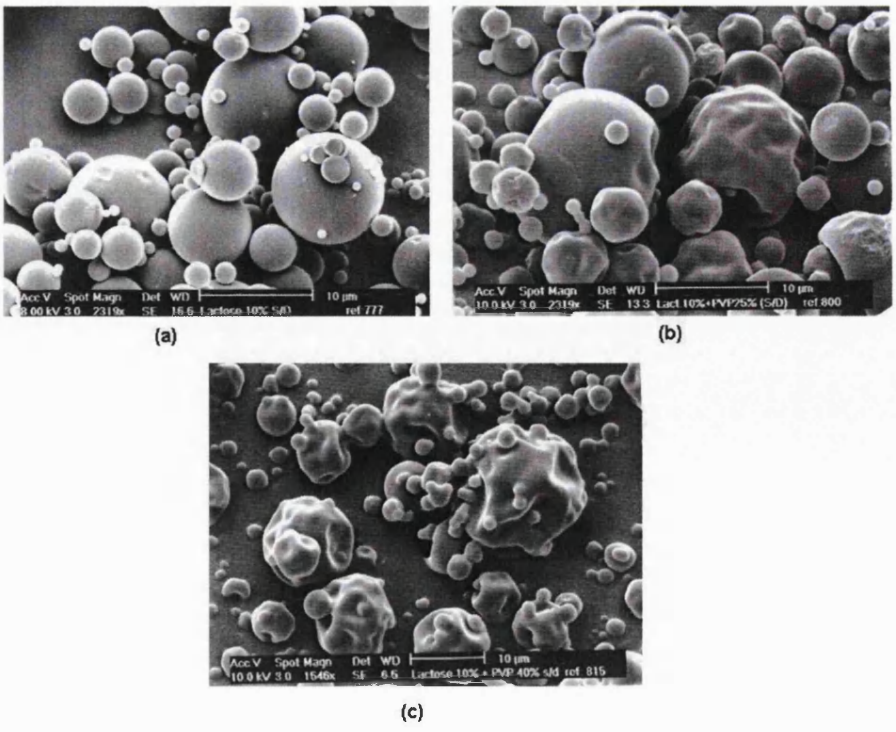

4.3.1.3 Determination of T_g

With the addition of PVP (K-25) to amorphous lactose the glass transition of the diluent will be affected so step scan DSC was employed to investigate this. The T_g's were determined for SD products of amorphous lactose and PVP (K-25). Table 4.3 summarises the experimental T_g's of the single and binary components. All T_g values quoted were taken at midpoint.

Table 4.3. A summary of the experimental heat capacities (ΔC_p) and glass transition temperatures (T_g) of the single and binary SD products of amorphous (amo.) lactose and PVP (K-25) (n=6).

Sample/ (w/w)	ΔC_p (J/g/°C)	T_g (°C)
Amo lactose	0.487 ± 0.048	115.9 ± 0.7
+ PVP 5%	0.450 ± 0.056	116.4 ± 0.6
+ PVP 10%	0.442 ± 0.035	116.7 ± 0.3
+ PVP 25%	0.430 ± 0.036	119.6 ± 0.9
+ PVP 40%	0.340 ± 0.013	123.5 ± 0.9
PVP (K-25)	0.253 ± 0.032	172.3 ± 0.5

The T_g of amorphous lactose has been determined as 115.9 °C ± 0.7 this is in keeping with recent literature values, of 114°C and 116°C (onset value: Taylor and Zografi, 1998; Hill et al., 1998; Schmitt et al., 1999). Previously a dry T_g value of amorphous lactose has been quoted as 101°C (Roos, 1993) and 104°C (Elamin et al., 1995). A recent study on the T_g of amorphous lactose (Brooks et al., 2001) showed that the difference between high and low values of T_g result from the use of non-hermatically and hermatically sealed sample pans. The use of hermatically sealed pans lead to low values of T_g for lactose, which was also found to retain a residual moisture content of ~1% when equilibrated over phosphorus pentoxide. The high values of T_g were obtained by using non-hermatically sealed pans where the residual water could be removed. As part of this study non-hermatically sealed pans were used. The residual moisture content of the SD products were also determined after drying and are shown in table 4.4.

Table 4.4. A summary of the residual moisture content of SD products of amorphous lactose and PVP (K-25) and their single counterparts after drying in vacuum oven under conditions described in section 4.2.2 (n=4).

Sample	% TGA residual moisture cont. after drying.
Amo lactose	1.31 ± 0.09
+ PVP 5%	1.46 ± 0.12
+ PVP 10%	1.53 ± 0.15
+ PVP 25%	1.81 ± 0.12
+ PVP 40%	1.90 ± 0.19
PVP	2.01 ± 0.2

All SD samples showed one glass transition temperature, which indicates that all the samples are a homogenous mix and they also showed a T_g that was reproducible for all steps of the method indicating the removal of residual moisture during the scans (Nair et al., 2001). Fig 4.7 shows step scan data for amorphous lactose and PVP (K-25) 40% w/w and the reproducibility of each step scan. This was seen for all single and binary component systems.

Fig 4.7. Step scan data for amo. Lactose and 40% PVP (K-25).

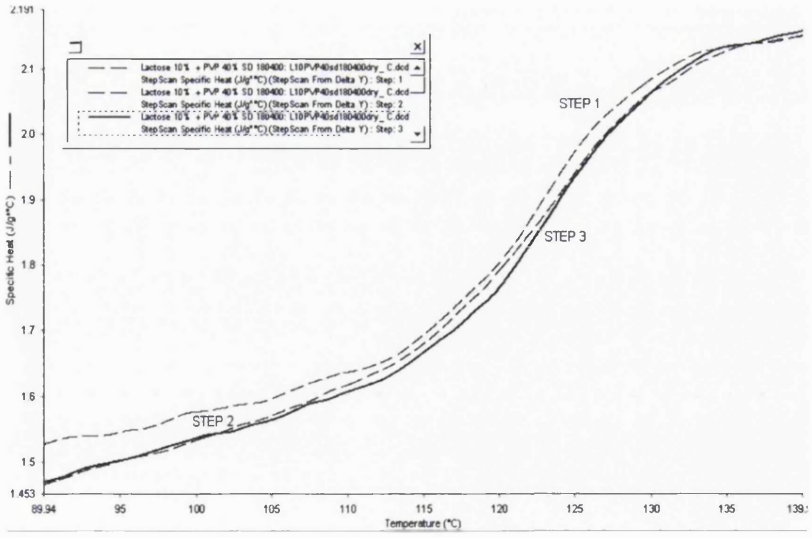

Table 4.3 shows there was a general increase in the T_g of the SD products with an increase in PVP (K-25) content. However at low concentrations of PVP (K-25) (5 and 10%) the T_g values are similar to amorphous lactose alone. This trend was also seen for colyophilised systems of amorphous sucrose and PVP (K-90) (Shamblin et al., 1996).

The increase in T_g could be due to a number of reasons; the increase in viscosity of the SD system with an increase in PVP, which would lead to a reduced mobility of lactose molecules (Ahlneck and Zografi, 1990; Shalaev et al., 1995) An increase in viscosity can also be related to a decrease of free volume in the system, which relates to the molecular size of PVP. This volume would be reduced with the addition of a high molecular weight polymer such as PVP (K-25). However, Hancock and Zografi, (1997) described how the addition of small amounts of a macromolecule to an amorphous sample of small molecular size would produce excess free volume to the system because of its much larger molecular size. The effect would be that the glass temperature of the system would not be elevated greatly. At lower concentrations of PVP (K-25) (5 and 10%) this effect was seen where there was very small deviation from the T_g of amorphous lactose. Finally, a specific interaction between the heterogeneous components may have occurred (usually hydrogen bonding (H-bond)). At high concentrations of PVP the effect of hydrogen bonding is increased as more PVP is present and there is also a decrease in the free volume which may have raised the T_g of the system. These are all possible reasons that can be investigated theoretically (see below) and experimentally.

The specific heat capacities of the SD samples (table 4.3) were also determined at the glass transition, where there was a decrease in the value with an increase in polymer concentration. This indicates an increased rigidity because of the large polymer structure (which is a strong glass former) and so molecular mobility at the glass transition is restricted (Hancock et al., 1995). The change in the specific heat capacity during the T_g transition for the single components can also be compared to literature, from which there is a good correlation for amorphous lactose with a value of 0.472 J/g/°C (Hancock and Zografi, 1997) and that of PVP 0.26 J/g/°C (Shamblin et al., 1998).

A number of theoretical equations have been used to generate values that can be compared to experimental values to assess whether any interactions have occurred within the binary SD product and also free volume effects. In recent years many studies have been conducted in this way, Nair et al., (2001) compared T_g studies using the Gordon-Taylor equation (Gordon and Taylor, 1952) and studies of FTIR using PVP (K-90) and various pharmaceutical drugs. Feldstein (2001) also used various equations to assess the bond interaction between PVP (K-90) and short chains of PEG 400.

All the equations that are used in the analysis were derived from ideal polymer blend systems, however this has not limited their use outside this field. With regards to lactose

and PVP (K-25) it is interesting to note that the binary SD product can be perceived as a polymer blend. Using the rule of thumb that the ratio of the melting temperature to glass transition temperature (T_m/T_g) is greater than 1.5, the sample can be classified as a strong glass former and resemble a high polymer in its thermomechanical properties (Slade and Levine, 1988). The ratio of Tm/Tg for lactose is ~1.8 (210/115.9) from experimental data and may be regarded as a polymer for the use of the following equations, which have been derived for polymer blends.

The Gordon-Taylor equation (Gordon-Taylor, 1952) described briefly in chapter one, section 1.3.6 was used to calculate the T_g for the SD products and compared to the experimental values. This provides us with an indicator of the strength of bonding in the binary systems. Deviation from ideal behaviour has been attributed to differences in the strength of intermolecular interactions between the individual components and those of the combined system. If the binary system has a higher T_g than expected, this indicates a stronger binding for the heterogeneous mix, this is because the stronger binding lowers the molecular mobility. Alternatively if there is a negative deviation from the calculated Gordon-Taylor values, this would indicate that there is stronger binding for homogenous molecules than a heterogeneous mix (Shamblin et al., 1996; Nair, et al., 2001; Van der Mooter, et al., 2001).

$$T_{gmix} = (w_1T_{g1}) + (Kw_2T_{g2}) / (w_1 + (Kw_2)) \qquad \text{.....equation 1.3}$$

where w_1 and w_2 represents the weight fractions of the components and K is a constant which can be calculated from the density (ρ) and T_g of each individual component.

$$K = (\rho_1T_{g1}) / (\rho_2T_{g2}) \qquad \text{.....equation 4.1}$$

The density measurement of dry amorphous lactose and PVP (K-25) were found to be 1.54 and 1.23 gcm^{-3} respectively both are in good agreement with literature (Kibbe, 2000; Hancock and Zografi, 1994). These values were determined using the pyconmeter under the experimental conditions listed in chapter two, section 2.11.3. The K value was then determined to be 1.09 where component 1 and 2 are amorphous lactose and PVP (K-25) respectively.

Where the densities are approximately equal for both components the Gordon-Taylor equation as shown in literature (Hancock and Zografi, 1994) can be modified to the Fox equation (1950) equation 4.2.

$$1/T_{gmix} = w_1/T_{g1} + w_2/T_{g2} \quad \text{.....equation 4.2}$$

where w_1 and w_2 are weight fractions of amorphous lactose and PVP respectively. T_{g1} and T_{g2} are the glass transition temperature of each component.

This equation is routinely used for synthetic and semi-synthetic polymers plasticized with water where the density ratios are approximately unity. However for low molecular weight glass materials such as pharmaceutical drugs and sugars the difference in density between water and the material will be significant (Hancock and Zografi, 1994). However in the case of dry amorphous lactose and PVP (K-25) the ratio of densities is approximately unity (~1.25) so this equation can be used to assess the experimental values along with the theoretical values and also compare with the Gordon-Taylor equation. In both equations (1.3 and 4.2) the assumption that the volume (weight fractions) of both components is additive. Also both equations are generally recognised to hold for miscible polymer blends with weak intermolecular interactions (Feldstein et al., 2001).

The Couchman-Karasz equation (equation 4.3) (Couchman and Karasz, 1978) is an equation, which is a modification of the Gordon-Taylor equation taking into account the heat capacities of the components in a mix at their respective glass transition. It assumes that the thermodynamics of mixing of both components is a combinatorial process. A negative deviation from the ideal (a negative deviation between the theoretical and experimental values) would indicate that mixing is not random between components (Shamblin et al., 1998). This could be extrapolated to bonding between heterogeneous molecules being weaker than the homogenous species. A positive deviation would indicate the opposite. Hancock and Zografi (1994) explain that several authors have found this equation to be useful for describing the plasticizing effect of low molecular weight materials in film forming samples.

$$Tg_{mix} = (w_1 T_{g1}) + ((\Delta C_{p2}/\Delta C_{p1})\, w_2 T_{g2}) / (w_1 + ((\Delta C_{p2}/\Delta C_{p1})\, w_2)) \quad \text{....equation 4.3}$$

Where ΔC_{p2} and ΔC_{p1} represent the heat capacities of PVP (K-25) and amorphous lactose respectively. The ratio of heat capacities is equivalent to a constant, which has the same meaning as the Gordon-Taylor equation.

Fig 4.8. A change in T_g as a function of amorphous lactose (w/w) in SD products with PVP (K-25). (■) experimental values, (●) calculated Gordon-Taylor values (▲) calculated Fox values (▼) calculated Couchman-Karasz values. (—) Kovacs critical temperature (T_c)

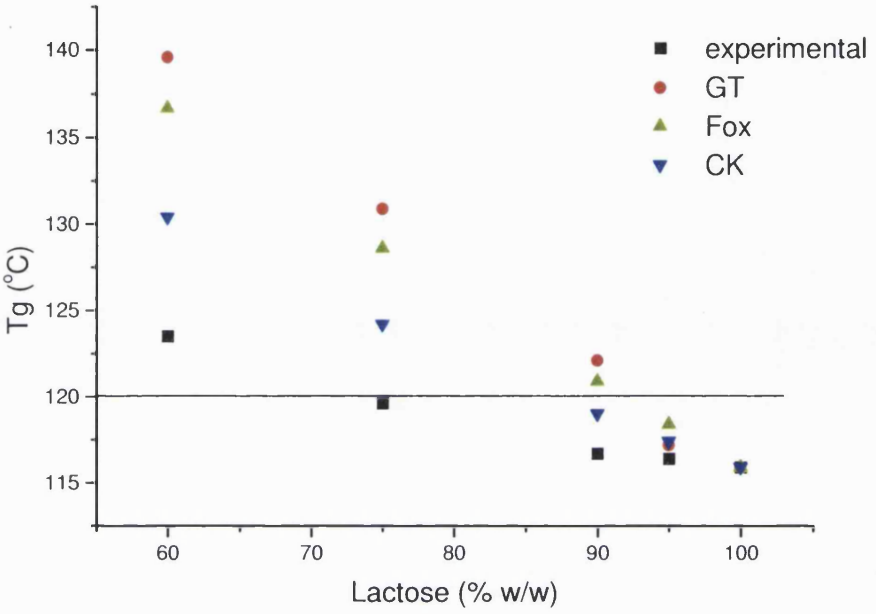

The results showed a negative deviation from the calculated values, which increases with increase in PVP content hence indicating in all cases that the bonding between lactose and PVP (K-25) was weaker than the interaction between like species. The Gordon-Taylor equation seemed to produce the highest theoretical results followed by the Fox and Couchman-Karasz equation respectively.

In terms of the different equations, the Gordon-Taylor equation (Gordon and Taylor, 1952) is based on the assumption that the volume fraction of each component is a completely additive affair. Except for 5% PVP (K-25) there is an appreciable difference between the experimental and calculated values.

The Fox equation (Fox and Flory, 1950) is based on the same assumption and predicts high values for T_g but which are relatively lower than the GT equation, which indicates a better fit when the density ratio is approximated to unity. This non-ideal behaviour could be due to non-additivity of the volumes of polymer and disaccharide, which could arise from excess volume contributions during mixing (Shamblin et al., 1998) or where one polymer does not contribute to the volume.

Kovacs (1963 via Shamblin et al., 1996) derived an equation that allows the calculation of a critical temperature (T_c) by which the volume effect of the higher T_g component in this case PVP (K-25) becomes zero or in some cases is described as meaningless as it tends to a negative result. Above this critical temperature the predicted and experimental T_g should coincide to assume ideal behaviour (i.e. additive volume fractions).

Kovacs (1963, via Shamblin et al., 1996) originally proposed this for mixtures of components where the difference of T_g for each respective component is large ($\geq$ 50°C). The author found that the T_{gmix} cannot be predicted because of the limited temperature range over which the free volume of additivity is valid (Aubin and Prud'homme, 1988; Shamblin et al., 1996). The equation used to predict the critical temperature (T_c) is shown as equation 4.4.

$$T_c = T_{g2} - (f_{g2}/\Delta\alpha_2) \qquad \text{.....equation 4.4}$$

Where f_{g2} is the fractional free volume and 2 denotes the component of PVP (K-25). $\Delta\alpha_2$ represents the thermal expansion coefficient for the free volume. Substituting values of 0.025 and 0.000484 for f_{g2} and $\Delta\alpha_2$ respectively which are universal values (Ferry, 1980). The T_c is calculated at ~ 120°C. This critical temperature is shown in Fig 4.5 as a horizontal line. Below this temperature we would expect the principle of volume of additivity to be non-applicable in accordance with the Kovacs equation, however above this the experimental and theoretical T_gs should coincide. There is only one point above T_c (SD amo. lactose and PVP 40%) but the values do not coincide. Hence the effects of non-additvity seem to apply throughout the graph (Kovacs, 1963 via Shamblin et al., 1996; Feldstein et al., 2001). As a consequence equation 4.4 does not take into consideration the effects of excess free volume upon mixing but it seems likely that there is contribution of excess free volume upon mixing of both lactose and PVP (K-25) above and below the critical temperature, which could lead to a negative deviation from ideal mixing and hence non-additvity.

The Couchman-Karasz equation (Couchman and Karasz, 1978) also produced a result where we have negative deviation of the calculated from the experimental value. However this deviation in comparison to the other equations was less. The difference in using the Couchman-Karasz equation, is the consideration of the entropy of mixing, where the assumption that there exist an additive effect of each component (Couchman and Karsz, 1978). Therefore it seems that entropy of mixing played a greater role in the

deviation from ideal behaviour for the SD products of amorphous lactose and PVP (K-25). Couchman and Karasz (1978) address the issue of deviation and provide equations to replace that of equation 4.3. Righetti et al., (1992) applied these equations to polymer-diluent systems and found that the entropy of mixing is not exclusively combinatorial but also arises from specific interactions, which the Couchman-Karsz equation (1978) does not take into account. This however has not limited the use of this equation or that of Gordon-Taylor, or Fox where the same assumption applies.

It follows, that although a negative deviation indicates a weaker interaction between components than expected and can be attributed to the excess free volume on mixing for both low and high concentrations of the polymer, it does not rule out any interaction. From the characterisation of SD products earlier and the T_g data specific interactions may exist for the higher concentrations of PVP (K-25) at 25 and 40%. To assess this and the volume of additvity the Schneider plot, which is based on the ideal behaviour to the GT equation and takes into account enthalpy and entropy changes, can be used.

4.3.1.4 Determination of the Schneider plot

The Schneider plot has been used to determine specific interactions between components predominately in polymer blends (Schneider, 1989; Hancock and Zografi, 1994; Feldstein, 2001). It is based on an equation that considers the interaction energies and entropy changes between components. Two constants are of importance K_1 and K_2 where the first constant is related to the difference between the energetic interactions (enthalpic changes) and induced conformational changes (entropic changes). Whereas K_2 is an additional constant which is based on the induced conformational changes only.

$$(T_{gmix}-T_{g1})/(T_{g2}-T_{g1})w_{2c} = (1+ K_1) - (K_1 + K_2)w_{2c} + K_2w_{2c}^2 \quad \text{.....equation 4.5}$$

Where w_{2c} is the corrected weight faction of the higher Tg component in this case PVP (K-25) at the glass transition temperature. The corrected fraction is calculated using the equation 4.6 (Brekner et al., 1988; Feldstein, 2001). This is calculated to account for the change in volume fraction during the glass transition for the higher component.

$$w_{2c} = Kw_2/ (w_1 + Kw_2) \quad \text{.....equation 4.6}$$

where K is the constant used in the GT equation, however the density of the samples approximates to unity and therefore K is the ratio of Tg_1/Tg_2 where 1 denotes lactose and 2 denotes PVP.

For volume of additivity to exist only in a binary blend K_1 and K_2 would be zero and hence equation 4.6 would equal one. The result would be a line about unity indicating there is no interaction. However if an interaction exists a straight line of slope K_1 (>0.5) would indicate that specific interactions would dominate the mixture or a curved line ($K_2 \neq 0$) would indicate changes in the interaction environment with changing composition mixture (Schneider, 1989; Hancock and Zografi, 1994).

Fig 4.9. A graphical representation of the Schneider plot for amorphous lactose and PVP (K-25) SD products.

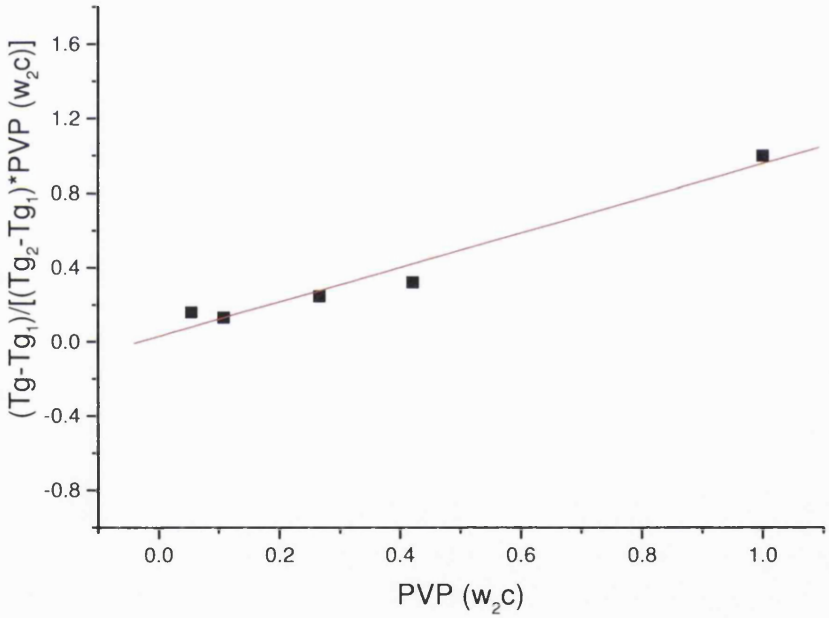

A K_1 value of – 0.89 was determined from the intercept and slope of the graph. This indicated that specific interactions are occurring with polymer and diluent, which maybe affecting the overall free volume of mixing and the T_g. However the effects of molecular size (a small amorphous molecule and macromolecule mixture) will affect the entropy of the constant term and this was reflected in the negative term of K_1 (Schneider, 1997). So it was difficult to assess whether the specific interactions arise from incompatibility of molecular size or from actual interactions (Schneider, 1989; Hancock and Zografi, 1994).

It seems likely that greater interactions will exist at higher concentrations of PVP (25 and 40% with raised T_g values) in the form of hydrogen bonding and also disruptions that would lead to entropic changes. However at low concentrations of the polymer (5 and 10% PVP) there was very little change in the T_g, which may be caused by the excess free volume due to the large macromolecule size. This would lead to an increase in the entropy of the system only. At these low concentrations of polymer less interactions in the form of hydrogen bonding may be taking place between PVP (K-25) and lactose that cannot be reflected in the T_g.

In conclusion the theoretical equations show that the addition of PVP (K-25) to amorphous lactose leads to entropic changes and excess free volume producing a lower T_g than expected. This reduces the capability of PVP to act as an effective stabilising material. However in light of this study and the results seen from the characterisation of the SD and PM products the samples that contained the higher concentration PVP (25 and 40%) and produced a higher T_g were assessed for interactions pertaining to hydrogen bonding using FTIR.

4.3.1.5 Determination of bonding: FTIR

The formation of H-bonds between different molecular species can be determined using FTIR, which can provide information on the extent and nature of interactions. The theory behind the use of IR to study binary compounds is that the mixing of two components at molecular level will cause changes in the oscillating dipole of the molecules. This change manifests itself as a change in the frequency and bandwidth of interacting groups. If there is an interaction, band shifts and broadening of spectra occurs relative to spectra taken of single components (Silverstein et al., 1974). As part of this study FTIR has been employed to assess the extent of interaction between diluent and polymer. The structures of lactose and PVP are shown in Fig 4.10 with the proton donating and accepting species of amorphous lactose and PVP highlighted.

Fig 4.10. The structure of (a) lactose, both α-and β-components and (b) PVP monomer.

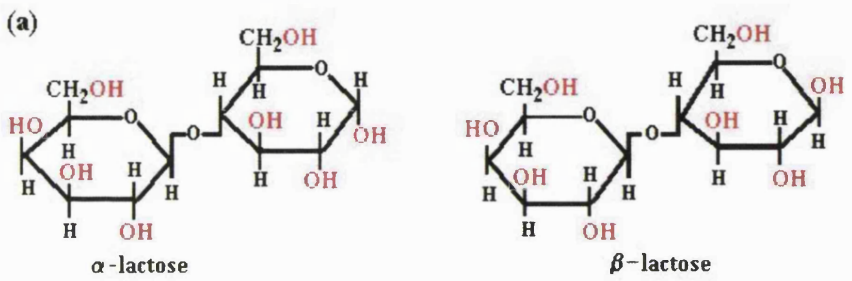

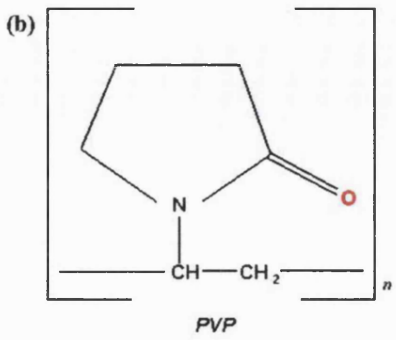

PVP

Lactose has a number of hydroxyl groups that have the potential to hydrogen bond. PVP can interact through either the oxygen (O) or the nitrogen (N) atoms of its pyrrole ring. Through these atoms it acts as a proton acceptor, attracting hydrogen from other species. The carbonyl group of PVP is considered the most favourable sight for interactions due to steric constraints on the nitrogen atom (Taylor and Zografi, 1997; Molyneux, 1985). Previous studies have also shown that this is the site of interaction for hydrogen bonds formed in binary amorphous systems both with other polymers and small molecules (Moskala et al., 1985 Sekizaki et al., 1995, Taylor and Zografi, 1997).

A comparison of SD products with mixes helped to identify any significant intermolecular bonding that has taken place between the two processes. The spectra were viewed at 2 major wave number sections: 1800-1600cm^{-1} which represents hydrogen bonding that has been associated with PVP (Molyneux, 1985). The latter section 1200-900cm^{-1} represents OH-deformation and C-O stretching vibrations on the lactose molecules.

The samples that have been studied are amorphous lactose and PVP (K-25) 25 and 40%, however, the T_g study showed a negative deviation from the calculated values for all concentrations. Nevertheless the higher concentrations of PVP (K-25) raised the T_g of lactose whereas at low concentrations of PVP (K-25) 5 and 10% w/w, the samples showed a similar T_g result to that of lactose alone. Moreover information from DSC and SEMS for the higher concentration of PVP (K-25) indicated that there may be some interaction between amorphous lactose and PVP (K-25).

The band 1800-1600cm^{-1} for both concentrations of polymer (Fig 4.11 shows PVP (K-25) 40% SD and PM products) showed a raised peak at 1654 cm^{-1} that represent the carbonyl stretch of the polymer. If hydrogen bonding has taken place this peak will be shifted to a lower wave number and will also broaden. In this instance there is a shift in wave number to 1650 cm^{-1} and the shape of the peak has broadened indicating hydrogen

bonding for the SD product. This was also seen for PVP (K-25) 25% SD product. However, this shift of 4cm^{-1} needs to be compared to literature (Taylor and Zografi, 1998, Shamblin et al., 1998), which shows a shift of this magnitude, is reasonable at the concentration of PVP (K-25) we are investigating. Both papers considered hydrogen bonding between sugars, namely sucrose and PVP (K-90). For the PM products of amorphous lactose and PVP, no shift was seen in this region indicating no hydrogen bonding between the polymer and the SD systems.

Fig 4.11 FTIR spectra (region 1800-1600cm^{-1}) for Key: DARK BLUE: PVP, MAVUE: amorphous lactose + PVP (K-25) 40% PM, RED: amorphous lactose + PVP (K-25) SD product: BLUE: amorphous lactose.

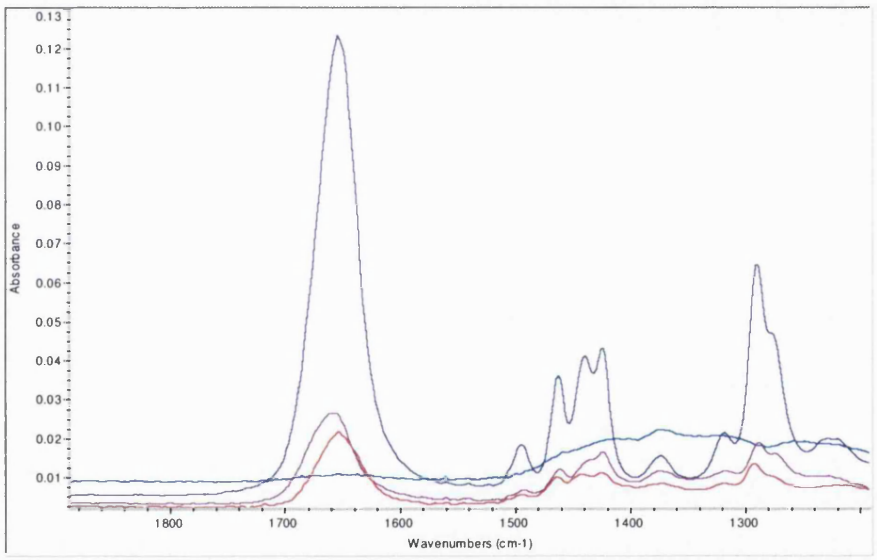

The peak that occurred at 1288cm^{-1} are due to C-N stretch associated with PVP structure (Molyneux, 1985). There was a decrease in intensity with the reduction in PVP concentration, which was greater for the SD systems (Fig 4.11, 25% PVP (K-25) not shown). This reflected the concentration of PVP within the binary products and also indicates that for the SD material the polymer is interacting with the lactose through intermolecular bonding. Therefore more PVP molecules are embedded in the structure as a consequence and are not detected by FTIR. Further evidence that hydrogen bonding has taken place was supported by section 1200-900cm^{-1} (Fig 4.12). Peaks observed at 1068 and 1035 cm^{-1} represented OH-deformation and C-O stretching vibrations on lactose molecules respectively. These peaks were depressed for the PM products, which was due to the concentration of lactose. For the SD product these peaks completely disappear, indicating bonding with PVP (K-25). Therefore it seems that hydrogen bonding does take

place but only in the SD products investigated. There was no hydrogen bonding detected for any of the PM products investigated.

Fig 4.12. FTIR spectra (region, 1200-900cm^{-1}) for: BLUE: amorphous lactose, PURPLE: amorphous lactose + PVP (K-25) 40% PM, PINK: amorphous lactose + 40% PVP (K-25) SD product, RED: PVP.

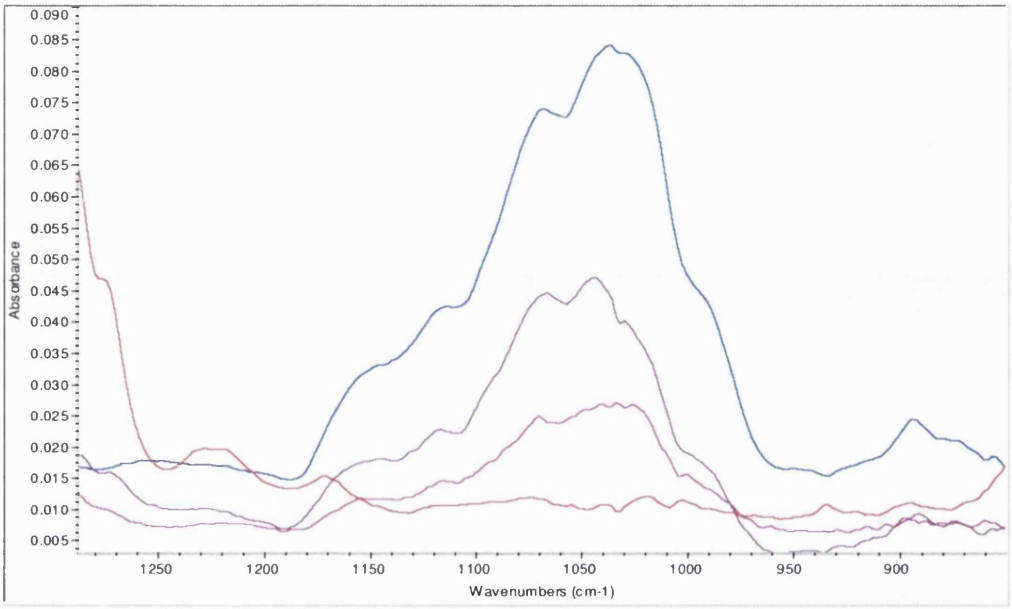

4.3.2 Studying Crystallisation using Isothermal microcalorimetry

4.3.2.1 The Onset of Crystallisation

Crystallisation was induced at 75% RH using the TAM in attempt to establish the onset of crystallisation and also quantify the amorphous content of lactose. Fig 4.13 is a graphical representation of TAM data for SD amorphous lactose and the respective PVP concentrations. Visual inspection showed that PVP (K-25) was affecting the crystallisation of amorphous lactose. By increasing the concentration of PVP (K-25) above 5% there was a delay in the onset of crystallisation of lactose. The peak heights of the TAM graphs were also suppressed and broadened with an increase concentration of the polymer, illustrating a possible change in the kinetics of crystallisation (Buckton and Darcy, 1995d). A comparison with the PM products in Fig 4.14 showed that the onset of crystallisation of amorphous lactose was not greatly affected by the presence of PVP (K-25) at any concentration in comparison to the SD data. The shape of the original amorphous lactose graph was also maintained with the addition of PVP (K-25) even

though the peak height was reduced. The crystallisation onset was determined for both binary systems in table 4.5.

Fig 4.13. A graphical representation of TAM data for SD products consisting of amorphous lactose and PVP (K-25) concentrations.

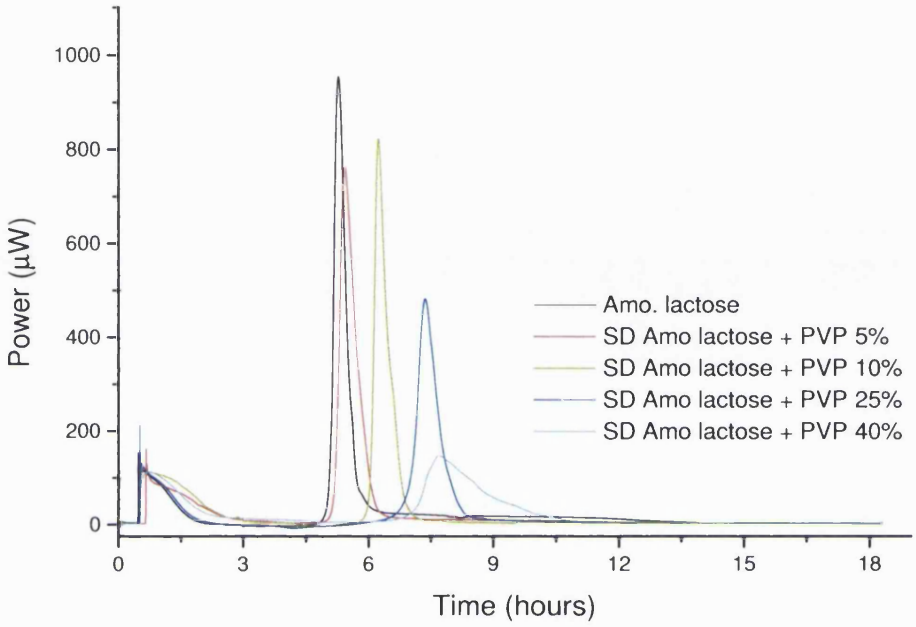

Fig 4.14. A graphical representation of TAM data for PM products consisting of amorphous lactose and PVP (K-25) concentrations.

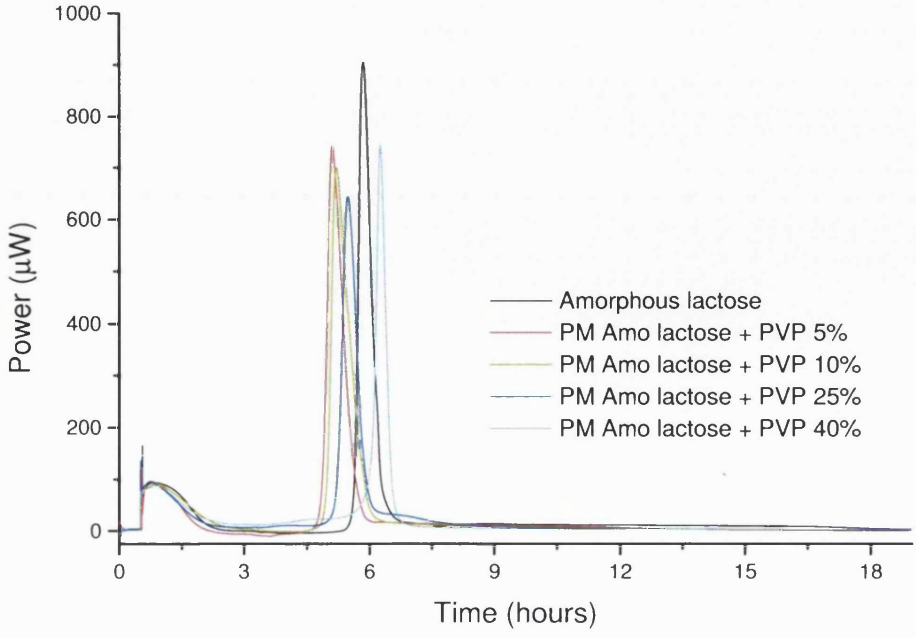

Table 4.5. A comparison between SD and PM products on the onset of crystallisation of amorphous lactose (n=4).

Product	Onset of crystallisation (hours) SD	Onset of crystallisation (hours) PM
Amo. lactose	5.3 ± 0.4	5.3 ± 0.4
+ PVP 5%	5.2 ± 0.7	4.6 ± 0.3
+ PVP 10%	5.9 ± 0.8	4.6 ± 0.7
+ PVP 25%	6.2 ± 0.3	4.8 ± 0.2
+ PVP 40%	7.7 ± 0.5	5.2 ± 0.5

There was an increase in the onset of crystallisation with an increase of PVP (K-25) in the SD product especially for the higher concentrations of polymer (25 and 40%). However the PM products gave the impression that the polymer has no effect on the onset of crystallisation along with the crystallisation kinetics (i.e. the shape of the graphs in Fig 4.14), in fact the time to crystallise was less than amorphous lactose alone. This reduction in the onset of crystallisation for amorphous lactose is not unexpected for a number of reasons: firstly if we consider the PM composition it would consist of amorphous lactose and PVP particles alone and a portion of miscible lactose and PVP (with the SD product, the polymer is embedded within the lactose structure, so there is more miscibility and interaction). The disaccharide, polymer and the miscible portion absorb the slow uptake of water provided by the TAM, this coupled by the second reason, which is the reduced weight of amorphous lactose leads to an earlier onset of crystallisation. We can increase the load of sample in the TAM to equate to ~30mg of amorphous lactose alone and compare the results. This would be justified to eliminate the effects of reduced weight on the onset of crystallisation, which are more apparent with a PM product (where there is less likely to be miscibility between components). Table 4.6 illustrates the increase in sample weight placed in the TAM, to produce a weight of 30mg amorphous lactose for each sample.

Table 4.6. The change in the sample load for TAM to counteract the effects of weight on the onset of crystallisation, where the sample weight of amorphous lactose equates to 30mg in each case.

PM product (%) w/w	Mass of mix needed to equate to 30mg lactose content (mg)
Amo. Lactose	30.00
+ PVP 5%	31.58
+ PVP 10%	33.33
+ PVP 25%	40.00
+ PVP 40%	50.00

Fig 4.15. The TAM graphs for amorphous lactose and PVP (K-25) PM (the graphs have been produced using a sample weight that corrects for lactose (30 mg)).

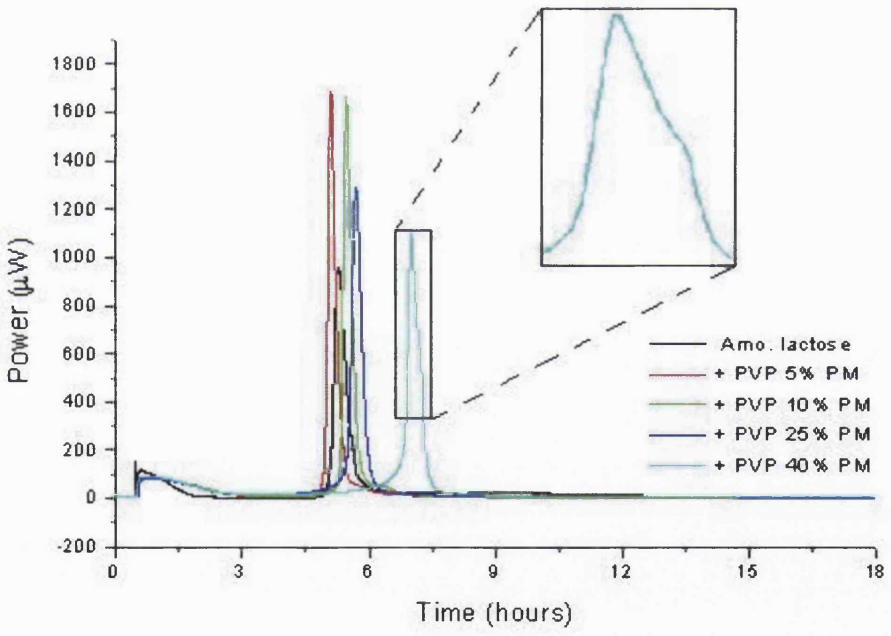

Fig 4.15 shows the correction of amorphous lactose sample weight, where we can see that there was a delay in the onset of crystallisation with increase in PVP (K-25) content except for 5% PVP. The shape of the graph for the PM, which contains PVP (K-25) 40%, was also distorted, as the picture reveals, which was not apparent in Fig 4.14. This has also been sited by Buckton and Darcy, (1995d), where saturation of the powder bed was not a cooperative process but a summation of small rate constants. The onset of crystallisation was determined for the corrected weight (table 4.7). The most significant change once the weight has been adjusted was with the higher concentrations of the

polymer. There was a delay in the onset of crystallisation at 40% PVP, at low concentrations of PVP 5 and 10% the crystallisation onset was still reduced.

Table 4.7. The onset of crystallisation determined from Fig 4.15 for amorphous lactose and PVP (K-25) PM products using the corrected weight for amorphous lactose (n=4).

PM product	Onset of crystallisation (hours)
Amo. lactose	5.3 ± 0.4
+ PVP 5%	4.7 ± 0.06
+ PVP 10%	5.0 ± 0.7
+ PVP 25%	5.4 ± 0.05
+ PVP 40%	5.9 ± 0.5

4.3.2.2 Quantifying the Amorphous content

The apparent enthalpies of crystallisation (ΔH_c) have been calculated for each graph, and a comparison of the SD and PM products was made. An accurate result of (ΔH_c) for amorphous lactose was achieved by subtracting the enthalpy associated with PVP and correcting for amorphous lactose weight. This was based on the assumption that the enthalpies of both lactose and PVP (K-25) are purely additive, this may be a reasonable assumption for a PM but highly unlikely with a SD product. However it was found that the enthalpies associated with PVP (K-25) were very small. These values were determined by weighing the (%) amount of PVP (K-25) in a binary product into an ampoule at 75% RH and lowered into the TAM. The PVP graph generated was integrated at the point of crystallisation of the SD product. Fig 4.16 and table 4.8 show examples of how the enthalpy of the polymer was determined and sample calculations respectively.

Fig 4.16. An example of how the enthalpy of the polymer was achieved. The vertical lines show where the graph of PVP was integrated. The SD product of amorphous lactose and PVP (K-25) at 40% w/w and PVP (K-25) at that weight alone are illustrated here. This was repeated for all concentrations of PVP for SD and PM.

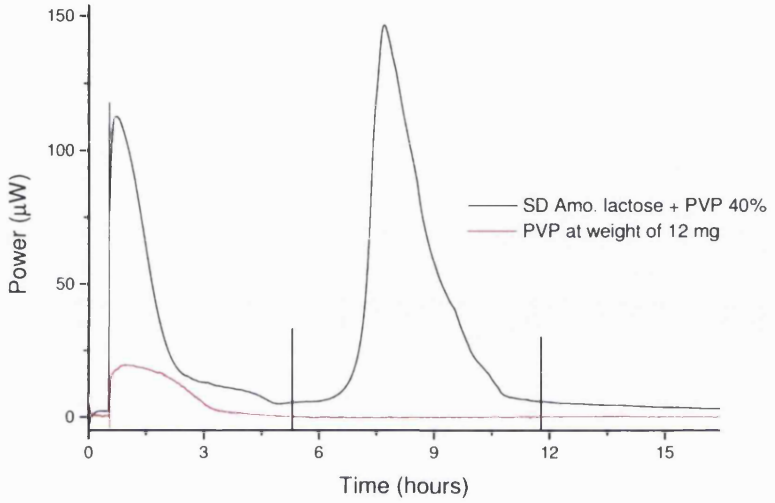

Table 4.8. Example calculations of the subtraction of the enthalpy related to PVP (K-25) from the apparent enthalpy of crystallisation of amorphous lactose. The final apparent enthalpy of crystallisation is divided by amount of lactose within the sample load (i.e. the corrected weight of lactose).

SD amo. lactose + PVP 40% w/w	Sample weight (mg)	Weight of lactose (mg)	(ΔH_c lactose) – (ΔH PVP) (J)	Apparent ΔH_c lactose (J/g)
L10p40a	29.8	17.9	829.2 – 4.5= 824.7	46.1
L10p40b	30.1	18.1	835.4 – 4.5= 830.9	45.9
L10p40c	30.0	18.0	834 – 4.5= 829.5	46.1

Table 4.9. A summary of the apparent enthalpy of crystallisation (ΔH_c) for amorphous lactose after subtraction of PVP enthalpy and correction of amorphous lactose weight (n=4).

SD Samples	Apparent ΔH_c (mJ/mg)	(%) Apparent amorphous content
Amo. Lactose	45.7 ± 1.7	100
Amo lac + PVP 5%	50.5 ± 1.5	110.5
Amo lac + PVP 10%	50.8 ± 3.2	111.2
Amo lac + PVP 25%	51.3 ± 1.5	112.3
Amo lac + PVP 40%	45.9 ± 0.4	100.4

Table 4.10. A summary of the apparent enthalpy of crystallisation (ΔH_c) for amorphous lactose after subtraction of PVP enthalpy and correction of amorphous lactose weight (n=4).

PM products	Apparent ΔH_c (J/g)	(%) Apparent amorphous content
Amo. Lactose	45.7 ± 1.7	100
Amo lac + PVP 5%	50.4 ± 3.9	110.3
Amo lac + PVP 10%	52.5 ± 1.5	114.9
Amo lac + PVP 25%	52.8 ± 0.9	115.5
Amo lac + PVP 40%	53.0 ± 1.5	116.0

A comparison of (ΔH_c) for both the SD and PM products would indicate that PVP (K-25) does not inhibit the crystallisation of amorphous lactose but only retards the process with an increase in the onset of crystallisation time. However the increase in the apparent enthalpy of crystallisation may be attributed to the increase of water being held in the system as PVP (K-25) is a hygroscopic material and acts as an internal desiccant. From chapter three (section 3.6.2) it was described that the crystallisation peak (Phase II) is a net effect of the desorption of water (endothermic) and the crystallisation process itself (exothermic). Fig 4.17 illustrates the effects of absorbed water and desorption which is relatively small due to the influence of PVP, this as a consequence alters the crystallisation peak. This event is likely, as there is a general increase in the enthalpy of crystallisation with an increase in PVP concentration in the PM products, where there is no bonding between lactose and PVP. Even though the enthalpy of PVP has been

subtracted under the assumption that the enthalpies are purely additive this is still possible as the TAM is a sensitive instrument.

Fig 4.17. A schematic representation of the net effects of the crystallisation peak (a) lactose alone and (b) with the addition of PVP.

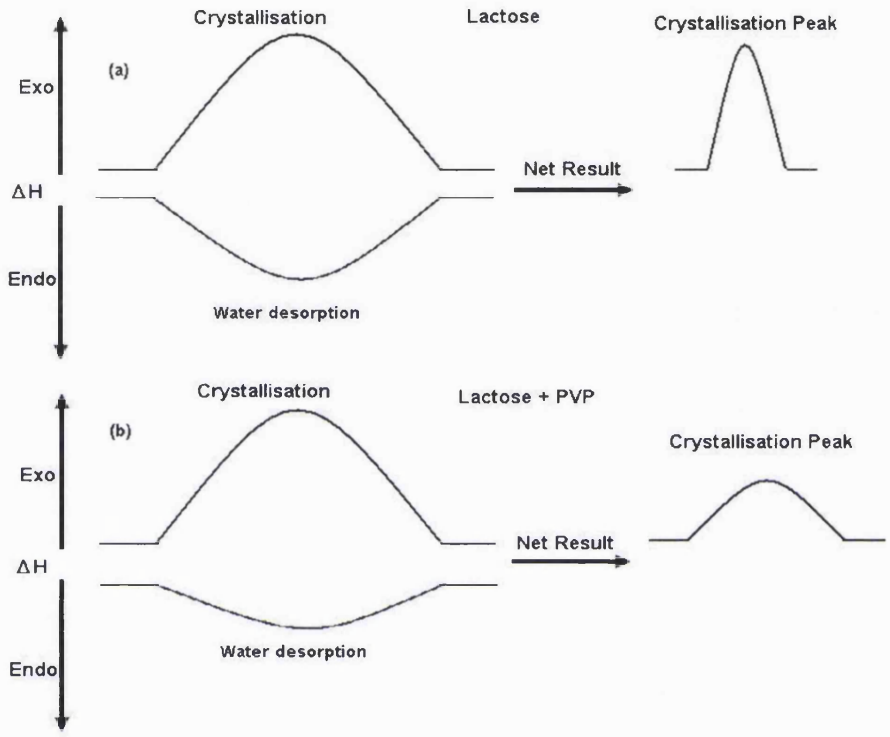

To prove that PVP is acting as an internal desiccant, and that this is contributing to the excess enthalpy of crystallisation we would expect the conditioned samples (ex-TAM) to contain excess desorbed water upto 100°C. This water is associated with absorbed water of the sample (Darcy and Buckton, 1997). Using TGA from samples taken from the TAM once the peak has returned to baseline, the quantity of water can be determined.

The results show (table 4.11) there was an increase in the amount of water with an increase in PVP (K-25) content, which is higher for the PM products. This supports the hypothesis that more water is retained in the samples hence leading to an increase in the apparent enthalpy of crystallisation. The lower concentrations of PVP (K-25) 5 and 10% SD products absorbed the same amount of water as their PM counterparts. For the higher concentrations of PVP (K-25) 25 and 40%, the polymer in the SD product was acting more intimately with amorphous lactose (hydrogen bonding) so less water will be absorbed by the system in comparison to the PM products of identical concentration. At these concentrations of the polymer, there was some inhibition of lactose crystallisation

due to hydrogen bonding, but quantification through the TAM may be unreliable due to retained absorbed moisture.

Table 4.11. A summary of the absorbed water (< 100 °C) for SD and PM products which have been removed from the TAM after crystallisation at 75% RH (n=4).

System (% w/w)	% TGA water sorbed < 100°C. SD product	% TGA water sorbed < 100°C. PM product
Amo. lactose	0	0
+ PVP 5%	1.1 ± 0.1	1.1 ± 0.1
+ PVP 10%	2.3 ± 0.3	2.1 ± 0.3
+ PVP 25%	4.0 ± 0.3	6.7 ± 0.4
+ PVP 40%	7.1 ± 0.9	9.0 ± 0.9

4.3.3 The investigation of crystallisation usingDVS

The crystallisation of SD and PM products of amorphous lactose and PVP (K-25) was also studied by DVS-NIRS. Initially the water saturation of the samples was investigated and the crystallisation kinetics determined using the Avrami equation (chapter three, section 3.6.4.2).

4.3.3.1 The Absorption of Water

Fig 4.18. A graphical representation DVS data of amo. lactose and PVP (K-25) (a) SD and (b) PM products.

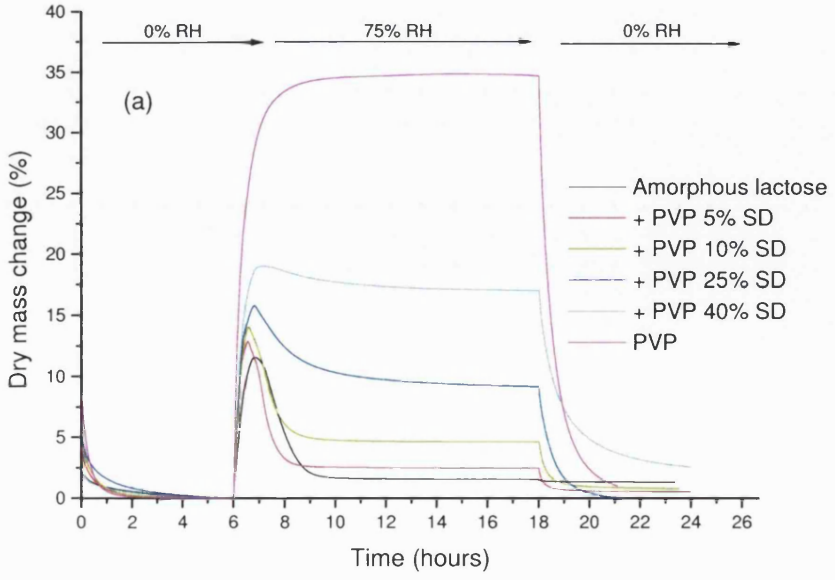

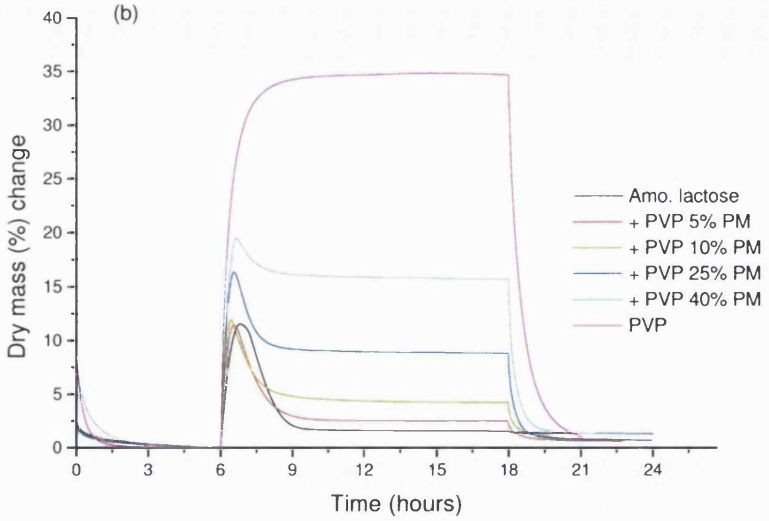

A visual interpretation of the graphs (Fig 4.18 (a) and (b)) showed that there was an increase in water content of both the SD and PM products with an increase in PVP (K-25) concentration. The graph also begins to take on the form of a PVP graph especially with higher concentrations of PVP (K-25), 25 and 40% w/w. To further investigate the amount of water absorbed for each system, the experimental values were plotted and compared to theoretical values. The theoretical values were calculated based on the assumption that each component was behaving as a single entity with no interaction and that saturation of each component was achieved. The water contribution was then calculated based on the sample weight of each component in the binary sample (Fig 4.19).

Fig 4.19. A graphical comparison of the experimental and calculated water content for the SD products.

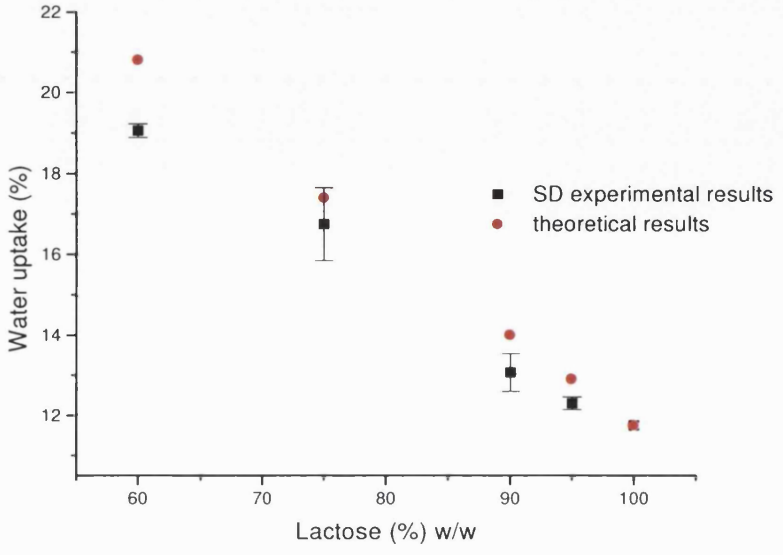

The practical and theoretical values of water absorption (Fig 4.19) were very similar to trends observed for Tg results, where a negative deviation from the calculated results was shown, for all SD products. It is worth noting that the use of water as a probe would be based on the accessibility of each single component and the form of each component. In terms of the state of each sample, earlier work showed that in all cases the SD products are amorphous (PXRD, DSC). Eliminating the presence of crystalline material, any inferences made are based on how accessible the components are and whether saturation of the powder bed has occurred. A negative deviation would indicate that not all components are accessible to water and that saturation of the powder bed is not achieved. This may be due to the increased embedment of PVP in the amorphous lactose structure (Imamura et al., 2001) and due to the hydrogen bonding between the polymer and disaccharide at high concentrations of PVP (K-25). However, recent studies have shown that any hydrogen bonding between blends of sugar and PVP are insufficient to prevent water accessibility to single components (Zhang and Zografi, 2001). Therefore it seems that powder bed saturation has not taken place before crystallisation of amorphous lactose. A comparison with the PM products was needed to confirm these results, where we know that no hydrogen bonding exists between lactose and PVP.

Fig 4.20. A graphical comparison of the experimental and calculated water content for the PM products.

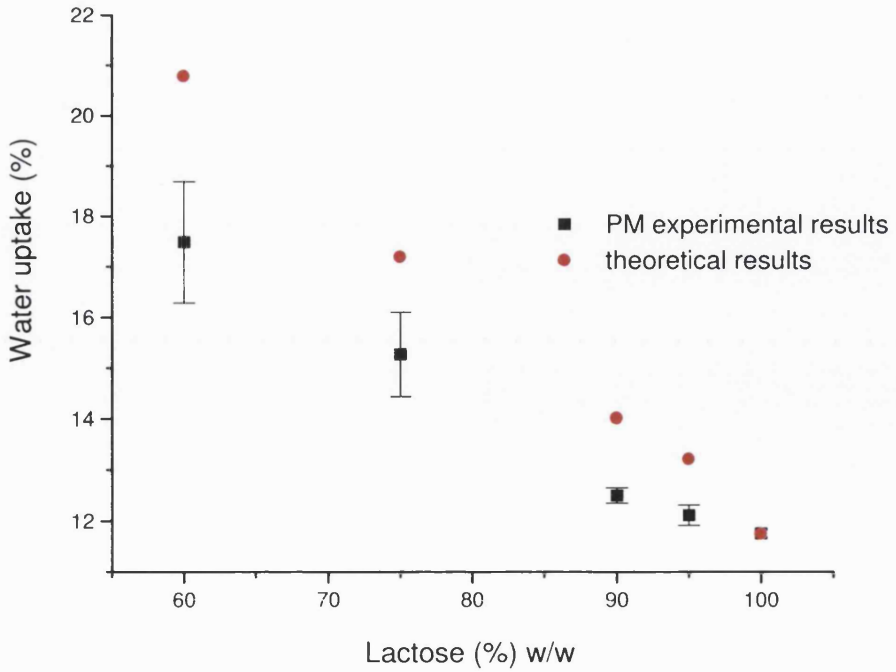

The PM products showed (Fig 4.20) that there was a negative deviation from the theoretical results across the concentrations of the polymer. This indicates that powder bed saturation did not occur before crystallisation of amorphous lactose. By comparing both graphs (Fig 4.19 and 4.20) visually there is a greater negative deviation between the theoretical and experimental results for the PM than the SD products. This would indicate that there is more amorphous lactose not miscible with PVP (K-25) than in the SD product. Hence less water is absorbed before crystallisation of lactose commences. Stubberud et al., (1998) also reported a negative deviation for PM blends of amorphous lactose and PVP (K-25). Therefore we would expect the crystallisation of amorphous lactose in PM blend to crystallise faster than the SD product, which has been observed by the TAM.

4.3.3.2 The Induction time

The induction time was defined in chapter three (section 3.6.4.2.3) as the most probable time from the beginning of isothermal crystallisation to the point at which a stable nucleus starts to grow (Kedward et al., 1998). The induction time has the same meaning as the onset of crystallisation described for TAM data, so the results can be compared. The difference between the DVS and TAM is in the delivery of water vapour; the relatively fast rate of water absorption when using the DVS makes the instrument less sensitive towards sample weight. Its operational feature is to assess mass change (with regards to water absorption and desorption) as a function of time. Hence when we compared the induction time of the SD and PM products there is a similar trend to that of the TAM without correcting for the weight of the PM products.

Table 4.12. A summary of the induction times determined by DVS for both SD and PM products (n=4).

Product	Induction time (mins) SD	Induction time (mins) PM
Amo. Lactose	33.0 ± 2.1	33.0 ± 2.1
+ PVP 5%	32.2 ± 1.5	31.5 ± 0.8
+ PVP 10%	37.0 ± 0.7	33.5 ± 0.9
+ PVP 25%	48.5 ± 0.5	39.2 ± 0.4
+ PVP 40%	70.5 ± 0.5	43.2 ± 0.6

From table 4.12 there was an increase in the induction time with an increase in PVP (K-25) concentration, which was more profound with the SD products. The increase in induction time infers a delay in the formation of a stable nucleus from which growth would occur. According to literature, there are two mechanism by which nucleation can be inhibited. Van Hook and Frulla, (1952) identified these processes as either a mass transport or orientation and incorporation step. Materials that compromise the role of water acting as a solvent alter the ability of molecules to diffuse and attain contact in order to form a stable nucleus, hence affect the mass transport or diffusion step. An example of this is a hygroscopic material which hydrogen bonds with water. Substances that prevent the correct orientation and incorporation of the crystallising material affect the orientation and incorporation step of the crystallisation process. An example of this is shown by Symthe (1967) where raffinose had a significant inhibitory effect on the growth rate of certain crystal faces of sucrose. More recent studies based on water absorption of sucrose with PVP have shown that the inhibitory effect of PVP on this sugar may well be attributed to molecular local mobility amongst other structural dynamics, which could interfere with the nucleation process (Shamblin and Zografi, 1999a; Zhang and Zografi, 2001) although further work is required in the area.

For SD products which contain high concentrations (25 and 40%) of PVP (K-25) we know that the polymer is hydrogen bonded with a portion of amorphous lactose from FTIR. There will also be an increase in viscosity of the system, making it difficult for lactose molecules to diffuse (Van Hook, 1971) to form a nucleus of critical size. PVP is also a hydrophilic molecule so will form hydrogen bonds with water reducing the amount of solvent in which lactose can dissolve and diffuse. This was also reported by Van Scoik and Carstensen (1990) for the study of sucrose crystallisation under the influence of various substances. All of these combinatorial processes are likely to have caused the delay of nucleation for amorphous lactose. At low concentrations of the polymer there seems to be little effect on the nucleation phase of amorphous lactose.

For the PM products, the nucleation phase at higher concentrations of PVP (K-25) delays the induction time but was relatively small in comparison to the SD products. This would indicate that not all the processes that delay the induction time for SD product are prevalent in the PM. There was no evidence of hydrogen bonding within the PM products studied and the viscosity of the PM product is highly unlikely to be high in comparison to the SD product, and these are factors that can be disregarded. The only factor, which would affect the nucleation phase, would be the interaction of PVP with water. The polymer will hydrogen bond and absorb water hence reducing the dissolution of lactose

within the water and diffusion of the molecules. In this role PVP is acting as an internal desiccant.

4.3.3.3 The kinetics of crystallisation for SD and PM products

The crystallisation kinetics for each SD and PM products was studied by application of the Avrami equation (chapter three, section 3.6.4.2,equation 3.2) a summary of the kinetic parameters is shown in table 4.13 and 4.14.

Table 4.13. A summary of the determined crystallisation kinetic parameters using the Avrami equation for SD products.

SD product	Avrami exp.(n)	linear fit (R^2)	Rate constant (k) (min^{-1})	linear fit (R^2)	Half–time ($t_{1/2}$) (min)
Amo. Lactose	1.73	1.0	0.018	1.0	44.95
+ PVP 5%	1.80	0.99	0.023	0.99	35.47
+ PVP 10%	1.77	0.99	0.019	0.99	42.79
+ PVP 25%	1.36	0.99	0.011	0.99	69.43
+ PVP 40%	1.12	0.99	0.007	0.99	102.99

Table 4.14. A summary of the determined crystallisation kinetic parameters using the Avrami equation for PM products.

PM product	Avrami exp. (n)	linear fit (R^2)	Rate constant (k) (min^{-1})	linear fit (R^2)	Half–time ($t_{1/2}$) (min)
Amo. Lactose	1.73	1.0	0.018	1.0	44.95
+ PVP 5%	1.52	0.99	0.018	0.99	43.65
+ PVP 10%	1.56	0.99	0.019	0.99	41.61
+ PVP 25%	1.32	0.99	0.017	0.99	44.56
+ PVP 40%	1.09	0.99	0.021	0.99	34.22

An overall interpretation of the results showed that PVP (K-25) exerts an effect on the crystal growth of amorphous lactose when spray-dried with the disaccharide. The addition of PVP (K-25) as a physical mix seems to have no effect on the crystallisation of amorphous lactose and was even reduced under the concentration of 40% PVP (K-25). This was deduced by comparing the isothermal crystallisation rate constant (k) and the time taken for the binary system to crystallise to double its original value (half time $t_{1/2}$). However when analysing the results for the PM product which contained 40% PVP, there

was more than one crystallisation rate constant resulting along the desorption phase of the graph. This supports the findings of the TAM data for this concentration and the result above. Therefore it seems that the Avrami equation would be less suited to describe the crystallisation kinetics of PM products as more than one rate constant describes the overall system. An attentive approach to the problem would be to assess the crystallisation half time ($t_{1/2}$) using the exponential model. This was also done for the SD product to compare results (table 4.15).

Table 4.15. The crystallisation half times ($t_{1/2}$) determined by fitting the data to an exponential model for both SD and PM products (n=4).

Product	$t_{1/2}$ (mins) SD	$t_{1/2}$ (mins) PM
Amorphous lactose	45.4 ± 0.5	45.4 ± 0.5
Amo. Lac + PVP 5%	37.1 ± 2.2	45.1 ± 1.2
Amo. Lac. + PVP 10%	44.9 ± 1.5	48.0 ± 0.7
Amo. Lac. + PVP 25%	110.4 ± 1.2	49.6 ± 1.7
Amo. Lac. + PVP 40%	137.3 ± 1.9	50.2 ± 0.9

A comparison of the results for the SD products using both the Avrami and the exponential model follow a similar trend, indicating that PVP (K-25) at and above 25% PVP (K-25) affects the crystal growth phase of amorphous lactose. The viscosity of the binary system along with hydrogen bonding is most likely slowing down the diffusion of the lactose molecules and hence the mass transfer to the critical nuclei. The orientation and incorporation step is also hindered by similar means.

The crystallisation half time for the PM products shows a gradual increase in this parameter as the concentration of PVP (K-25) increases. This is more prominent for the higher concentrations of PVP (K-25) 25 and 40%, which is identical to the findings for the SD products. However a comparison with the SD products of identical polymer concentration, indicate that the change may not be significant. Therefore it seems at higher concentrations of PVP in the PM products there is an effect on the nucleation phase by the increase in the induction time (section 4.3.3.2) of lactose crystallisation but a much slower rate is adopted for the crystal growth stage. A similar finding was reported by Sarciaux and Hageman (1997) where the addition of a protein to sucrose co-lyophilised was found to delay the nucleation stage of sucrose but have less effect on the crystal growth.

The Avrami exponents generated describes the nucleation mechanism and the number of dimensions in which growth is occurring. For the SD product the Avrami exponent remains relatively the same at low concentrations of PVP (5 and 10%) indicating no effect on the nucleation mechanism and growth of amorphous lactose. At higher concentrations of PVP (25 and 40%) the Avrami exponent decreases in value, this might indicate that the polymer is affecting the nucleation mechanism and the dimensions of growth, which was concluded by the induction time and the crystallisation half times. For the PM products the Avrami exponent is not considered, as it may not represent the actual crystallisation of amorphous lactose due to different rates of desorption of water.

4.3.4 The study of crystallisation using NIRS

In chapter three (section 3.6.5) NIRS was used to follow the phase transition of amorphous lactose to the crystalline state, where it was established that amorphous lactose undergoes absorption of water, collapses and in the process of doing so crystallises. In this case NIRS has also been used to see whether the crystallisation of lactose was altered with the addition of polymer at varying concentrations. Kinetic data from DVS has already proved that the crystallisation of lactose was hindered by the addition of the polymer, however investigating the NIR spectra will be a novel approach in the study of the amorphous to crystalline phase transition. NIR spectra was analysed for both the SD and PM products during the crystallisation stage, at the end of the cycle at 75% RH and also at the end of the second drying phase, in order to assess the crystalline material in a dry state.

4.3.4.1 Following the Amorphous to Crystalline phase transition

After drying the SD and PM samples at 0% RH for 6 hours, crystallisation was induced at 75% RH. It was found that the SD and PM samples containing 5 and 10% PVP, crystallised in a similar manner to amorphous lactose alone (Fig 4.21), which can be compared to chapter 3, Fig 3.14(b). The sample absorbs water, where the spectrum taken at 40 mins shifts to lower wavelengths and also broadens in appearance indicating a wide range of interaction energies. Multiple peaks formed at 1908 and 1956 nm for the spectrum taken at 70 mins at 75% RH which shift to higher energy states and disappear once crystallisation is complete. Also during this stage the monohydrate peak becomes more sharply defined from 1926 to 1934 nm and increases in intensity.

Fig 4.21. SNV 2nd der. NIR spectra following the amorphous to crystalline phase transition for SD amo. lactose and PVP 10% (this figure is also representative of SD and PM samples of amo. lactose and PVP 5% and the PM product containing 10% PVP).

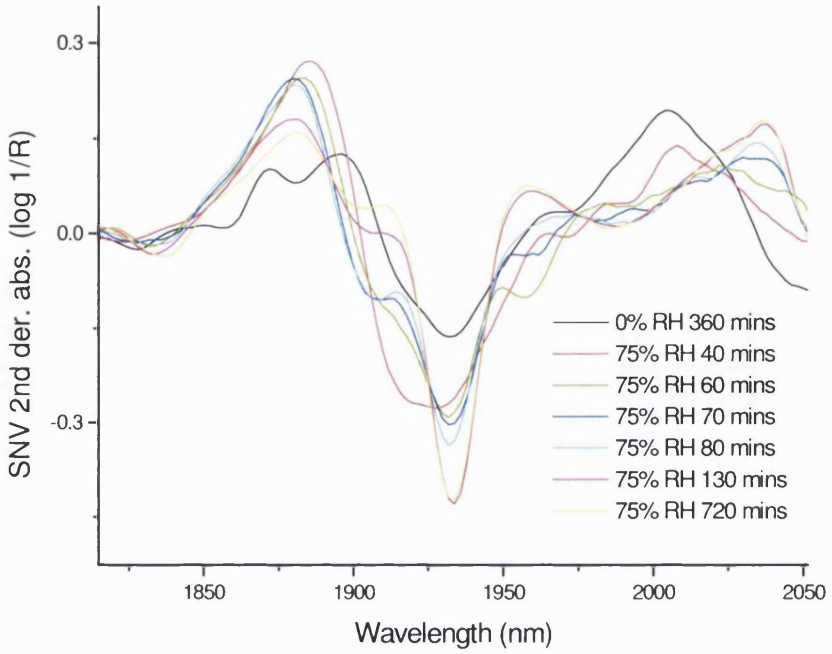

For the SD products containing amorphous lactose and PVP 25 and 40% w/w the onset of crystallisation for amorphous lactose was delayed, supporting the increase in induction time seen in table 4.11. Fig 4.22 shows spectra of co spray-dried amorphous lactose and PVP 40%, which is also representative of SD product containing amorphous lactose and PVP 25%, the only difference is the spectra time. From the spectra in Fig 4.22 it was difficult to assess whether crystallisation of amorphous lactose had occurred or was complete just by considering the spectra around 1900 nm. This was due to the decrease in concentration of amorphous lactose within the co-spray dried products containing higher concentrations of PVP. This problem was resolved by considering another area of spectra which is related to the uptake of water and crystallisation of lactose. The spectra at 1436 nm represents a first overtone O-H stretch that shifts gradually from 1438 nm to 1450 nm once crystallisation was complete (Fig 4.22 (b)).

Fig 4.22. SNV 2nd der. NIR spectra of co-spray dried amorphous lactose and PVP (K-25) 40% w/w (a) 1900 nm and (b) 1400 nm.

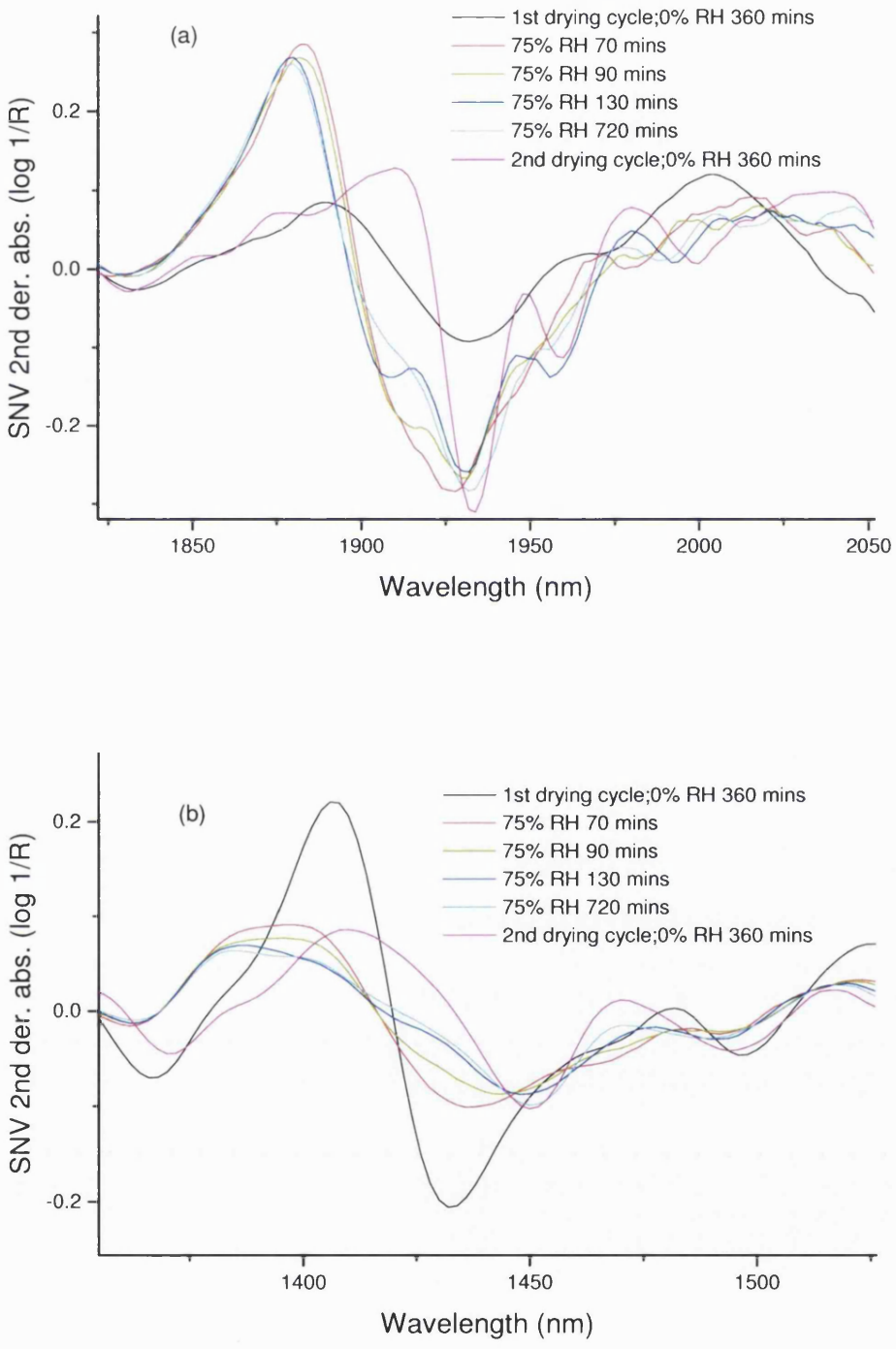

From table 4.11 the induction time of co-spray dried amorphous lactose and PVP (K-25) 40% w/w was determined at ~ 70 mins, at this point the desorption of water was seen.

The spectra in Fig 4.22 (a) supports this, where at 70 mins the sample was shown to be wet and plasticized, with the peak being displaced from 1930 nm to 1926 nm and also increases in intensity indicating the absorption of water. At the same time within the region of 1400 nm (Fig 4.22 (b)) the intensity of the spectra decreases and shifts from 1432 nm to 1438 nm. After 130 mins at 75% RH the wavelength has gradually shifted to 1930 nm indicating the onset of crystallisation with multiple peaks formed at 1908 and 1956 nm. Simultaneously the peak at 1438 nm has shifted to a higher wavelength and hence lower interaction energy to 1448 nm also indicating the onset of crystallisation. By 720 mins at 75% RH there have been gradual changes in spectra from the disappearance of multiple peaks and change in intensity to a permanent shift of wavelength to 1932 nm which represents the formation of a monohydrate. However at 1448 nm the peak is displaced permanently to 1450 nm by 250 mins at 75% RH with very little change in spectra after this point in this region, indicating that crystallisation may have been complete by this stage. An interesting feature of the NIR spectra is that it is very difficult to see the sharp monohydrate peak at 1932 nm, this could be due to a number of reasons; firstly the decrease concentration of lactose and secondly the elevated absorbed water within the SD product due to PVP, which may be obscuring the NIR spectra. This could be a likely cause simply because once the sample is exposed to the second drying stage after crystallisation at 0% RH for 360 mins a sharp monohydrate peak along with a shoulder peak at 1960 nm is observed. The presence of the latter peak for co-spray dried products containing a higher concentration of PVP (K-25) especially after drying represents C=O stretch second overtone and thus may indicate the presence hydrogen bonding between lactose and PVP during crystallisation.

The amorphous to crystalline phase transition using NIRS for the PM products was similar to their SD counterparts except for the timing. The PM products containing amorphous lactose and PVP at concentration 5 and 10% crystallised in similar manner and showed spectral changes, which were similar to amorphous lactose alone, and co-spray dried with PVP 5 and 10%. The PM products containing higher concentrations of PVP at 25 and 40% except for timing showed similar spectral transitions to that of co-spray dried amorphous lactose and PVP 25 and 40%. Fig 4.23 shows spectral changes which occurred with time for PM product of amorphous lactose and PVP 25%.

Fig 4.23. SNV 2nd der. NIR spectra of PM product amorphous lactose and PVP (K-25) 25% w/w (a) 1900 nm and (b) 1400 nm.

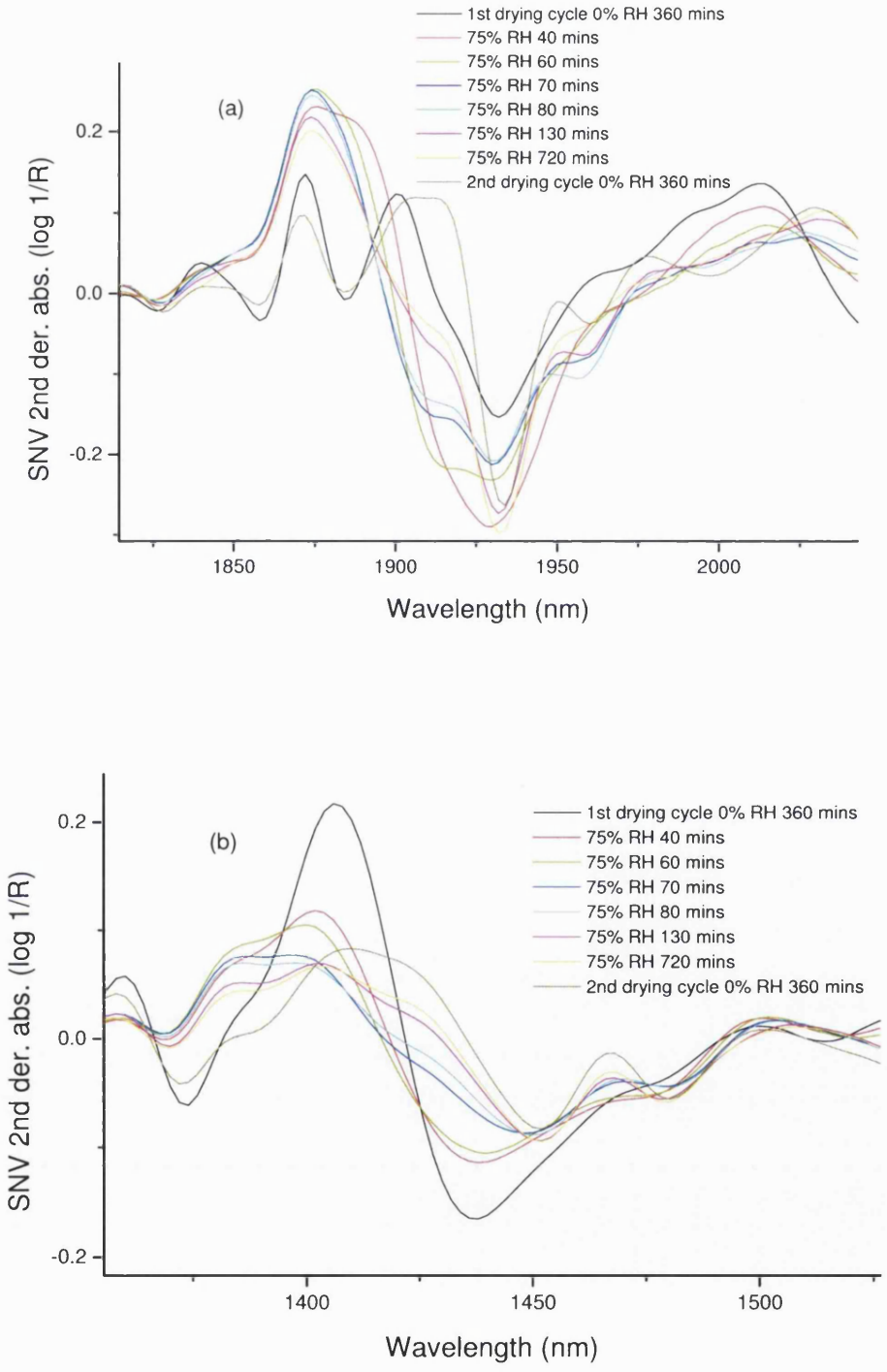

Plasticization occurred as water was taken up by the sample, this was followed by the onset of crystallisation with the formation of multiple peaks at 1906 and 1956 nm on

either side of the monohydrate peak. The onset of crystallisation and formation of a monohydrate was also confirmed with a shift of the peak at 1436 nm to 1450 nm. At the end of 75% RH the monohydrate peak formed in comparison to the final dried spectra of the experiment is not sharp. With the aid of drying a sharp monohydrate peak with a shoulder peak at 1960 nm was observed.

A comparison of the SD and PM products at the end of the second drying stage would give a better indication of whether the SD samples have formed a sharp monohydrate peak at the end of the experiment. The increased water absorbed under the influence of PVP (K-25) was removed (Fig 4.24). The difference in intensity represents the concentration of lactose in the sample as the spectra can be compared to PM products in Fig 4.25.

Fig 4.24. SNV 2nd der. NIR spectra of crystalline lactose and PVP SD products taken at the end of the DVS cycle; at 0% RH for 6 hours (The 2nd drying phase).

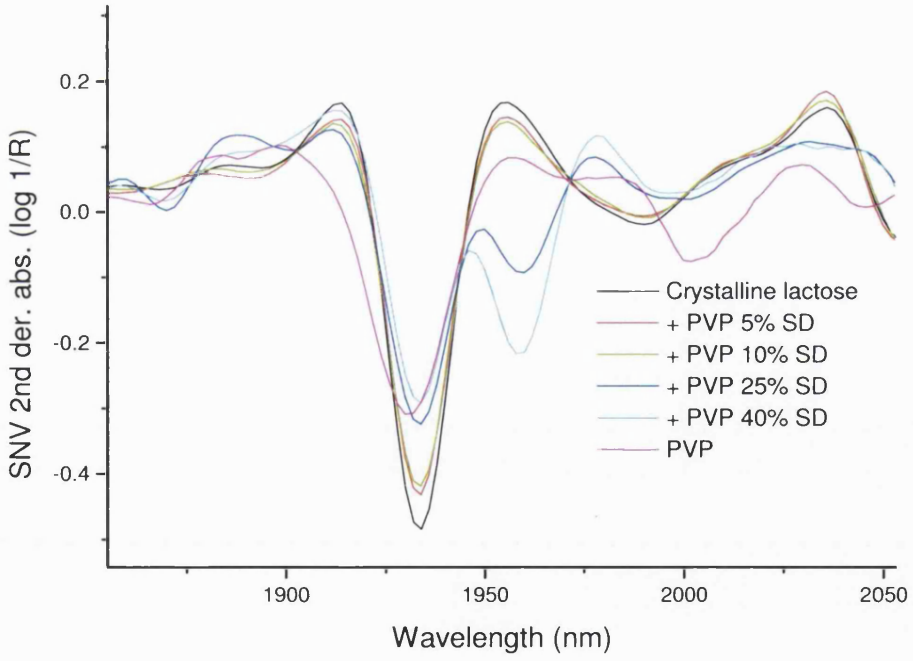

Fig 4.25. The NIR spectra of crystalline lactose and PVP PM products taken at the end of the DVS cycle; at 0% RH for 6 hours (The 2nd drying phase).

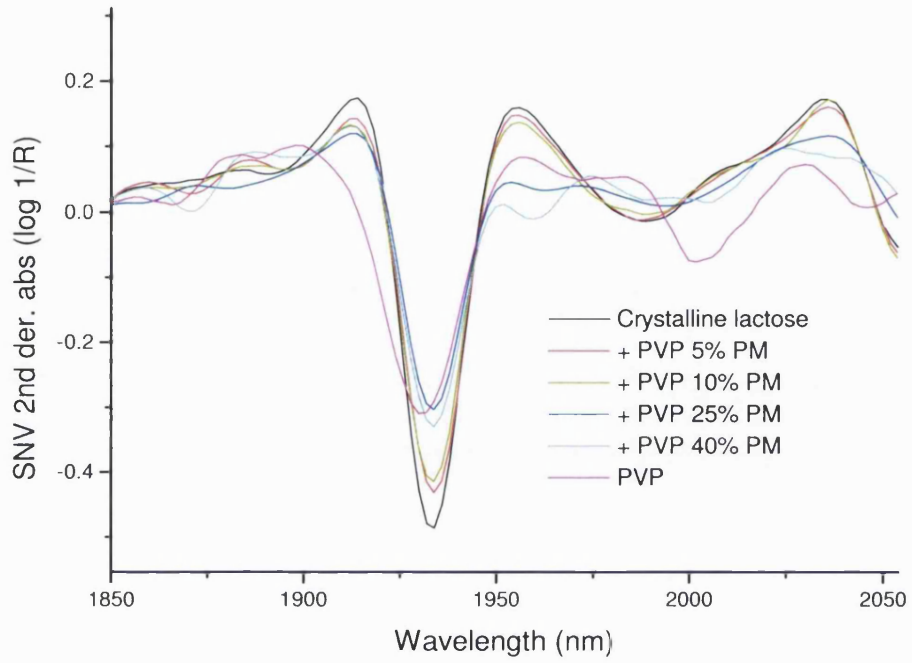

4.3.4.2 Intermolecular Bonding; Hydrogen bonding

After assessing the spectra during crystallisation it was apparent that the crystalline product containing higher concentrations of PVP (K-25) both SD and the PM product (25 and 40%) were different from the remaining products. Not only do we see the extra peak at 1960 nm which may represent hydrogen bonding but also spectra between the region 1400-1600 nm show the formation of new peaks which represent intermolecular hydrogen bonding. Fig 4.26 (a) taken at the end of the second drying stage shows the SD products of amorphous lactose and PVP (K-25) where the new peaks can be identified at 1540 and 1590 nm. These peaks correspond to 1st overtone O-H stretch and represent intermolecular hydrogen bonding. Fig 4.26 (b) represents the PM products where the two new peaks are evident for the PM product containing PVP 40% at 1536 and 1590 nm. These peaks along with the peak that occurs at 1960 nm indicate that the crystalline samples containing a high concentration of PVP (K-25) (SD product 25 and 40% and the PM product containing 40%) are hydrogen bonding during crystallisation but there is also formation of the monohydrate. From this analysis it can be inferred that PVP (K-25) does

inhibit crystal growth of amorphous lactose by hydrogen bonding with the sample during crystallisation in place or along with water.

Fig 4.26. SNV 2nd der. NIR spectra for amorphous lactose and PVP (K-25) at ascending concentration of PVP for (a) SD and (b) PM products.

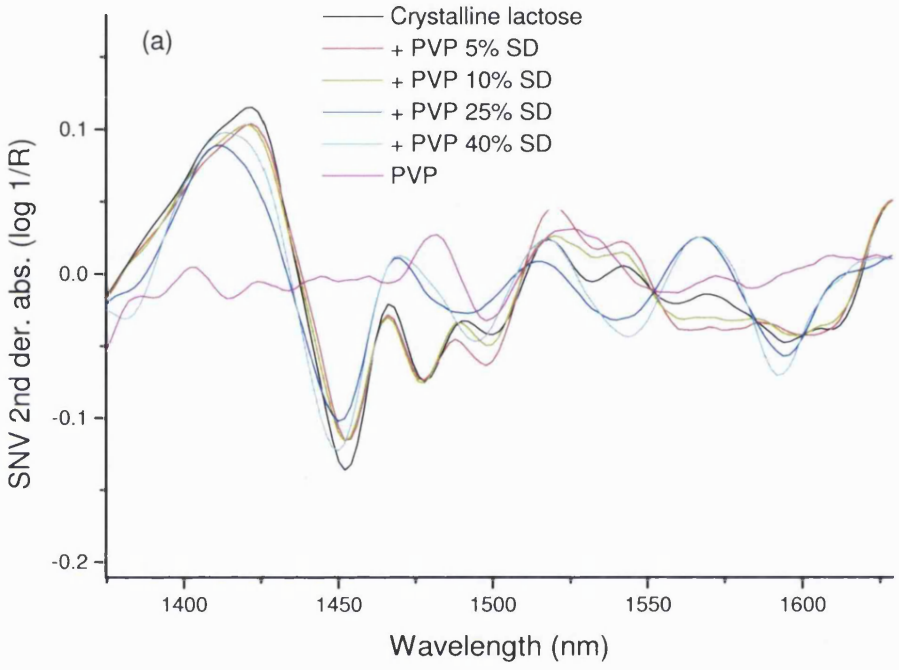

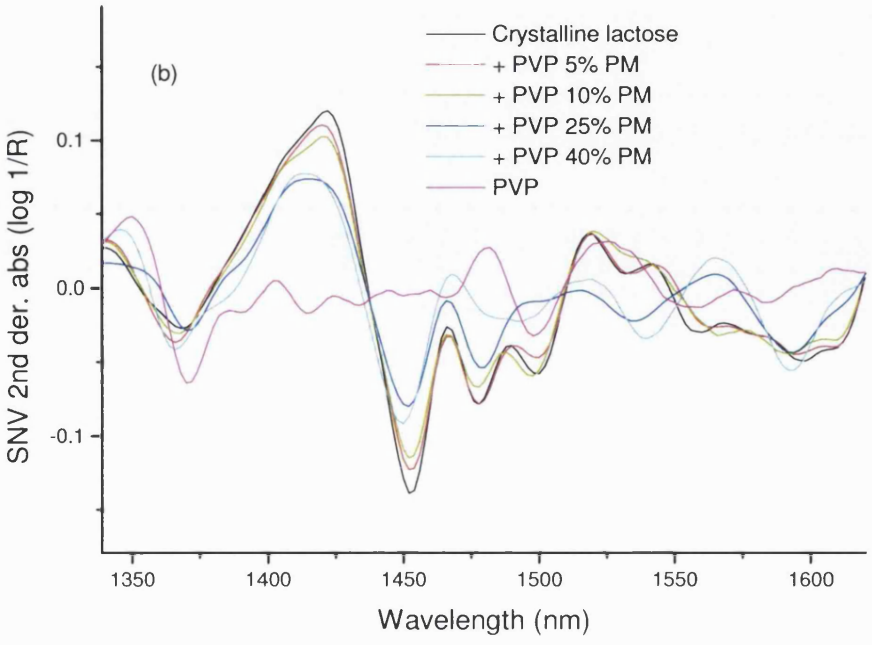

4.3.4.3 The Anomeric Region

The effects of PVP (K-25) on the anomeric region of lactose (2000-2200 nm) were similar to previous findings. The SD and PM products that contained low concentrations of PVP (5 and 10%) were found to crystallise to the monohydrate and β-anhydrous which is detected at 2104 and 2126 nm (Fig 4.27). The SD and PM products (with the exception of PM product containing 25% w/w) containing a high concentration of PVP presented a monohydrate peak as well as an α-peak at 2094 nm. This would indicate that no β-anhydrous was formed within the sample or that NIRS is not sensitive to detect the latter anomer. From literature (Buckton et al., 1998; Lane and Buckton, 2000) it seems that only one anomer is detected within this region at any particular time.

Fig 4.27. SNV 2nd der. NIR spectra showing the anomeric region of (a) SD and (b) PM products.

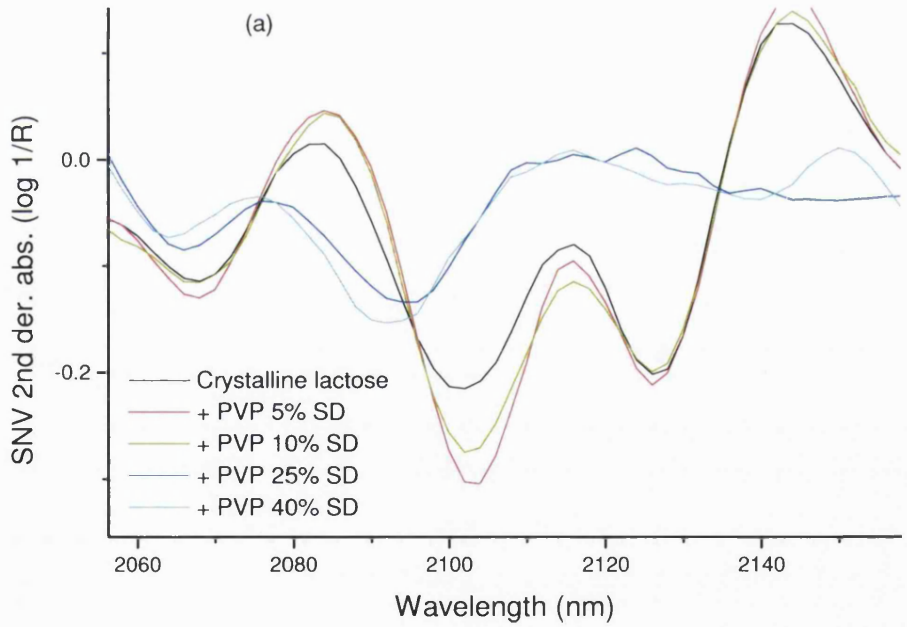

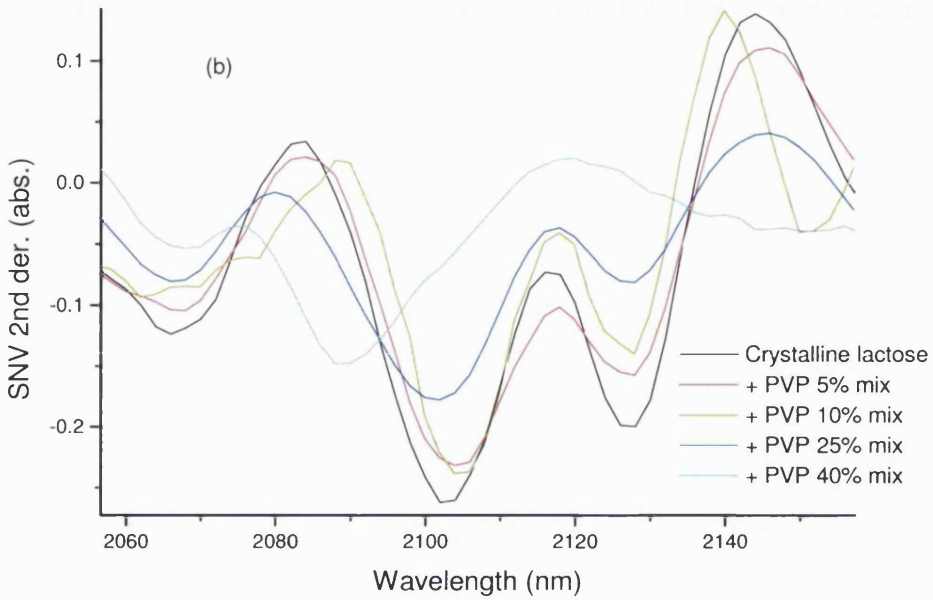

The crystallisation of lactose under the influence of the hygroscopic nature of PVP coupled with the rapid uptake of water vapour would seem to favour the production of the α-anomer. This therefore tips the ratio of α to β, where the α-anomer was detected in favour of the β-form. This is expected as the β-anomer converts to the α-form under the influence of water vapour at a high relative humidity (> 94%, Angberg et al., 1991). However with a hygroscopic material which absorbs and retains large amounts of water the RH within the sample will be elevated rapidly and maintained for along time promoting mutarotation.

In conclusion NIRS has shown that the nucleation phase was indeed delayed by the addition of PVP (K-25) at high concentrations for the SD products. This was monitored by the onset of crystallisation. The time taken for crystallisation to be complete was difficult to assess, as there were ongoing gradual changes in the spectra throughout the experimental cycle. However once crystallisation was complete, the formation of a monohydrate peak was seen for all concentrations of PVP in both the SD and PM products. This would indicate that lactose crystallisation was not inhibited. Although a closer look at the spectra for SD and PM samples containing 25 and 40% PVP showed that hydrogen bonding may have taken place during the elevated RH period between lactose and PVP from the peaks identified in section 4.3.4.2. This may have inhibited some of the lactose from crystallising to form a monohydrate.

4.3.5 Quantification of PVP content using NIRS

After qualitatively assessing the NIR spectra it became apparent that the amount of PVP (K-25) within the SD products could be quantified. This was done at a number of points along the experiment, which again highlights the advantage of combining NIRS and DVS. The pharmaceutical applications of NIRS have been discussed in chapter two as relatively new applications. Moffat (1998) has defined a case for the use of NIR as a primary method of analysis. In terms of quantification, Moffat (1998) explains "there is no reason why the spectral values measured by NIR cannot be directly related to mass..." and this includes the mixture of two solids. Quantitative studies that have been published in literature have been described in chapter two section 2.8.1.

The aim of this study was to investigate whether PVP could be quantified under a variety of experimental and physical changes of the sample. The quantity of PVP within the spray dried system was assessed at the beginning of the experiment: untreated sample, at the end of the first drying stage: when all the samples are dry and we have only amorphous lactose and PVP; At the end of the crystallisation stage at 75% RH, and at the end of the 2nd drying stage; crystallised dry sample of lactose and PVP (K-25). The SNV 2nd derivative of absorbance has been used to assess the NIR spectra as described in chapter three, section 3.3.6.

4.3.5.1 The Quantification Process

The quantification process consists of a calibration set, which was used to generate an equation to help predict the validation set. Mathematical processing which consisted of multiple linear regression (MLR) technique was used to generate the calibration equation across the full wavelength range of 1100-2500nm. This method is often chosen when the relationship to be established is linear and the spectral noise is low.

A NIR absorbance spectrum was chosen and entered into the database along with its actual PVP content (termed the reference value) known from sample preparation. The spectra of 18 samples (which also derive from different batches) are randomly selected into two groups at a 60:40 ratio, which form the calibration and validation set respectively. A mathematical treatment was then chosen to remove multiplicative interferences such as scatter and particle size of the samples. In keeping with previous results the SNV-2nd derivative (absor.) was chosen. The MLR technique was then applied

to the calibration set using the Vision software. An equation was then recorded along with the wavelength at which the correlation was found to be at its peak between the reference PVP content and the SNV 2nd derivative NIR calculated values. A number of wavelengths can be added to the calibration equation to improve the correlation but there is danger in overfitting the data. In either case it was found that a good correlation was achieved with the one chosen wavelength from the software.

The quantification process was conducted on four spectra along the DVS experimental run to determine the PVP content in the spray dried samples under various physical forms. The initial spectrum studied was when the sample contained residual water (point (a) along Fig 4.28). The second spectrum was when the sample was dry (spectra taken at the end of the initial drying phase, 0% RH at 6 hours, point (b) along Fig 4.28). A crystalline sample with residual water (spectra taken at the end of 75% RH at 12 hours point (c) along Fig 4.28) was also quantified. Finally a dry crystalline sample (the final spectra of the experimental run at 0% RH for 6 hours point (d) along Fig 4.28).

Fig 4.28. A DVS graphical representation of the physical state and where the spectra have been taken along the experiment.

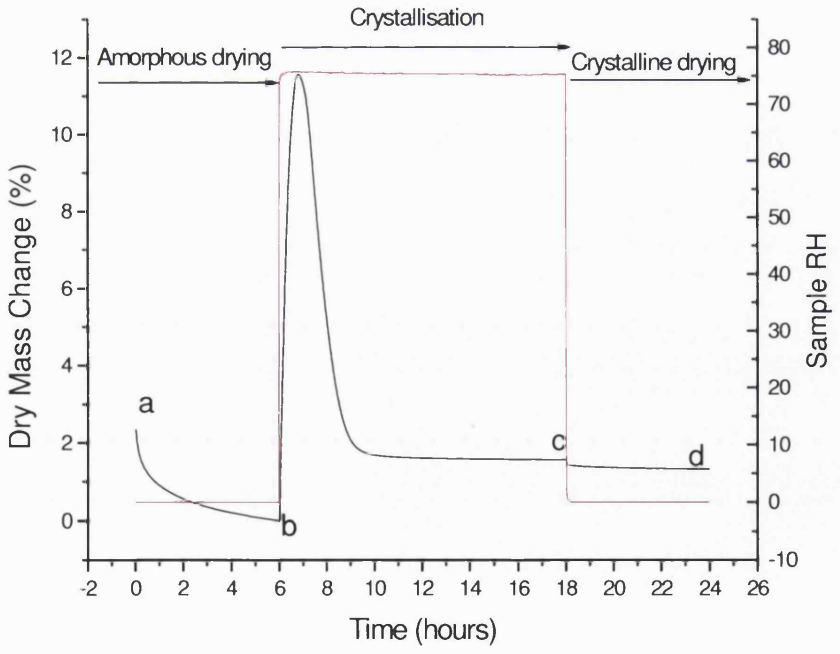

A number of mathematical parameters can be quoted to assess how well the data can be quantified and validated. The F value (equation 4.7) is a useful tool for the indication of possible "overfitting" of the calibration to the reference set and the determination of how many wavelengths should be used in the calibration equation. It is also an indication of the effectiveness of the wavelength chosen (Wilson et al., 2001). In all cases in this study the one wavelength was used as chosen by the software, which has been described above.

$$F = R^2 (n-K-1) / K (1- R^2) \quad \text{..... equation 4.7}$$

Where n is the number of samples, K is the number of wavelengths and R^2 is the multiple correlation coefficient.

The residual sum of squares (RSS) represents the difference between the reference and NIR calculated values squared. This value can be used to calculate the standard error of calibration (SEC), equation 4.9.

$$RSS = \sum_{i=1}^{n} (y_i - Y_i)^2 \quad \text{..... equation 4.8}$$

$$SEC = \sqrt{\frac{RSS}{n-p}} \quad \text{.....equation 4.9}$$

Where y is the reference value of PVP content (%) from the SD products, Y is the NIR calculated value of the PVP content (%), n is the number of samples and p is the number of coefficients in the calibration equation. The wavelength chosen for each spectrum quantified along with the appropriate mathematical parameters is shown in table 4.16 and a graphical representation in Fig 4.29.

Table 4.16. The spectrum chosen for quantification along with the wavelength where the correlation was the greatest. The F-value and the SEC is also shown for the calibration sets.

Spectra	Physical state of sample	Wavelength (nm)	R^2	F-value	S.E.C (% w/w)
(a)	Amorphous untreated	1686.0	0.99	4504.6	2.02
(b)	Amorphous dry	1170.0	0.99	634.7	1.85
(c)	Crystalline	1688.0	0.99	4180.6	1.43
(d)	Crystalline dry	1660.0	0.99	1465.7	2.35

Fig 4.29. A graphical representation of the calibration sets for the quantification of PVP content (%) in SD products for the different spectra which represents the samples (a) untreated (b) dry amorphous (c) crystalline (d) dry crystalline.

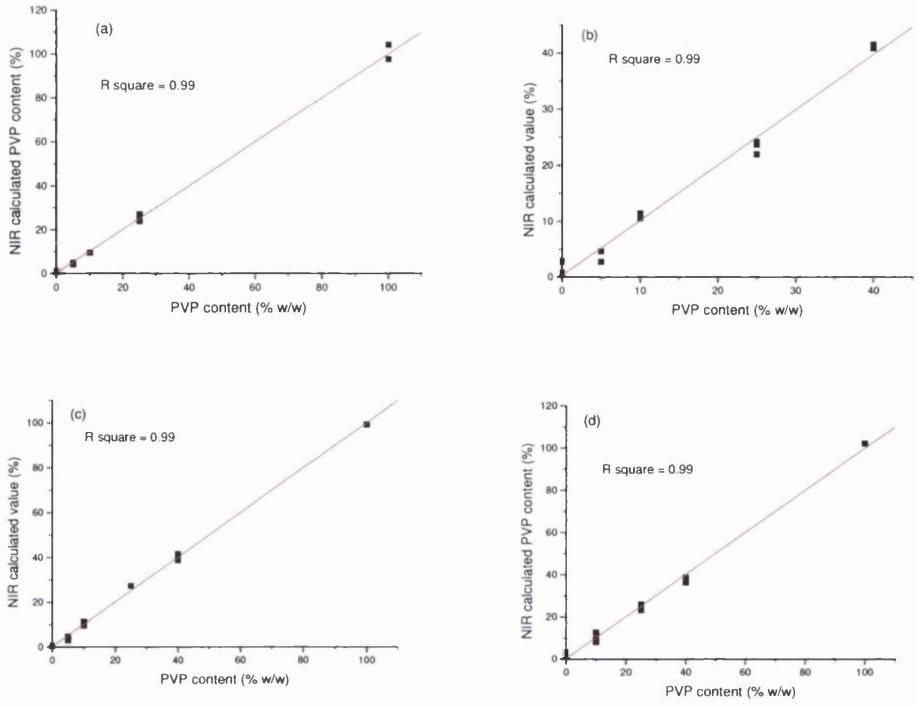

All four spectra showed a good correlation with the calibration equation, thus indicating that the PVP (%) content can be quantified regardless of the physical state of the sample and external conditions of the environment. The chosen wavelengths by the NIRS (Fig 4.30 shows the areas of interest) also confirm that we are quantifying the PVP content as they correspond to PVP overtones that arise from its structure.

The F value is relatively high for all four spectra in comparison to literature (Wilson et al, 2000) indicating a very good fit to the wavelength chosen. The value is lowest for spectra where the samples have been exposed to a drying state, this may be explained by the fact that NIRS prime use is in the study of water behaviour in materials particularly in the food industry, where its use is prevalent. The main reasons for this are its low absorptivity for water and its usefulness in the study of hydrogen bonding (Osborne et al., 1993). Therefore this may explain the reason for low F value for spectra taken from the drying stages of the DVS cycle and the relatively high SEC values.

Fig 4.30. NIR spectra of lactose and PVP (K-25). The regions boxed are the wavelength spectra chosen by the quantification process, which occurs where PVP spectrum is most prominent.

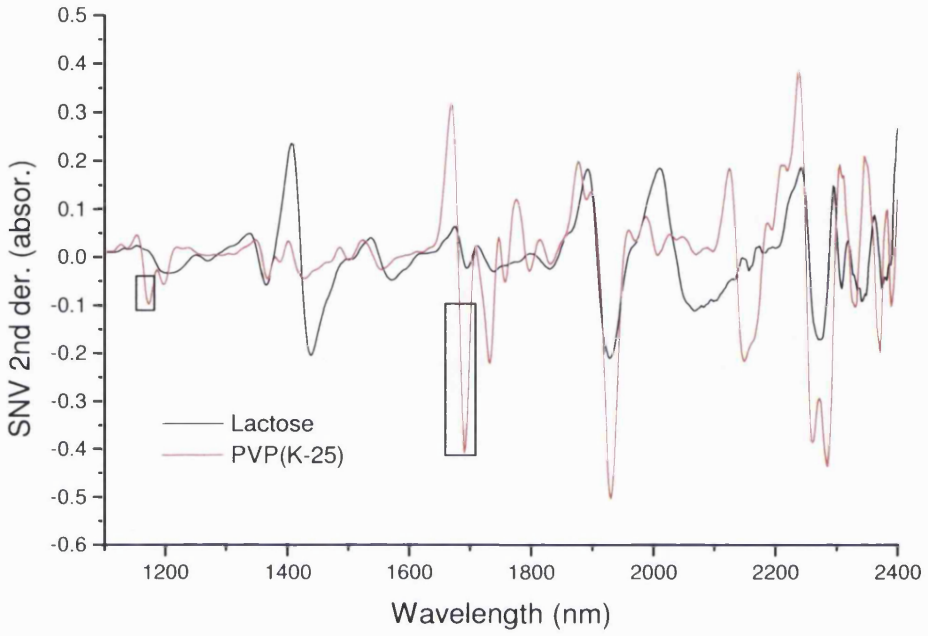

4. 3.5.2 Validation of the Calibration equation

The calibration equation was validated by application to a validation set. This was conducted for all four spectra values as shown in table 4.17. The standard error of prediction was calculated using the same equation for SEC except p=0, which represents the number of coefficients in the equation.

Table 4.17. A summary of the validation of NIR spectra at different physical states of the SD sample along the DVS cycle.

Spectra	Physical state of sample	Wavelength (nm)	R^2	S.E.P (% w/w)
(a)	Amorphous untreated	1686.0	0.99	2.72
(b)	Amorphous dry	1170.0	0.99	4.70
(c)	Crystalline	1688.0	0.98	5.03
(d)	Crystalline dry	1660.0	0.99	3.80

The validation data (table 4.17) showed there was a good correlation for all NIR spectra at different physical states. The SEP was lowest for the samples that are amorphous and

contain residual water. Furthermore at a concentration greater than 5% PVP the quantification of the polymer can be confidently assessed for all physical states. The study was also conducted on PM product (results not shown), which also produced a good correlation for PVP content at each physical state of the sample.

4.3.5.3 Quantification of PVP using Spectra in Combination

In this section the combination of all the spectra in one group (a total of 72 spectra) has been quantified for PVP content to investigate whether a good correlation between different physical state spectra could also be produced. Fig 4.31 shows the calibration graph for 43 spectra (note the spectra is divided in to a calibration and validation set at a 60 to 40 ratio as described in section 4.3.5.1).

Fig 4.31. A graphical representation of the calibration set for the quantification of PVP content (%) in SD products for the different spectra.

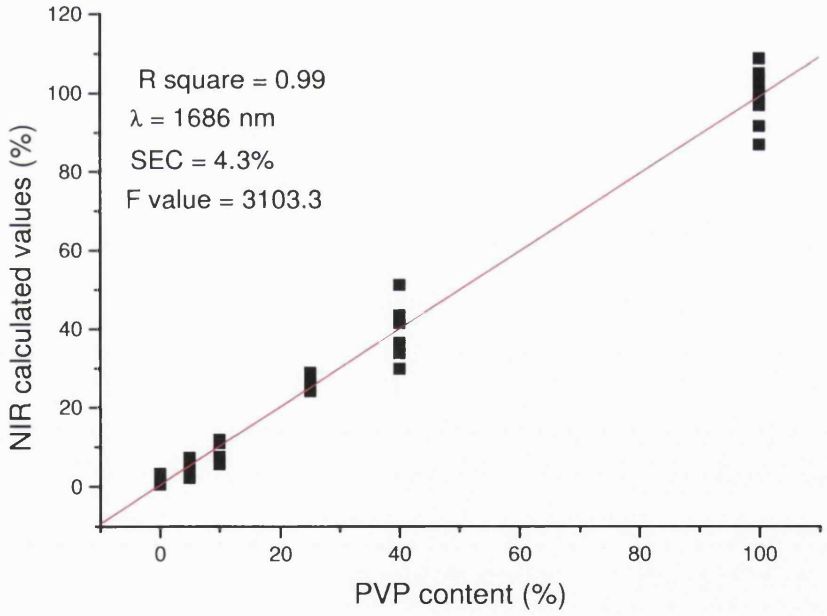

The results show that NIR is non-specific to the physical state of the product and that we can quantify a component regardless of the state by one common wavelength. Although this is possible we do lose some sensitivity at lower concentrations with the SEC and SEP at 4.3 and 8.7% respectively. There is a good correlation with the calibration equation at 0.99 but this falls slightly using the validation set at 0.97. The approach of using NIRS is

a novel way of quantification in pharmaceutics as we can simply quantify a material off the shelf in a non-invasive and rapid manner regardless of its physical state. The build up of a library to quantify a material can also be produced at whatever state the material is in; wet, dry, amorphous or crystalline. This would be particularly useful during the early stages of formulation in pharmaceutics where there are very little amounts of sample. From this preliminary study it seems that the spectra that we have collected during one DVS experimental run (144 in total) would be quantifiable for PVP content. If we include repeats of an experimental run a large amount of spectra has been collected for this chapter (4320 spectra). The spectra could all be used to produce a database and quantify the PVP content in a binary blend of amorphous lactose and PVP (K-25).

4.3.6 Characterisation of the SD products after crystallisation

Characterisation of the SD products after crystallisation at 75% RH in the TAM was conducted to investigate whether the anomeric composition of amorphous lactose was affected during crystallisation. The crystalline samples were also exposed to heat under the influence of the DSC to assess the effects of PVP on lactose during crystallisation, however we need to be aware that in pan transitions could take place.

4.3.6.1 GC

GC data were obtained using the procedure outlined in chapter two (section 2.10.3), the crystalline material removed from the TAM was immediately derivatised and studied for its anomeric ratio. The results were also compared to the anomeric ratio of the co-spray dried products before proceeding with crystallisation.

From table 4.18 PVP (K-25) seems to have no effect on the anomeric composition when co-spray dried with lactose. The ratios are fairly consistent with ascending PVP concentration. After crystallisation in the TAM at 75% RH there was a marginal increase in the α-anomeric composition for the higher concentration of PVP (K-25) 25 and 40%. It was interesting to note that the increase in the α-content occurs for the co-spray dried products containing the higher concentration of PVP (K-25). This was also seen by NIRS for these products, where in the anomeric region (4.3.4.2) only the α-peak at 2096 nm was seen. Although a direct comparison between data cannot be made as the uptake of water vapour for each technique is different and this may affect the anomeric ratio, as the presence of water vapour promotes β to α mutarotation. Nevertheless it does seem that

when we add a hygroscopic material to lactose, where a large amount of water is absorbed and retained the α-anomer is favoured.

Table 4.18. The anomeric composition of the SD products after exposure to 75% RH in the TAM (n=4).

SD product.	Before crystallisation		After crystallisation	
	α	β	α	β
Amo lactose	41.7	58.3	46.0	54.0
Amo lac + PVP 5%	40.9	59.1	46.0	54.0
Amo lac + PVP 10%	40.8	59.2	46.2	53.8
Amo lac + PVP 25%	40.6	59.4	49.3	50.7
Amo lac + PVP 40%	40.5	59.5	49.5	50.5

4.3.6.2 DSC

The DSC thermographs (Fig 4.32) taken after crystallisation in the TAM for SD and PM products at polymer concentration 5, 25 and 40% (10% is represented by the 5% thermograph) showed a very similar trend. The thermographs for all PVP (K-25) concentration lack the differences or the specification shown by other techniques, hence indicating that the disaccharide and polymer are interacting under the influence of heat. The main observation was the increased formation of the endotherm followed by the exothermic peak seen after the monohydrate peak with an increase in PVP concentration. The endothermic peak has been described in literature as the melting of unstable α-anhydrous followed by the crystallisation of α/β complex. Under the influence of heat PVP promotes the formation of unstable α-anhydrous to form the anomeric complex.

Fig 4.32. The DSC thermographs of crystalline lactose and PVP (K-25): (a) SD and (b) PM products.

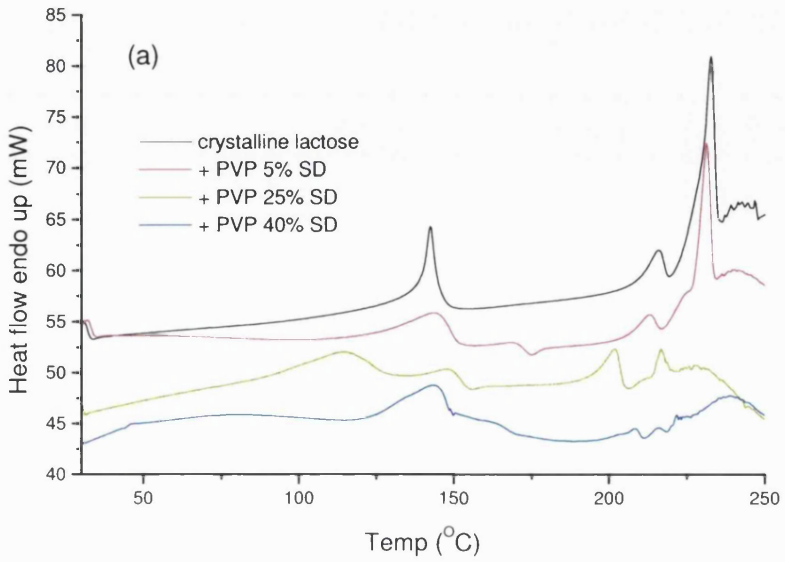

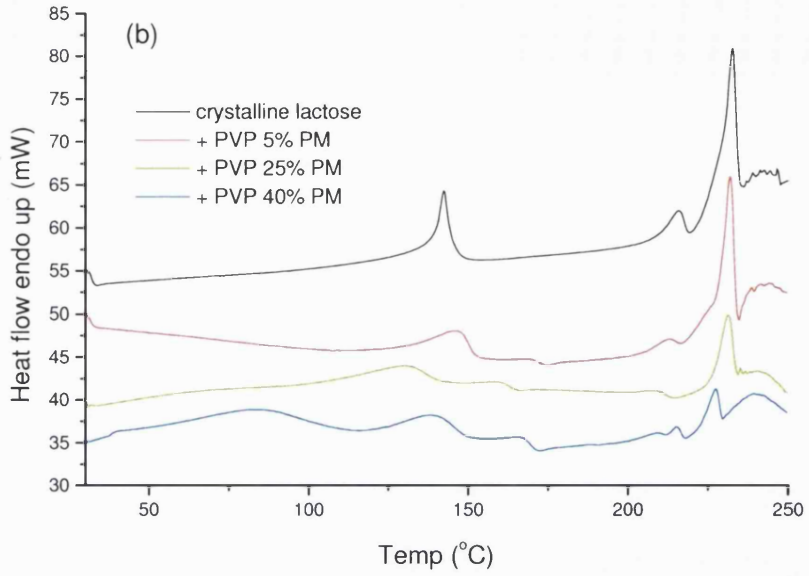

4.4 Conclusions

From the results presented the characterisation and the study of the crystallisation of amorphous lactose and PVP (K-25) at ascending concentration has been achievable by combining a variety of techniques. Prior to crystallisation, PVP at higher concentrations (25 and 40% w/w) was found to exert its effects on amorphous lactose when both components were spray dried together. Hydrogen bonding along with the increase in viscosity stabilised amorphous lactose. However an increase in entropy and excess free volume due to molecular size and steric hindrance provided a negative deviation from the theoretical equations used to assess molecular interactions and prevented an increase in Tg. For co-spray dried lactose and PVP at low concentrations 5 and 10% any significant interaction to exist was hindered by the presence of a small amount of macromolecule in a large amount of small disaccharide molecule. With the PM products, no interaction was seen between the components.

PVP (K-25) was seen to delay crystallisation of amorphous lactose by affecting nucleation phase for both the SD and PM products that contained a higher concentration of PVP (K-25) 25 and 40%. The hygroscopic nature of PVP (K-25) along with the molecular size of the polymer was responsible for this. However once nucleation of a critical size was achieved it was difficult to assess whether crystal growth of lactose was affected and inhibition had occurred. With the aid of DVS-NIRS it was possible to identify intermolecular hydrogen bonding for the crystalline products from co-spray dried

amorphous lactose and PVP (K-25) 25 and 40% and their PM counterparts. This would inevitably inhibit crystal growth of amorphous lactose.

Quantification of PVP in the SD and PM products was possible regardless of the physical state of the sample. There was a good correlation for the PVP content when the different spectra were all grouped together although some specification was lost. This does have some advantages as a library for quantification of a material can be produced and used as a database regardless of the physical state of a product.

SECTION B: Partially Amorphous Lactose and PVP (K-25)

The study of amorphous lactose and PVP (K-25) was extended to include the effects of PVP on a sample of lactose that contained amorphous and crystalline material. Partially amorphous lactose was chosen which was spray-dried from a prepared suspension of lactose 30% w/v (see chapter three, section 3.4). The suspension was determined by isothermal microcalorimetry to have an amorphous and crystalline content of 89.6 and 10.4% respectively. Chidavaenzi et al. (2001) also studied different feed concentrates of lactose with PEG 4000 with unexpected results. The study found that there was a difference in the co-spray dried product of lactose and PEG 4000 depending on whether the feed concentrate of lactose was a solution or a suspension. Other studies have followed namely Corrigan et al. (2002), which described similar findings.

The majority of this study was conducted in a similar manner as described in section A of this chapter, with the experimental techniques, methodology and materials been identical. The aim of this study was to establish the effects of PVP on partially amorphous lactose in a SD and a PM product at an ascending concentration. In addition particle sizing was also determined for the SD products using the experimental methodology described in chapter two, section 2.12.

4.5 Results and Discussion

4.5.1 Characterisation of SD products prior to crystallisation

4.5.1.1 PXRD, DSC, TGA

PXRD along with DSC was used to characterise the SD and PM products of partially amorphous lactose (pa. amo.) and PVP. The PXRD diffractograms (examples are shown in Fig 4.33) showed all the samples whether SD or a PM showed a peak at 12.6°, a range of peaks at 19-20° (2θ) and also at 22.0°, this is similar to SD lactose from 30% feed concentrate. The peaks were identified with the aid of DSC to correspond to stable α-anhydrous lactose (see chapter three, section 3.6.1.1). For the SD product containing 40% PVP, the diffractogram showed the sample contained a greater amount of crystalline matter. Peaks for the SD product containing 40% PVP were identified at 12.5, 16.5 and 20°, which represented α-lactose monohydrate. Further confirmation, was seen by DSC thermographs (Fig 4.34) where an α-lactose monohydrate dehydration peak was seen at ~

145°C for co-spray dried pa. amorphous lactose and 40% PVP. For the SD products at concentrations of PVP 5, 10, and 25%, the DSC traces were similar to partially amorphous lactose alone. With the PM products of all concentrations of PVP (K-25), the DSC traces produced were all similar to partially amorphous lactose alone (not shown).

Fig 4.33. PXRD diffractograms of Pa. Amo. Lactose + PVP (K-25) (a) 5% SD (b) 25 % PM and (c) 40% SD.

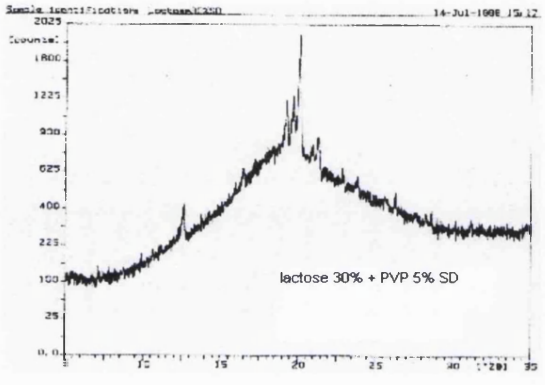

(a)

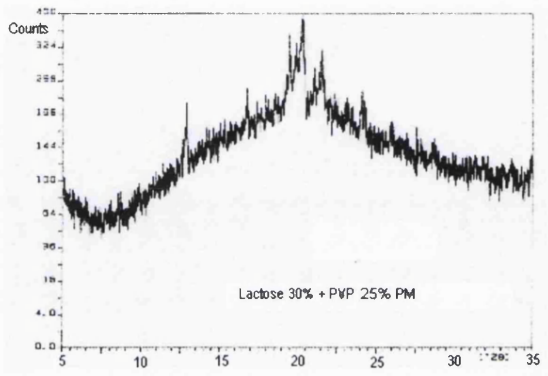

(b)

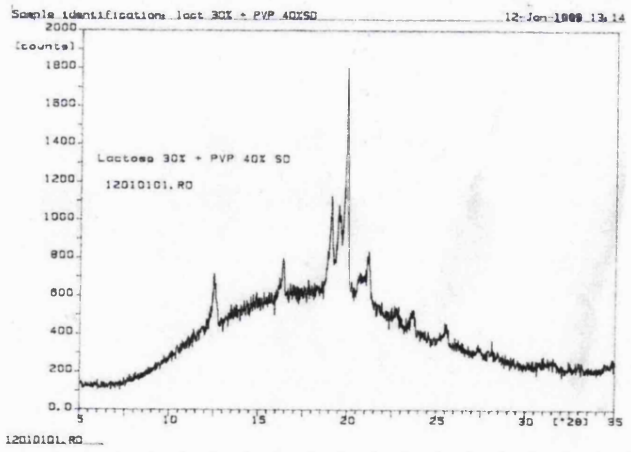

(c)

Fig 4.34. DSC thermographs of SD pa. amo. lactose alone and 40% PVP (K-25).

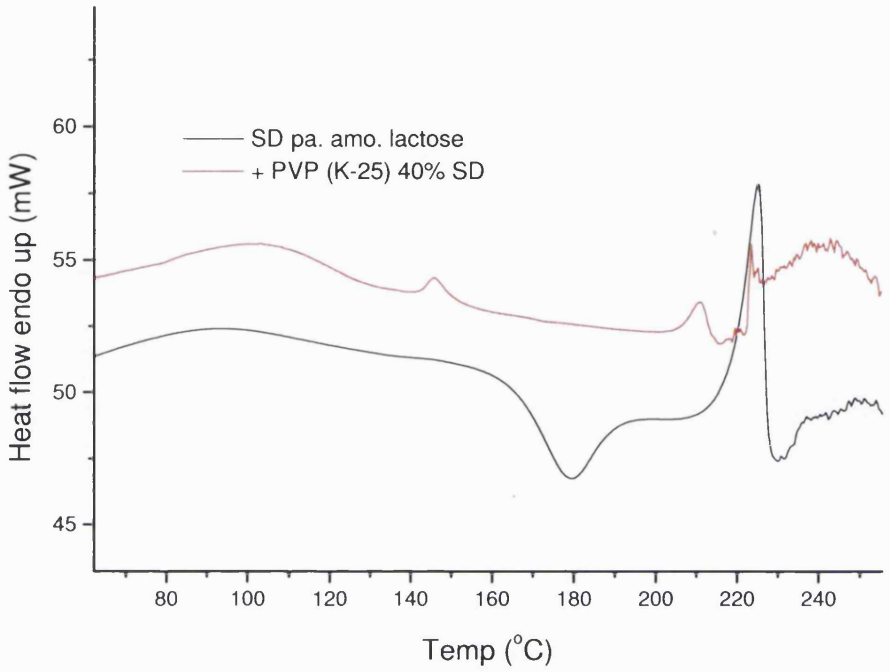

The quantity of α-lactose monohydrate in co-spray dried pa. amo. lactose and 40% PVP (K-25) can be estimated using TGA. The TGA thermograms (Fig 4.35 (a)) showed that 0.93% (± 0.12, n = 8) water was attributed to the monohydrate. From this percentage, we can calculate the amount of crystalline monohydrate present in the sample. This is achievable as the (%) water monohydrate has been determined for the starting material lactose monohydrate as 5.48%, which contains 94% α-lactose monohydrate. From these figures the (%) water content per percent of lactose monohydrate is 0.058% (5.48 / 94). A simple division of 0.93/0.058 tell us that SD pa. amo. lactose with PVP (K-25) 40% w/w contains approximately 16.0% monohydrate.

Fig 4.35. A TGA thermogram of (a) Pa . amo. lactose + PVP (K-25) 40% SD product and (b) "as received" lactose monohydrate .

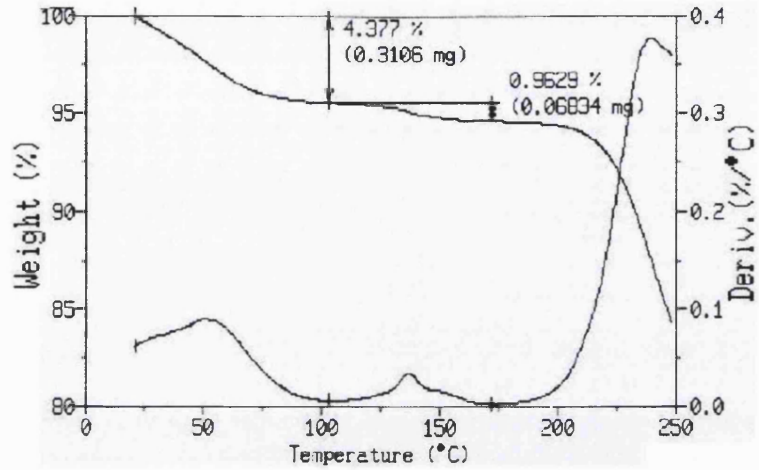

(a)

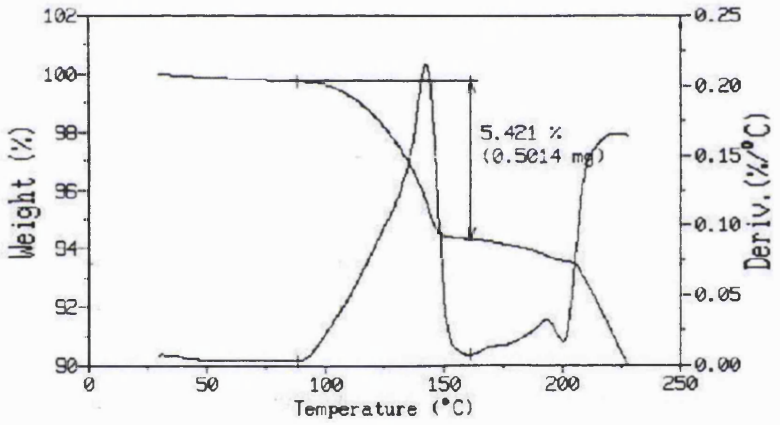

(b)

From the characterisation of SD products using DSC, PXRD, and TGA, we were able to determine the composition of each sample (table 4.19). The increase in the small monohydrate content for SD pa. amo lactose with 40% PVP (K-25) may be due to the increase load of material when spray drying. During the process of atomisation coupled with the increase in pump rate, there is a reduction in residence time in the atomiser, so therefore not all the monohydrate was milled and converted to the amorphous state. Therefore there would be an increase in particle size with an increase in load of the sample, which was investigated in the following section.

Table 4.19. The anomeric composition of SD pa. amo. lactose and PVP (K-25) products at ascending concentration of the polymer.

SD product lactose	Composition (%) Amorphous	α-monohydrate	α-anhydrous	β-anhydrous
30 % w/v	89.6	0	10.4	0
+ PVP 5%	89.6	0	10.4	0
+ PVP 10%	89.6	0	10.4	0
+ PVP 25%	89.6	0	10.4	0
+ PVP 40%	84.0	16.0	0	0

4.5.1.2 Particle Sizing and SEMS

Table 4.20 showed that the addition of PVP (K-25) to partially amorphous lactose showed no change in the overall particle size of the system except for 40% PVP (K-25) where the value of 90% undersize was relatively high with respect to partially amorphous lactose alone. This reflects the α-lactose monohydrate within the binary blend, which can be compared to the starting material of α-lactose monohydrate and the increase in pump rate due to an increase spray drying load. The particle size data was also verified by SEMS taken by the samples (Fig 4.36). Fig 4.36(d) represents SD pa. amo. lactose and PVP (K-25) 40% which showed that there was on average large particles produced by the spray drying process.

Table 4.20. A representation of particles size for the SD products of partially amorphous lactose and PVP (K-25)(n=15).

	10%undersize (μM)	50%undersize (μM)	90% undersize (μM)
Lactose mono.	2.9 ± 0.3	16.3 ± 1.0	40.9 ± 4.0
Pa. Amo. Lactose	1.1 ± 0.8	8.2 ± 0.6	20.4 ± 1.2
+ PVP 5% w/w	0.9 ± 0.3	5.6 ± 0.9	17.7 ± 0.5
+ PVP 10% w/w	2.0 ± 0.6	7.4 ± 0.2	21.3 ± 0.4
+ PVP 25% w/w	0.7 ± 0.2	1.6 ± 0.5	16.8 ± 1.4
+ PVP 40% w/w	0.7 ± 0.2	1.5 ± 0.7	38.2 ± 2.1

Fig 4.36. SEMS of (a) partially amorphous lactose + PVP (K-25) (b) 10% (c) 25% (d) 40% SD products.

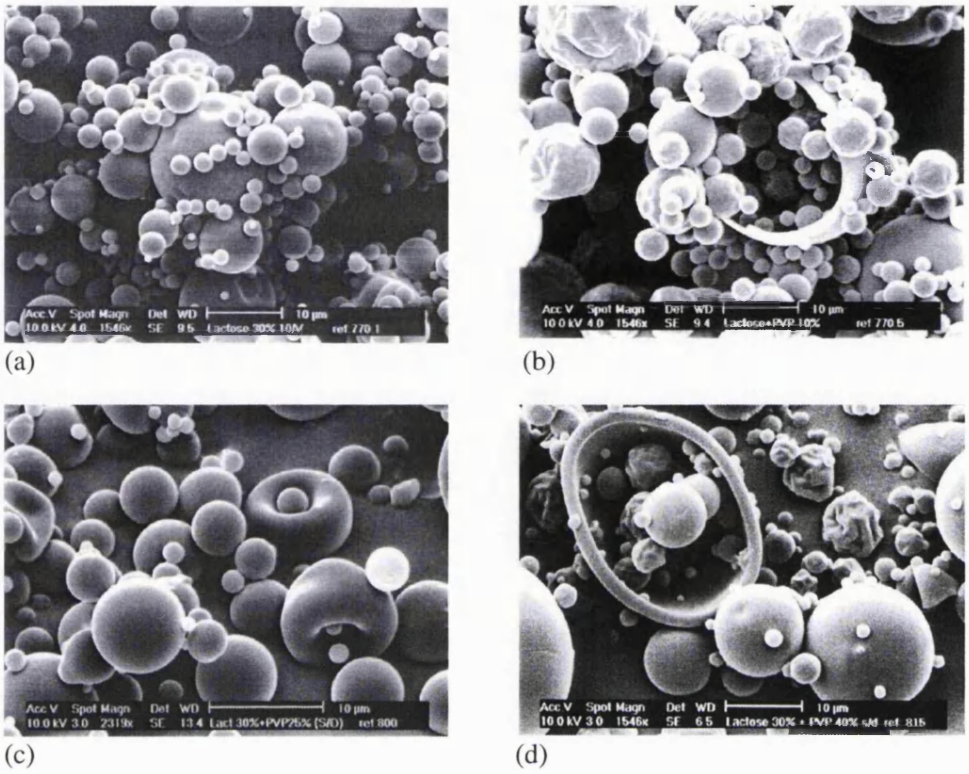

4.5.1.3 Determination of T_g

Since the preliminary characterisation of SD pa. amo. lactose and PVP (K-25) showed a difference in composition in comparison to co-spray dried amo. lactose and PVP (K-25), the T_g of the SD products was also investigated to compare results (table 4.21). The T_g and specific heat capacity of partially amorphous lactose are lower in relation to amorphous lactose. The T_g of a material is independent of the degree of crystallinity but with an increase in crystallinity the transition becomes difficult to detect (Ford and Timmins, 1989). With a partially amorphous material the specific heat capacity would be expected to decrease but the T_g to remain the same. The T_g value reported is within literature values for a material that is 100% amorphous (Hancock and Zografi, 1994). The glass transition of a material usually occurs over 20°, it is likely that with a decrease in ΔC_p there will be a small change in the reported T_g value. All samples showed one glass transition, which indicates miscibility between polymer and the low molecular weight sugar.

Table 4.21. A summary of the ΔC_p and T_g of co-spray dried partially amorphous lactose and PVP (K-25) (n=4).

SD product	ΔC_p (J/g/°C)	T_g (°C)
Pa. Amo lactose	0.366 ± 0.044	112.3 ± 1.1
+ PVP 5%	0.388± 0.0.33	112.3 ± 0.4
+ PVP 10%	0.433 ± 0.040	115.0 ± 1.2
+ PVP 25%	0.373 ± 0.038	121.4 ± 0.9
+ PVP 40%	0.257± 0.037	127.6 ± 1.2

In comparison to co-spray dried amorphous lactose and PVP (K-25) there was a greater increase in the T_g of pa. amo. lactose with the addition of PVP (K-25). This was especially the case at a high concentration of the polymer (40%) where there is an increase in the T_g of ~15° compared to a 7° increase for amorphous lactose and PVP (K-25) SD. PVP (K-25) seems to be acting as a relatively effective antiplastiscing agent with partially amorphous lactose than a sample that is 100% amorphous. A plausible explanation could be a decrease in the free volume of the system with an increase in PVP content at a concentration of 10% and greater coupled with crystalline material, which may fill the voids produced. This may lead to **less** excess free volume been generated on mixing and hence the consequence would be a higher T_g. There is also the increase in rigidity with the addition of PVP (K-25) and hence a decrease in molecular mobility of amorphous lactose which would raise the T_g. For co-spray dried pa. amo. lactose and 40% PVP where the largest difference in T_g and ΔC_p was observed, the polymer has a smaller quantity of amorphous lactose to "interact" with. So the addition of PVP is more profoundly seen. A rise in T_g in the presence of crystalline material has also been reported by Okhamafe and York (1987).

How effective the increase in T_gs are for the SD products can be determined using the theoretical equations described in section 4.3.1.3. The density of a dry sample of partially amorphous lactose was determined by pyconometry at 1.53 gcm^{-3}. The K value was calculated to be 1.08. Component 1 and 2 in the equations were lactose and PVP (K-25) respectively. Fig 4.37 illustrates the trend between the Tg and the lactose percentage using the theoretical equations.

Fig 4.37. A change in T_g as a function of partially amorphous lactose (w/w) co-spray dried with PVP (K-25). (■) experimental values, (●) calculated Gordon-Taylor values (▲) calculated Fox values (▼) calculated Couchman-Karasz values. (—) Kovacs critical temperature (T_c)

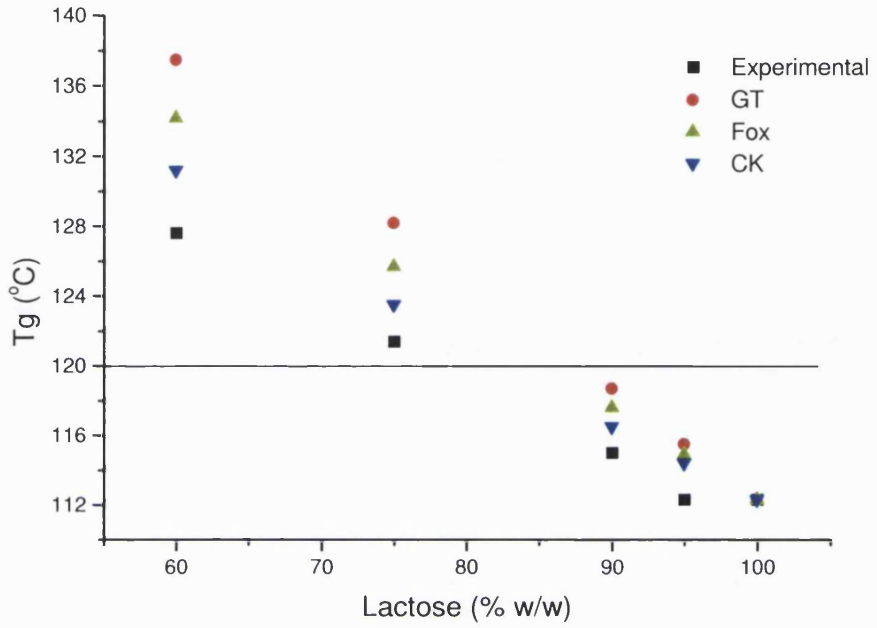

Although there was an increase in the T_g with the binary blends which contain crystal seeds, a similar trend to that of co-spray dried amorphous lactose and PVP (K-25) was seen. There was a negative deviation from all analytical equations, indicating that the reasons for deviation are similar to that of amorphous lactose and PVP (K-25) SD products. From section 4.3.1.3 it was found that there was an increase in the entropic changes which lead to an increase in free volume on mixing that provides a negative deviation from the calculated values.

4.5.2 The use of TAM in the crystallisation of partially amorphous lactose binary systems.

Crystallisation for co-spray dried and PM products were induced at 75% RH in a similar manner as described in section 4.3.2. The aim was to quantify the amorphous content after and to establish whether crystallisation was delayed or inhibited by the addition of PVP (K-25) in the presence of seed crystals. Fig 4.38 shows the TAM data for co-spray dried products of pa. amo. lactose and PVP (K-25), where visually we can see that there was a delay in the onset of crystallisation.

Fig 4.38. A TAM graphical representation of SD products consisting of partially amorphous lactose and PVP (K-25).

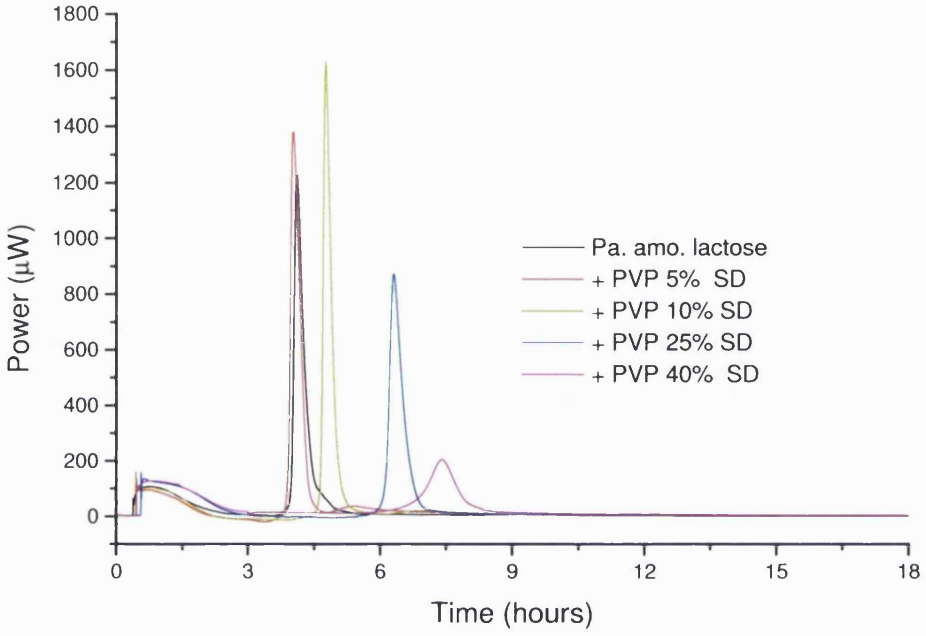

The addition of PVP (K-25) above 5% delays the onset of crystallisation, which has been determined in table 4.22. This shows a similar trend to the T_g data where there was an increase in the T_g above 5% PVP (K-25). At a concentration of 10% or greater, PVP (K-25) the delay in the onset of crystallisation represents a delay in the nucleation phase, which occurs regardless of crystal seeds of lactose been present. The shapes of the peak also indicate that there was a change in the crystallisation kinetics of lactose with an increase in PVP (K-25) concentration.

Table 4.22. A summary of the onset of crystallisation for partially amorphous lactose and PVP (K-25) SD product (n=4).

SD product	Onset of crystallisation (hours)
Pa amo. lactose	3.5 ± 0.09
+ PVP 5%	3.5 ± 0.17
+ PVP 10%	4.0 ± 0.03
+ PVP 25%	5.5 ± 0.50
+ PVP 40%	5.6 ± 0.08

To determine the enthalpy of crystallisation for co-spray dried partially amorphous lactose and PVP (K-25), the sample has to be corrected for lactose weight as described in section 4.3.2.2 as well the amount of crystalline material in each SD sample. An example calculation is shown in table 4.23 and the values for the SD products in table 4.24.

Table 4.23. Example calculations of the subtraction of the enthalpy related to PVP (K-25) from the apparent enthalpy of crystallisation of amorphous lactose. The final apparent enthalpy of crystallisation was divided by the amount of lactose within the sample load. This was achieved by subtracting the weight of PVP (K-25) and the amount of crystalline material in the sample which is 16.0% in this case.

SD pa amo. lactose + PVP 40% w/w	Sample weight (mg)	Sample weight of amo. lactose	(ΔH_c lactose) – (ΔH PVP) (J)	Apparent ΔH_c lactose (J/g)
L30p40a	30.3	30.3 × (1- (0.4 + 0.16)) = 13.3	618.7–11.7= 607.0	45.6
L30p40b	30.0	30.0 × (1- (0.4 + 0.16)) = 13.2	605.5–11.7= 593.8	45.0
L30p40c	30.0	30.0 × (1- (0.4 + 0.16)) = 13.2	593.2–11.7=5 81.5	44.1

Table 4.24. A summary of the apparent enthalpy of crystallisation (ΔH_c) for amorphous lactose after subtraction of PVP enthalpy and correction of amorphous lactose weight for SD products (n=4).

SD product	ΔH_{cry} (mJ/ mg)	(%) Apparent amorphous content
Pa. amo. Lactose	40.9 ± 1.9	100
+ PVP 5 %	46.6 ± 2.4	113.9
+ PVP 10 %	48.1 ± 3.0	117.6
+ PVP 25%	50.8 ± 0.5	124.2
+ PVP 40%	44.9 ± 0.8	109.8

Table 4.25. A summary of the apparent enthalpy of crystallisation (ΔH_c) for amorphous lactose after subtraction of PVP enthalpy and correction of amorphous lactose weight for PM products (n=4).

PM product	ΔH_{cry} (mJ/mg)	% Apparent amorphous content
Pa. amo lactose	40.9 ± 1.9	100
+ PVP 5 %	48.5 ± 1.3	118.6
+ PVP 10 %	49.7 ± 1.2	121.5
+ PVP 25%	51.3 ± 1.6	125.4
+ PVP 40%	52.4 ± 0.3	128.1

A comparison of the enthalpy of crystallisation for the SD and PM products (tables 4.24 and 4.25) present a similar result to amorphous lactose and PVP products (section 4.3.2.2). There is excess water retained within the products during crystallisation which makes it difficult to quantify the amorphous content. Therefore the conclusion that can be drawn is that the quantification of amorphous material is not accurately possible with the addition of a hygroscopic material.

4.5.3 The investigation of crystallisation using DVS for partially amorphous lactose binary systems.

Fig 4.39. A DVS graphical representation for pa. amo. lactose and PVP (K-25) (a) SD and (b) PM products.

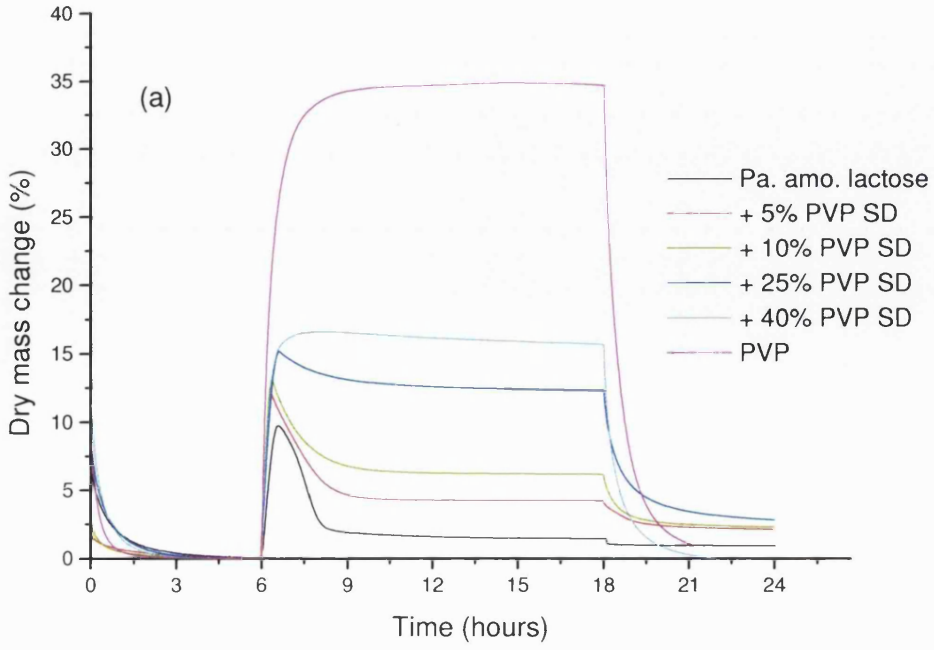

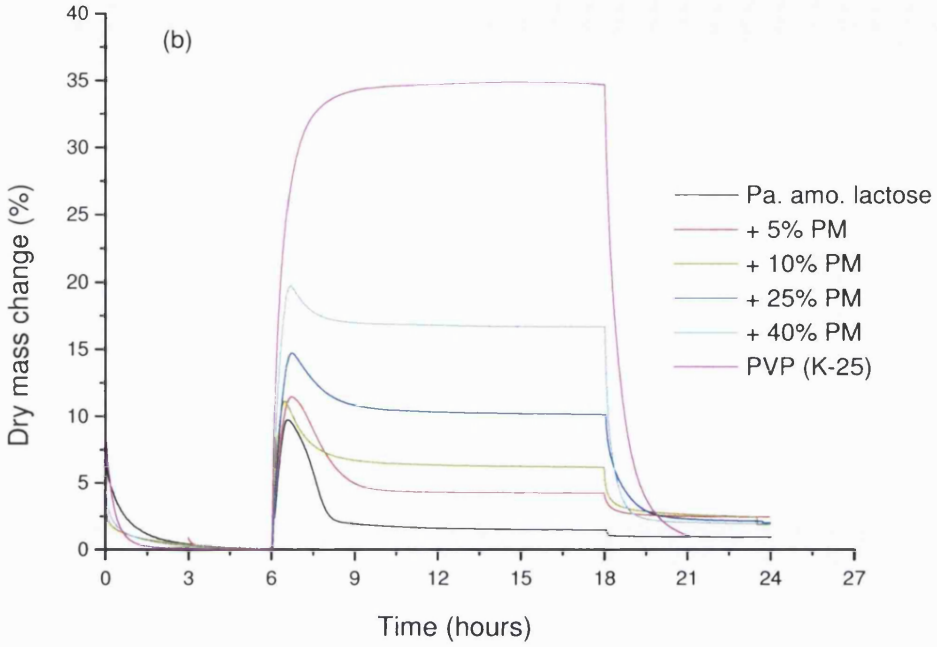

From previous sections it has been apparent that the use of DVS has been vital in assessing water sorption, desorption of binary products, and hence has been used in this section. The aim of this study was to assess the crystallisation kinetics of the SD and PM products using similar methods discussed in section 4.6.1. Fig 4.39 shows the DSC profiles of SD and PM products, which are very similar to co-spray dried and PM products of amorphous lactose and PVP (K-25). There was an increase in the water uptake with an increase in the PVP concentration for both the SD and PM products. The induction time was also determined (table 4.26), where there was a gradual increase in the induction time with ascending concentration of polymer for the PM products, but these values do not seem significant due to large standard deviations. For the SD products there was a gradual increase in the induction time above 5% polymer, and a more significant increase at 40% PVP. This reflects a similar trend to TAM data and would confirm that the presence of PVP was affecting the nucleation phase of crystallisation regardless of the presence of crystal seeds. However the marked increase in the induction time for the SD product containing 40% PVP seems to suggest that we may have a more complex situation which would need to be investigated in detail with NIRS.

Table 4.26. A summary of the induction time for partially amorphous lactose and PVP (K-25) SD products (n=4).

Product	Induction time (mins) SD	Induction time (mins) PM
Pa. Amo. Lactose	33.7 ± 1.5	33.7 ± 1.5
+ PVP 5%	32.2 ± 5.1	36.5 ± 12.7
+ PVP 10%	34.9 ± 3.6	36.3 ± 7.7
+ PVP 25%	40.5 ± 2.1	38.8 ± 10.7
+ PVP 40%	124 ± 4.5	39.2 ± 1.6

The crystallisation half time was assessed using the exponential model (table 4.27) which showed that there was also a general increase in the half time for the SD products, which was extensively prolonged for the product containing 40% PVP. With the addition of crystalline material in the sample, one would expect that the crystallisation process would proceed at a relatively fast rate due to seeding, however we witness a delay in the nucleation phase as well as a delay in the crystal growth. For the PM products the crystallisation half times (not shown) did not show a conclusive trend. A number of reasons for this could be due to the different water desorption rates of amorphous lactose and PVP. The addition of crystalline material would not affect the water desorption, however the actual mass may hinder or alter the rate at which water is removed from the sample in a closed humidified chamber. The reason that this could be a plausible cause was the comparison of data with the PM products containing amorphous lactose and PVP alone (table 4.14, section 4.3.3.3). A trend in crystallisation half time was seen by applying the exponential model to the PM products which did not contain crystalline seeds.

Table 4.27. The crystallisation half times ($t_{1/2}$) determined by fitting the data to an exponential model for SD samples (n=4).

Product	SD $t_{1/2}$ (mins)
Pa. Amo. Lactose	46.5
Pa Amo. Lac + PVP 5%	51.1
Pa.Amo. Lac. + PVP 10%	51.5
Pa. Amo. Lac. + PVP 25%	66.1
Pa. Amo. Lac. + PVP 40%	257.8

In conclusion both T_g and isothermal microcalorimetry data along with DVS data suggest that there was a delay in the crystallisation process for partially amorphous lactose when co-spray dried with PVP. The only possible explanations are the increase rigidity and hence decrease mobility that supersedes the crystalline presence and hence has an influence in hindering crystallisation. Further confirmation that that crystallisation of partially amorphous lactose was actually hindered should be supported by NIRS.

4.5.4 Studying crystallisation using NIRS

4.5.4.1 The crystallisation of SD partially amorphous lactose

NIRS was coupled with DVS to follow the amorphous to crystalline phase transition as we have described in chapter three, section 3.6.4 and 3.6.5, in this part of the study the crystallisation of SD lactose from different feed concentrates is described. The results using NIRS showed that SD amorphous lactose (10% feed solution) and pa. amo. lactose (30% feed suspension) crystallised in a similar manner. The difference between the samples was the onset of crystallisation which was clearly highlighted by the TAM data (section 3.6.2.1). The crystallisation of SD pa. amo. lactose is shown in Fig 4.40 so that a comparison between NIRS spectra relating to co-spray dried pa. amo. lactose and PVP (K-25) can be made.

Fig 4.40. SNV 2nd der. NIR spectra of SD pa. amorphous lactose during the amorphous to crystalline phase transition at (a)1900 nm and (b) 1400 nm region.

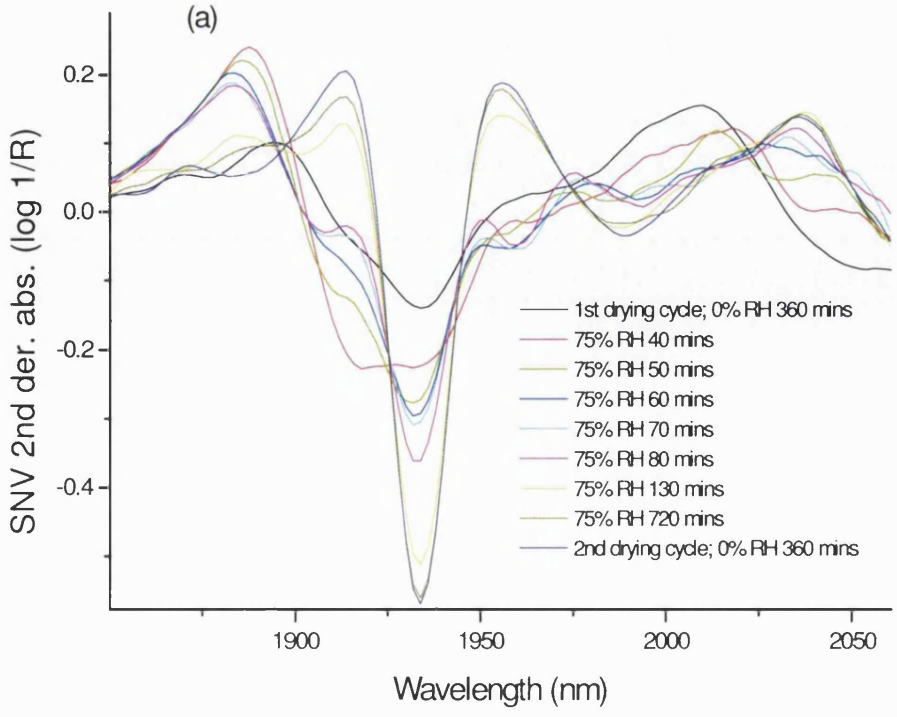

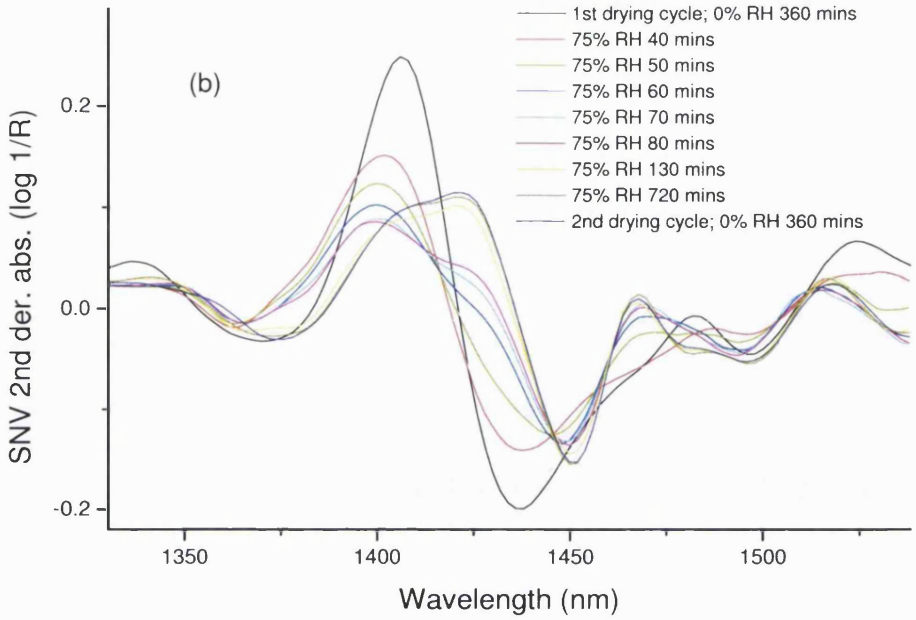

Fig 4.40 (a) showed that after 6 hours of drying, the sample was exposed to 75% RH where there was a rapid uptake of water. The spectrum taken at 40 mins showed a shift to a lower wavelength to 1920 nm indicating plastiscization. At 50 mins the onset of crystallisation was seen by a monohydrate peak seen at 1932 nm which with time becomes permanently displaced at 1934 nm. Multiple peaks formed at 70 mins at 75% RH which shifted to a higher energy state and disappeared just before crystallisation was complete. There was very little change in the monohydrate region at 1934 nm after 150 mins indicating that crystallisation was complete. There was also very little difference in the spectra during the second drying cycle of the experiment at 0% RH for 6 hours. Fig 4.40 (b) shows another area of spectra, where at 1436 nm represents a lactose first overtone O-H stretch that shifted gradually from 1438 nm to 1450 nm once crystallisation was complete. The anomeric region (not shown) of lactose at 2000 nm also showed the gradual formation of β-lactose at 2104 and 2126 nm.

4.5.4.2 The crystallisation of co-spray dried partially amorphous lactose and PVP (K-25)

The crystallisation of co-spray dried partially amorphous lactose and PVP (K-25) at 5 and 10% (NIR spectra not shown) was similar to SD partially amorphous lactose alone at 1450 and 1934 nm where these areas represent water molecules interaction in relation to monohydrate formation. The onset and duration of crystallisation was also very similar to partially amorphous lactose alone. In accordance with DVS data, both the induction time and the crystallisation half time were similar to partially amorphous lactose alone.

For co-spray dried partially amo lactose and PVP (K-25) at 25 and 40%, it was very difficult to see the crystallisation process as was described in section 4.3.4.1 due to the excess absorbed water. The problem was resolved by considering both areas of spectra pertaining to crystallisation at 1900 and 1400 nm. Co-spray dried pa. amorphous lactose and PVP 25% (Fig 4.41) showed that the onset of crystallisation occurred at 40 mins, which reflects the induction time determined by DVS (table 4.8). The spectrum (Fig 4.41 (a)) taken at 40 mins at 75% RH showed the uptake of the absorbed water and a shift in wavelength to 1932 nm. By 80 mins the spectrum taken at 75% (Fig 4.41 (a) and (b)) showed the formation of a monohydrate peak at 1934 nm and a shift in wavelength to 1448 nm. After this point, there are gradual changes in the spectra, the intensity of the peak increases along with permanent shifts to the monohydrate regions. However, a sharp monohydrate is not seen until the end of the second drying stage. This was also observed in the earlier section of 4.3.4.1

Fig 4.41. SNV 2nd der. NIR spectra of co-spray dried pa. amorphous lactose and 25% PVP (K-25) during the amorphous to crystalline phase transition at (a)1900 nm and (b) 1400 nm region.

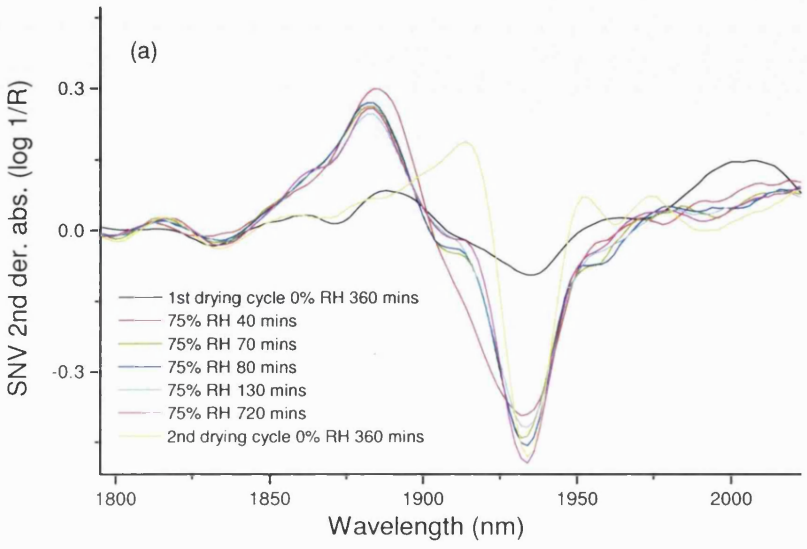

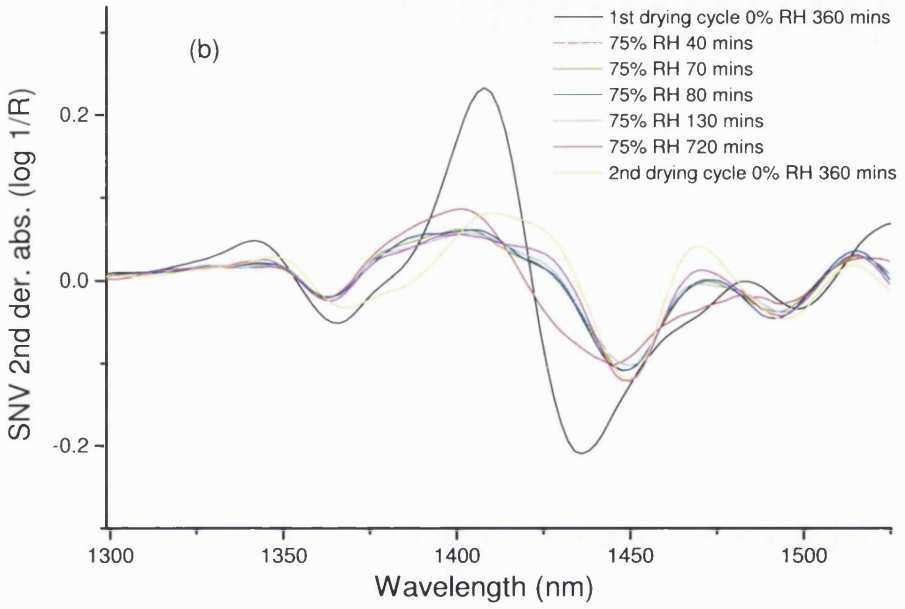

The NIR spectra relating to the crystallisation of co-spray dried partially amorphous lactose and 40% PVP (K-25) showed differences in the onset and rate of crystallisation. Fig 4.42 (a) and (b) showed that crystallisation proceeds and was completed before the desorption of water. The onset of crystallisation was seen between 50 and 60 mins and continued up until 70 mins at the elevated RH. Whereas the data verified by DVS (table 4.26) showed that desoprtion was not detected until 124 mins. A more detailed look at Fig 4.42(a) showed that the dry spectrum (0% RH, 360 mins) of co-spray dried pa. amo. lactose and 40% PVP (K-25) showed a monohydrate peak at 1934 nm representative of the monohydrate content within the sample. However, Fig 4.42(b) showed the peak at 1434 nm represented the amorphous state of the sample with no crystallisation peak seen at 1450 nm. With the uptake of water at 75% RH, gradually with time, the monohydrate peak at 1934 nm (Fig 4.42(a)) increased in intensity up until 70 mins at 75% RH. During the same time the peak at 1434 nm (Fig 4.42(b)) shifted to 1450 nm indicating crystallisation to the monohydrate. However the characteristic feature of a sharp monohydrate peak was not seen until the sample was exposed to a second drying stage where the absorbed water was removed. Fig 4.42 (a) and (b) shows the last spectrum of experiment at 0% RH at 360 mins where a sharp monohydrate peak was observed. A closer look at the drying stage after crystallisation in Fig 4.43 showed that there was a gradual transformation of the monohydrate peak at 1934 nm. At 1450 nm the peak in this region increases in intensity with no other change.

Fig 4.42. SNV 2nd der. NIR spectra of co-spray dried partially amorphous lactose and 40% PVP (K-25) (a) at 1900 nm region and (b) at 1400 nm region.

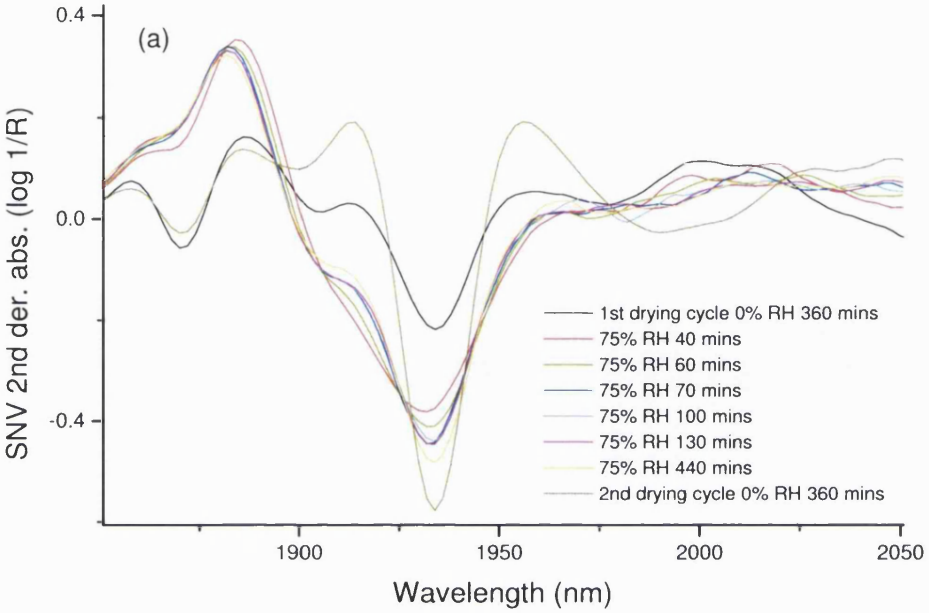

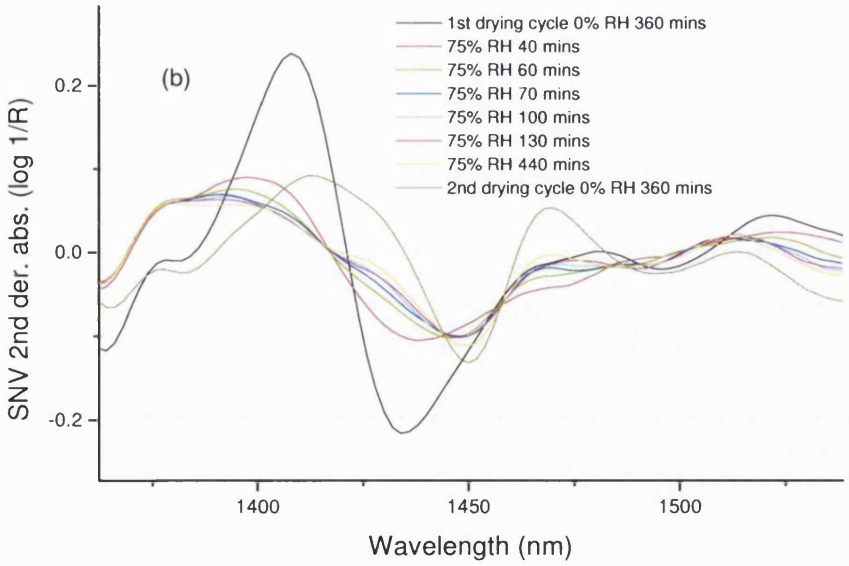

Fig 4.43. SNV 2nd der. NIR spectra of co-spray dried partially amorphous lactose and 40% PVP (K-25) at 0% RH for 6 hours after crystallisation at 75% RH.

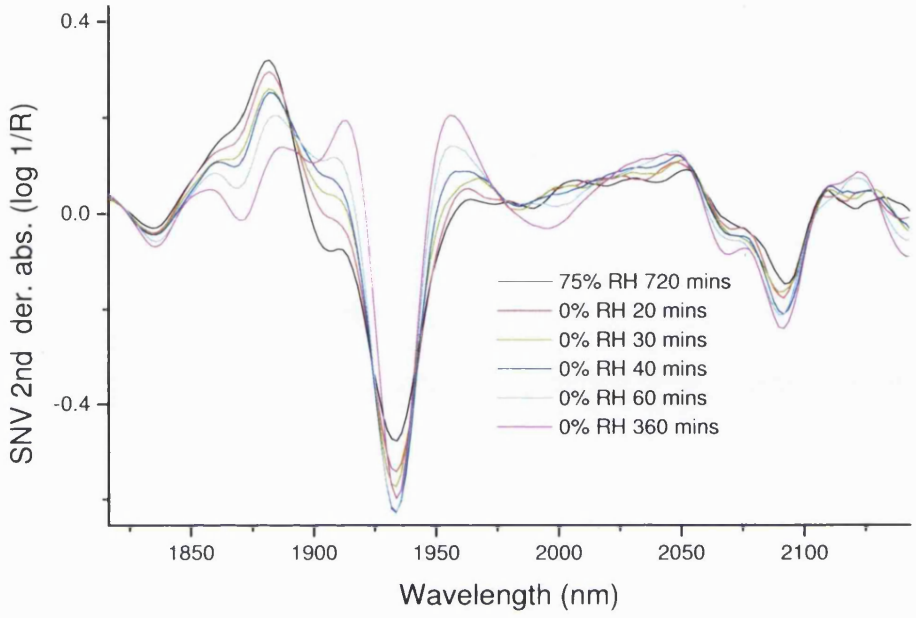

The samples were subjected to drying after crystallisation to assess the physical state of the material without the presence of water. The last spectra from this latter stage have been investigated in section 4.3.4.1 which proved to be informative in supporting and facilitating any conclusion drawn from previous sections. In a similar manner, the spectra in this section have also been studied for both SD and PM products (Fig 4.44 and 4.45). The dry crystalline samples of partially amorphous lactose and PVP (K-25) SD products (Fig 4.44) showed a monohydrate peak for all the samples. The intensity of the peaks shown in the inset picture show the intensity of the monohydrate greatest for 40% PVP, this can be attributed to the fact that the starting material had crystalline α-monohydrate present. The anomeric region also observed in Fig 4.44, showed that the α-form was favoured in SD products containing PVP at high concentrations at 25 and 40% after crystallisation. However in the case of the latter SD product the starting material contained α-monohydrate.

Fig 4.44. The NIR spectra of crystalline lactose and PVP SD products taken at the end of the DVS cycle; at 0% RH for 6 hours (The 2nd drying phase).

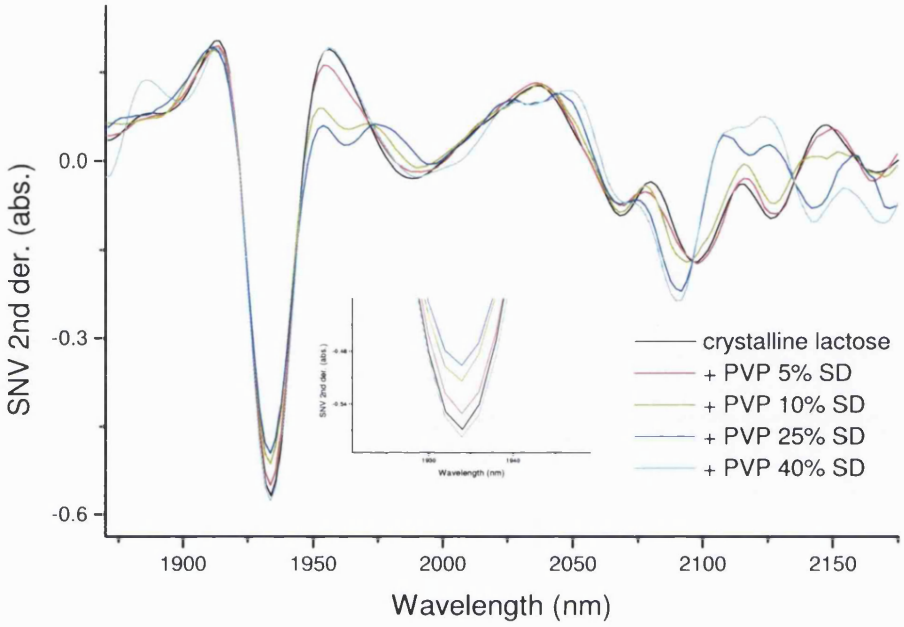

Fig 4.45. The NIR spectra of crystalline lactose and PVP PM products taken at the end of the DVS cycle; at 0% RH for 6 hours (The 2nd drying phase).

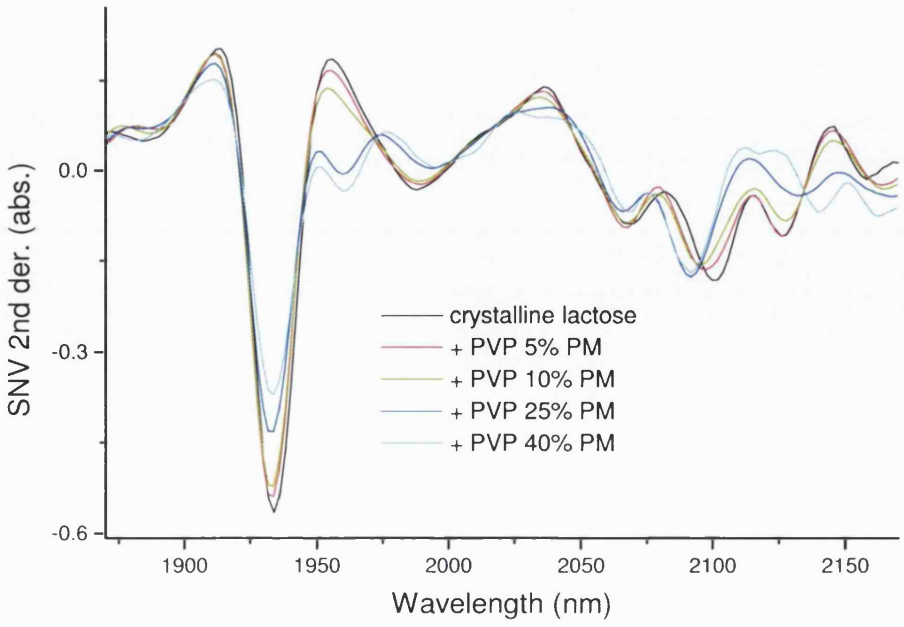

The PM products (Fig 4.45) showed that a monohydrate peak was seen for all concentrations of PVP (K-25) however the intensity of the peak decreased with an increase in PVP concentration. At higher concentrations of the polymer 25 and 40% PVP the α-anomer is again favoured by PVP. This has been the trend at higher concentrations of PVP for both work presented in section A and B. Confirming with a hygroscopic material such as PVP, the RH is maintained to promote the mutarotation of the β-anomer to the α-form (section 4.3.4.2).

In conclusion to these results, crystallisation does proceed when crystal seeds of lactose are present in the SD product. The amorphous content of co-spray dried products at 5% and 10% PVP with crystalline seeds at a concentration of 10% seems to crystallise at a similar rate according to the NIRS, TAM, and DVS with no significant change in the induction time and crystallisation half time. For the amorphous content of co-spray dried product containing 40% PVP and 16.0% seed crystals, crystallisation proceeds at a faster rate than partially amorphous lactose alone according to NIRS. The induction time and water desorption rate determined by TAM and DVS would suggest otherwise, however the crystallisation process with three entities (crystalline and amorphous lactose and PVP) is a difficult process with regards to the release and desorption of water. For the amorphous content of co-spray dried lactose at 25% PVP, the polymer does seem to supersede the presence of crystalline seeds and delay the onset of crystallisation with a reasonable delay in the onset of crystallisation both seen with TAM, DVS and NIRS. This is summarised in Fig 4.46 in a schematic representation.

Fig 4.46. A schematic representation of the effects of crystal seeds of lactose and PVP on the crystallisation of amorphous lactose.

Crystallisation proceeds ← Amorphous lactose → Crystallisation retarded

(Crystal seeds) (PVP)

↓ ↓

SD product 5% PVP SD product 25% PVP

SD product 10% PVP

SD product 40% PVP

4.6 Conclusions

The characterisation and crystallisation of amorphous lactose in the presence of seed crystals has been studied under the influence of PVP at ascending concentration. With a combination of techniques, it was possible to unravel the complex nature of the tertiary systems. The use of water as a probe alone was not sufficient in providing conclusive results into the co-spray dried products although the hyphenation of DVS and NIRS proved to be vital in this study.

From the results it was shown that the presence of crystalline matter with PVP had counteracting effects on the crystallisation of amorphous lactose depending on the concentration of each entity. The rigidity of the polymer and amorphous lactose was influenced by the presence of seed crystals which was observed by a rise in the Tg. This made it very difficult for the sample to desorb water, hence the slow rate of desorption seen by DVS for the samples followed a similar trend to the Tg and TAM data. However with the employment of NIRS, the crystalline seeds actually aided the crystallisation process of amorphous lactose and counteracted the effects of PVP except for co-spray dried lactose and 25% PVP.

Chapter Five
Lactose and SDS

5.1 Introduction

The co-spray drying of lactose and sodium dodecyl sulphate (SDS) has been undertaken as an investigation to study the effects of the surfactant on the physical characteristics and crystallisation of amorphous lactose. Many pharmaceutical formulations exist where both lactose and SDS are included; however the effects that one excipient may exert on the other has not been studied. Recent literature reports based on SDS are primarily focused on interactions with protein-based compounds (Waninge et al., 1996; Wang et al., 1999; Vermeer and Norde., 2000). One study has used SDS in an attempt to identify interactions between the surfactant and another pharmaceutical excipient; magnesium stearate (Wang and Chowhan, 1990). Other pharmaceutical reports are based on calorimetric observations and detection of the critical micelle concentration (cmc) (Volpe and Filho, 1995; Fox et al., 1997; Wang and Olofsson, 1998).

The aim of this study was to determine the effects of SDS on the characteristics of amorphous lactose under spray dried conditions. This was achieved by spray drying lactose with SDS at concentrations of 1, 2, and 3%. PM products were also produced in an attempt to understand the difference between the PM and SD systems.

5.2 Experimental Methodology

SD products were produced under the experimental conditions outlined in chapter two section 2.2.3. The percentage yield of the SD products increased with the addition of surfactant, however remained fairly constant with the increase in surfactant concentration.

Table 5.1. The percentage (%) yield for each SD product of amorphous lactose and SDS under similar spray drying conditions (n=3).

Sample (w/w)	(%) yield
Amorphous lactose	10.0
+ 1% SDS	21.16
+ 2 % SDS	21.04
+ 3% SDS	22.67

Characterisation of the SD and PM products was undertaken using DSC, TGA and GC. The experimental method was described in chapter two under each section heading for

each instrument. Particle sizing was also conducted using the calculated ratio of the refractive index (R.I) of lactose and SDS (see chapter two, section 2.12.3). The crystallisation of amorphous lactose and SDS (SD and PM) was studied using the TAM and DVS-NIRS. The experimental background was reported in chapter two sections 2.3.4 and 2.8.4 respectively.

5.3 Results and Discussion

5.3.1 Characterisation of lactose and SDS SD products before crystallisation

5.3.1.1 Particle Sizing and SEMS

The particle sizing of the SD products was determined using the Malvern as described in chapter two, section 2.12.3. Table 5.2 shows that the particle size of the SD system greatly increased with the addition of surfactant for concentrations 1 and 3%, however with the addition of 2% SDS, the particle size was of similar value to amorphous lactose alone. This variation in particle size without a trend seems to indicate that the varying pump rate during the spray drying process may have influenced this property.

Table 5.2. Particle size analysis of amorphous lactose and SDS SD products (n=15).

Product	10% undersize (μM)	50% undersize (μM)	90% undersize (μM)
Amo lactose	1.11 ± 0.7	8.22 ± 1.9	20.43 ± 5.3
+ SDS 1%	2.95 ± 1.5	20.17 ± 4.8	57.78 ± 9.5
+ SDS 2%	1.30 ± 0.2	9.40 ± 1.5	24.15 ± 3.4
+ SDS 3%	3.56 ± 1.2	18.49 ± 3.0	45.50 ± 7.8
SDS	10.83 ± 3.1	31.46 ± 4.5	75.69 ± 11.1

The SEMS of the SD products further substantiate the above particle size findings (Fig 5.1). Hence this correlation excludes any experimental or instrumental error, which could have influenced the particle size analysis. A comparison at 20 μm showed the samples with large spheres were the SD products that contained 1 and 3%. There was also greater fragmentation with the addition of the surfactant. This change in morphology and particle size could be attributed to the increase in evaporation rate. This was controlled by the inlet temperature where high initial drying rates will lead to larger particles with thin shells and fracture and low initial drying rates will lead to smaller particles with thick shells. The inlet temperature however remained fairly constant at 185-190°C, so therefore

it may be that with the addition of SDS the evaporation of moisture from the surface of the particle increases. Although this hypothesis contradicts the physical characteristic, that SDS increases the wetting of a material, but by facilitating water transport across the surface of the particle, SDS also facilitates the removal of unbound moisture under drying conditions. However, this factor alone would not explain why this was seen for 1 and 3% but not 2% SDS. An increase in particle size must also be due to the increased pump rate to maintain the outlet temperature.

Fig 5.1. SEMS of (a) amorphous lactose and SDS SD products + (b) 1%, (c) 2%, (d) 3%.

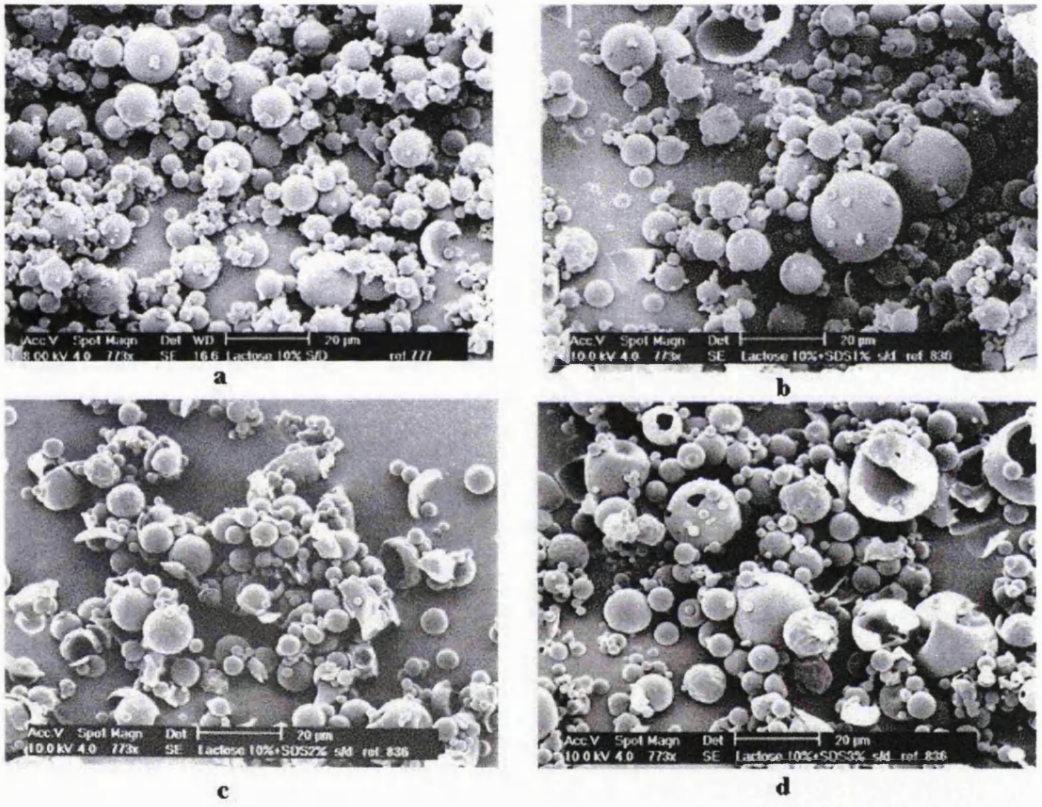

5.3.1.2 GC

The change in the anomeric ratio of amorphous lactose was investigated using GC, table 5.3, which showed a marginal increase in the α-anomer for the SD products and very little change for the PM products. In comparison with these results, the change in the anomeric ratio was mainly due to spray drying with the addition of SDS. Roetman and Van Schaik (1975) also found that mutarotation takes place during the spray drying process.

Table 5.3. The anomeric ratio of amorphous lactose and SDS products determined by GC (n=3).

Product	Anomeric composition (SD)		Anomeric composition (PM)	
	α (%)	β (%)	α (%)	β (%)
Amo lactose	41.7	58.3	41.7	58.3
+ SDS 1%	51.4	48.6	41.5	58.5
+ SDS 2%	53.4	46.6	44.0	56.0
+ SDS 3%	50.3	49.7	44.4	55.6

5.3.1.3 TGA

The TGA results (table 5.4) showed the level of moisture within the sample. Above 1% of SDS there was a marginal increase in the residual moisture content. With such a small increase in the residual moisture with no apparent trend, this reflects the difference in spray drying the feed concentrates. As well as determining the moisture content for the samples the TGA thermograms (Fig 5.2) showed that no crystalline material was present, with no monohydrate peak detected. The detection of the monohydrate is within means of the sensitivity of the TGA, where the instrument is documented to have an accuracy of 0.1% and a resolution of 0.1 μg.

Table 5.4. The percentage (%) absorbed water determined by TGA for amorphous lactose and SDS SD products (n=4).

SD products	% TGA absorbed water
Amo lactose	4.35 ± 0.06
+ SDS 1%	4.11 ± 0.36
+ SDS 2%	5.53 ± 0.10
+ SDS 3%	5.54 ± 0.32

Fig 5.2. TGA thermograms for (a) amorphous lactose and (b) + SDS 2% SD products, which also represents that of 1 and 3% SD.

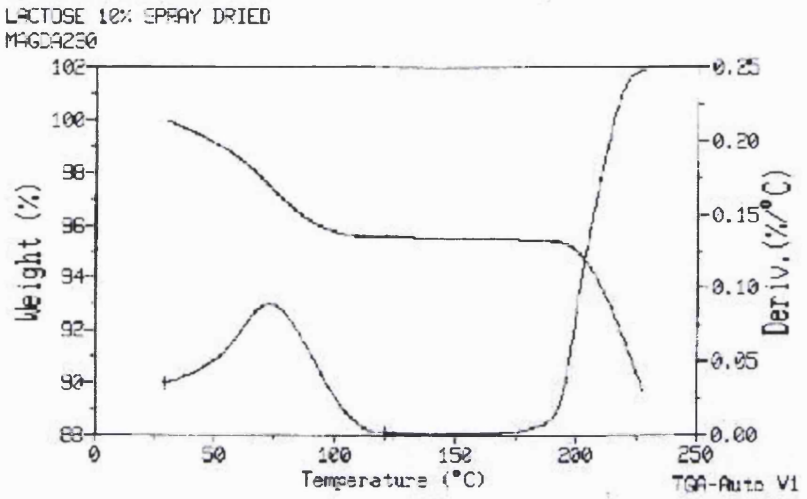

(a)

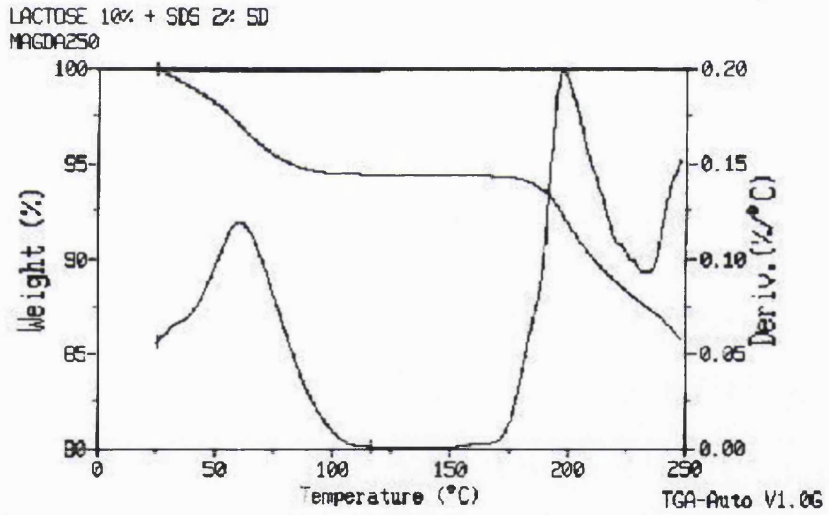

(b)

5.3.1.4 DSC

The DSC thermographs produced for the SD products (Fig 5.3) showed premature crystallisation of amorphous lactose (table 5.5) this was then almost instantly followed by an endothermic peak, which was subsequently followed by an α-melt. Table 5.5 represents the onset averages of these thermal events with an increase in surfactant concentration. The decrease in the apparent onset of crystallisation may be due to the

increase in water content of the SD sample which was supported from the TGA results. However this can not be the only reason because for 1% SDS the moisture content was low. Hence the presence of SDS must increase the wettability of the sample with the addition of the surfactant, which in turn lowers the Tg of amorphous lactose, increasing mobility and causing premature crystallisation.

Fig 5.3. DSC thermographs of amorphous lactose and SDS SD products.

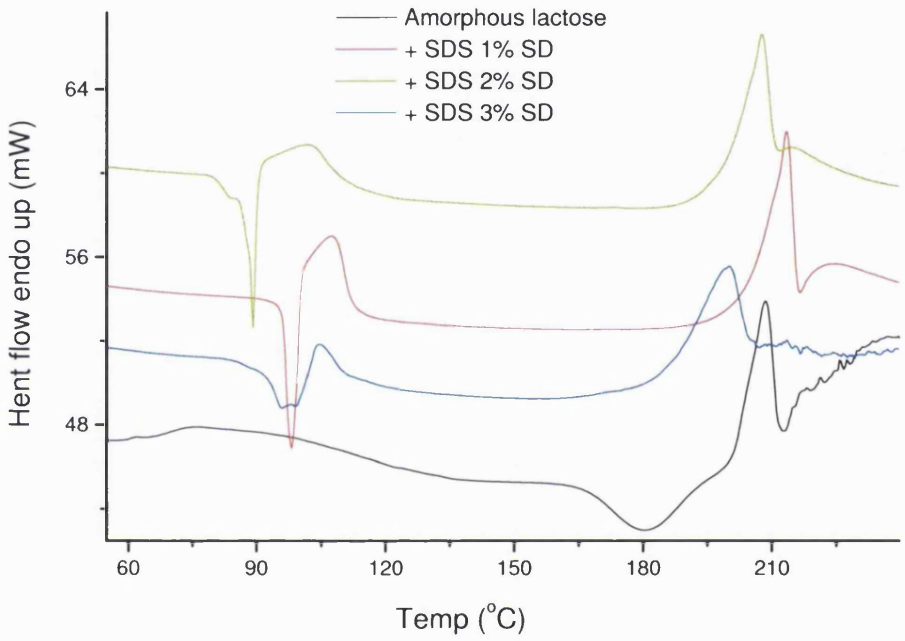

Table 5.5. A summary of DSC physical parameters of amorphous lactose and SDS SD products (n=4).

SD product	Crystallisation onset (°C)	α-melt onset (°C)
Amo lactose	179.0 ± 5.4	210.85 ± 1.5
+ SDS 1%	105.1 ± 5.2	207.5 ± 1.9
+ SDS 2%	100.1 ± 3.5	202.1 ± 0.9
+ SDS 3%	102.1 ± 7.8	196.2 ± 2.1

The endothermic peak after crystallisation is likely due to monohydrate loss, as a result of formation due to crystallisation. Kedward et al., (1998) reported similar findings for lactose crystallisation under non-isothermal conditions using different scanning rates. This type of exo-endotherm sequence is opposite to the endo-exotherm seen in the study

with PVP after crystallisation (section 4.3.6.2) at a higher temperature range. The endo followed by an exothermic peak at ~170 and 180°C respectively was attributed to an unstable α-anhydrous melt followed immediately by crystallisation of β/α complex (Lerk et al., 1984; Olano et al., 1977; Olano et al., 1983; Jouppila et al., 1997). So it is more likely that this is one form of lactose transformation.

The PM products of amorphous lactose and SDS DSC thermographs (Fig 5.4) were similar in shape to that of amorphous lactose alone. The amorphous lactose in the PM products was seen to crystallise at an earlier temperature (table 5.6), this was then followed by an α-melt. The difference between the SD and PM products was that no lactose transformation was seen.

Fig 5.4. DSC thermographs of amorphous lactose and SDS PM products (amorphous lactose alone not included).

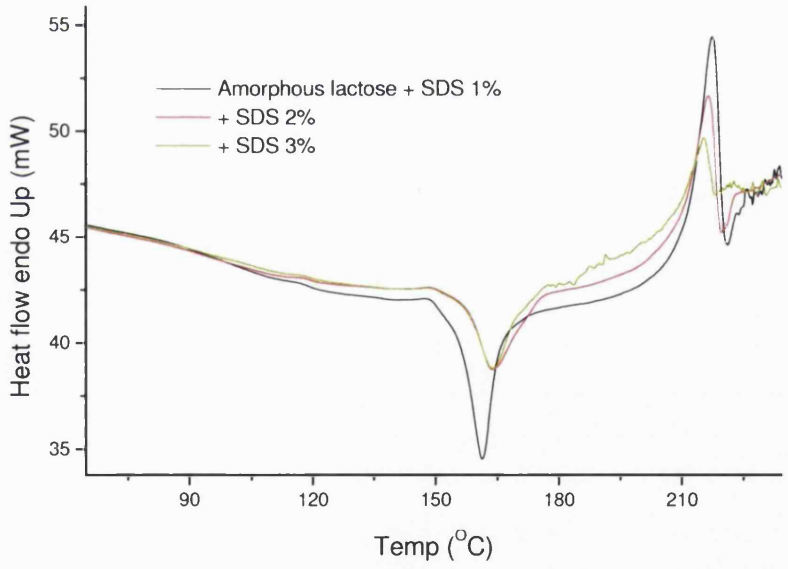

Table 5.6. A summary of DSC physical parameters of amorphous lactose and SDS PM products (n=4).

SD product	Crystallisation onset (°C)	α-melt onset (°C)
Amo lactose	179.0 ± 5.4	210.9 ± 1.5
+ SDS 1%	155.7 ± 0.6	210.8 ± 0.4
+ SDS 2%	156.6 ± 0.6	208.3 ± 0.8
+ SDS 3%	156.9 ± 0.9	210.6 ± 1.4

In conclusion, spray drying amorphous lactose and SDS at concentrations of 1, 2, and 3% had an effect on the physical properties of amorphous lactose, where the particle size of the product increased along with a change in morphology. This has been attributed to the increase in evaporation of moisture at the surface of the particles leading to an increase fragmentation and an increase in the pump rate. There was no change in the physical state of amorphous lactose with the addition of surfactant, where only amorphous lactose was produced for each SD product. SDS seems to promote lactose crystallisation followed by monohydrate loss under the influence of heat. For the PM products, the effects of SDS were not so profound but amorphous lactose did crystallise at an earlier temperature. Thus supporting the findings that in the presence of SDS molecules, lactose crystallises at a faster rate.

5.3.2 The Study of crystallisation using Isothermal Microcalorimetry (TAM)

The crystallisation of SD and PM products was undertaken using the TAM and DVS-NIRS by induction due to water vapour. The amorphous content was quantified along with the onset of crystallisation using the TAM. The crystallisation kinetics was determined using the shape of peaks where Full Width Half Maximum (FWHM) was determined with the aim of comparing the different effects of SDS concentration on the crystallisation of amorphous lactose. DVS was employed to investigate water absorption of the SD and PM products.

Fig 5.5 Typical TAM responses for SD amorphous lactose alone and with SDS following exposure to 75% RH.

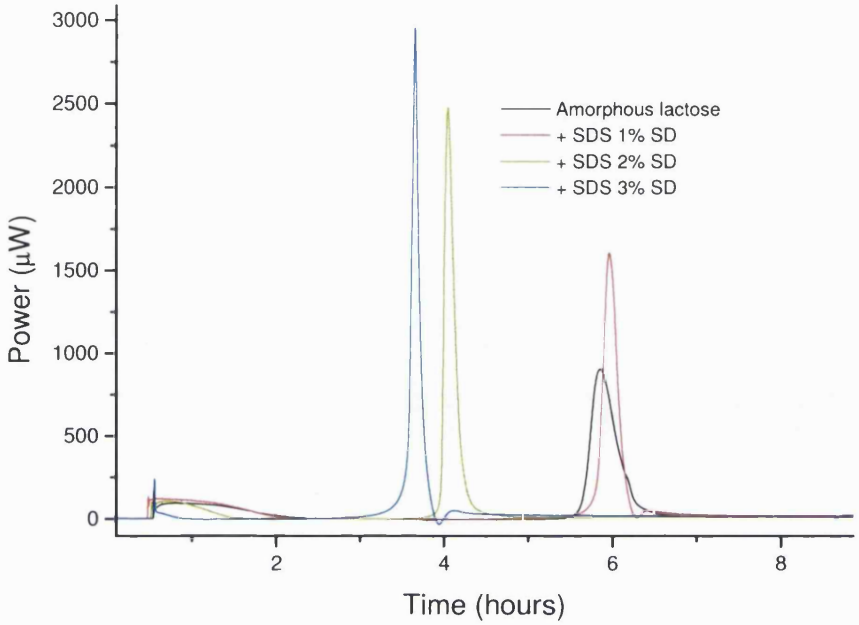

Table 5.7. A summary of FWHM and induction time for the TAM data for amorphous lactose and SDS SD (n=4).

SD product	FWHM (mins)	Induction time (hours)
Amo. lactose	18.7 ± 0.6	5.3 ± 0.4
+ SDS 1%	11.2 ± 0.5	5.5 ± 0.3
+ SDS 2%	7.3 ± 0.1	3.7 ± 0.1
+ SDS 3%	6.0 ± 0.5	3.4 ± 0.0

Fig 5.5 showed that with the addition of SDS, there was a decrease in the induction time above 1% surfactant concentration. Moreover the FWHM decreases with an increase in SDS concentration, which indicates a relatively rapid cooperative crystallisation process (table 5.7). The presence and size of the SDS molecule was expected to delay the nucleation and crystal growth of amorphous lactose by physically hindering the approach of lactose molecules to form a crystal nuclei. However, the opposite effect was seen this could be due to the increased wetting response under the influence of the surfactant, along with the SDS particle providing nucleation sites. Also SDS is not a hygroscopic material hence does not hydrogen bond with water to cause delay or inhibition of crystallisation.

During spray drying the lactose and SDS particles must be interacting in one form or another. SDS may be coating the particles with the hydrocarbon chain, with the SDS hydrophilic head on the outside. This would cause an increase in the wetting and interaction in bringing the lactose together. This would accelerate the mass transport mechanism for nucleation. Crystal growth would also be affected in a similar manner (Van Scoik and Carstensen, 1990).

For the PM products Fig 5.6 and table 5.8 showed that at 1% and above SDS concentration, there was a reduction in the induction time but the crystallisation kinetics were not greatly influenced in comparison to the SD products. This is possible as documented by Sarciaux and Hageman, (1997). From these results, SDS would be expected to interact with the lactose molecules, however the extent of interaction would not be as great hence the difference in data.

Fig 5.6. Typical TAM responses for amorphous lactose alone and with SDS (PM) following exposure to 75% RH.

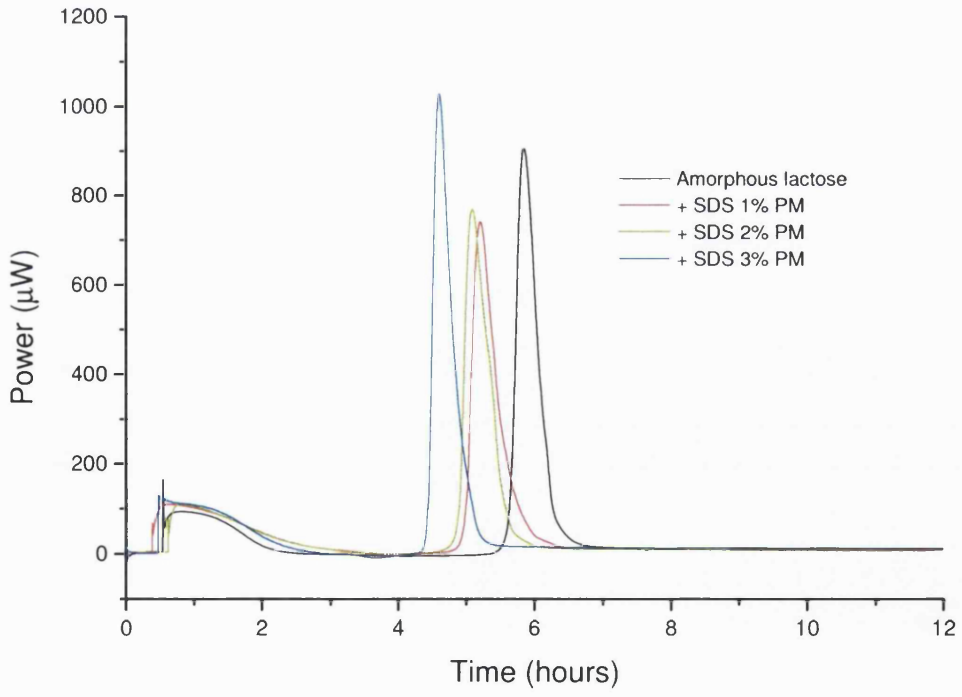

Table 5.8. A summary of FWHM and induction time for the TAM data for amorphous lactose and SDS PM (n=4).

SD product	FWHM (mins)	Induction time (hours)
Amo. lactose	18.7 ± 0.6	5.3 ± 0.4
+ SDS 1%	20.8 ± 0.5	4.7 ± 0.4
+ SDS 2%	20.1 ± 2.4	4.5 ± 0.2
+ SDS 3%	15.8 ± 1.6	4.3 ± 0.3

5.3.2.1 The enthalpy of crystallisation (ΔH_{cry})

Integrating the TAM peaks gives an indication of the amount of amorphous material crystallising (see chapter three section 3.6.2). Although from the previous chapter we learned that the apparent enthalpy of crystallisation was affected by a secondary component that may alter the wetting of lactose. Such findings therefore must be further substantiated with a secondary technique. NIRS data taken during crystallisation in DVS under similar experimental conditions of the TAM are shown to correlate well (see chapter three section 3.6.5 and chapter four, section 4.3.4). A comparison with DVS-NIRS data would therefore show the intensity of the monohydrate peak and if there indeed was a difference in the crystallisation of amorphous lactose.

In this case the integration of the TAM peaks initially proved difficult with the shape of the graph affected by the surfactant. If we look closely at the shape of the graphs (Fig 5.7(a)) we can clearly see phase III (see chapter three, section 3.6.2) of the TAM peak becoming more prominent with the addition of surfactant for the SD products. An investigation into the TAM graphs of the PM products show that phase III is not intensified with the addition of the surfactant (Fig 5.7 (b))

Fig 5.7. Phase III transition of amorphous lactose and SDS (a) SD and (b) PM products shown at a magnification.

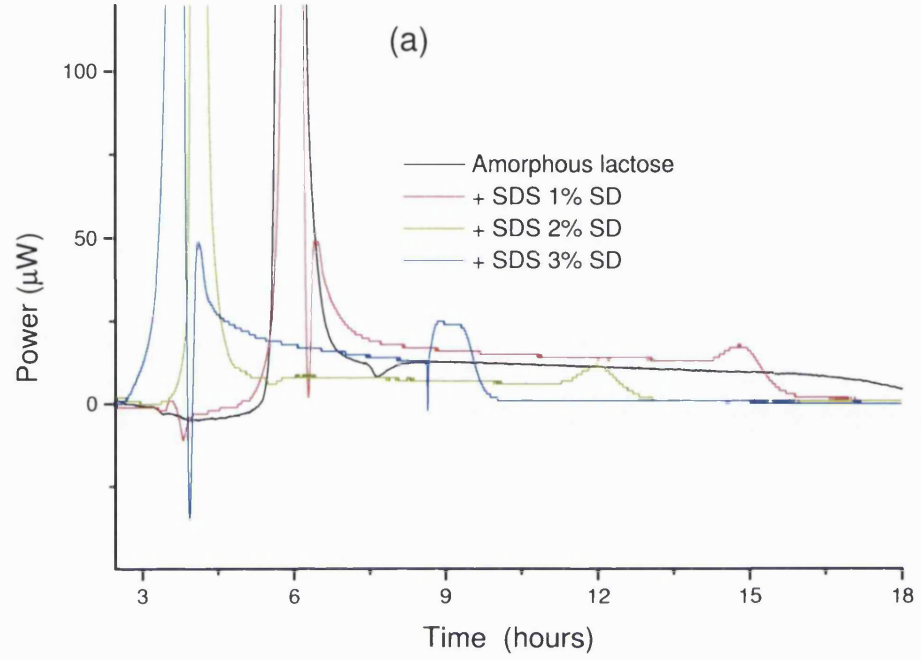

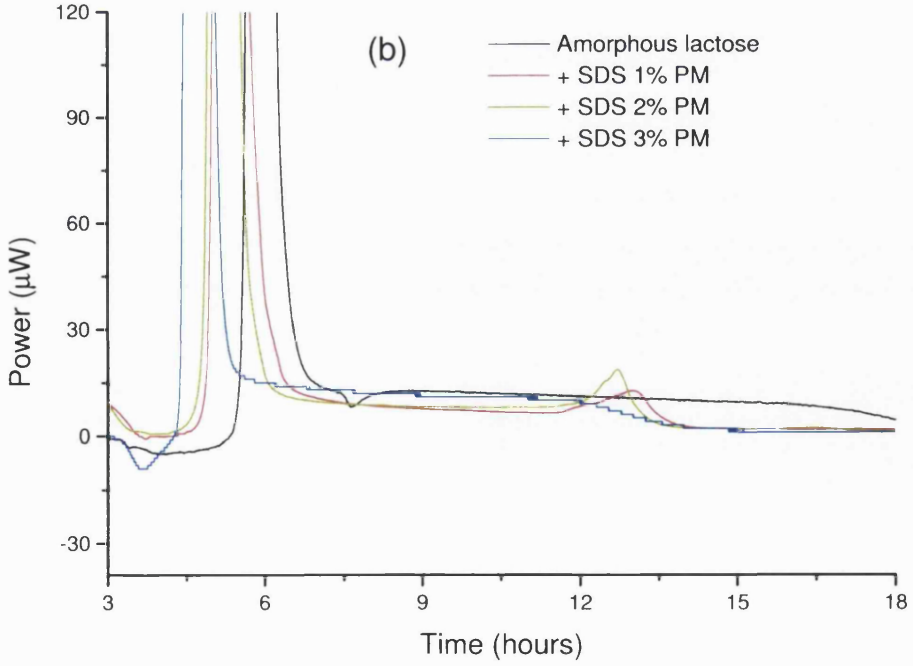

Phase III of the graph has been attributed to a number of physical changes of amorphous lactose, which are reported to take place after crystallisation. Briggner et al., (1994) have suggested that it could be due to mutarotation of the β-form to the α-form. Sebhatu et al., (1994) has hypothesised that the secondary peak could be due to water incorporation of the crystalline α-anhydrous to form a monohydrate. Angberg (1995) has suggested that phase III could be attributed to the composition of α-lactose monohydrate, anhydrous α-lactose and β-lactose. Nevertheless phase III has not been studied under the influence of a binary system before. It is also interesting to note that this particular peak was intensified with SDS for the SD products, which may be correlated to the DSC thermographs, where the endothermic peak seen after crystallisation has been attributed to lactose transformations from this study (Kedward et al., 1998). Studying this section may also confirm or provide an alternative hypothesis as to what is occurring for the DSC thermographs.

In order to identify clearly what was occurring at phase III and more importantly to establish whether this phase should be considered for integration to determine ΔH_{cry}, this peak was investigated for the SD products. The TAM experiment was stopped after the crystallisation peak (phase II) and just before the beginning of phase III (Fig 5.8), a DSC experimental run was then conducted on the sample (Fig 5.9). The DSC thermograph was compared to another trace (Fig 5.10) taken at the end of the TAM experiment (at the end of phase III).

Fig 5.8. A TAM graph representative of amorphous lactose and SDS SD products, at the end of phase II, where a sample was taken for a DSC experimental run.

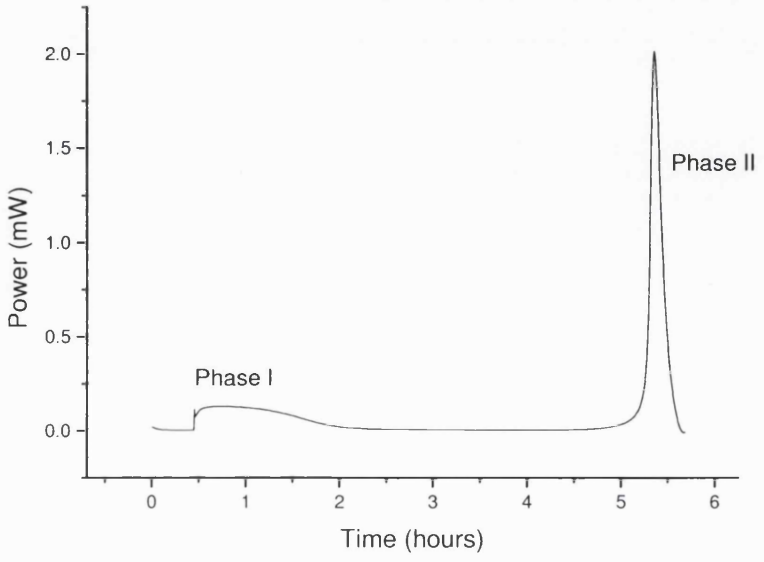

Fig 5.9. A DSC thermograph of lactose and SDS 1% SD product after the crystallisation peak (phase II) of and just before phase (III) (see Fig 5.8). The SD products containing lactose and SDS 2 and 3% also showed similar traces.

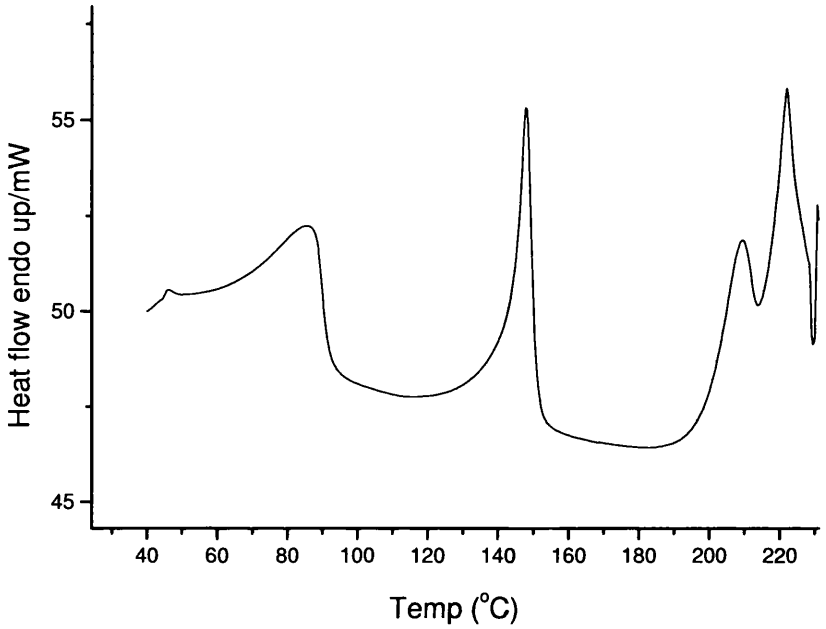

Fig 5.9 representing a DSC thermograph of lactose and SDS 1% SD taken at the end of the crystallisation peak shows a large endothermic peak below 100°C, which is attributed to absorbed water with the sample. An endothermic peak at approximately 140°C represents dehydration of the monohydrate which has occurred at phase II. The absence of an exothermic crystallisation peak indicates that all the crystallisation has taken place during phase II of the TAM peak. This has been proven in literature by PXRD after phase II (Briggner et al., 1994). Further along the DSC thermograph we observe an α-and β-melt at approximately 214 and 220°C.

At the end of the TAM experiment, approximately 18 hours later, a DSC experiment was also conducted for all the SD products and compared to Fig 5.9. The DSC trace shown in Fig 5.10 was representative of all the SD systems, there are differences between the thermographs which would suggest that a physical process has taken place along the duration of phase III of the TAM graph.

Fig 5.10. A DSC thermograph of lactose and SDS 1% SD product after phase (III) of the TAM graph. The SD products containing lactose and SDS 2 and 3% also showed similar traces.

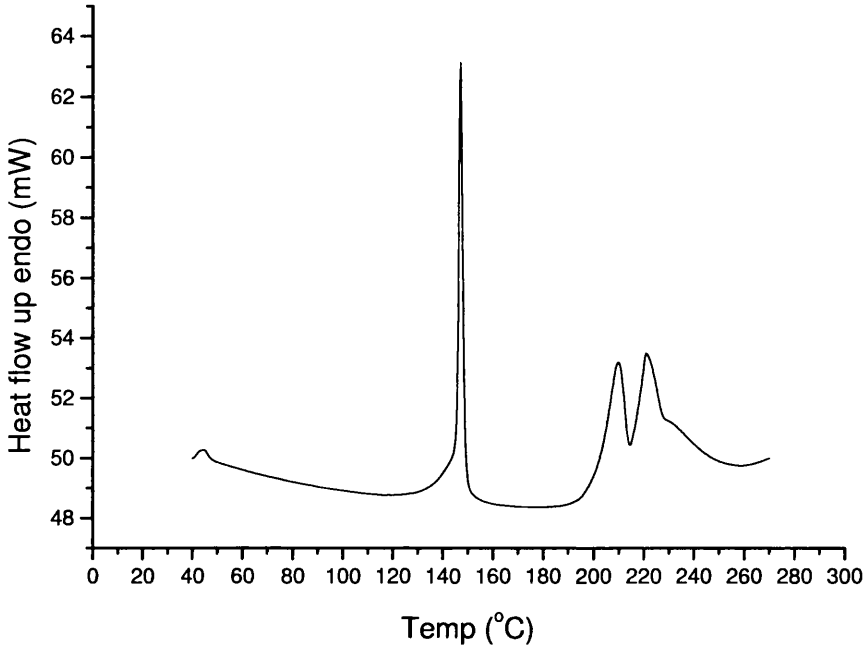

The initial observation was there was no endothermic peak below 100°C representing absorbed water, this suggested that during this phase water has been desorbed or been incorporated in the anhydrous form to produce a monohydrate (Sebhatu et al., 1994). It is more likely that the latter process was occurring which is an exothermic process where bonds are forming between the water and crystalline α-anhydrous lactose as phase III is seen as an exothermic peak and hence a positive peak in the TAM. Desorption of water from the sample would be an endothermic process as seen in the DSC and would lead to a negative peak in the TAM. However, both processes can take place but the incorporation of water was the dominant feature. To further support this hypothesis, a sharp monohydrate peak (Fig 5.10) relative to Fig 5.9 indicates that more monohydrate was present at the end of the TAM experiment. However to confirm this, integrating the dehydration peaks and correcting for lactose weight for each SD product needs to be conducted. This would determine the amount of crystalline material present at the end of each stage (table 5.9).

Table 5.9. The enthalpy of dehydration (ΔH_{deh}) determined by DSC thermographs peaks for traces taken at the end of phase II and III of a TAM experiment for each SD product (n=4).

Sample	ΔH_{deh} (J/g) phase II	ΔH_{deh} (J/g) phase III
Amo lactose alone.	----	58.6 ± 2.2
Amo. Lactose + SDS 1%	75.4 ± 7.7	93.1 ± 1.8
Amo lactose + SDS 2%	64.5 ± 4.0	97.9 ± 2.5
Amo lactose + SDS 3%	57.7 ± 5.3	95.3 ± 1.1

The results show that there was more monohydrate formed at the end of phase III with respect to phase II and crystalline lactose alone. However a comparison with a dehydration peak of a sample which was ~100% α-lactose monohydrate was ~142 J/g (determined by DSC). This suggests that we do not have complete monohydrate formation. Another observation was the similar enthalpy of dehydration seen for all SD products containing SDS, leading to the inference that the same amount of monohydrate was formed at the end of the TAM process.

A comparison with TGA data taken at the end of TAM graph (table 5.10) also showed that a similar amount of monohydrate was formed for each SD product containing different concentrations of SDS. This confirmed the fact that the crystalline product contains the same amount of monohydrate sample regardless of SDS concentration.

Table 5.10. TGA data for crystalline lactose and SDS SD products (n=3)

SD product	(%) TGA hydrate water
Crystalline lactose	2.95 ± 0.01
+ SDS 1%	3.39 ± 0.02
+ SDS 2%	3.39 ± 0.09
+ SDS 3%	3.35 ± 0.05

Considering the GC data taken at the end of phase III can support the difference in the anomeric ratio between crystalline lactose alone and the crystalline products that contain the surfactant, where there should be an increase in the α-anomer. Table 5.10 shows there was an increase in the α-anmoeric form of lactose with the addition of SDS but the increase was essentially the same for the different SDS concentration. This coincides with the same amount of monohydrate formed under the influence of SDS for DSC data.

Table 5.11. GC data for crystalline samples of lactose and SDS SD products from the TAM at 75% RH and 25 ℃.

Product	G.C Result After crystallisation	
	α (%)	β (%)
Crystalline lactose	46.0	54.0
+ SDS 1%	54.5	45.5
+ SDS 2%	54.8	45.2
+ SDS 3%	54.5	45.5

After this preliminary study the apparent enthalpy of crystallisation can now be calculated for the SD products containing lactose and SDS, with a clearer understanding of how to integrate the TAM peaks to achieve an accurate result. Where appropriate the graphs have been integrated using phase II only as complete crystallisation was shown to have occurred at this stage through this study and through literature (Briggner et al., 1994; Sebhatu et al., 1994).

Table 5.12. The apparent enthalpy of crystallisation (ΔH_{cry}) for amorphous lactose and respective SDS concentrations for SD products (n = 4). The data has been corrected for lactose weight.

SD product	ΔH_{cry} (J/ g)	(%) Apparent amorphous content
Amo. Lactose	45.7 (1.7)	100
+ SDS 1 %	45.2 (0.8)	98.9
+ SDS 2 %	44.7 (1.2)	97.8
+ SDS 3 %	42.6 (1.9)	93.2

Table 5.13. The apparent enthalpy of crystallisation (ΔH_{cry}) for amorphous lactose and respective SDS concentrations for PM products (n = 4). The data has been corrected for lactose weight.

PM product	ΔH_{cry} J/ g	% Apparent amorphous content
Amo lactose	45.7 (1.7)	100
+ SDS 1 %	39.8 (0.9)	87.1
+ SDS 2 %	40.1 (1.4)	87.7
+ SDS 3 %	41.7 (0.7)	91.2

Table 5.12 representing the SD products shows a small decrease (6.8%) in the apparent enthalpy of crystallisation with addition of SDS above 1%. This contradicts the data shown above by the DSC, TGA and GC where there is a clear indication that all the amorphous material has crystallised and that there was an increase in the formation of α-monohydrate formed. A possible explanation could be that an inhibition of 6.8% in the crystallisation of amorphous lactose falls below the detection limit of DSC, which is 10% or greater (Sebhatu et al., 1994). The TAM is well documented for its increased sensitivity and a detection limit of 0.5% or greater (Buckton and Darcy, 1995). Another reason could be the difference between the crystallisation exothermic and the desorption endothermic peak which provides the net crystallisation peak that is integrated. To support this theory, table 5.12 represents the apparent enthalpy of crystallisation for the PM products, which are less than their SD products counterparts. In this case the interaction between amorphous lactose and SDS molecules is weak relative to the SD products, so the presence of SDS and its non-hygroscopic nature expels an excess amount of desorbed water from the material. This is the opposite effect seen with PVP which is a hygroscopic material and willingly absorbs and retains water leading to an increase in the apparent enthalpy of crystallisation (section 4.3.2.2). Fig 5.11 shows the net effect of crystallisation and desorption of water with and without SDS on the apparent enthalpy of crystallisation.

Fig 5.11. A schematic representation of the net effects on the TAM crystallisation peak with (a) lactose alone and (b) with the addition of SDS.

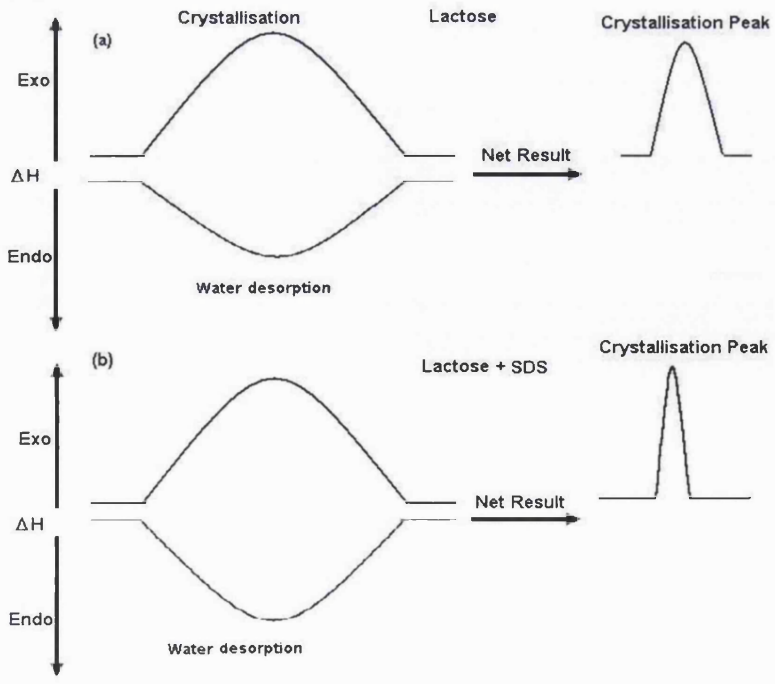

5.3.3 Crystallisation investigated using DVS

DVS data throughout the course of this thesis has supported and also added insight into TAM experiments. If SDS does indeed increase the wetting of lactose by coating we would expect to see an increase in the water uptake relative to amorphous lactose alone. Measuring water absorption can test the hypothesis that SDS increases the wetting of lactose. DVS is able to measure the moisture uptake of a material after drying the sample (0% RH for 360 mins). Fig 5.12 represents the DVS profile of amorphous lactose and SDS SD, which are similar to the TAM graphs with respect to shape and width by general observation.

Fig 5.12. DVS profiles of amorphous lactose and SDS SD products under experimental conditions already described in chapter two, section 2.8.4.

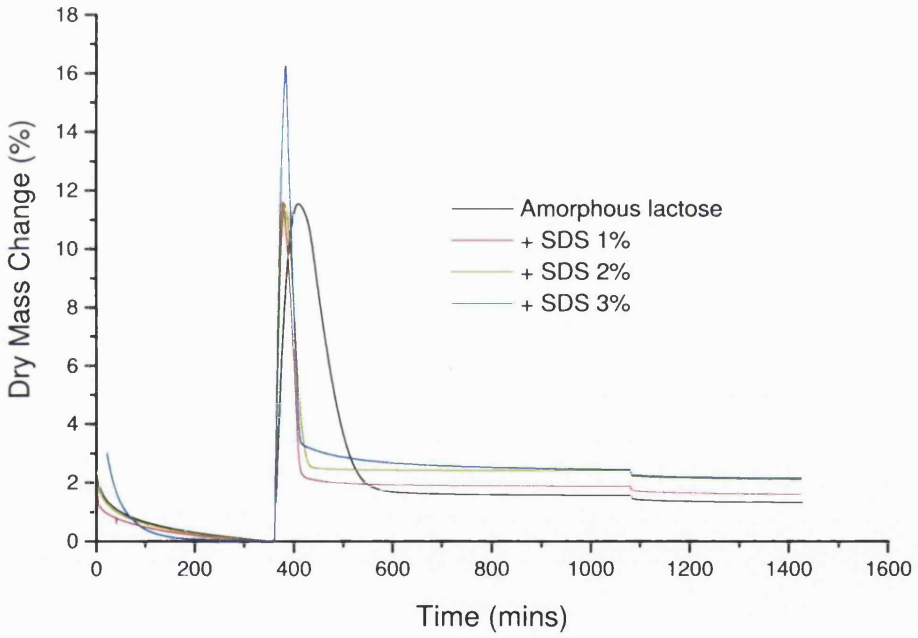

Visual observations include the noticeable increase in water uptake with SD product containing SDS 3%. Table 5.14 shows the actual uptake of moisture with a small increase for water with 1 and 2% SD products. A comparison with the PM products shows only a small increase in the water content for SDS 3% indicating the difference in interaction between the SD and PM products with respect to SDS.

Table 5.14. DVS water uptake for amorphous lactose and SDS SD products at 75% RH (and 25 ℃) after drying at 0% RH for 360 mins (n=4).

Product	% Water Uptake, SD	% Water Uptake, PM
Amo. Lactose	11.75 ± 0.2	11.75 ± 0.2
+ SDS 1%	11.99 ± 0.1	11.75 ± 0.5
+ SDS 2%	12.50 ± 0.4	11.89 ± 0.2
+ SDS 3%	15.63 ± 0.6	12.15 ± 0.3

5.3.4 Studying crystallisation using NIRS

NIR data taken during crystallisation in DVS under similar experimental conditions supported the rapid rate of crystallisation seen under the influence of the surfactant by the TAM and DSC. Fig 5.13 shows the crystallisation of co-spray dried amorphous lactose and SDS 3%. The crystallisation process of amorphous lactose was not affected except for the rate for all the SD products.

Fig 5.13. SNV 2nd der. NIR spectra for co-spray dried lactose and SDS 3% at 1900 nm.

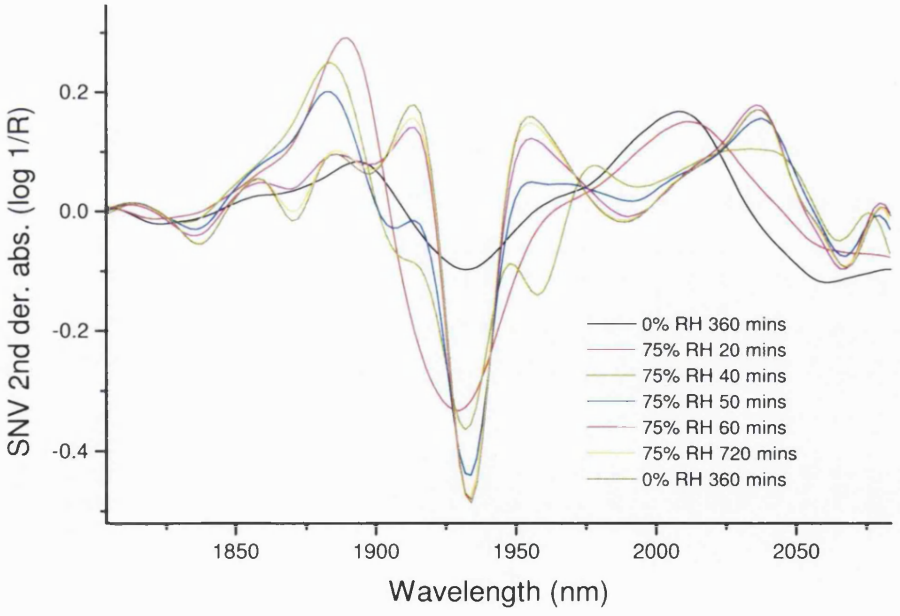

From Fig 5.13, amorphous lactose was seen to absorb water and shift to lower wavelength and broaden within 20 mins at 75% RH. The onset of crystallisation and the formation of the monohydrate was evident at 40 mins at 75% RH, where multiple peaks are formed at 1926, 1934 and 1960 nm. After this time the monydrate peak at 1934 nm

increased in intensity and the multiples peaks on either side shifted to higher energy states and disappear within 20 mins of first development (at 75% RH 60 mins). After 60 mins at 75% RH there is very little change in the spectra except for a gradual increase monohydrate intensity thus indicating that all the major changes have occurred within 60 mins at 75% RH. This can be compared to amorphous lactose alone where the crystallisation was seen to be complete within 180 mins (chapter three, section 3.6.5.1). At the end of the cycle at 75% at 720 mins there was no apparent change in spectrum presented and that between the final spectrum of the experiment (0% RH and 360 mins) during the second drying phase. This indicated that all water was expelled and crystallisation was complete much earlier on at the elevated RH. It is also interesting to note that the shapes of the crystallisation peaks presented in Fig 5.13 were also much sharper, indicating the rapid crystallisation kinetics in comparison to amorphous lactose alone (chapter three, section 3.6.5.1) and amorphous lactose and PVP (section 4.3.4.1). The observations presented here are also representative of co-spray dried lactose with 1 and 2% SDS except for the rate at which crystallisation occurred.

Fig 5.14 representing NIR spectra taken at the end of 12 hours at 75% RH, shows there was very little difference between the intensity spectra of crystalline lactose and the products that contain SDS. This indicates that amorphous lactose was crystallising with no apparent change in quantity. Hence, it seems more likely that the wetting and desorption of water under the influence of SDS affects the apparent enthalpy of crystallisation as explained by the TAM data rather than inhibition of crystallisation of amorphous lactose.

Fig 5.14. NIR spectra taken at 75% RH for 12 hours for crystalline lactose and SDS SD products.

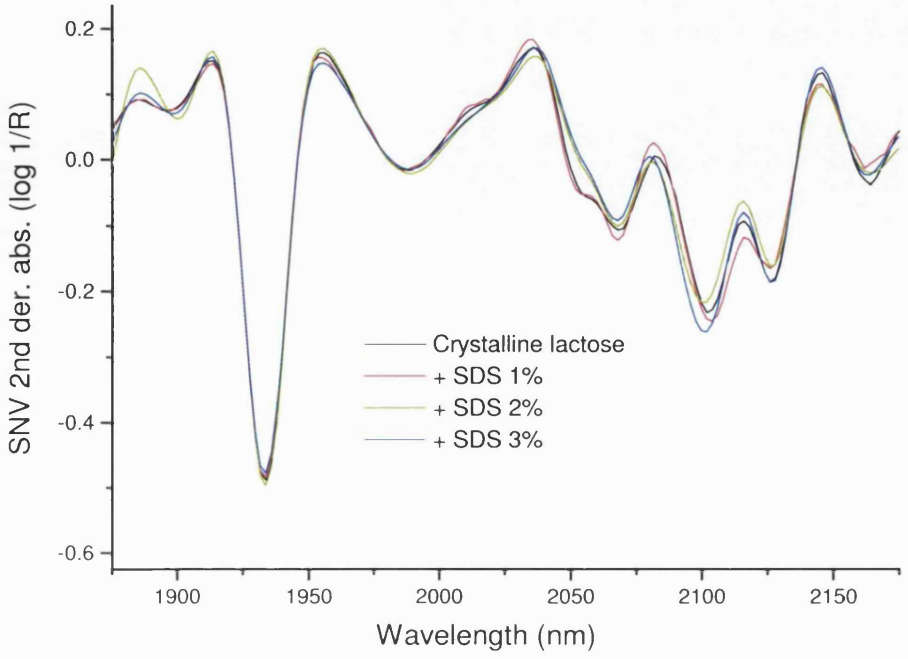

5.4 Conclusions

Spray drying amorphous lactose with SDS was investigated to assess any effects on the physical state and the phase transition of amorphous lactose to the crystalline state. There was no change in the amorphous state of lactose with the addition of SDS when spray dried together; the only difference in the physical state is the increase in particle size, and fragmentation which was observed for SD products containing SDS 1 and 3%. This could be attributed to an increase in the pump and evaporation rate during spray drying.

Once crystallisation had been induced, a reduction in the onset of crystallisation was observed. Under the influence of heat amorphous SD lactose with SDS seems to crystallise to the monohydrate which is lost immediately after. However with the TAM data, an exothermic event was seen after crystallisation, where it was determined that mainly the incorporation of water was the physical process taking place. This is more likely to be seen with the addition of SDS as the wetting response is increased.

The TAM data provided a more conclusive trend with a decrease in the induction time above 1% SDS concentration. The explanation we have provided is based on the increase in wetting of amorphous lactose, which increases the mass transport process during nucleation. SDS within the PM product showed that the induction time was also decreased but the crystallisation kinetics were not greatly influenced. Along with other data this indicated that there were stronger interactions between lactose and SDS when spray-dried compared to the PM samples.

Hence in conclusion SDS when added to lactose and SD will produce the amorphous state, however this is not stable in the formulation once under the influence of heat or water vapour. Crystallisation occurs relatively rapidly in terms of nucleation and crystal growth. Therefore where amorphous lactose is used in formulations as a stabilising agent, and the addition of SDS is required; the effects of the surfactant on amorphous lactose need to be considered.

General Conclusion and Future Work

General Conclusions

The study of binary systems has been achieved by using a variety of specialised analytical tools, the introduction of the hyphenated technique DVS-NIRS has proved to be reliable and essential in the study of the amorphous to crystalline phase transition. The technique has been able to provide answers to problems which would have otherwise proved to be difficult to answer without carrying out further experiements.

An introduction to the behaviour of the single components and their physical properties was described in chapter three. Lactose was investigated at different feed concentrations, where it was found that the amorphous content of lactose when spray dried was determined by the feed concentrate of the product. By keeping the spray-drying parameters constant and increasing the feed concentrate, the amount of crystalline material increased in the SD product. The TAM was able to quantify the amorphous and crystalline content of each feed accurately. It was found that the SD products from feed concentrates in solution 10% and 20% w/v were found to be approximately 100 and 96% amorphous. The SD products from feed concentrate in suspension at 30 and 40% w/v were approximately 89 and 55% amorphous with the remainder crystalline. Crystallisation kinetics determined by DVS data using the Avrami equation was also able to distinguish between the SD products from different feed concentrates. In conjunction with NIRS amorphous lactose alone (SD lactose from 10% w/v feed) and in the presence of seed crystals (SD lactose from 20 and 30% w/v feed) was found to crystallise in a similar manner. Amorphous lactose with a higher quantity of crystalline material (~50%, SD lactose from 40% feed) crystallised in a cooperative and rapid manner. This proved that the novel combination of DVS and NIRS was a reliable and innovative technique. In addition, it can be concluded that the SD product is dependent on the feed concentrate of a material providing that the spray-drying parameters are kept fairly constant.

PVP was studied as a single entity using both TAM and DVS-NIRS. The TAM data showed a large exothermic peak which when investigated was attributed to the wetting of the polymer. Light microscopy showed a gradual change in the physical morphology along with TGA data which showed increased water absorption. It was also found that the Tg of the material could not be detected by the TAM as an enthalpy change. DVS-NIRS was able to follow the structural changes of PVP whilst drying and wetting of the sample was conducted. Hydrogen bonding between PVP and water was also detected and the change in the PVP structure due to absorption and desorption of water was also observed. DVS-NIRS provides a rapid means of collecting a substantial quantity of information in a short space of time. This is one of the many advantages for those who employ the technique.

The study of lactose and PVP both SD and as PM products was presented in chapter four. The spray drying of amorphous lactose and PVP produced an amorphous material with no crystalline content as observed by DSC and PXRD. Tg data showed an increase in the Tg for co-spray dried products at 25% PVP and above. FTIR also showed that hydrogen bonding existed with these SD products. However, with the theoretical equations employed a negative deviation from the ideal behaviour was seen. This deviation is less when applying the Couchman-Karsz equation (Couchman and Karsz, 1978) indicating that an entropy-based analysis was better suited for the study. Non-additivity of volume was assessed by the Kovacs equation which showed that excess free volume above and below the critical temperature (T_c) existed.

The effects of the combination of entropy and free volume were summarised in the Schneider plot, which produced a negative gradient, this indicated that specific interactions were responsible for the negative deviation and are affecting the overall free volume. The negative term represents a large conformational entropic contribution. Hence, it seems that entropy is a cause for deviation from ideal behaviour as well as specific interactions (hydrogen and non-hydrogen bonding) leading to changes in the overall free volume. The increase in entropy may be explained by the following terms; Lactose is a molecule that self associates (i.e. forms hydrogen bonds in the pure form) and so it would be difficult to break these bonds. The addition of PVP (a large macromolecule to a small amorphous molecule) will cause disruption of the lactose structure and hence hydrogen bond breaking via the embedment of the polymer into the glassy state. This leads to an increase in the entropy term. At low concentrations (5 and 10%) of PVP (K-25), the entropy effect coupled with the excess free volume leads to a greater negative deviation from the Schneider plot and no change in the Tg value. At high polymer concentrations (25 and 40%), the addition of PVP (K-25) will cause disruption and hydrogen bond breaking but there was hydrogen bonding between polymer and diluent. However this does not compensate for the disruption that has occurred in the lactose structure as the ratio of hydrogen bonds broken in comparison to the number of bonds formed will be high due to steric hindrance and the size of the PVP polymer (Painter et al., (1991).

Once the products were exposed to water and crystallised using both the TAM and DVS-NIRS, it was found that the SD and PM products containing the higher concentration of PVP (25 and 40% w/w) showed a delay in the onset of crystallisation indicating a delay in the nucleation phase. The hygroscopic nature of PVP (K-25) hydrogen bonding with water reduces the mobility of lactose molecules and increases the viscosity. The analysis of the crystallisation kinetics (using Avrami equation and the exponential model) showed a delay in

the crystalline growth by an increase in the crystallisation rate constant as well as the crystallisation half time. The inhibition of amorphous lactose crystallising was difficult to assess by quantification using the TAM. The affinity of PVP to retain water and behave as an internal desiccant distorted the shape of the graph leading to a larger than expected apparent enthalpy of crystallisation. However with NIRS following crystallisation and showing that intermolecular hydrogen bonding existed in the final crystallised product of the SD and PM products at 25 and 40% w/w PVP. This evidence coupled with hydrogen bonding existing in the co-spray dried products prior to crystallisation would indicate that crystallisation was indeed inhibited. Hence, the limitation of the TAM in providing a quantifiable answer was resolved by combining the observations of other techniques used.

The co-spray drying of partially amorphous lactose with PVP resulted in an increase in the monohydrate content at 40% PVP concentration. This was due to the increase load when spray drying. This has been an important part of the study where the concentration of the feed has influenced the physical properties of the SD products as a result of the spray drying process. These findings should allow the operator to predict and control the SD product for future reference.

The study of the tertiary system of partially amorphous and crystalline lactose and PVP was complex but nevertheless problems were overcome using the techniques in conjunction and in particular with the employment of DVS-NIRS. It was found that the addition of PVP to partially amorphous lactose had different effects on the amorphous to crystalline phase transition depending on the amount of crystalline material and PVP content within the system. At lower concentrations of PVP (5 and 10% w/w) no change was observed in the nucleation and crystal growth of lactose. At 25% PVP the crystallisation process was retarded and at 40% w/w PVP with 16% crystalline content amorphous lactose was seen to crystallise rapidly. However, with the use of water sorption as a probe alone (TAM and DVS) the results were misleading to believe that there was a delay in the onset of crystallisation with an increase in PVP content regardless of the crystalline content. This is because a tertiary system is a complex one where the addition of a hygroscopic material such as PVP has a precedent effect on the water absorption of other components and hence "disguises" the results. This is evident from the quantification of the apparent amorphous content of these systems and the different water desorption rates seen by both the TAM and DVS.

The anomeric ratio of lactose was altered when a hygroscopic material was added to the disaccharide. With the GC and NIRS at higher concentrations (25 and 40% w/w) of PVP for both SD and PM products the α - anomer was favoured. As a result of the presence of PVP,

the relative water uptake was high at high concentrations of PVP resulting in an increased amount of water within the systems leading to mutarotation of the β-lactose to the α-form. Quantification of PVP in the SD and PM products for both the binary and tertiary products (results of the latter not included) was possible regardless of the physical state of the sample. There was a good correlation for the PVP content when the different spectra were all grouped together although some specification was lost. However, an advantage would be a library for quantification of a material can be produced and used as a database regardless of the physical state of a product.

Chapter five was based on the co-spray drying of amorphous lactose and SDS at ascending concentration along with the PM products. The characterisation of the samples showed that all the SD products were amorphous with no crystalline content. Under the influence of heat (DSC) and water vapour (TAM) crystallisation occurred prematurely. SDS also seemed to promote lactose transformation with the monohydrate lost relatively quickly after crystallisation under heat and more monohydrate formation under water vapour clearly detectable by the TAM. The premature crystallisation may be attributed to the increase wetting of lactose under the presence of SDS, which was found to be more profound for the SD products than the PM samples.

The prime objective of this thesis has been to investigate the co-spray drying and the crystallisation of lactose under the influence of additives. Many of the findings and observations were possible by combining the results from experimental data of all the investigative techniques. By conducting this study the limitations of experimental techniques such as the TAM and DVS have also been developed which will help future work to be conducted more thoroughly.

Future Work

Some interesting concepts have been developed from this study which have been tested with the experiments described. In order to develop the findings further, future work is required in some areas. The study of lactose with PVP could be substantiated by increasing the concentration of polymer above 40% to test the findings and predict the result. Using different molecular weight polymers at a single concentration initially with lactose would also be interesting to see if there is any effect on the crystallisation of amorphous lactose. All of these ideas are plausible as lactose and PVP are model components as single and as binary entities.

The work conducted with lactose and SDS has scope to expand by thoroughly testing the hypothesis that SDS does increase the wetting response of lactose when spray dried by surface energy studies.

The use of DVS-NIRS has been fully exploited in these studies which has proved extremely advantageous. Studying tertiary systems and applying various crystallisation kinetics at different relative humdities will further develop the capacity and limits of this technique which are beginning to be understood by the help of the work presented here. There were limitations to the technique which were found from this study that warrant further investigations. For example the different rate of water absorption for each product although this was overcome by application of the exponential model.

Adding a model hydrophobic drug to the binary systems was an idea initially presented at the beginning of the study but due to time constraints of this project it was not possible. Therefore adding a model hydrophobic/hydrophilic drug to the binary systems would be interesting to investigate and further understand and develop the amorphous to crystalline phase transition.

References

A

Ahlneck, C. and Zografi, G., 1990. The molecular basis of moisture effects on the physical and chemical stability of drugs in the solid–state. Int. J. Pharm. 62, 87-95.

Ahmed, H., Buckton, G. and Rawlins, D.A., 1996. The use of isothermal microcalorimetry in the study of small degrees of amorphous content of a hydrophobic powder. Int. J. Pharm., 130, 195-201.

Aldridge, P. K., Evans, C. L., Ward, and Colgan, S.T., 1996. NIR detection of polymorphism and process-related substances. Anal. Chem., 68, 997-1002.

Andronis, V., Yoshioka, M. and Zografi, G., 1997. Effects of sorbed water on the crystallisation of indomethacin from the amorphous state. J. Pharm. Sci. 86, 3, 346-351.

Angberg, M., Nystrom, C. and Castensson, S., 1991. Evaluation of heat-conduction microcalorimetry in pharmaceutical stability studies. III. Crystallographic changes due to water vapour uptake in anhydrous lactose powder. Int. J. Pharm., 73, 209-220.

Angberg, M., 1995. Lactose and thermal analysis with special emphasis on microcalorimetry. Therm. Acta. 248, 161-176.

Angell, C. A., 1995. The formation of glasses from liquids and biopolymers. Sci. 267, 1924-1935.

Arvanitoyannis, I., and Blanshard, J.M.V., 1994. Rates of crystallisation of dried lactose-sucrose mixtures. J. Food Sci., 59, 1, 197-205.

Atkins, P.W., 1998. Physical chemistry. 6th edition. Oxford university press.

Aubin, M. and Prud'homme, R.E., 1988, Analysis of the glass transition temperature of miscible polymer blends. Macromol. 21, 2945-2949.

Aulton, M. E., 2002. Pharmaceutics, The Science of dosage form design. Churchill livingstone.

Avrami, M., 1940. Kinetics of Phase change. II Transformation-time relations for random distribution of nuclei. J. Chem. Phys. 8, Feb., 212-224.

B

Berlin, E., Kilman, P.G., Anderson, B.A. and Pallansch, M.J., 1971. Calorimetric measurement of the heat of desorption of water vapour from amorphous and crystalline lactose. Thermochem. Acta., 2,143-152

Black, D. B. and Lovering, E. G., 1977. Estimation of the degree of crystallinity in digoxin by X-ray diffraction and infrared method. J. Pharm. Pharmac. 29, 684-687.

Brekner, M.J., Schneider, H.A., and Cantow, H.J., 1988. Approach to the composition dependence of the glass transition temperature of compatible polymer blends: The effect of local chain orientation. Makromol. Chem., 189, 2085-2097.

Briggner, L. E., Buckton, G., Bystrom, K. and Darcy, P., 1994. The use of isothermal microcalorimetry in the study of changes in crystallinity induced during the processing of powders. Int. J. Pharm. 105, 125-135.

Brittain, H. G., Bogdanowich, S. J., Bugay, D. E., DeVincentis, J., Lewen, G. and Newman, A. W., 1991. Physical characterization of pharmaceutical solids. Pharm. Res. 8, 8, 963-973.

Brittain, H. G., Bogdanowich, S. J., Bugay, D. E., DeVincentis, J., Lewen, G. and Newman, A. W., 1991a. Analytical profiles of drug substances, Lactose, anhydrous., Vol 20, Academic Press, p369-380.

Brittain, H.G., 1997. Spectral methods for the characterisation of polymorphs and solvates. J. Pharm. Sci. April, 86, 4, 405-412.

Broadhead, J., Edmound Rouan, S. K. and Rhodes, C. T. 1992. The spray drying of pharmaceuticals. Drug. Dev. Ind. Pharm. 18, 11, 1169-1206.

Brooks, G. F., Paterson, A. H. J. and Bronlund, J. E., 2001. Residual moisture in amorphous lactose and its effect on Tg.
http://www.fsci.umn.edu/Ted_Labuza/PDF_files/Presentations/lactoseColorFull.pdf

Buckton, G. and Beezer, A., 1991. The applications of microcalorimetry in the field of physical pharmacy. Int. J. Pharm. 72, 181-191.

Buckton, G., 1995. Applications of isothermal microcalorimetry in the pharmaceutical industry. Thermochim. Acta, 248, 117-129.

Buckton, G. and Darcy, P., 1995a. the use of gravimetric studies to assess the degree of crystallinity of predominately crystalline powders. Int. J. Pharm. 123, 265-271.

Buckton, G., Darcy, P. and Mackellar, A. J., 1995b. The use of isothermal microcalorimetry in the study of small degrees of amorphous content of powders. Int. J. Pharm. 117, 253-256.

Buckton, G. and Darcy, P., 1995c. The influence of additives on the recrystallisation of amorphous spray dried lactose. Int. J. Pharm., 121, 81-87.

Buckton, G. and Darcy, P., 1996. Water mobility in amorphous lactose below and close to the glass transition temperature. Int. J. Pharm. 136, 141-146.

Buckton, G., Yomnemuochi, E., Hammond, J., and Moffat, A., 1998a. The use of near infrared spectroscopy to detect changes in the form of amorphous and crystalline lactose. Int. J. Pharm. 168, 231-241.

Buckton, G. and Darcy, P., 1999. Assessment of disorder in crystalline powders- a review of analytical techniques and their application. Int. J. Pharm. 179, 141-158.

Buckton, G., 2002. Chapter 9: Solid-state properties. Pharmaceutics, The Science of dosage form design. Editor: Aulton, M., Churchill livingstone.

Burt, H. and Mitchell, A. G., 1981. Crystal defects and dissolutions. Int. J. Pharm. 9, 137-152.

Byrn, S., 1982. Solid-State chemistry of drugs. Academic Press, New York, pp 4-11.

Byrn, S., Pfeiffer, R., Ganey, M., Hoiberg, C. and Poochikian, G., 1995. Pharmaceutical Solids: A strategic approach to regulatory considerations. Pharm. Res. 12, 7, 945-954.

C

Carpenter, J.F. and Chang, B.S., 1996. Lyophilisation of protein pharmaceuticals. In: Avis, K.E., Wu, V.L. (Eds), Biotechnology and Biopharmaceutical Manufacturing. Processing and Preservation. Interpharm Press, 199-264.

Chidaveanzi, O., Buckton, G., Koosha, F. and Pathak, R., 1997. The use of thermal techniques to assess the impact of feed concentration on the amorphous content and polymorphic forms present in spray dried lactose. Int. J. Pharm. 159, 67-74.

Chidavaenzi, O., 1999. The effect of spray drying on the physicochemical properties of products. PhD thesis.

Chidaveanzi, O., Buckton, G. and Koosha, F., 2001. The effect of co-spray drying with polyethylene glycol 4000. on the crystallinity and physical form of lactose. Int. J. Pharm., 216, 43-49.

Coleman, M. and Painter, P., 1984. Fourier transform infrared spectroscopy: probing the structure of multicomponent polymer blends. Appl. Spectrosc. Rev., 20, 3-4, 255-346.

Columbano, A., Buckton, G. and Wikely, P., 2002. A study of the crystallisation of amorphous salbutamol sulphate using water vapour sorption and near infrared spectroscopy. Int. J. Pharm. 237, 171-178.

Corrigan, O. I. and Holohan, E. M., 1984. Amorphous spray dried hydroflumthiazide-polyvinylpyrrolidone systems: physicochemical properties. J. Pharm. Pharmcol., 36, 217-221.

Corrigan, O.I., Holohan, E.M. and Reilly, M.R., 1985. Physicochemical properties of indomethacin and related compounds co-spray dried with polyvinylpyrrolidone. Drug Dev. Ind. Pharm. 11, 2 & 3, 677-695.

Corrigan, D., Healy, A. M. and Corrigan, O. I., 2002. The effect of spray drying solutions of polyethylene glycol (PEG) and lactose/PEG on their physicochemical properties. Int. J. Pharm., 235, 193-205.

Couchman, P.R. and Karasz, F.E., 1978. A classical thermodynamic discussion of the effect of composition on glass transition temperatures. Macromolecules, 11, 1, 117-119.

Coulson, J.M., and Richardson, J.F. 1991 Chemical Engineering. Volume 2. 4th ed. Pergamon press.

D

Darcy, P. and Buckton, G., 1997. The influence of heating/drying on the crystallisation of amorphous lactose after structural collapse. Int. J. Pharm. 158, 157-164.

Darcy, P. and Buckton, G., 1998. Quantitative assessments of powder crystallinity: Estimates of heat and mass transfer to interpret isothermal microcalorimetry data. Thermochem. Acta., 316, 29-36.

David, R. and Giron, D., 1998. Chapter 7: Crystallisation. Handbook of Powder technology. Vol 9. Editors: Chuila, D., Deleuil, M. and Pourcelot, Y., Powder technology and pharmaceutical processes. Elseivier science.

De Bruijn, T.J.W., De Jong, W.A. and Van den berg, P.J., 1981. Kinetic parameters in Avrami-Erofeev type reactions form isothermal and non-isothermal experiments. Thermochem. Acta. 45, 315-325.

Duncan-Hewitt, W. C. and Grant, D. J. W., 1986. True density and thermal expansivity of pharmaceutical solids: comparison of methods and assessment of crystallinity. Int. J. Pharm. 28, 75-84.

Dweivedi, S. K. and Mitchell, A. G., 1989. Gas chromatographic analysis of anomeric composition of lactose. J. Pharm. Sci. 78, 12, 1055-1056.

E

Ediger, M. D., Angell, C. A. and Nagel, S. R., 1996. Supercooled liqiuds and glasses. J. Phys. Chem. 100, 13200-13212.

Elamin, A.A, Sebhatu, T. and Ahlneck, C., 1995. The use of amorphous model substances to study mechanically activated materials in the solid state. Int. J. Pharm. 119, 25-36.

Elliott, S.R., 1994. Chapter 4: Amorphous solids: An introduction. Defects and disorder in crystalline and amorphous solids. Editor: Catlow, C.R.A., Kluwer academic Pub.

F

Feldstein, M.M., 2001. Peculiarities of glass transition temperature relation to the composition of poly(N-vinylpyrrolidone) blends with short chain poly (ethylene glycol). Polymer, 42, 7719-7726.

Fell, J. T., and Newton, J. M., 1970. The characterisation of the form of lactose in spray dried lactose. Pharm. Acta Helv. 45, 520-522.

Ferry, J.D., 1980. Viscoelastic properties of polymers, 3rd edition. John Wiley and sons. NY.

Flink, J.M., 1983. Chapter 17: Structure and Structure transitions in dried carbohydrate materials. Physical properties of foods. Editors; Peleg, M. and Bagley, E.B., AVI publishing.

Ford, J.L., 1986. The current status of solid dispersions. Pharm. Acta. Helv., 61, 2, 69-88.

Ford, J.L. and Timmins, P., 1989. Pharmceutical Thermal Analysis: Techniques and Applications. John Wiley and Sons, NY.

Fox, T.G. and Flory, P., 1950. Second order transition temperatures and related properties of polystyrene. I. Influence of molecular weight. J. Appl. Phys., 21, 581-591.

Fox, G.J., Bloor, D.M., Holzwarth, J.F., and Wyn-Jones, E., 1997. Use of isothermal titration microcalormetry to monitor the adsorption/desorption processes of sodium dodecyl sulphate with neutral polymers. Langmuir, 14, 1026-1030.

Franks, F. Water solubility and sensitivity – hydration effects. 1981. In: Finch, C.A. (Ed), Chemistry and Technology of water soluble Polymers, Plenum Press, New York. 157-178.

G

Giron, D., 1995. Thermal analysis and calorimetric methods in the characterisation of polymorphs and solvates. Thermochem. Acta. 248, 1-59.

Gordon, M. and Taylor, J.S., 1952. Ideal copolymers and the second-order transitions of synthetic rubbers. I non-crystalline copolymers. J. Appl. Chem., 2, Sept, 493-500.

H

Haines, P. J., 2002. Principles of thermal analysis and calorimetry. Royal society of chemistry.

Hancock, B. C. and Zografi, G., 1994. The relationship between the glass transition temperature and the water content of amorphous pharmaceutical solids. Pharm. Res. 11, 4, 471-477.

Hancock, B. C., Shamblin, S. L. and Zografi G., 1995. Molecular mobility of amorphous pharmaceutical solids below their glass transition temperatures. Pharm. Res. 12, 6, 799-806.

Hancock, B. C. and Zografi, G., 1997. Characteristics and Significance of the amorphous state in pharmaceutical systems. J. Pharm. Sci. 86, 1, 1-12.

Hill, V.L., Craig, D.Q.M. and Feely, L.C., 1998. Characterisation of spray dried lactose using modulated differential scanning calorimetry. Int. J. Pharm., 161, 95-107.

Hogan, S. and Buckton, G., 2000. The quantification of small degrees of disorder in lactose using solution calorimetry. Int. J. Pharm. 207, 57-64.

Hogan, S. and Buckton, G., 2001. The application of near infrared spectroscopy and dynamic vapour sorption to quantify low amorphous contents of crystalline lactose. Pharm. Res. 18, 1, 112-116.

Hogan, S. and Buckton, G., 2001(a). Water sorption/desorption – near IR and calorimetric study of crystaslline and amorphous raffinose. Int. J. Pharm. 227, 57-69.

I

Ibrahim, H.G., Pisano, F., and Bruno, A., 1977. Polymorphism of phenylbutazone: properties and compressional behaviour of crystals. J. Pharm. Sci., 66, 669-673.

Imamura, K., Iwai, M., Ogawa, T., Sakiyama, T., and Nakanishi, K., 2001. Evaluation of the hydration states of proteins in freeze-dried amorphous sugar matrix. J. Pharm. Sci. 90, 12, 1955-1963.

Imaizumi, H., Nambu, N. and Nagai, T., 1983. Stabilisation of amorphous state of indomethacin by solid dispersion in polyvinylpyrrolidone. Chem. Pharm. Bull. 31, 7, 2510-2512.

J

Jacobs, P.W., 1997. Formation and growth if nuclei and the growth of interfaces in the chemical decomposition of solids: New insights, J. Phys. Chem. B., 101, 1086-1093.

Jolley, J.E., 1970. The microstructure of photographic gelatine binders. Photo. Sci. Eng., 14, 3, 169-177.

Jouppila, K., Kansikas, J. and Roos, Y. H., 1997. Glass transition, water plasticization and lactose crystallisation in skim milk powder. J. Dairy. Sci. 80, 3152-3160.

K

Kawashima, Y., Lin, S. Y., Taekenaka, H. J., 1983. put title in. Drug Dev. Ind. Pharm. 9, 8, 1445-1463.

Kauzmann, W., 1948. Nature of the Glassy state. Chem. Rev., 43, 220-238.

Kedward, C.J., MacNaughtan, W., Blanshard, J.M.V. and Mitchell, J.R., 1998. Crystallisation kinetics of lactose and sucrose based on isothermal differential scanning calorimetry. J. Food Sci., 63, 2, 192-197.

Kedward, C.J., MacNaughtan, W. and Mitchell, J.R., 2000. Crystallisation kinetics of amorphous lactose as a function of moisture content using isothermal differential scanning calorimetry. J. Food. Sci., 65, 2, 324-328.

Kerč, J. and Srčič, S., 1995. Thermal analysis of glassy pharmaceuticals. Therm. Acta., 248, 81-95.

Kibbe, A., 2000. The handbook of pharmaceutical excipients, 3rd edition. Editor: Arthur Kibbe. American Pharmceutical Assoc. and Pharm. Press., 276-285.

Kreft, K., Kozamernik, B. and Urleb, U., 1999. Qualitative determination of polyvinylpyrrolidone type by near-infrared spectrometry. Int. J. Pharm., 177, 1-6.

Kussendrager, K., De Hoog, P. and Van Leverink., 1981. Some physical properties of spray-dried lactose with stability and compression. Acta. Pharm. Seuc., 18, 2, 94-95.

L

Lane, R. and Buckton, G., 2000. The novel combination of dynamic vapour sorption gravimetric analysis and near infrared spectroscopy as a hyphenated technique. Int. J. Pharm. 207, 49-56.

Lerk, C.F., Andreae, A.C., De Boer, A.H., De Hoog, P., Kussendrager, K. and Van Leverink, J., 1984. Transitions of lactose by mechanical and thermal treatments. J. Pharm. Sci. 73, 6, 857-859.

Lerk, C.F., Andreae, A.C., De Boer, A.H., De Hoog, P., Kussendrager, K. and Van Leverink, 1984a. Alterations of α-lactose during differential scanning calorimetry. J. Pharm. Sci. 73, 6, 856-857.

Levine, H., and Slade, L., 1987. Water as a plasticiser: Physico-chemical aspects of low-moisture polymeric systems. Water Sci. Rev. Editor: Franks, F., Camb. Uni. Press. 79-185.

Liu, J., Rigsbee, D.R., Stotz, C. and Pikal, M.J., 2002. Dynamics of pharmaceutical amorphous solids: The study of enthalpy relaxation by isothermal microcalorimetry. J. Pharm. Sci. 91, 8, 1853-1862.

M

Mackin, L., Zanon, R., Park, J. M., Foster, K., Opalenik, H. and Demonte, M., 2002. Quantification of low levels (< 10%) of amorphous content in micronised active batches using dynamic vapour sorption and isothermal microcalorimetry. Int. J. Pharm. 231, 227-236.

Maffezzoli, A., Kenny, J.M. and Torre, L., 1995. On the physical dimensions of the Avrami constant. Thermochem. Acta, 269/270, 185-190.

Makower, B. and Dye, W. B., 1956. Equilibrium moisture content and crystallisation of amorphous sucrose and glucose. Agr. Food Chem., 4, 1, 72-77.

Masters, K. 1990. Spray drying handbook, 5th edition.

Mazzobre, M.F., Soto, G., Aguilera, J.M., and Buera, M.P., 2001. Crystallisation kinetics of lactose in systems co-lypophilised with trehalose. Analysis by differential scanning calorimetry. Food Res. Int., 34, 903-911.

Molyneux, P., 1985. Water soluble synthetic polymers: Properties and behaviour, Vol. 1 & 2. CRC press.

Moffat, A., 1998. the case for the use of near-infrared spectroscopy as a primary method of analysis. J. Pharm. Pharmcol. Suppl., 50, 46.

Moskala, E.J., Varnell, D.F. and Coleman, M.M., 1985. Concerning the miscibility of poly(vinyl phenol) blends-FTIR study. Polymer, 26, Feb, 228-234.

Mullins, J. W., Crystallisation, 3rd edition, 1993. Butterworth-Heinemann, Oxford.

Mysels, K.J., 1986. Surface tension of solutions of pure sodium dodecyl sulphate. Langmuir, 2, 423-428.

N

Nair, R., Nyamweya, N., Gonen, S., Martinez-Miranda, L.J. and Hoag, S.W., 2001. Influence of various drugs on the glass transition temperature of poly(vinylpyrrolidone): a thermodynamic and spectroscopic investigation. Int. J. Pharm. 225, 83-96.

O

Oakley, D.E., Oct. 1997. Produce uniform particles by spray drying. Chem. Eng. Prog. 48-54.

Okhamafe, A.O. and York, P., 1987. Thermal characterisation of drug/polymer and excipient/polymer interactions in some film coating formulation. J. Pharm. Pharmacol. 41, 1-6.

Oksanen, C. and Zografi, G., 1990. The relationship between the glass transition temperature and water vapour absorption by poly(vinylpyrrolidone). Pharm. Res. 7, 6, 654-657.

Olano, A., Bernhard, R.A. and Nickerson, T.A., 1977. Alteration in the ratio of α- to β-lactose co-crystallised from organic solvents. J. Food Sci., 42, 4, 1066-1068.

Olano, A., Corzo, N. and Martinez-Castro, I., 1983. Studies on β-lactose crystallization. Milchwissenschaft. 38, 8, 471-474.

Osborne, B. G., Fearn, T. and Hindle, P. H., 1993. Practical NIR spectroscopy with applications in food and beverage analysis. 2nd edition. Longman scientific and technical Press.

Otsuka, M., Ohtani, H., Kaneniwa, N. and Higuchi, S., 1991. Isomerisation of lactose in solid-sate by mechanical stress during grinding. J. Pharm. Pharmcol. 43, 148-153.

P

Painter, P. C., Graf, J.F. and Coleman, M.M, 1991. Effect of hydrogen bonding on the enthalpy of mixing and the composition dependence of the glass transition temperature in polymer blends, Macromol., 24, 5630-5638.

Patel, R., 1999. Studies of drug-surfactant interactions. University of London Phd. Thesis.

Phipps, M. A. and Mackin, L. A., 2000. Application of isothermal microcalorimetry in solid state drug development. Pharm. Sci. and Tech. Today, 3, 9-17.

Pikal, M. J. and Grant, D. J. W., 1987. A theoretical treatment of changes in energy and entropy of solids caused by additives or impurities in solid solution. Int. J. Pharm. 39, 243-253.

R

Read, W.T., 1953. Dislocations in crystals. Mcgraw-Hill, New York.

Righetti, M.C., Ajroldi, G. and Pezzin, G., 1992. The glass transition temperature of polymer-diluent systems. Poly., 33, 22, 4779-4784.

Robards, K., Haddad, P. R., and Jackson, P. E., 1994. Principles and practice of modern chromatographic methods. Academic press limited.

Robinson, B. V., Sullivan, F.M., Borzelleca, J.F. and Schwartz, S.L. (1990) PVP: A critical review of the kinetics and toxicology of polyvinylpyrrolidone (Povidone). Lewis Publishers.

Roetman, K., and Van Schaik, M. 1975. The β/α ratio of lactose in the amorphous state. J. Dairy Milk. 29, 225-237.

Roos, Y. and Karel, M., 1992. Crystallisation of Amorphous lactose. J. of Food Sci, 57, 3, 775-777.

Roos, Y., 1993. Melting and glass transitions of low molecular weight carbohydrates. Carbo. Res., 238, 39-48.

S

Sarciaux, J.M.E., and Hageman M.,J., 1997. Effects of bovine somatotropin (rbSt) concentration at different moisture levels on the physical stability of sucrose in freeze dried rbSt/sucrose mixtures. J. Pharm. Sci., 86, 3, 365-371.

Saleki-Gerhardt, A., and Zografi, G., 1994. Non-isothermal and isothermal crystallisation of sucrose from the amorphous state. Pharm. Res., 11, 8, 1166-1173.

Saleki-Gerhardt, A., Ahlneck, C. and Zografi, G., 1994. Assessment of disorder in crystalline solids. Int. J. Pharm. 101, 237-247.

Schmitt, E. A., Law, D. and Zhang, G. G. Z., 1999. Nucleation and crystallisation kinetics of hydrated amorphous lactose above the glass transition temperature. J. Pharm. Sci. 88, 3, 291-296.

Schneider, H. M., 1989. Polymer review; Glass transition behaviour of polymer of compatible polymer blends. Polymer., 771-779.

Schneider, H. M., 1997. Conforamtional entropy contributions to the glass temperature of blends of miscible polymers. J. Res. Nat. Inst. Stan. Tech., 102, 2, March-Apr., 229-248.

Sebhatu, T., Angberg, M. and Ahlneck, C., 1994. Assessment of the degree of disorder in crystalline solids by isothermal microcalorimetry. Int. J. Pharm. 104, 135-144.

Sekikawa, H., Nakano, M. and Arita, T., 1978. Inhibitory effect of polyviynlpyrrolidone on the crystallisation of drugs. Chem. Pharm. Bull., 26, 1, 118-126.

Sekizaki, H., Danjo, K., Eguchi, H., Yonezawa, Y., Sunada, H. and Otuska, A., 1995. Solid state interactions of ibuprofen and polyvinylpyrrolidone. Chem. Pharm Bull., 43, 6, 988-993.

Shalaev, E. Y., amd Franks, F., 1995. Structural glass transitions and thermophysical processes in amorphous carbohydrates and their supersaturated solutions. J. Chem. Soc. Farad. Trans., 9, 10, 1511-1517.

Shamblin, S.L., Huang, E. Y. and Zografi, G., 1996. The effects of co-lyophilised polymeric additives on the glass transition temperature and crystallisation of amorphous sucrose. J. Therm. Anal., 47, 1567-1579.

Shamblin, S.L., Taylor, L.S. and Zografi, G., 1998. Mixing behaviour of colypholilised binary systems. J. Pharm. Sci., 87, 6, 694-701.

Shamblin, S. L., Tang, X., Chang, L., Hancock, B. and Pikal., 1999. Characterisation of the time scales of molecular motion in pharmaceutically important glasses. J.Phys. Chem. B. 103, 4113-4121.

Shamblin, S.L. and Zografi,G., 1999a. The effect of absorbed water on the properties of amorphous mixtures containing sucrose. Pharm. Res., 16, 1119-1124.

Shaw, D.J., 1992. Introduction to colloid and surface chemistry, 4th edition. Butterworth-Heineman Ltd.

Sichina, W. J., Enhanced characterisation of the glass transition event using stepscan DSC. Pharmaceutical technical note.

Silverstein, R.M., Bassler, G.C. and Morrill, T., 1974. Spectrometric identification of organic compounds. 3rd edition, John Wiley and Sons Inc. p73-83.

Simonelli, A.P., Mehta, S. C. and Higuchi, W. I., 1969. Dissolution rates of high energy polyvinylpyrrolidone (PVP) –Sulfathiazole coprecipitates. J. Pharm. Sci., 58, 5, 538-549.

Simonelli, A.P., Mehta, S. C. and Higuchi, W. I., 1976. Dissolution rates of high energy sulfathiazole-povidone coprecipitates II: characterisation of form of drug controlling its dissolution rate via solubility studies. J. Pharm. Sci. 65, 3, 355-361.

Smythe, B.M., 1967. Sucrose crystal growth, II. Rate of crystal growth in the presence of impurities. Aust. J. Chem., 20, 1097-1114.

Stubberud, L., Arwidsson, H.G., Hijortsberg, V., and Graffner, C., 1996. Water solid interactions. III. Effect of glass transition temperature and processing on tensile strength of compacts of lactose and lactose/polyvinylpyrrolidone. Pharm. Dev. Tech., 1, 2, 195-204.

Stubberud, L. and Forbes, R. T., 1998. The use of gravimetry for the study of the effect of additive on the moisture induced recrystallisation of amorphous lactose. Int. J. Pharm. 163, 145-156.

Sugisaki, M., Suga, H. and Seki, S., 1968. Calorimetric study of the glassy state. IV, heat capacities of glass water and cubic ice. Bull. Chem. Soc. Jpn. 41, 2591-2599.

Suryanarayanan, R., and Mitchell, A.G. 1985. Evaluation of two concepts of crystallinity using calcium gluceptate. Int. Pharm, 24, 1-17.

T

Tantishaiyakul, V., Kaewnopparat, N. and Ingkatawornwong, S., 1999. Properties of solid dispersions of piroxicam in polyvinylpyrrolidone. Int. J. Pharm. 181, 143-151.

Taylor, L.S. and Zografi, G., 1997. Spectroscopic characterisation of interactions between PVP and indomethacin in amorphous molecular dispersions. Pharm. Res., 14, 12, 1691-1698.

Taylor, L.S. and Zografi, G., 1998. Sugar-polymer hydrogen bond interactions in lyophilised amorphous mixtures. J. Pharm. Sci., 87, 12, 1615-1620.

Tan, Y.Y. and Challa, G., 1976, The glass transition temperature of poly(N-vinylpyrrolidone) and the effect of water. Polymer, 17, August, 739-740.

Thiel, P.A. and Madey, T.E., 1987. The interaction of water with solid surfaces: Fundamental aspects. Surf. Sci. Rep., 7, 211-385.

To, E.C., and Flink, J.M., 1978. Collapse, A structural transition in freeze-dried carbohydrates. II. Effect of solute composition. J. Fd. Tech., 13, 567-581.

Turnball, D., and Fischer, J.C., 1949. Rate of nucleation in condensed systems, J. Chem. Phys., 17, 71-73.

Turner, D.T. and Schwatrz, A., 1985. The glass transition temperature of poly(N-vinylpyrrolidone) by differential scanning calorimetry. Polymer, 26, May, 757-762.

V

Van den Mooter, G., Wuyts, M., Blaton, N., Busson, R., Grobet, P., Augustijns, P. and Kinget, R., 2001. Physical stabilisation of amorphous Ketoconazole in solid dispersions with polyvinylpyrrolidone K25. Euro. J. Pharm. Sci. 12, 261-269.

Van Hook, A. and Frulla, F., 1952. Nucleation in sucrose solutions. Ind. Eng. Chem., 44, 1305-1308.

Van Hook, A., 1971. Nucleation. Sug. Tech. Rev., 1, 232-238.

Van Scoik, K. G. and Cartensen J.T., 1990. Nucleation phenomena in amorphous sucrose systems. Int. J. Pharm., 58, 185-196.

Vermeer, A.W.P., and Norde, W., 2000. The influence of the binding of low molecular weight surfactants on the thermal stability and secondary structure of IgG., Colloids And Surf. A: Physicochem. Eng. Asp. 161, 139-150.

Volpe, P.L.O. and Filho, E.A.S., 1995. Calorimetric study of SDS micelle formation in water and in NaCl solution at 298K. Thermochem. Acta, 257, 59-66.

Vromans, H., Bolhuis, G.K., Lerk, C.F., Biggelaar, V. D. and Bosch, H., 1987. Studies on tableting properties of lactose. VII. The effect of variations in primary particles size and percentage of amorphous lactose in spray dried lactose products. Int. J. Pharm., 35, 29-37.

W

Wade, A. and Weller, P. J., 1994. Handbook of pharmaceutical excipients. 2nd edition. The Pharmaceutical Press.

Walstra, P., 2003. Physical Chemistry of Foods. Marcel Dekker Inc.

Wang, L.H., and Chowhan, Z.T., 1990. Drug excipient interaction resulting from powder mixing. V. Role of sodium lauryl sulphate. Int. J. Pharm., 60, 61-78.

Wang, G., and Olofsson, G., 1998. Titration calorimetric study of the interaction between ionic surfactants and uncharged polymers in aqueous solutions. J. Phys. Chem. B., 102, 9276-9283.

Wang, G., Pelton, R., and Zhang, J., 1999. Sodium dodecyl sulfate binding to poly(N-isopropylacrylamide) microgel latex studied by isothermal titration calorimetry. Colloids And Surf. A: Physicochem. Eng. Asp. 153, 335-340.

Waninge, R., Paulsson, M., Nylander, T., Ninham, B. and Sellers, P., 1998. Binding of Sodium dodecyl sulphate and dodecyl trimethyl ammonium chloride toβ-lactoglobulin: A calorimetric study. Int. Diary J., 8, 141-148.

White, G.W., and Cakebread, S.H., 1966. The glassy state in certain sugar-containing food products. J. Food. Tech., 1, 73-82.

Wilson, N., Watt, R.A. and Moffat, A.C., 2001. A near-infrared method for the assay of cineole in eucalyptus oil as an alternative to the official BP method. J. Pharm. Pharmcol., 53, 95-102.

Williams, M.L., Landel, R.F., and Ferry, J.D., 1955. The temperature dependence of relaxation mechanisms in amorphous polymers and other glass-forming liquids. J. Am. Chem. Soc., 77, 3701-3706.

Y

Yoon W.L, Jee, R.D. and Moffat, A. C., 1998. Optimisation of sample presentation for near-infrared spectra of pharmaceutical excipients. Analyst, 123, May, 1029-1034.

York, P., 1983. Solid-state properties of powders in the formulation and processing of solid dosage forms. Int. J. Pharm. 14, 1-28.

Yoshioka, M., Hancock, B. and Zografi, G., 1995. Inhibition of indomethacin crystallisation in poly(vinylpyrrolidone) coprecipatates. J. Pharm. Sci., 84, 8, 983-986.

Z

Zheng, M. X., Martin, G.P. and Marriott, C., 2001. Effects of molecular weight of poylvinylpyrrolidone on the glass transition and crystallisation of co-lyophilised sucrose. Int. J. Pharm., 218, 63-73.

Zhang, J. and Zografi, G., 2001. Water vapour absorption into amorphous sucrose-poly(vinylpyrrolidone) and trehalose-poly(vinylpyrolidone) mixtures. J. Pharm. Sci., 90, 9, Sept., 1375-1385.

Zhou, D., Zhang, G.G.Z., Law, D., Grant, D.J.W., and Schmitt, E.A., 2002. Physical Stability of amorphous pharmaceuticals: importance of configurational thermodynamic quantities and molecular mobility. J. Pharm. Sci., 91, 8, 1863-1872.

Zografi, G., 1988. States of water associated with solids. Drug. Dev. Ind. Pharm. 14, 14, 1905-1926.